



Technische Universität München  
Fakultät für Chemie

---

**Investigation of Pyridoxal Phosphate-Dependent  
Enzymes and Deciphering Their Role as Novel  
Antibiotic Targets in Critical Bacterial Pathogens  
by a Chemical Proteomic Strategy**

---

Dissertation zur Erlangung des akademischen Grades eines  
Doktors der Naturwissenschaften von

**Martin Pfanzelt**





Technische Universität München  
Fakultät für Chemie

**Investigation of Pyridoxal Phosphate-Dependent  
Enzymes and Deciphering Their Role as Novel  
Antibiotic Targets in Critical Bacterial Pathogens  
by a Chemical Proteomic Strategy**

**Martin Pfanzelt**

Vollständiger Abdruck der von der Fakultät für Chemie  
der Technischen Universität München zur Erlangung eines

**Doktors der Naturwissenschaften (Dr. rer. nat.)**

genehmigten Dissertation.

Vorsitzende:

Prof. Dr. Cathleen Zeymer

Prüfer der Dissertation:

1. Prof. Dr. Stephan A. Sieber

2. apl. Prof. Dr. Wolfgang Eisenreich

Die Dissertation wurde am 09.03.2022 bei der Technischen Universität München  
eingereicht und durch die Fakultät für Chemie am 30.03.2022 angenommen.



*Für meine Eltern, Familie und Freunde*



DIE VERGANGENHEIT IST OHNE BEDEUTUNG, DENN DU KANNST SIE NICHT MEHR VERÄNDERN. DEINE ZUKUNFT HINGEGEN IST LEBENDIG WIE EIN JUNGER BAUM. DU ENTSCHEIDEST, WO ES SICH FÜR IHN LOHNT, ZU WURZELN, UND WIE WEIT ER SEINE KRONE IN DEN HIMMEL STRECKEN SOLL.

– *Uwe Eckardt (Die Savanten)*





# ABSTRACT

---

Vitamin B<sub>6</sub> plays a vital role in the metabolism of all living organisms. Its bioactive form pyridoxal 5'-phosphate (**PLP**) serves as a cofactor of pyridoxal 5'-phosphate-dependent enzymes (**PLP**-DEs) and catalyses a large number of different reactions. Due to the involvement of **PLP**-DEs in many basic metabolic processes, some of these enzymes play critical roles in human diseases and are already addressed as important drug targets.

Based on a previous study in our lab, we synthesised novel pyridoxal (**PL**)-probes derivatised at the C2'-, C3'- and C6-position for the investigation of bacterial **PLP**omes. For the biological evaluation and suitability of the 13 **PL**-probes as cofactor mimics, we first investigated their kinetics in phosphorylation studies with bacterial pyridoxal kinases (PLKs), which revealed sufficient activation for the majority of our probes. Growth studies and analytical labelling experiments confirmed probe uptake, activation and their ability to function as activity-based probes. For the initial experiments, we worked with *S. aureus* and *E. coli* mutants that are both lacking **PLP** *de novo* synthesis. We started to optimise our previous preparative labelling conditions in the *S. aureus* mutant strain by comparing different media and probe concentrations. Compared to our previous study, we enhanced the labelling efficiency by 35%. We then applied our refined conditions to an *E. coli* mutant strain. Moreover, we were able to exploit the **PLP**ome of the GRAM-negative *P. aeruginosa* wild type strain by a set of selected **PL**-probes. For all three organisms, a large number of known and putative or poorly characterised **PLP**-DEs could be accessed by quantitative mass spectrometry-based proteomics, using label free quantification (LFQ). Next, we selected five putative **PLP**-DEs from the analysed organisms and confirmed **PLP**-binding as well as catalytic insights into the function of the aminotransferases *PA3659* and *PA3798* (*P. aeruginosa*), the serine/threonine dehydratase *PA2683* (*P. aeruginosa*), the transcriptional regulator *ydcR* (*E. coli*) and the cysteine desulfurase *A0A0H2XXHJ5* (*S. aureus*) by a series of different biochemical methods, including UV/Vis spectroscopy and targeted metabolomics. Finally, we screened a library of putative **PLP**-DE inhibitors for their antibiotic activity and investigated the targets of four hit compounds by competitive **PLP**ome profiling. Two target **PLP**-DEs of the antibiotic compound phenelzine were further verified by *in vitro* assays, showcasing that our method is a powerful tool in drug development to unravel (off)-target proteins in a holistic approach, covering the whole proteome.

In addition, based on the pro-tide strategy in drug design, we established the synthesis of a **PL3** phosphoramidate probe, which can be used as a PLK independent cofactor surrogate. Especially the human PLK is highly restricted to its substrates, which is why the novel probe **PL3PA** could bypass this fundamental issue.



# ZUSAMMENFASSUNG

---

Vitamin B<sub>6</sub> nimmt eine wichtige vitale Rolle im Stoffwechsel aller lebenden Organismen ein. Seine bioaktive Form Pyridoxal-5'-phosphat (**PLP**) dient als Cofaktor von Pyridoxal-5'-phosphat-abhängigen Enzymen (**PLP**-DEs) und katalysiert eine große Anzahl verschiedener Reaktionen. Da **PLP**-DEs an vielen grundlegenden Stoffwechselprozessen beteiligt sind, spielen einige dieser Enzyme eine entscheidende Rolle bei der Entwicklung von Krankheiten und sind bereits als Angriffsziele für Arzneimittel bekannt.

Auf der Grundlage einer früheren Studie in unserem Labor haben wir neuartige Pyridoxal (**PL**)-Sonden entwickelt, die an der C2'-, C3'- und C6-Position modifiziert sind, um bakterielle **PLP**-DEs zu untersuchen. Zur biologischen Bewertung und Eignung der 13 **PL**-Sonden als Cofaktor-Mimetika untersuchten wir zunächst ihre Kinetik in Phosphorylierungsstudien mit bakteriellen Pyridoxal-Kinasen (PLKs), die eine ausreichende Aktivierung für die meisten unserer Sonden zeigten. Wachstumsstudien und analytische Labellingsexperimente bestätigten die Aufnahme der Sonden, ihre Aktivierung und ihre Fähigkeit als aktivitätsbasierte Sonden zu fungieren. Für die initialen Experimente arbeiteten wir mit *S. aureus* und *E. coli* Mutanten, bei denen die **PLP** *de novo* Synthese ausgeschaltet wurde. Zunächst optimierten wir unsere früheren präparativen Labellingsbedingungen im *S. aureus* Mutantenstamm, indem wir verschiedene Medien und Sondenkonzentrationen verglichen. Im Vergleich zu unserer früheren Studie konnten wir die Labellingeffizienz um 35% steigern. Anschließend wandten wir unsere verbesserten Bedingungen auf beide Mutanten an. Darüber hinaus konnten wir das **PLP**om des GRAM-negativen *P. aeruginosa* Wildtyp-Stamms mit einer Reihe ausgewählter **PL**-Sonden zugänglich machen. Für alle drei Organismen konnte eine große Anzahl bekannter und mutmaßlicher oder schlecht charakterisierter **PLP**-DEs durch quantitative, massenspektrometrie-basierte Proteomik signifikant angereichert werden. Anschließend wählten wir fünf mutmaßliche **PLP**-DEs aus den untersuchten Organismen für ausführlichere Analysen aus. Wir bestätigten die **PLP**-Bindung und konnten katalytische Einblicke in die Funktion der Aminotransferasen *PA3659* und *PA3798* (*P. aeruginosa*), der Serin/Threonin-Dehydratase *PA2683* (*P. aeruginosa*), des Transkriptionsfaktors *ycdR* (*E. coli*) und der Cystein-Desulfurase *A0A0H2XXHJ5* (*S. aureus*) mit einer Reihe verschiedener biochemischer Methoden, einschließlich UV/Vis-Spektroskopie und Metabolomik, gewinnen. Schließlich untersuchten wir eine Bibliothek mutmaßlicher **PLP**-DE Inhibitoren auf ihre antibiotische Aktivität und konnten vier zelluläre Zielstrukturen (Targets) durch kompetitive Proteomikexperimente aufklären. Zwei der Enzyme, die mit dem Antibiotikum Phenelzin interagieren, wurden durch *in vitro* Assays weiter verifiziert. Deshalb ist unsere chemische Proteomik-Methode ein

leistungsfähiges Werkzeug für die Arzneimittelentwicklung, um (Off-)Target-Proteine in einem ganzheitlichen Ansatz zu entschlüsseln, der das gesamte Proteom umfasst.

Darüber hinaus haben wir auf der Grundlage der pro-tide Strategie für die Entwicklung von Medikamenten die Synthese einer **PL3** Phosphoramidat-Sonde erarbeitet, die als PLK-unabhängiges Cofaktor-Surrogat verwendet werden kann. Insbesondere die humane PLK ist in Bezug auf ihre Substrate stark eingeschränkt, weshalb die neuartige Sonde **PL3PA** dieses grundlegende Problem umgehen könnte.

# ACKNOWLEDGEMENTS

---

Dass „die Zeit [jeden] promoviert“, wie ein geschätzter, ehemaliger Kollege<sup>1</sup> zu sagen pflegte, stimmt so nicht. Auf dem langen Weg dorthin erhält man Hilfe von sehr vielen Personen, ohne die es niemals möglich wäre, alles zu bewältigen. An dieser Stelle möchte ich mich an meine Freunde, Familie und Kollegen wenden, um ihnen von ganzem Herzen zu danken.

Zunächst gilt mein Dank meinem Doktorvater PROF. STEPHAN SIEBER, der mich in seinen Lehrstuhl aufgenommen und mich bis zum Schluss immer unterstützt hat. Seine Fähigkeit, Lösungen für allerlei Probleme zu finden, war immer bemerkenswert. Ganz besonders hat mir die Freiheit gefallen, eigene Ideen und Experimente einzubringen und diese auch ausführen zu dürfen. Besonders hervorheben möchte ich auch seine bedingungslose Unterstützung bei meiner Bewerbung für ein Stipendium bei der STUDIENSTIFTUNG DES DEUTSCHEN VOLKES, für das ich mich hiermit auch beim Verein selbst bedanken möchte. PROF. MANFRED SARGL hat mich sehr herzlich aufgenommen und die Treffen mit unsere Gruppen waren immer lustig und unterhaltsam. Auf das Angebot einer Skitour in Kufstein komme ich gerne zurück!

Ohne freiwillige Lektoren könnte man eine solche Arbeit nicht veröffentlichen. Herzlichen Dank an den Briten DIETRICH MOSTERT, der den Fließtext durch seine Sprachgewandtheit enorm aufgewertet hat. Vielen Dank auch an CAROLIN GLEISSNER, MICHAELA aka SERGEANT aka MICHA FIEDLER und DOMINIK SCHUM für ihre gründliche Korrektur dieser Arbeit und ihre hilfreichen Anmerkungen.

Ein großes Dankeschön geht an meine Kooperationspartner während der Promotion, DR. SABINE SCHNEIDER und PROF. WOLFGANG EISENREICH für die zahlreichen Gespräche zu *Q2FF14*, THOMAS MAHER (godverdomme jongen!) für seine tatkräftige Unterstützung in seinem 9-monatigen Praktikum, MARKUS SCHWARZ für seine Hilfe mit den *Pseudomonas*-Proteinen (Primer sollten wir jetzt genügend haben) und RAMONA ABSMEIER für die Klonierung und Expression der beiden Transkriptionsfaktoren. Danke dir RAMONA auch insbesondere für deine hilfsbereite und gesellige Art. Auf „a guads Allgäuer Bier“ können wir uns gerne mal treffen. Dir MARKUS gute Nerven mit unserer Orbi XL und dir MICHAELA aka SERGEANT aka MICHA FIEDLER gutes Gelingen mit dem Phosphoramidat-Projekt. Glaub mir, das wird gut! Außerdem danke ich ISABEL WILKINSON für die gute Zusammenarbeit.

Ohne MONA WOLFF wären wir im Labor wohl aufgeschmissen. Wir wären nicht nur arm, weil wir alles doppelt und dreifach bestellt hätten, sondern das Labor würde einem Schlachtfeld gleichen, da wir wegen deiner Aufräumaktionen verlernt haben, unsere Dinge selbst wieder einzuräumen. Außerdem möchte ich mich bei unseren Azubis

---

<sup>1</sup>Mathias W. Hackl


LINDA, ALINA, MARIE, ISABELLA und TANJA für ihre Unterstützung im täglichen Laboralltag und bei einigen Experimenten bedanken. KATJA BÄUML hat verhindert, dass wir uns nicht alle aus Versehen umgebracht haben und die Massenspektrometer nicht in Flammen aufgegangen sind. Danke KATJA für deine direkte, manchmal fordernde, aber ehrliche Art! Außerdem gilt mein Dank HOLGER LEUTUNG, der durch seine ruhige und durchdachte Art sehr dazu beigetragen hat, dass ich mich genauer mit Massenspektrometern auseinandergesetzt habe. Auf die richtige Menge Diamantin kommt es an!

Die Fäden im Hintergrund richtig zu ziehen verstanden CHRISTINA BRUMER und BARBARA SEIBOLD besonders gut. Ihr habt es immer rechtzeitig geschafft, die Arbeitslosigkeit abzuwenden, auch wenn die Hürden der Vertragsverlängerung noch so groß waren. Herzlichen Dank euch zwei!


Man lernt selbst sehr viel, wenn man Praktikanten betreut. Danke an RAMON RANKA, MICHAEL ZOLLO, AZIZA EL HARIRY, MARIA WEYH, PATRICK RAUNFT, DARIO MDROVIC, der alte Gratler, CORINNA VOLLEI und FRANZISKA HELD für die Unterstützung bei zahlreichen Projekten. Ich werde jedes sich rotierende Etwas auf 108 Umdrehungen stellen, egal ob du willst und nicht! Außerdem überlasse ich die Definition eines sogenannten Gratlers ab jetzt DARIO, der Ehrenechse. MICHI, viel Spaß beim Spachteln von Roststellen und bei den teuren Reparaturen an deinem Stern. Kleiner Tipp: hol dir einen Schweden.

Der AK Sieber ist bekannt für den guten Zusammenhalt unter den Kollegen und eine lustige, ausgelassene Atmosphäre. Das kann ich nur bestätigen und mich bei allen ehemaligen und aktiven Kollegen dafür bedanken. Alle Mitglieder des harten Kerns, aber auch des mittelharten, dreiviertelweichen und natürlich des weichen Kerns werden hiermit angesprochen.

Ganz besonders bedanke ich mich bei CAROLIN GLEISSNER für ihre lustige und herzliche Art während all der Jahre am Lehrstuhl. Außerhalb der Arbeit haben wir auch viel erlebt, wir waren auf den verschiedensten Bergen, Loipen und Radwegen. Alles gerne wieder, nur nicht bei 35 °C in der Sonne! Außerdem stehen noch einige Skitouren aus, Pieps und Schaufel haben wir ja jetzt. Aber was wäre CARO ohne VOLKER KIRSCH gewesen? VOLKER hat eine derart sympathische Art, dass ihn nicht nur jeder mag und mit seinem Charakter klarkommt, er vermag es auch, jede schlechte Stimmung zu heben und Hoffnung zu schenken. Danke VOLKI für die lustige Zeit im Labor und natürlich den fachlichen Wissenstransfer bezüglich unseres Schlachtroßes, der Orbi! Ich hoffe, wir bekommen bald eine Probe für unser ausstehendes Duet hin! Auch bei DOMINIK SCHUM, dem besten Konditor Bayerns, und MICHAELA aka SERGEANT aka MICHA FIEDLER möchte ich mich für die lustige Zeit im neuen Gebäude bedanken.

Bei meinen Laborkollegen ANGELA WEIGERT-MUÑOZ, THERESA RAUH, PAVEL KIELKOWSKI, JAN-NIKLAS DIENEMANN und am Ende THOMAS GRONAUER  und

---

PATRICK ALLIHN bedanke ich mich für die tolle Atmosphäre, die lustigen oder ernstesten Gespräche und die geteilten Sußigkeiten. Es war mir eine Freude mit den berühmten Laborhemmem(!) THERESA und THERESA zu arbeiten. Auch unsere mittlerweile leider aufgelöste Kaffe-Gang (THOMAS, DIDI, CARO, VOLKER und RAMONA) war immer sehr unterhaltsam. Dass die thermodynamische Senke Leuvens so in Erinnerung bleiben wird, hätte keiner gedacht. Danke INES HÜBNER, ROBERT MACSICS und STEPHAN HACKER für die lustige Zeit während der ABPP-Konferenz in Belgien, oder doch Holland? Sorry, but I don't understand ... THIS language. Auch unserer Fußballmannschaft, der Eintracht und Zweittracht Prügel, sozusagen dem harten Fußballkern, CHRISTIAN FETZER, MATHIAS HACKL, THOMAS GRONAUER, TILL REINHARDT, DIETRICH MOSTERT, PATRICK ALLIHN, MARKUS SCHWARZ, JONAS DRECHSEL, VOLKER KIRSCH, PATRICK ZANON, KYU-MYUNG LEE und PHILIPP LE danke ich für die tollen Trainingseinheiten und Turniere. Für einen heißen Sommertag noch nichts geplant? Wie wäre es mit einer Session PAMELA aka SERGEANT aka FIEDLER im Dreck vor dem Klärwerk? Das fanden auch ALEXANDRA GEISSLER und JAN-NIKLAS DIENEMANN besonders toll und ein Muskelkater war immer vorprogrammiert. Eine Frage bleibt bestehen: TILL REINHARDT, haben wir dich wirklich gebrochen? Einen richtigen Grantler aus den Bergen durfte ich mit JOSEF BRAUN kennenlernen. Danke für die tägliche Schokoladenration, die es nach einem Fluch und Beschimpfungen immer gab. Ohne KONSTANTIN ECKEL  hätte ich meine Bakterienpellets in Zentrifugenröhrchen niemals weggeräumt. DAVIDE BOLDINI wünsche ich viel Spaß beim Crypto-Mining und MARTIN KÖLLEN beim Synthetisieren aller möglichen Antibiotikaderivate. Meinem nordirischen, mittlerweile „lechoanerischen“ Freund STUART RUDELL wünsche ich alles Gute für die Zukunft in seinem neuen Job und hoffe, dass ihm sein Knie nicht so weh tut, wie er immer behauptet! Den angehenden Doktoranden LAURA ECK, MAX BOTTLINGER und AZIZA EL HARIRY wünsche ich einen guten Start und viel Erfolg!

Auch bei allen anderen, noch nicht genannten Ehemaligen möchte ich mich bedanken: MATTHIAS STAHL, ELENA KUNOLD, MARKUS LAKEMEYER, BARBARA EYERMANN, VADIM KOROTKOV, DORA BALOGH, JOHANNES WENGER, KATJA GLIESCHE, TOBIAS BECKER, IGOR PAVLOVIĆ, JULIA FRIEDERICH, JOHANNES RÖSSLER und WEINING ZHAO. Ein ganz besonderer Dank gilt aber ANNABELLE HOEGL, die mich während zwei Praktika und meiner Masterarbeit betreut hat und mir dann das große Pyridoxalprojekt anvertraut hat. Ich wünsche dir eine schöne Zeit mit deiner kleinen Familie in Dänemark und man sieht sich hoffentlich in der Heimat bald wieder! Außerdem möchte ich mich bei meiner Mentorin FRANZISKA MANDL bedanken, wir waren immer auf einer Wellenlänge! Danke für dein Vertrauen und die lustigen Momente.

Ganz besonders will ich mich hiermit bei KONRAD HÖRMANN, „m Ruadl Bua“ bedanken, meinem längsten und besten Kumpel seit Kindergartenzeiten. Wie ein geschätzter Nachbar schon öfter gesagt hat, ergänzen wir uns sehr gut und sind ein super

Team. Egal was zu tun ist, wir helfen zusammen und sind dadurch schnell und effizient. Die Arbeiten aller Art, sei es im Holz, am Trockenbau oder am Schreibtisch, waren und sind immer ein perfekter Ausgleich. Glaube mir, auf uns kommen noch glorreiche Jahre zu! Immer Spaß gemacht haben die Proben und Konzerte unseres Klaviertrupps mit Frontmann GERALD SÜTTINGER, PHILIPP DIETERICH und ANDREAS KIRSTEIN. Nicht nur die Klavierproben, auch die Segelausflüge auf dem Ammersee waren immer wunderbar und lustig. Bei dir GERALD möchte ich mich nochmal ganz besonders bedanken, für deine große Empathie und die große musikalische Weiterentwicklung, die ich dank dir erlebt habe.

Bei meinen Burggener Freunden PHILIPP DIETERICH, MATTHIAS STELZNER, ROBERT HÖRMANN, VINZENZ KARGL, JOHANNES DIETERICH, CORNELIUS MANDAK, VERONIKA SCHOBER und den Aushilfsburggenern GABRIEL STÖGER, LAURA KECK, TERESA STOLZ und PIA JUST bedanke ich mich ganz besonders! Immer lustig waren die Ausflüge und süffigen Abende in diversen Garagen und Hütten. Danke auch VRONI für die Kaffeekränzchen während meiner Zeit im Homeoffice, die durch einen „Bauragrauß“ durch das Fenster angekündigt wurden, und deine leckeren Muffins, des war TOLL! Meinem Bruder MANUEL PFANZELT auch ein großer Dank für die stete Gastfreundschaft, Hilfe bei allerlei Dingen und den großen Zusammenhalt.

Liebe Wohltäterin HILDEGARD LIEPOLD, „mei liabs Dotle“, herzlichen Dank für all die Unterstützung als meine Patentante! Ich bin immer gerne bei dir zum Ratschen oder Klavierspielen. Den namloser Wetterspitz schaffen wir schon noch! Danke auch GÜNTHER und SABINE ZUBE, dass mir/uns euer Stanzacher Haus immer offen steht! Danke auch JÜRGEN BADER für die Unterstützung und Versorgung für das leibliche Wohl. Liebe USCHI, danke für deine natürliche Art und deine Begeisterung für Kräuter aller Art, ich habe viel dabei gelernt!

Für die gemeinsame Zeit bedanke ich mich bei LISA SCHLOR, dass du mich immer auf andere Gedanken gebracht und mich immer wieder aufgebaut hast! Auch wenn sich unsere Wege getrennt haben, wünsche ich dir alles Gute für deine Zukunft und bleib genauso wie du bist!

Zum Schluss gilt mein größter Dank meinen Eltern BRIGITTE und JÜRGEN PFANZELT für all die Unterstützung in meinem Leben. Ihr seid die besten Eltern, liebevoll, fürsorglich und immer mit passenden, aufbauenden Worten ausgestattet. MAMA, danke für dein bedingungsloses Verständnis, deine positive Art und positiven Zusprüche. PAPA, danke für deine ruhige, bodenständige, weltoffene Art, dein künstlerisches Geschick und deine immerwährende Unterstützung in allen Lebensbereichen. Ohne euch wäre nichts möglich gewesen.

*Martin Pfanzelt*

*Burggen, 2022*



# PUBLICATIONS AND CONFERENCES

---

## Journal Publications

- I A. Hoegl, M. Nodwell, V. C. Kirsch, N. Bach, M. Pfanzelt, M. Stahl, S. Schneider, S. A. Sieber, *Nat. Chem.* **2018**, *10*, 1234–1245.
- II A. Fux, M. Pfanzelt, V. C. Kirsch, A. Hoegl, S. A. Sieber, *Cell Chem. Biol.* **2019**, *26*, 1461–1468.
- III M. Pfanzelt, T. E. Maher, R. M. Absmeier, M. Schwarz, S. A. Sieber, *Angew. Chem. Int. Ed.* **2022**, e202117724, DOI: 10.1002/anie.202117724.
- IV I. Wilkinson, M. Pfanzelt, S. A. Sieber, *Angew. Chem. Int. Ed.* **2022**, e202201136, DOI: 10.1002/anie.202201136.
- V D. Ranava, C. Scheidler, M. Pfanzelt, S. A. Sieber, S. Schneider, M.-N. F. Yap, **2022**, manuscript submitted.

## Conferences

- I ABPP Conference  
27<sup>th</sup>–29<sup>th</sup> March 2019, Leuven, Belgium  
*Poster Presentation:* Investigation of Pyridoxal Phosphate-Dependent Enzymes in GRAM-negative bacteria using a chemical proteomic strategy
- II EMBL Chemical Biology  
2<sup>nd</sup>–5<sup>th</sup> September 2020, Virtual Conference  
*Poster Presentation:* Investigation of PLP-dependent enzymes using a chemical proteomic strategy



# CONTRIBUTIONS

---

The project was initiated by A. HOEGL, M. NODWELL, N. C. BACH and S. A. SIEBER. MN established synthesis of **PL1**, AH developed synthesis of **PL2** and **PL3** as well as the **PLP**ome detection strategy in *S. aureus*. A. S. FUX established **PL1** labelling in human cells. M. PFANZELT synthesised probes **PL4** and **PL5** in an internship under the supervision of AH. MP continued with synthesis of **PL6-PL12** in his Master's thesis and synthesised probes **PL13** and **PL3PA** during his PhD. MP conducted experiments concerning the biological evaluation of all probes and performed labelling experiments in *S. aureus*, *E. coli* and *P. aeruginosa*. MP screened the compound library against several bacterial strains and performed competitive labelling experiments in *E. coli*. T. E. MAHER synthesised the phenelzine library and conducted competitive labelling experiments in *S. aureus* during an internship under the supervision of MP. R. M. ABSMEIER cloned and expressed *ydcR* and *yjiR* and performed analytical gel-based labelling experiments with **PL3PA** in HeLa cells during her Master's thesis under the supervision of MP. M. SCHWARZ cloned and expressed *PA2683* and *PA3798* during his Master's thesis under the supervision of MP. MP did all other experiments including cloning, expression and validation assays. SAS devised the project and supervised experiments.



# CONTENTS

---

<b>1</b>	<b>Background and Motivation</b>	<b>1</b>
1.1	Cofactors . . . . .	2
1.2	Vitamin B6 . . . . .	3
1.3	PLP-Dependent Enzymes . . . . .	7
1.4	Inhibition of PLP-Dependent Enzymes . . . . .	10
1.5	A Chemical Proteomic Tool . . . . .	16
1.5.1	PLPome Investigation by ABPP . . . . .	16
1.5.2	Competitive ABPP for Antibiotic Target Screening . . . . .	19
1.6	Objectives . . . . .	21
<b>2</b>	<b>Results and Discussion</b>	<b>23</b>
2.1	Synthetic Strategy . . . . .	24
2.1.1	PL-Derived Probes . . . . .	26
2.1.2	Pro-Tide Probe PL3PA . . . . .	30
2.1.3	Synthesis of Phenelzine Analogues . . . . .	39
2.2	Biological Evaluation of the Probes . . . . .	41
2.2.1	Phosphorylation by <i>pdxK</i> and SaPLK . . . . .	41
2.2.2	Growth Studies . . . . .	43
2.2.3	Analytical Labelling . . . . .	45
2.2.4	A Refined Preparative Labelling Strategy . . . . .	46
2.2.5	The Pro-Tide Probe PL3PA . . . . .	47
2.3	PLPome Profiling . . . . .	51
2.3.1	<i>S. aureus</i> PLPome . . . . .	51
2.3.2	<i>E. coli</i> PLPome . . . . .	53
2.3.3	<i>P. aeruginosa</i> Wild Type PLPome . . . . .	55
2.4	Validation Experiments . . . . .	57
2.4.1	The Aminotransferases <i>PA3659</i> and <i>PA3798</i> . . . . .	58
2.4.2	The Serine/Threonine Dehydratase <i>PA2683</i> . . . . .	61
2.4.3	The Transcriptional Regulator <i>ydcR</i> . . . . .	63
2.4.4	The Cysteine Desulfurase <i>A0A0H2XHJ5</i> . . . . .	66
2.5	Application: Screening for Potential Inhibitors . . . . .	69
2.5.1	Phenelzine in <i>S. aureus</i> . . . . .	70
2.5.2	Benserazide in <i>S. aureus</i> . . . . .	75
2.5.3	CCG-50014 in <i>S. aureus</i> . . . . .	77
2.5.4	MAC173979 in <i>E. coli</i> . . . . .	81
<b>3</b>	<b>Summary and Outlook</b>	<b>87</b>
3.1	Summary . . . . .	88
3.2	Outlook . . . . .	91

---

<b>4</b>	<b>Material and Methods</b>	<b>93</b>
4.1	Chemistry . . . . .	94
4.1.1	General Methods . . . . .	94
4.1.2	Synthesis . . . . .	96
4.2	Biochemistry . . . . .	162
4.2.1	Culture Media . . . . .	162
4.2.2	Cloning and Expression of Proteins . . . . .	162
4.2.3	Protein Purification of STREP Tagged Proteins . . . . .	169
4.2.4	Purification of His Tagged Proteins <i>ydcR</i> and <i>yjiR</i> . . . . .	169
4.2.5	UV/Vis Measurements . . . . .	170
4.2.6	Probe Phosphorylation Studies with <i>pdxK</i> and SaPLK . . . . .	170
4.2.7	Loading State Studies . . . . .	170
4.2.8	Intact Protein Mass Spectrometry . . . . .	171
4.2.9	Assay for <i>PA2683</i> Activity . . . . .	171
4.2.10	EMSA – Electrophoretic Mobility Shift Assay . . . . .	172
4.2.11	Growth Studies . . . . .	172
4.3	Proteomics . . . . .	173
4.3.1	Analytical Labelling . . . . .	173
4.3.2	Preparative Labelling . . . . .	174
4.4	Targeted Metabolomics Assays . . . . .	179
4.4.1	Substrate Screen for <i>PA2683</i> . . . . .	179
4.4.2	Substrate Screen for <i>PA3659</i> and <i>PA3798</i> . . . . .	179
4.4.3	Inhibition Assay for <i>A0A0H2XII6</i> with Phenelzine . . . . .	179
4.4.4	Inhibition Assay for <i>A0A0H2XHJ5</i> with Phenelzine . . . . .	180
4.4.5	Further Sample Preparation . . . . .	180
4.4.6	MS Measurement and Analysis . . . . .	180
4.5	Compound Screen . . . . .	183
	<b>References</b>	<b>191</b>
	<b>List of Figures</b>	<b>207</b>
	<b>List of Schemes</b>	<b>209</b>
	<b>List of Tables</b>	<b>211</b>
<b>A</b>	<b>Appendix</b>	<b>213</b>
A.1	Supplementary Figures . . . . .	214
A.2	Supplementary Tables . . . . .	221
A.3	NMR-Spectra . . . . .	230
A.4	Licences . . . . .	264
A.5	Curriculum Vitae . . . . .	265

# PREFACE

---

This thesis was submitted to the Faculty of Chemistry, Technical University of Munich to obtain the PhD degree (Dr. rer. nat.). The work presented was carried out in the years 2017-2022 in the laboratory of PROF. STEPHAN A. SIEBER.

The thesis is a direct continuation of my Master's thesis titled "Synthesis of Pyridoxal Derivatives for the Investigation of Pyridoxal Phosphate Dependent Enzymes" from 2017. Some of the results are therefore included, as they are relevant for the further results. Parts of the dissertation are based on publications I and III (see Publications and Conferences).

## THESIS OBJECTIVES

The objectives of this thesis are

- the synthesis of pyridoxal derived probes, which can be used for proteomics
- the profiling of the **PLP**omes in *E. coli*, *S. aureus* **PLP** *de novo* synthesis knockout strains
- the profiling of the *P. aeruginosa* wild type **PLP**ome
- the investigation of unknown or poorly studied putative **PLP**-DEs using a selection of different biochemical methods
- the screening of a library of known *in vitro* **PLP**-DE inhibitors and other potentially inhibitory molecules against different bacterial strains
- the competitive profiling of hit compounds in *S. aureus* and *E. coli* knockout strains
- the validation of hit enzymes obtained from the competitive experiments by inhibition assays
- the synthesis of a novel, pro-tide strategy based pyridoxal phosphoramidate probe, termed **PL3PA**
- the first evaluation of this probe in bacteria and human cells

## TYPESETTING

This thesis was written with L<sup>A</sup>T<sub>E</sub>X. For providing the original header and layout I want to warmly thank JEPPE FOCK ([link](#)) and SØREN PREUS ([link](#)).





# LIST OF ABBREVIATIONS

---

<b>AA</b>	Amino acid
<b>ABMP</b>	Activity-based metabolomic profiling
<b>ABPP</b>	Activity-based protein profiling
<b>ABP</b>	Activity-based probe
<b>AcOH</b>	Acetic acid
<b>ADC</b>	4-Amino-4-deoxychorismate
<b>AdoCbl</b>	Adenosylcobalamin
<b>ADP</b>	Adenosine diphosphate
<b>A<math>\beta</math>BP</b>	Affinity based probe
<b>AGC</b>	Automatic gain control
<b><i>alr</i></b>	Alanine racemase
<b>AMP</b>	Adenosine monophosphate
<b>Asc</b>	Ascorbate
<b>AT</b>	Aminotransferase
<b>aTet</b>	Anhydrotetracycline
<b>ATP</b>	Adenosine triphosphate
<b>AZT</b>	3'-Azidothymidine
<b>B</b>	Broth
<b>BCAT</b>	Branched-chain L-amino acid aminotransferase
<b>Boc</b>	<i>tert</i> -Butyloxycarbonyl
<b>BTAA</b>	2-{4-{ {Bis{[1-( <i>tert</i> -butyl)-1 <i>H</i> -1,2,3-triazol-4-yl]methyl}amino}methyl}-1 <i>H</i> -1,2,3-triazol-1-yl}acetic acid
<b>bp</b>	Base pairs
<b>calcd.</b>	Calculated
<b>CAM</b>	Ceric ammonium molybdate
<b>CBL</b>	Cystathionine $\beta$ -lyase
<b>CBS</b>	Cystathionine $\beta$ -synthase
<b>CDM</b>	Chemically defined medium
<b>CGS</b>	Cystathionine $\gamma$ -synthase
<b>CID</b>	Collision-induced dissociation
<b>CSE</b>	Cystathionine $\gamma$ -lyase
<b>CNS</b>	Central nervous system

<b>CuAAC</b>	Copper catalysed alkyne-azide cycloaddition
<i>cysK</i>	Cysteine synthase
<i>dadX</i>	Alanine racemase
<b>DABCO</b>	1,4-Diazobicyclo[2,2,2]octane
<b>DAT</b>	D-Aminoacid transaminase
<b>DBDMH</b>	1,3-Dibromo-5,5-dimethylhydantoin
<b>DCM</b>	Dichloromethane
<b>DCS</b>	D-Cycloserine
<i>ddl</i>	D-Ala-D-ala-ligase
<b>DHODase</b>	Dihydroorotate dehydrogenase
<b>DIPA</b>	Diisopropylamine
<b>DIPEA</b>	Diisopropylethylamine
<b>DMF</b>	Dimethyl formamide
<b>DMP</b>	<i>N,N'</i> -Dimethylaminopyridine
<b>DMSO</b>	Dimethylsulfoxide
<b>DOPA</b>	Dihydroxyphenylalanine
<b>DTT</b>	Dithiothreitol
<b>DXP</b>	1-Deoxy-D-xylulose 5-phosphate
<b>EDTA</b>	Ethylenediaminetetraacetic acid
e.g.	Exempli gratia
eq	Equivalent
<b>ESI</b>	Electrospray ionization
<b>Et</b>	Ethyl
<i>et al.</i>	Et alii
<b>EtOAc</b>	Ethyl acetate
<b>fwd</b>	Forward
<b>g</b>	Gram
<b>GABA</b>	$\gamma$ -Aminobutyric acid
<b>GABA-AT</b>	$\gamma$ -Aminobutyric acid aminotransferase
<b>h</b>	Hour
<b>HC</b>	Heat control
<b>HCD</b>	Higher-energy C-trap dissociation
<b>HCV</b>	Hepatitis C virus
<b>HEPES</b>	4-(2-Hydroxyethyl)-1-piperazineethanesulfonic acid
<b>HESI</b>	Heated electrospray ionization

---

<b>HILIC</b>	Hydrophilic interaction chromatography
<b>HIV</b>	Human immunodeficiency virus
<b>HPLC</b>	High pressure liquid chromatography
<b>HRMS</b>	High resolution mass spectrometry
<b>HTH</b>	Helix-turn-helix
<b>HTS</b>	High throughput screening
<b>Hz</b>	Hertz
<b>IBCF</b>	<i>iso</i> -Butyl chloroformate
<b>IC<sub>50</sub></b>	Half maximal inhibitory concentrations
<b>IP-MS</b>	Intact protein mass spectrometry
<b>IPTG</b>	<i>iso</i> -Propyl- $\beta$ -D-1-thiogalactopyranoside
<b><i>J</i></b>	Coupling constant
<b>KAT</b>	Kynurenine aminotransferase
<b>L</b>	Liter
<b>LB</b>	Lysogeny broth
<b>LC-MS/MS</b>	Liquid chromatography coupled to tandem mass spectrometry
<b>LDA</b>	Lithium diisopropylamide
<b>LDH</b>	Lactate dehydrogenase
<b>LFQ</b>	Label free quantification
<b>LTQ</b>	Linear trap quadrupole
<b>LysC</b>	Endoproteinase LysC
<b>M</b>	Molar
<b>M</b>	Molecular mass
<b>m</b>	Multiplet
<b>MBP</b>	Maltose binding protein
<b><i>m</i>-CPBA</b>	<i>meta</i> -Chloroperoxybenzoic acid
<b>Me</b>	Methyl
<b>MeCN</b>	Acetonitrile
<b>MeOH</b>	Methanol
<b>min</b>	Minute
<b>MOM</b>	Methoxy methyl
<b>MOPS</b>	3-( <i>N</i> -Morpholino)propanesulfonic acid
<b>MS</b>	Mass spectrometry
<b>Ms</b>	Mesyl
<b>MW</b>	Molecular weight

<b>MWCO</b>	Molecular weight cut-off
<b>NADH</b>	Nicotinamide adenine dinucleotide
<b><i>n</i>-BuLi</b>	<i>n</i> -Butyllithium
<b>NMR</b>	Nuclear magnetic resonance
<b>OAc</b>	Acetate
<b>OAT</b>	Ornithine aminotransferase
<b>ODC</b>	Ornithine decarboxylase
<b>o/n</b>	Overnight
<b>ORF</b>	Open-reading frame
<b>P</b>	Phosphate
<b>PA</b>	Phosphoramidate
<b>PABA</b>	<i>para</i> -Aminobenzoic acid
<b>PAS</b>	<i>para</i> -Aminosalicylic acid
<b>PBS</b>	Phosphate-buffered saline
<b>PCR</b>	Polymerase chain reaction
<b>PEP</b>	Phosphoenolpyruvate
<b>PG</b>	Protective group
<b>Ph</b>	Phenyl
<b>Piv</b>	Pivaloyl
<b>PK</b>	Pyruvate kinase
<b>PL</b>	Pyridoxal
<b>PLK</b>	Pyridoxal kinase
<b>PLP</b>	Pyridoxal-5'-phosphate
<b>PLP-DE</b>	Pyridoxal-5'-phosphate dependent enzyme
<b>PLPHP</b>	Pyridoxal-5'-phosphate homeostasis protein
<b>PM</b>	Pyridoxamine
<b>PMB</b>	<i>para</i> -Methoxy benzyl
<b>PMP</b>	Pyridoxamine-5'-phosphate
<b>PN</b>	Pyridoxine
<b>PNP</b>	Pyridoxine-5'-phosphate
<b>PPADS</b>	Pyridoxal-5'-phosphate-6-phenylazo derivatives
<b>ppm</b>	Parts per million
<b>PR</b>	Promoter region
<b>PRM</b>	Parallel reaction monitoring
<b>R5P</b>	Ribose 5-phosphate

---

<b>rev</b>	Reverse
<b><math>R_f</math></b>	Retention factor
<b>RGS</b>	Regulator G-protein signaling
<b>rpm</b>	Revolutions per minute
<b>r.t.</b>	Room temperature
<b>satd.</b>	Saturated
<b>SDS-PAGE</b>	Sodium dodecyl sulfate polyacrylamide gel electrophoresis
<b>SHMT</b>	Serine hydroxymethyltransferase
<b>SIM</b>	Single ion monitoring
<b>SLIM</b>	Site-directed, ligase-independent mutagenesis
<b>SSM</b>	Secondary structure matching
<b>TAMRA</b>	5-Carboxytetramethylrhodamine
<b>TBAF</b>	Tetrabutylammonium fluoride
<b>TBDMS, TBS</b>	<i>tert</i> -Butyldimethylsilyl
<b>TEAB</b>	Triethylammonium bicarbonat
<b>TEV</b>	Tobacco etch virus
<b>TFA</b>	Trifluoro acetic acid
<b>TFAA</b>	Trifluoro acetic acid anhydride
<b>THF</b>	Tetrahydrofuran
<b>THPG</b>	Tetrahydropteroylglutamate
<b>TLC</b>	Thin layer chromatography
<b>TMS</b>	Trimethylsilyl
<b>Tn</b>	Transposon
<b>TR</b>	Transcriptional regulator
<b>TRIS</b>	Tris(hydroxymethyl)aminomethane
<b><math>t_R</math></b>	Retention time
<b>UV</b>	Ultraviolet
<b>Vis</b>	Visible
<b>wt</b>	Wild type



# 1

## BACKGROUND AND MOTIVATION

---

*The first chapter introduces pyridoxal phosphate, the importance of pyridoxal phosphate dependent enzymes and a chemical proteomic strategy to unravel novel protein functions and possible antibiotic target enzymes.*

### Contents

---

<b>1.1</b>	<b>Cofactors . . . . .</b>	<b>2</b>
<b>1.2</b>	<b>Vitamin B6 . . . . .</b>	<b>3</b>
<b>1.3</b>	<b>PLP-Dependent Enzymes . . . . .</b>	<b>7</b>
<b>1.4</b>	<b>Inhibition of PLP-Dependent Enzymes . . . . .</b>	<b>10</b>
<b>1.5</b>	<b>A Chemical Proteomic Tool . . . . .</b>	<b>16</b>
<b>1.6</b>	<b>Objectives . . . . .</b>	<b>21</b>

---

## 1.1 Cofactors

Cofactors (lat.: co-: together, with; lat.: factor: maker)<sup>[1]</sup> are essential for cellular function in all living organisms. A further distinction is made here between coenzymes, which are only bound to the enzyme during catalysis, and prosthetic groups, which are constantly bound to their enzymes.<sup>[2]</sup>

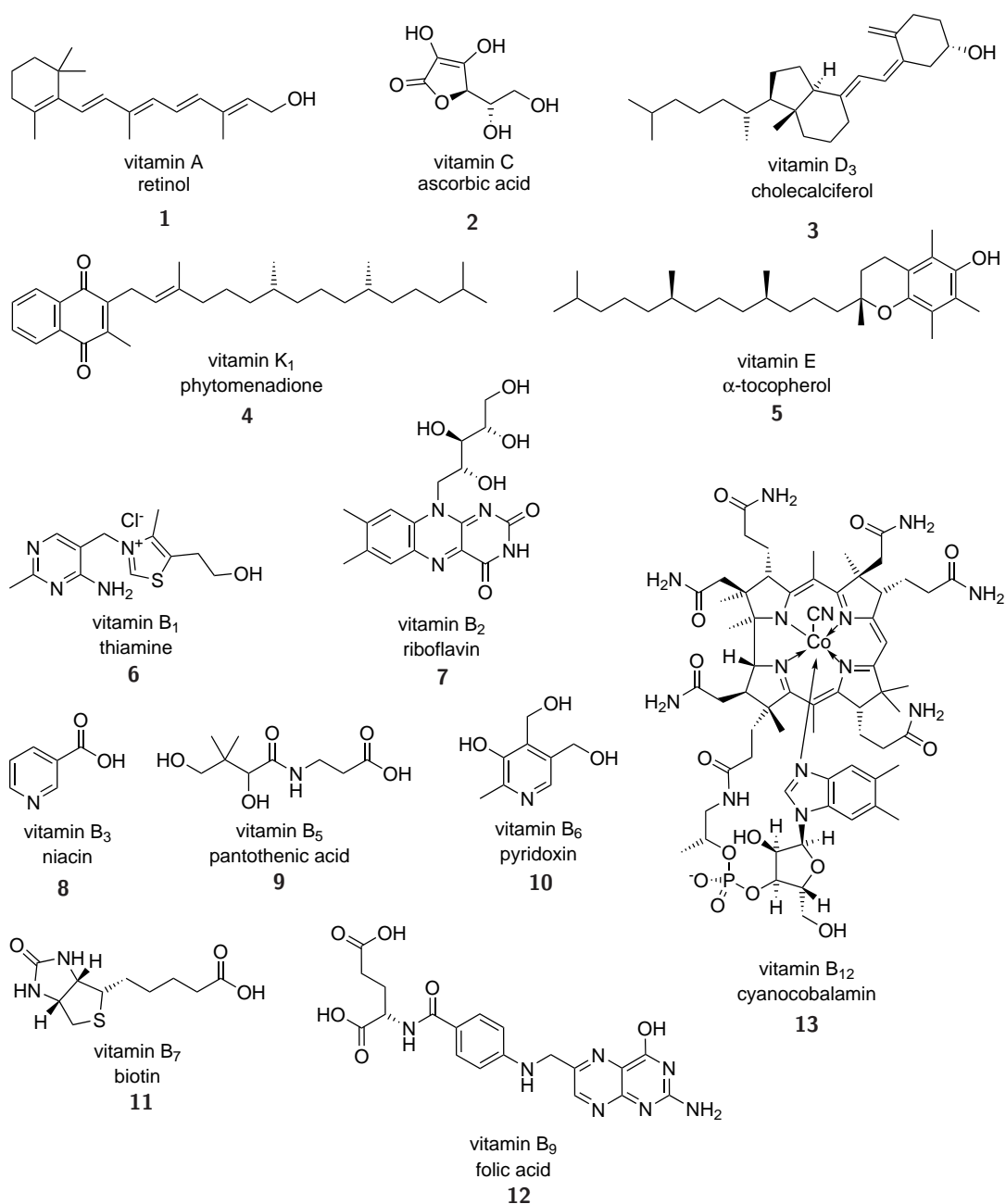


**Figure 1.1:** Structures of the 13 vitamins A (1), B<sub>1</sub> (6), B<sub>2</sub> (7), B<sub>3</sub> (8), B<sub>5</sub> (9), B<sub>6</sub> (10), B<sub>7</sub> (11), B<sub>9</sub> (12), B<sub>12</sub> (13) C (2), D<sub>3</sub> (3), E (5) and K<sub>1</sub> (4)



Cofactors can be organic compounds (e.g. vitamins), metal ions, metal-complexes (e.g. iron-sulfur complexes) or organometallic complexes (e.g. heme).<sup>[1]</sup> They all specifically bind to their corresponding apoenzymes and actively take part in catalysis.<sup>[1,2]</sup> In most cases, apoenzymes are inactive without their cofactor, highlighting their relevance in a biological context.<sup>[3]</sup> In fact, nearly half of all enzymatic reactions are dependent on a specific cofactor, underlining their importance in all forms of life.<sup>[2]</sup>

Vitamins (from vital amine, coined by CASIMIR FUNK<sup>[4]</sup>), 13 in total, are organic cofactors needed for normal physiological function (figure 1.1).<sup>[5,6]</sup> Usually, they can not be synthesized by humans in sufficient amounts which is why they need to be taken up by nutrition.<sup>[7,8]</sup> However, plants, fungi and bacteria can synthesize those compounds themselves.<sup>[5]</sup> Recently, attention on vitamin metabolic pathways greatly increased due to the vital importance of vitamins and their involvement in the development of certain human diseases.<sup>[6]</sup> Due to the involvement of vitamin dependent enzymes in crucial metabolic pathways, many of them are already recognized as drug targets.<sup>[9]</sup>

## 1.2 Vitamin B<sub>6</sub>

Vitamin B<sub>6</sub> is a collective term for the interconvertible pyridine compounds pyridoxine (**10**), pyridoxamine (**14**), pyridoxal (**15**) and their 5'-phosphates pyridoxine phosphate (**16**), pyridoxamine phosphate (**17**) and pyridoxal phosphate (**18**) (figure 1.2).

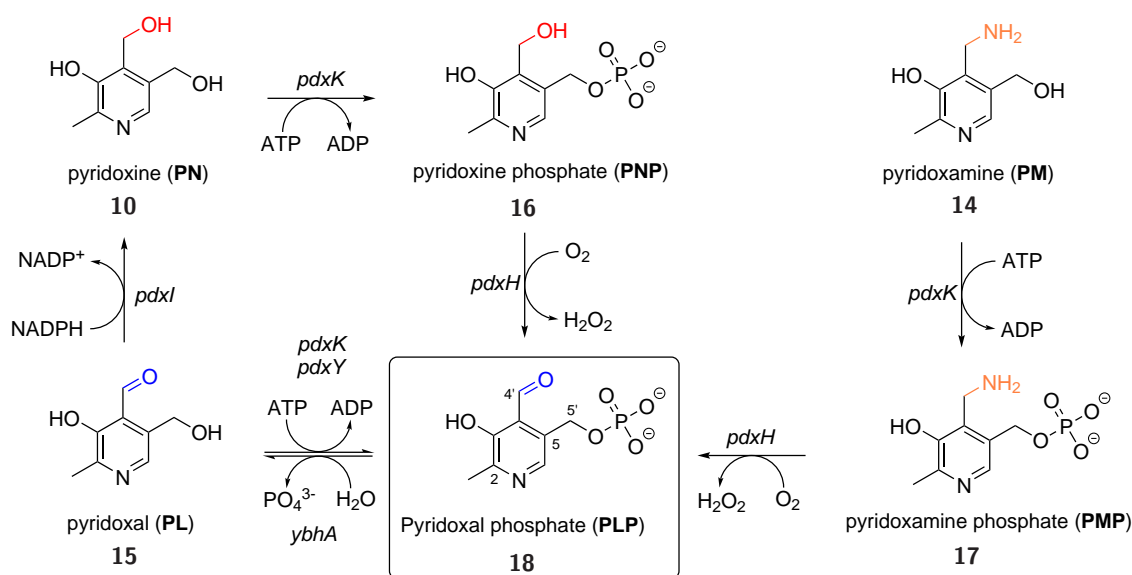


**Figure 1.2:** Structures and salvage pathways of the vitamin B<sub>6</sub> ensemble in *E. coli* consisting of pyridoxine (**10**), pyridoxamine (**14**), pyridoxal (**15**) and their 5'-phosphates pyridoxine phosphate (**16**), pyridoxamine phosphate (**17**) and pyridoxal phosphate (**18**).<sup>[10,11]</sup>

In general, two enzymes encoded by the genes *pdxK* and *pdxH*, are responsible for **PLP**-salvage in *E. coli*.<sup>[10]</sup> Pyridoxal kinase (PLK, *pdxK*) phosphorylates the C5'-alcohol of **PN**, **PM** and **PL**. Further, **PNP** and **PMP** can be oxidized to **PLP** by pyridoxine/pyridoxamine 5'-phosphate oxidase (PNPOx, *pdxH*).<sup>[12,13]</sup> Moreover, **PLP** can be dephosphorylated by a phosphatase (*ybhA*) and a recently identified pyridoxal reductase (*pdxI*) is able to reduce **PL** to **PN**, which complements the important **PL** salvage enzymes in *E. coli*.<sup>[14]</sup>

**PLP** is the bioactive compound of vitamin B<sub>6</sub>, a ubiquitous, versatile cofactor of pyridoxal phosphate-dependent enzymes (**PLP**-DEs). Plants and microorganisms are able to synthesize **PLP** *de novo* either through the deoxyxylulose 5-phosphate (DXP) dependent pathway, found in *E. coli* and other  $\gamma$ -proteobacteria<sup>[15]</sup>, or through the D-ribose 5-phosphate (R5P) dependent pathway, which appears in all kingdoms of life (i.a. fungi, plants, bacteria, animals).<sup>[10,12]</sup> Humans and other mammals rely on vitamin B<sub>6</sub> uptake from diet. However, a similar salvage mechanism can also be found there.<sup>[10,16]</sup>

In order to gain an understanding of **PLP** and its biological function, one has to take a closer look at its reactivities. First, **PLP** is able to react with amines to imines at its aldehyde. Second, it stabilizes carbanionic intermediates due to its pyridine nitrogen atom and hydroxyl group.<sup>[17,18]</sup> In a biological environment, **PLP** binds to the active lysine residue of **PLP**-DEs *via* a reversible imine bond ("Schiff-base"), known as the *internal aldimine*. The active enzyme-cofactor complex can now react with incoming substrate amines, such as amino acids, in a transamination reaction. Here, the bond with the active lysine is broken and a new Schiff-base is formed between the substrate and **PLP**, called the *external aldimine*, within the enzymes active pocket (figure 1.3).<sup>[19,20]</sup>

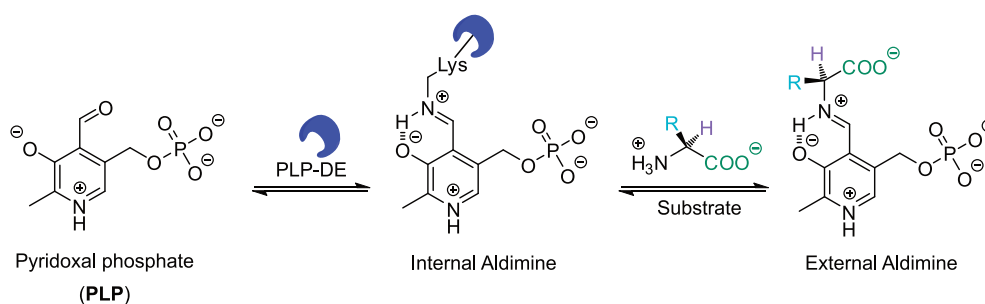


**Figure 1.3:** **PLP** forms an internal aldimine with the active lysine of a **PLP**-DE. Transamination with substrate amines such as amino acids leads to the formation of an external aldimine.

Due to the pyridine nitrogen atom of **PLP**, which is often protonated during catalysis, polarisation of the aldimine complex occurs leading to an enhancement of electrophilicity at the C4' position. Furthermore, aldimines are stabilised by the C3 phenoxide *via* hydrogen bonding and resonance stabilisation.<sup>[18]</sup> All these effects lead to an electronic sink, meaning that the nitrogen atom withdraws electrons from the substrates C<sub>α</sub> (fig-

ure 1.4 A). This effect results in a weakening of the adjacent  $\sigma$ -bonds of the substrates and a stabilisation of resulting carbanions by the extended  $\pi$ -conjugation.<sup>[21]</sup> The external aldimine can undergo a series of reactions, depending on the enzyme and the character of its catalytic pocket.<sup>[21,22]</sup> No matter which of the three  $C_{\alpha}$ -groups is removed, it leads to the formation of a quinonoid structure, which is able to react further. If the proton is removed first, further transaminations, racemizations or eliminations can occur. In addition, decarboxylations and side-chain cleavages of aldimines are typical chemical transformations in **PLP-DEs** (figure 1.4 B).<sup>[21,22]</sup>

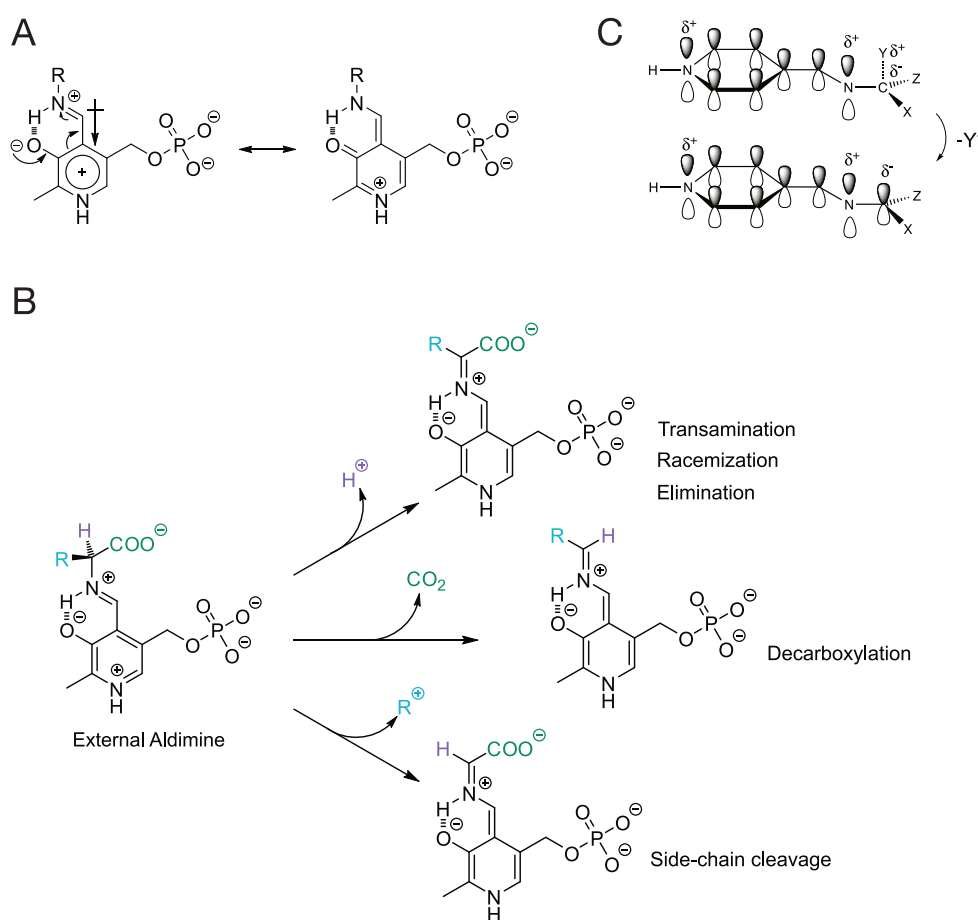


**Figure 1.4:** Reactions catalysed by **PLP-DEs**. **(A)** Dipole moment of aldimines illustrating the electronic sink properties. **(B)** External aldimines can undergo a series of reactions, depending on which group of the  $C_{\alpha}$  is cleaved.<sup>[21,22]</sup> **(C)** Reaction specificity through stereoelectronic effects (DUNATHAN'S hypothesis).<sup>[18,21,23]</sup>

Reaction specificity of **PLP-DEs** is kinetically controlled by their catalytic site environment and the resulting stereochemical arrangement of the  $C_{\alpha}$ -groups.<sup>[18]</sup> According to DUNATHAN'S hypothesis, the bond, which is preferably cleaved, has to be in a plane that is perpendicular to that of the delocalised  $\pi$ -system (figure 1.4 C).<sup>[18,20,21,23]</sup> The schematic illustration of the aldimine orbitals shows, that the bond being broken ( $C-Y$ ) leads to an extended  $\pi$ -system. Evolution of distinct active pockets in **PLP-DEs** has

led to specific enzymes catalysing certain reaction types. Therefore it is not surprising that mutations in the active pockets of certain **PLP**-dependent enzyme classes resulted in different reaction types and rates.<sup>[24,25]</sup>

**PLP** alone is able to catalyse reactions, too. These include elimination, transamination and racemisation reactions, some of which can be accelerated with  $\text{Al}^{3+}$  and  $\text{Cu}^{3+}$ .<sup>[17,18,26,27]</sup> Additionally, its role as antioxidant, modifier of expression, immune function regulator and antiepileptic agent must not be underestimated.<sup>[28-32]</sup>

Another important aspect of **PLP** is its 5'-phosphate group, which functions as a firm anchor that can be bound by **PLP**-DEs in their so-called "phosphate-binding cup".<sup>[18,33]</sup> *Denesyuk et al.* could show that **PLP**-DEs from all five fold types share common recognition patterns for the phosphate group of their **PLP**-cofactors.<sup>[33]</sup> A less important group for catalysis is the 2'-methyl substituent. It does not seem to have any function and is according to *Hill et al.* only a relic from its biosynthesis.<sup>[34]</sup> This property is going to be important for the whole study of **PLP**-DEs, as most probes will be derivatised at this position.

Due to the high reactivity of **PLP** towards nucleophilic amines and thiols, its concentration needs to be well regulated and be held at a low level.<sup>[35]</sup> **PLP** can be involved in aldehyde stress reactions, e.g. altering of protein structures, inhibition of enzyme activities and damage of DNA leading to mutagenesis.<sup>[35-38]</sup> In eukaryotic cells, **PLP**-levels are therefore maintained at around  $1 \mu\text{M}$  to avoid toxic effects.<sup>[10,35]</sup> Homeostasis of **PLP** is mainly regulated by pyridoxal phosphatase, pyridoxine/pyridoxamine 5'-phosphate oxidase and pyridoxal kinases.<sup>[10]</sup> The latter two enzymes are inhibited by **PLP** and can serve as transport enzymes, because they can bind to other **PLP**-DEs at high **PLP** concentrations leading to the transfer of **PLP** to apo-enzymes.<sup>[39-41]</sup> Generally, it is believed that not only free **PLP**, which is kept at low concentrations, serves as cofactor source for apo-enzymes but also **PLP**-amino acid adducts and **PLP**-binding proteins like the **PLP**-homeostasis protein (PLPHP), which is widely distributed in eukaryotes and bacteria.<sup>[10,11,42]</sup>

In humans, **PLP**-deficiency is linked to several disorders of neurological and non-neurological nature. Often, malfunction of PLK or PNPOx due to mutations or drug/natural products induced inhibition are responsible for this effect. The consequences are often severe and partly responsible for diseases like Parkinson's-disease, diabetes, cancer, Alzheimers-disease, schizophrenia, autism, epilepsy and others.<sup>[10,13,43-50]</sup> Those tremendous implications on organisms shows that a well regulated **PLP**-homeostasis is essential for its health.

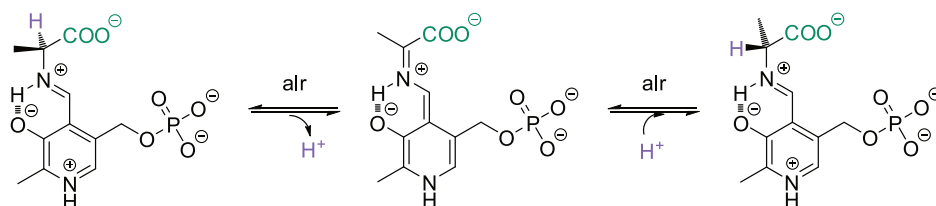
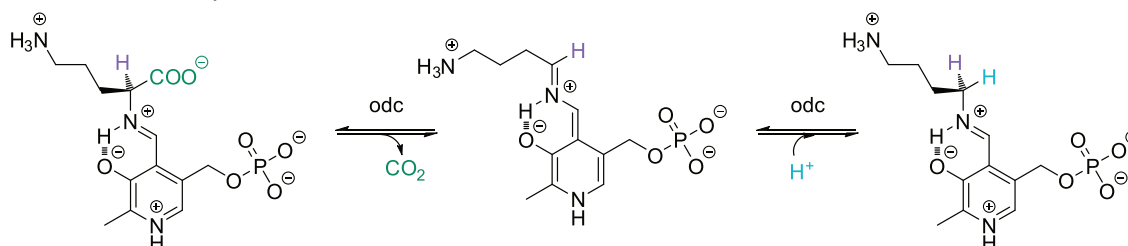
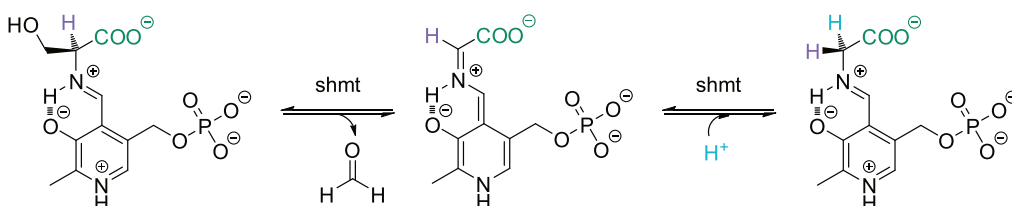
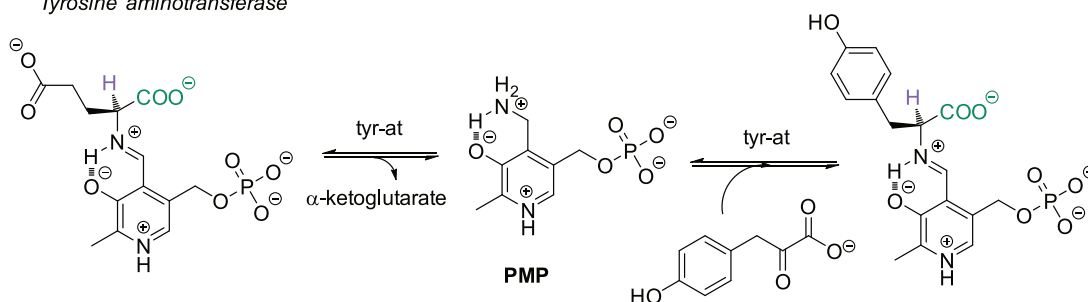
## 1.3 PLP-Dependent Enzymes

**PLP**-DEs already came into existence 1500 to 1000 million years ago, before the biological kingdoms of life diverged.<sup>[51]</sup> In total, **PLP**-DEs were split into seven enzyme clusters (fold types), five were suggested by *Grishin et al.*<sup>[52]</sup> and later two more by *Percudani and Peracchi*<sup>[22]</sup>. Fold type I, termed aspartate aminotransferase family, is the most diverse family of **PLP**-DEs including five of the six enzyme classes defined by the international union of biochemistry and molecular biology.<sup>[53,54]</sup> The tryptophan synthase family (fold type II) is similar to fold type I but fold type II enzymes are evolutionary divers.<sup>[54,55]</sup> Fold type III (alanine racemase family) enzymes catalyse amino acid racemisations and decarboxylations.<sup>[56,57]</sup> The second aminotransferase class is summarized in fold type IV (D-amino acid aminotransferase family) **PLP**-DEs, which transform strictly either (*S*)- or (*R*)-substrates.<sup>[58]</sup> Fold type V (glycogen phosphorylase family) enzymes use **PLP** in a different way compared to all other fold types. They do not use it as an electrophilic catalyst but involve the 5'-phosphate group in an acid-base catalytic mechanism.<sup>[18,59]</sup> Adenosylcobalamin (AdoCbl) dependent fold type VI (lysine 5,6-aminomutase family) and *S*-adenosyl methionin (SAM) dependent fold type VII (lysine 2,3-aminomutase family) differ from other **PLP**-DEs in their structure and were therefore independently categorized.<sup>[22,60,61]</sup>

All seven fold types are responsible for 348 distinct activities, which are listed in the B6-DataBase (link).<sup>i</sup> These include reactions at the substrates C<sub>α</sub>, like racemisation, decarboxylations, eliminations, transaminations and replacements (figure 1.5). Replacements and eliminations also apply to both the β- and γ-positions of substrates. Fold type VI and VII act through a radical mechanism utilizing AdoCbl or SAM as radical source.<sup>[20]</sup> The number of **PLP**-DEs varies widely among organisms. In general, procaryotic genomes encode a larger proportion (≈1.5%) for **PLP**-DEs than most eucaryotes, although the total number of **PLP**-DEs in eucaryotes is higher.<sup>[62]</sup> In bacteria, the number of **PLP**-DEs correlates with their genome size. Based on recent literature searches (*UniRule*<sup>[63]</sup>, *UniProt*<sup>[64]</sup>, *InterPro*<sup>[65]</sup> and *GO*<sup>[66]</sup>), *S. aureus* USA300 encodes 48 known and predicted **PLP**-DEs at a genome size of around 2.87 Mbp<sup>[67]</sup>, while *E. coli* K12 encodes 63 known and predicted **PLP**-DEs at a genome size of around 4.64 Mbp<sup>[68]</sup>. Even more known and predicted **PLP**-DEs are encoded by *P. aeruginosa* PAO1 with a genome size of 6.26 Mbp<sup>[69]</sup>. Here, 83 proteins were found to be at least putative **PLP**-dependent. These numbers were already predicted by *Percudani and Peracchi* in 2003.<sup>[62]</sup>

---

<sup>i</sup>23.02.2022

Reactions on the substrates  $\alpha$ -Positiona Racemisation  
*Alanine racemase*b Decarboxylation  
*Ornithine decarboxylase*c  $\alpha$ -Elimination and Replacement  
*Serine hydroxymethyltransferase*d Transamination  
*Tyrosine aminotransferase*

**Figure 1.5:** Simplified examples of **PLP-DEs** catalysing reactions at the substrates  $C_{\alpha}$  position.<sup>[54]</sup> All reactions start at the external aldimine stage followed by the loss of one of the groups at  $C_{\alpha}$ . Re-protonation or transamination leads to the formation of the product aldimines. Alanine racemase (*alr*) catalyses the conversion of L- to D-alanine. Ornithine decarboxylase (ODC) produces putrescine after hydrolysis of the product aldimine. After formaldehyde has been cleaved from serine, serin hydroxymethyltransferase (SHMT) is able to form glycine in the end. Tyrosine aminotransferase (*tyr-AT*) was chosen as an example of a transamination reaction, starting from glutamate aldimine. After amine transfer to **PLP**, which is called the first half reaction of an aminotransferase, hydroxyphenylpyruvate forms the product aldimine, which can then be released to form L-tyrosine.

Recently, an indolmycin biosynthesis protein from *Streptomyces griseus* was shown to be an unprecedented **PLP**-DE utilizing molecular oxygen for the oxidation of L-arginine.<sup>[70,71]</sup> Moreover, **PLP**-dependent *MocR*-like transcriptional regulators (TRs) from the *GntR*-TR family are widespread among eubacteria.<sup>[72]</sup> A well-studied example for this is *GabR* from *Bacillus subtilis*, which gets activated by the small neurotransmitter  $\gamma$ -aminobutyric acid (GABA) and **PLP**, causing a conformational rearrangement with enhanced DNA-binding capability.<sup>[73–75]</sup> Lastly, **PLP** was described to have an additional role in protein folding, because some **PLP**-DEs need their cofactor to be refolded *in vivo*.<sup>[76]</sup> As a paradigm of the versatility of **PLP**-dependent reactions, one only has to take a closer look at its role in the synthesis of natural products, which is always a fruitful source for novel bioactive compounds.<sup>[71]</sup>

However, reactions catalysed by **PLP**-DEs can not be predicted by their fold type or structure. In fact, many **PLP**-DEs are able to catalyse several different reactions.<sup>[77]</sup> The three aspects of reactions specificity are: stereochemical effects, protonation state of the external aldimine and the interaction of the substrate with the enzymes side chains in its active pocket.<sup>[21]</sup> For example, SHMT, a fold type I **PLP**-DE, shows a broad range of reaction specificity in the absence of its actual substrate, tetrahydropteroylglutamate (THPG). Beside the transfer of C $_{\beta}$  of serine to THPG it can then also catalyse retroaldol cleavage, racemisation, transamination and decarboxylation.<sup>[78]</sup> Enzymes offering a broad range of catalysed reactions must have recognition patterns for several substrate within their active site in order to distinguish from non-substrates. In fact, for aspartate aminotransferase it was shown that a single substitution of an active site residue increased its activity towards dicarboxylic and aromatic substrates. It even resulted in  $\beta$ -decarboxylation of L-aspartate.<sup>[79]</sup> This versatility of **PLP**-DEs drives research in the field of protein engineering towards novel or unprecedented reactions, including biocatalytic reactions<sup>[80–83]</sup> used for pharmaceutical compound synthesis or biotechnological tools for the synthesis of unnatural amino acids.<sup>[18,84]</sup>

**PLP**-DEs do not only play a role in the synthesis, interconversion or degradation of amino acids, but are also involved in the modulation of steroids, the metabolism of neurotransmitters (e.g. GABA, dopamine), immune regulation and many other important metabolic pathways.<sup>[13]</sup> Due to the involvement of **PLP**-DEs in these processes, some play a role in the development of diseases and are already recognized as drug targets.<sup>[9]</sup>

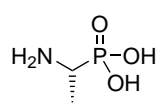
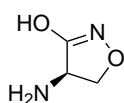
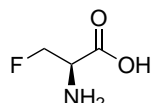
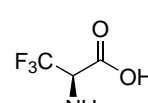
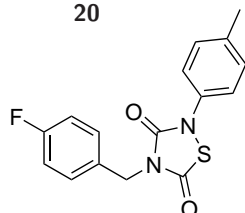
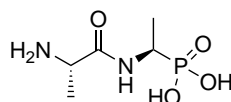
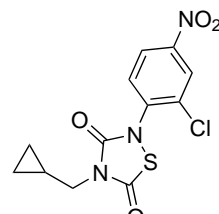
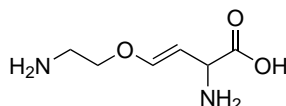
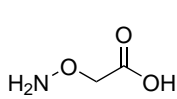
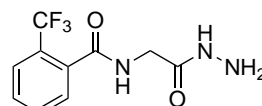
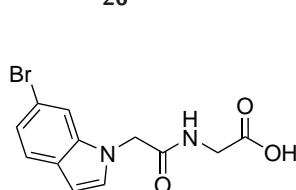
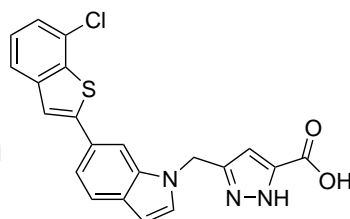
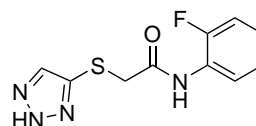
## 1.4 Inhibition of PLP-Dependent Enzymes

Taking into account that bacteria share only a third of their **PLP**ome with humans, **PLP**-DEs represent valuable antibacterial targets.<sup>[62]</sup> However, since **PLP**-DEs share high structural similarity even at low sequence similarity, selectivity of inhibitors, often derived from amino acids, tends to be a big problem.<sup>[54]</sup> This is especially true for alanine racemase (*alr*) inhibitors, like D-cycloserine (DCS, **19**), a clinical second line antibiotic against tuberculosis, which is known to exhibit severe side effects such as central nervous system (CNS) toxicity.<sup>[85–88]</sup> DCS is a natural product produced by *Streptomyces garyphalus* and *Streptomyces lavendulae* and known to inhibit alanine racemases *via* a mechanism based route, meaning that DCS binds as enzyme substrate, which forms an irreversible complex with the target enzyme after it is transformed into a reactive species by *alr*.<sup>[89]</sup> Additionally to inhibiting *alr*, DCS inhibits D-ala-D-ala-ligase (*ddl*)<sup>[90,91]</sup> and D-aminoacid transaminase (DAT)<sup>[92]</sup>, both enzymes involved in bacterial peptidoglycan synthesis. Alanine racemase is universal to bacteria and mycobacteria, since they need D-alanine for their cell wall biosynthesis, but absent in most eukaryotes, including humans.<sup>[9,93–95]</sup> *Milligan et al.* was able to show that *Mycobacterium smegmatis alr* deletion mutants were unable to grow on media lacking D-alanine.<sup>[96]</sup> These circumstances make *alr* an attractive clinically druggable antibiotic target.<sup>[9]</sup>

Of note, several bacteria (e.g. *E. coli*, *P. aeruginosa*, *S. aureus*, *A. baumannii*) have two alanine racemases: *alr*, which is the main source for D-alanine and constantly expressed at low levels and *dadX*, which is induced by L-alanine and thus is most active when L-alanine is used as a carbon source instead of glucose.<sup>[97–100]</sup> Hence, bacteria with two genes encoding for alanine racemase make it difficult to target both enzymes at once.<sup>[101]</sup>

Owed to the introduced facts about *alr*, many different inhibitors were investigated, partly through high-throughput screening (HTS). Among these are aminoethyl phosphonic acid (**20**)<sup>[9,93,101]</sup>,  $\beta$ -fluoro alanine (**21**)<sup>[9,93,101]</sup>, trifluoro alanine (**22**)<sup>[101]</sup> and alafosfalin (**23**)<sup>[101,102]</sup>, which are structurally related to alanine, but also non-substrate like thiadiazolidinone inhibitors CCG-50014 (**24**) and 401-7 (**25**)<sup>[103,104]</sup> (figure 1.6).



**A Alanine racemase inhibitors**aminoethyl  
phosphonic acid  
**20**D-cycloserine  
**19** $\beta$ -fluoro alanine  
**21**trifluoro alanine  
**22**CCG-50014  
**24**alafosfalin  
**23**401-7  
**25****B Sulfur metabolism inhibitors**L-aminoethoxy-  
vinyl glycine  
**26**aminoxyacetic acid  
**27***N*-Hydrazinocarbonylmethyl-  
2-trifluoromethylbenzamide  
**28**NL1  
**29**NL3  
**30**TAT1  
**31**

**Figure 1.6:** (A) The alanine racemase inhibitors aminoethyl phosphonic acid (**20**), DCS (**19**),  $\beta$ -fluoro alanine (**21**), trifluoro alanine (**22**), CCG-50014 (**24**), alafosfalin (**23**) and 401-7 (**25**). (B) Inhibitors against sulfur metabolism enzymes L-aminoethoxyvinyl glycine (**26**), aminoxyacetic acid (**27**), *N*-hydrazinocarbonylmethyl-2-trifluoromethyl benzamide (**28**), NL1 (**29**), NL3 (**30**) and TAT1 (**31**).

Another druggable bacterial enzyme class is represented by **PLP-DEs** involved in trans-sulfur metabolism.<sup>[105]</sup> Especially cystathionine  $\beta$ -lyase (CBL) and cystathionine  $\gamma$ -synthase (CGS) are of interest due to their absence in mammals.<sup>[9]</sup> Recently, it was shown in some bacteria, that also human orthologs of cystathionine  $\gamma$ -lyase (CSE) and cystathionine  $\beta$ -synthase (CBS) are encoded in the bacterial genome, which suggested an important function.<sup>[106]</sup> Nevertheless, due to a similar mechanism of the  $\beta$ - and  $\gamma$ -enzymes of bacteria and humans, specific inhibition of bacterial enzymes only is difficult.<sup>[9]</sup> While L-aminoethoxyvinyl glycine (**26**) and aminoxyacetic acid (**27**)<sup>[9,107,108]</sup> do not exhibit high selectivity for one of the transsulfuration enzymes,

*N*-hydrazinocarbonylmethyl-2-trifluoromethyl benzamide (**28**)<sup>[105]</sup> was found by HTS and showed specific inhibition of bacterial CBL as well as antimicrobial activity against *E. coli*.

A remarkable discovery was recently made about several inhibitors of the bacterial enzyme CSE including NL1 (**29**) and NL3 (**30**).<sup>[109]</sup> These inhibitors affect the H<sub>2</sub>S-mediated defense system, which protects bacteria against oxidative stress, rendering pathogenic bacteria highly sensitive to a range of different antibiotics.<sup>[106,110]</sup> *Shatalin et al.* showed that those inhibitors potentiate fluoroquinolones,  $\beta$ -lactams, and aminoglycosides in *S. aureus* and *P. aeruginosa*.<sup>[109]</sup> Moreover, biofilm formation and the number of persister cells could be reduced. This novel finding is a precious contribution towards fighting the antibiotic crisis, because combinational antibiotic treatments with those inhibitors could reduce emergence or spreading of antibiotic resistance.<sup>[109]</sup>

Another inhibitor class manipulating sulfur metabolism, cysteine metabolism more precisely, are *N*-(phenyl)thioacetamide-linked 1,2,3-triazoles, discovered by *Wallace et al.* in 2019.<sup>[111]</sup> The authors showed that TAT1 (**31**) was able to disrupt cysteine metabolism in *E. coli* by inhibiting cellular cysteine synthase A (*cysK*). Moreover, *cysK* is absent in humans and is important in essential bacterial metabolic pathways. The mode of action is most likely caused by a false product formation leading to growth inhibition.<sup>[111]</sup>

GABA aminotransferase (GABA-AT) is an ubiquitous enzyme catalysing the reversible conversion of GABA to succinic semialdehyde.<sup>[112]</sup> After conversion into succinate by succinic acid semialdehyde dehydrogenase, it enters the citric acid cycle. GABA fulfills certain physiological functions in plants<sup>[113]</sup>, mammals<sup>[114]</sup> and bacteria<sup>[115]</sup>. In bacteria, GABA is involved in carbon and nitrogen metabolism. In vertebrates, GABA is the major inhibitory neurotransmitter in the CNS, where it binds to chloride-selective ion channel receptors (GABA<sub>A</sub>, GABA<sub>C</sub>) and G-protein coupled receptors (GABA<sub>B</sub>), controlling neuronal activity *via* hyperpolarisation of the postsynaptic membrane.<sup>[116–119]</sup> Low GABA levels can lead to severe diseases, among them epilepsy<sup>[120]</sup>, Huntington's chorea<sup>[121]</sup>, Parkinson's disease<sup>[122]</sup>, Alzheimer's disease<sup>[123]</sup> and tardive dyskinesia<sup>[124]</sup>. The need for drugs targeting those diseases is therefore of great interest.<sup>[125]</sup> Of note, GABA concentration can not be increased by administration of GABA itself, as it can not cross the blood-brain barrier. Thus, the use of specific, brain-accessible GABA-AT inhibitors offers a possibility to increase GABA levels.<sup>[9]</sup>

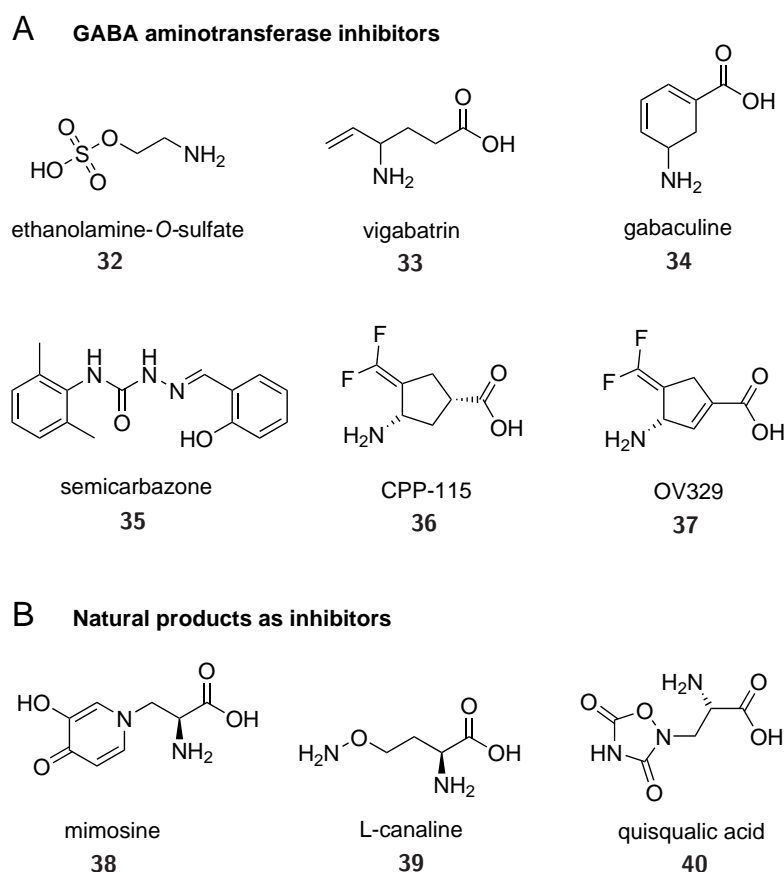
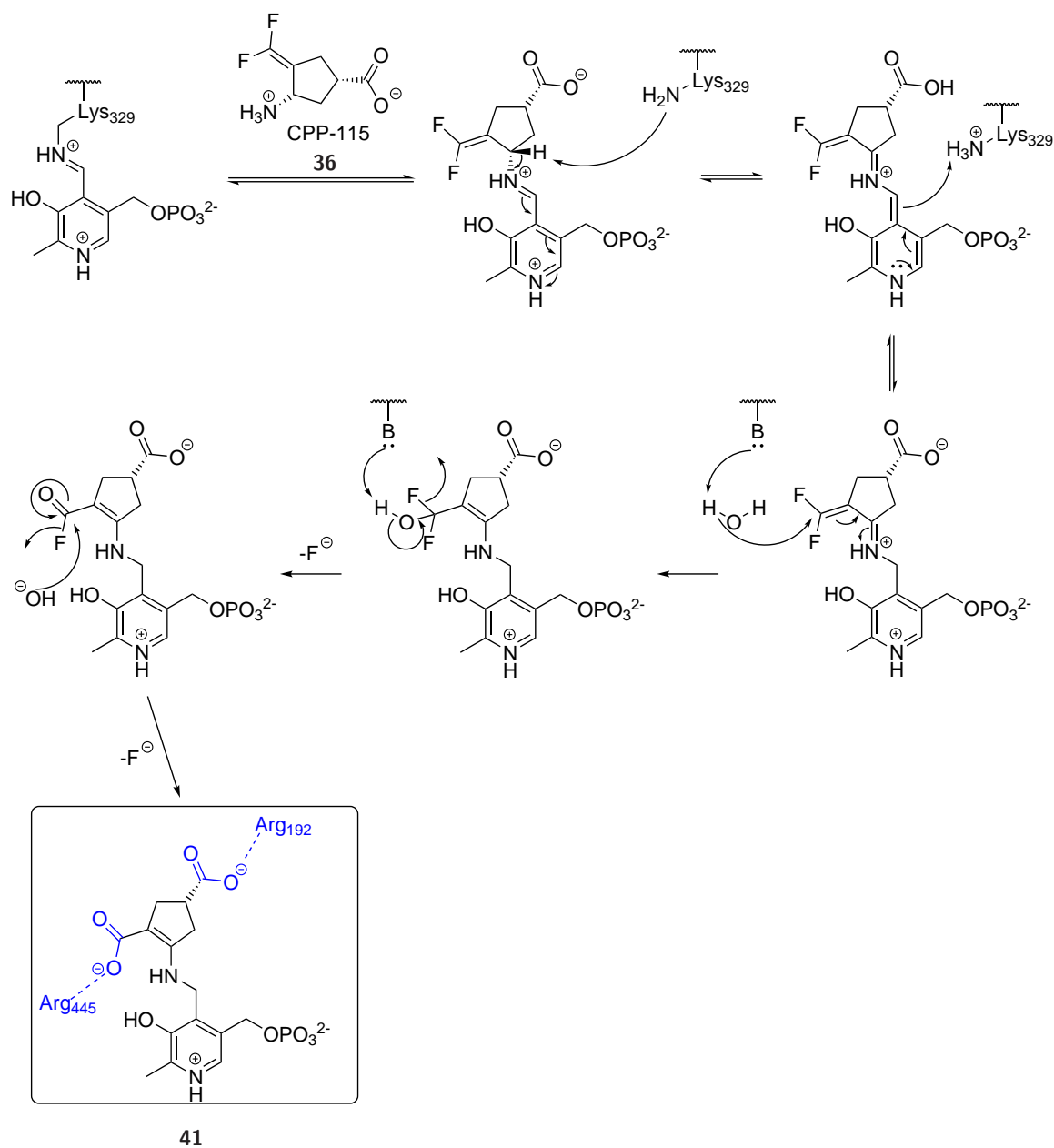


**Figure 1.7:** (A)  $\gamma$ -Aminobutyric acid aminotransferase inhibitors ethanolamine-*O*-sulfate (**32**), vigabatrin (**33**), gabaculine (**34**), the semicarbazone **35**, CPP-115 (**36**) and OV329 (**37**). (B) Structures of natural compounds inhibiting **PLP**-DEs: mimosine (**38**), L-canaline (**39**) and quisqualic acid (**40**).

Ethanolamine-*O*-sulfate (**32**) was the first GABA-AT inhibitor reported in literature.<sup>[126]</sup> In contrast to this compound, a GABA analogue named vigabatrin (**33**) became the only clinically used mechanism based inhibitor of GABA-AT, which is used for the treatment of convulsion in patients being resistant to other drugs.<sup>[127–129]</sup> As is the case for most **PLP**-DE inhibitors, vigabatrin causes several severe side-effects. The worst is probably the irreversible loss of peripheral vision, which happens in 30-40% of patients.<sup>[130,131]</sup> Another compound developed in the 1970's is gabaculine (**34**), which could not be used in patients because of its toxicity and poor ability to cross the blood-brain barrier.<sup>[9,132]</sup>

Aryl semicarbazones, such as semicarbazone **35** were able to increase GABA concentrations in rats without showing neurotoxicity.<sup>[133]</sup> Recently, novel fluorinated cyclic aminoacid compounds were developed: CPP-115 (**36**)<sup>[134]</sup> and OV329 (**37**)<sup>[116]</sup>, which is a refined, mechanism-based GABA-AT inhibitor and synthesised from CPP-115. CPP-115 itself, completed clinical phase I by now<sup>[135]</sup>, is 186 times more potent than vigabatrin and the newer compound OV329 is 10 times more potent than CPP-115. Furthermore, OV329 has low off-target activities and good pharmacokinetic prop-

erties.<sup>[116]</sup> The inhibition mechanism of CPP-115 is well studied and depicted in scheme 1.1.<sup>[116,134]</sup>



**Scheme 1.1:** Mechanism based inhibition of human GABA-AT by CPP-115 (**36**). After Schiff-base formation, tautomerisation and subsequent hydrolysis of the difluoromethylenyl group, adduct **41** is formed, which binds to Arg<sub>192</sub> and Arg<sub>445</sub> via electrostatic interactions leading to an inhibition of the enzyme.<sup>[116]</sup>

Schiff-base formation of CPP-115 with **PLP** and tautomerization of the external aldimine leads to an enhanced electrophilicity at the CF<sub>2</sub> carbon (MICHAEL-acceptor). Subsequent hydrolysis of the difluoromethylenyl group results in formation of dicarboxylate **41**. This complex causes a conformational change of the enzyme, enhancing

electrostatic binding to Arg<sub>192</sub> and Arg<sub>445</sub>.<sup>[116]</sup> Such inhibitors, which form strong non-covalent interactions with amino acid residues of the active site and lead to a loss of activity of the enzyme, are called transition-state mimics.<sup>[136]</sup> These must be distinguished from suicide inhibitors, which bind irreversibly to the enzyme *via* a reactive intermediate.<sup>[137]</sup>

Natural products often represent a fruitful source for bioactive compounds, since some of these secondary metabolites exhibit antibacterial or antifungal properties, making producers more resistant to pathogenic organisms.<sup>[138]</sup> Serin hydroxymethyltransferase (SHMT) is linked to cancer since growth and proliferation of cancer cells are supported by different metabolic changes, among them the folate-dependent one-carbon metabolism.<sup>[139]</sup> This enzyme therefore has high potential as an anticancer target.<sup>[140]</sup> A natural product produced by *Mimosa* plants, mimosine (**38**), was shown to be an active anti-neoplastic drug through inactivation of SHMT.<sup>[141]</sup> A more recent study claims, that mimosine acts **PLP** independently with respect to SHMT inhibition.<sup>[142]</sup>

L-Canaline (**39**) and its precursor L-canavanine are naturally occurring metabolites in leguminous plants, which were found to be toxic to peripheral blood mononucleocytes. L-canaline is an oxygen isostere of L-ornithine and shows inhibition of ornithine decarboxylase (ODC), which is a **PLP-DE** catalysing the rate limiting step in polyamine biosynthesis.<sup>[143,144]</sup>

Degradation of tryptophane through the kynurenine pathway involves several important neuroactive intermediates and therefore misregulation of enzymes involved in this process are linked to human CNS diseases.<sup>[145]</sup> Kynurenine aminotransferase (KAT) is a **PLP-DE** responsible for the transamination of kynurenine and 3-hydroxykynurenine to kynurenic acid and xanthurenic acid, respectively.<sup>[9]</sup> KAT II, mainly located in the brain, prefers L-kynurenine as substrate. *Schwarcz et al.* were able to demonstrate several inhibitory active compounds against KAT II, among them quisqualic acid (**40**) with an IC<sub>50</sub> in the low micromolar range.<sup>[145]</sup>

In summary, many different inhibitors, natural products or artificial compounds, against several **PLP-DEs** were developed to date. They often mimic enzymes substrates and lead to an inactivation due to a mechanism-based inhibition, like CPP-115. The biggest challenge in the development of more selective drug candidates against **PLP-DEs** is the functional assignment of uncharacterised enzymes, especially **PLP-DEs**, since they represent the biggest class of off-targets. Moreover, studying **PLP-DEs** of pathogenic organisms could open up new paths to find suitable antibiotic targets. Furthermore, mining the cell for the **PLP-DE** class would allow to narrow down the function of uncharacterised enzymes to a limited number of possible chemical transformations enabling a functional characterisation.

Investigation of **PLP-DEs** is difficult due to the lack of a comprehensive method gaining a global overview. Several bioinformatics studies on **PLP-DEs** analysing conserved active-site characteristics resulted in identification and classification of these

enzymes, but generally, structural information is needed.<sup>[146–149]</sup> Due to the vast and long evolution of **PLP**-DEs, they often do not share high sequence similarity, even though their structural similarity is high and has led to the fold-type categorisation.<sup>[22,55]</sup> Although, some methods were developed for visualizing the **PLP**ome, e.g. by western-blot analysis using anti-pyridoxine antibodies, these methods are unsuitable to quantify distinct **PLP**-DEs, not to mention unable to detect differences in modified **PLP**-DEs.<sup>[150]</sup>

Fortunately, we were recently able to fill the gap in profiling **PLP**-DEs by a chemical proteomic method in order to study the **PLP**ome of a *S. aureus*<sup>[151]</sup> (by *Hoegl et al.*) transposon mutant lacking **PLP** *de novo* synthesis as well as different human cancer cell lines<sup>[152]</sup> (by *Fux et al.*) in their native environment. The method is based on activity-based protein profiling (ABPP) involving functionalised **PL**-mimics bearing a clickable handle.

## 1.5 A Chemical Proteomic Tool

---

### 1.5.1 PLPome Investigation by ABPP

---

A proteomic tool for the visualisation or quantification of interactions of small molecules with the whole proteome was first developed by *Cravatt et al.*<sup>[153–159]</sup> and *Bogyo et al.*<sup>[160–163]</sup> This powerful technology, termed activity-based protein profiling (ABPP), allows to investigate proteins in their native biological environment by their activity without influence of their abundance.<sup>[164]</sup>

In general, activity-based probes (ABPs) contain a reactive moiety able to covalently react with its target protein or protein class in a selective manner. In most cases electrophilic groups like MICHAEL-acceptors, fluorophosphonates, vinylsulfones and epoxyketons are incorporated to react with nucleophilic residues in the enzymes active-site, mostly cysteines, serines or lysines.<sup>[156]</sup> In some cases, other strategies to irreversibly attach the probe to the enzymes have to be considered, either due to the inability of introducing a reactive moiety or because of a lack of reactive amino acid residues in near proximity. One way to overcome these issues is the introduction of photoreactive groups like diazirines, arylazides, tetrazoles or benzophenones which are able to form stable covalent bonds upon UV-irradiation.<sup>[165,166]</sup> These probes are then called affinity-based probes (*Af*BP). Another way is, as we do with our **PL**-derived probes, to trap covalent intermediates of a probe bound to its enzyme *via* chemical modification, e.g. reduction. Besides the selective covalent interaction of the probe with its target enzyme(s), ABPs need a functional reporter group (e.g. fluorophore, enrichment tag, alkyne, azide, cycloalkenes) allowing direct visualisation or enrichment

or selective reaction with a reporter tag (fluorophore such as rhodamine or enrichment tag such as biotin) *via* copper(I)-catalysed azide-alkyne cycloaddition (CuAAC)<sup>[154]</sup> or STAUDINGER-ligation<sup>[167,168]</sup> with phosphines (figure 1.8).

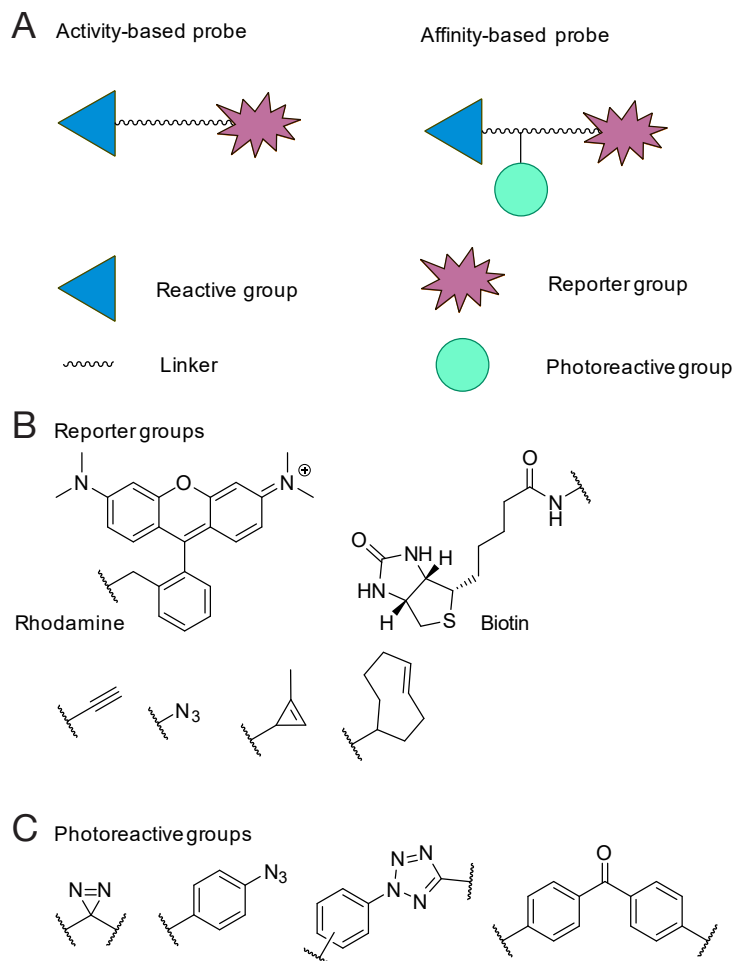


**Figure 1.8:** (A) Schematic illustration of activity- and affinity-based probes. (B) Selection of possible reporter groups. Either fluorescent or enrichment tags are already installed or small functional groups allow downstream coupling with reporter tags. (C) The most commonly used photoreactive groups in affinity-based protein profiling (AfBPP).

Fluorophore reporter groups allow analysis of labelled proteins *via* SDS-PAGE and subsequent fluorescent readout.<sup>[153,169]</sup> On the other hand, affinity-enrichment tags such as biotin allow qualitative identification of labelled proteins *via* mass-spectrometry based methods, such as LC-MS/MS (liquid chromatography coupled to tandem mass spectrometry).<sup>[157]</sup> The biotin labelled proteins are first enriched by biotin-avidin affinity chromatography, followed by a tryptic digest of bead-bound proteins, LC-MS/MS analysis and bioinformatic evaluation resulting in statistical distribution, often visualised in so called volcano plots.

As shown in figure 1.8, ABPs or AfBPs can be miniaturised by only adding a small chemical handle, which can be later functionalised by a reporter tag and additionally

enhances cell permeability and protein binding in contrast to bulky residues. Inspired by this methodology, our group developed a **PLP**ome detection strategy utilising **PL**-surrogates equipped with alkyne or azide tag.<sup>[151]</sup> In this thesis, novel probes will be presented, functionalised at the C2', C3' or C6 position (figure 1.9).

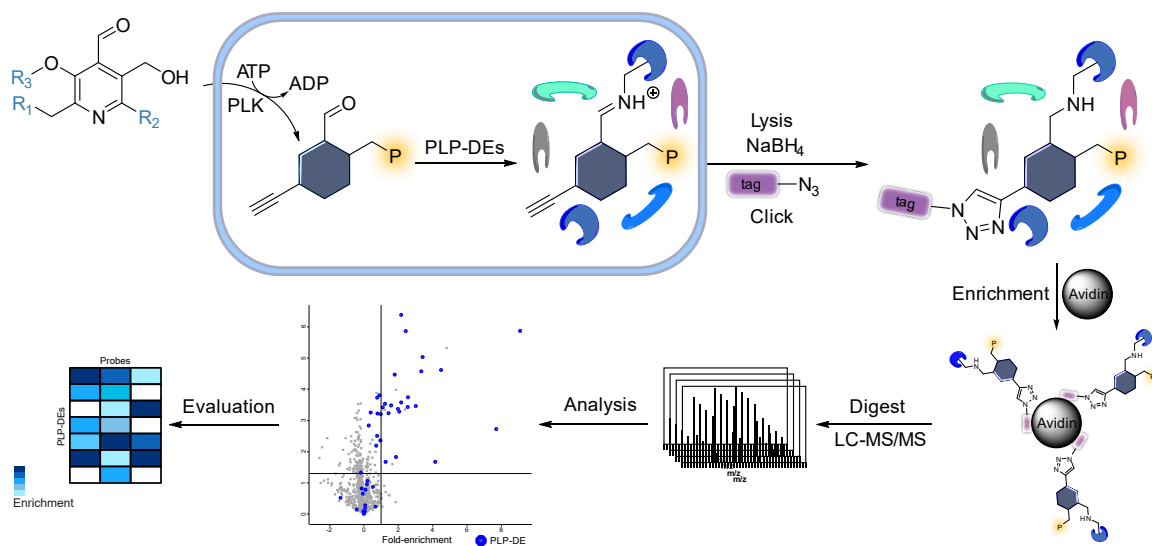


**Figure 1.9:** A chemoproteomics strategy for the investigation of **PLP**-DEs in live cells.<sup>[151]</sup> Functionalised cofactor mimics derivatised at the C2', C3' or C6 position are able to enter bacterial cells and are subsequently phosphorylated by cellular PLK. The activated probes can bind to **PLP**-DEs as internal aldimines. After cell lysis, reduction with sodium borohydride forms stable amines, which are necessary for the downstream process. Next, labelled proteome can be enriched by biotin-avidin affinity chromatography, followed by tryptic digest and LC-MS/MS measurement. Statistical analysis provides valuable data about the investigated **PLP**ome. Adapted from *Pfanzelt et al.*<sup>[170]</sup>

First, functionalised cofactor mimics are taken up by bacterial cells and are subsequently phosphorylated by cellular PLK. The phosphorylated probes can bind to **PLP**-DEs as internal aldimines. After cell lysis, reduction with sodium borohydride forms stable amines, which are necessary for the downstream process.<sup>[171]</sup> Next, the labelled proteome can be enriched by interaction of biotin with avidin agarose beads, followed by tryptic digest and LC-MS/MS measurement. After statistical evaluation of MS data, up- or downregulated proteins can be easily visualised by plotting the  $\log_2$ (enrichment) values with their respective *p*-values.

Until the 2000s, MS-based proteomic methods were only of qualitative nature giving protein lists without information about abundance and distribution. For quantification, a comparison between different states, e.g. probe treated and untreated cells, is required and can be achieved by both stable isotope labelling or label-free quantification (LFQ) methods, both of which have characteristic advantages and disadvantages.<sup>[172,173]</sup> LFQ methods are unlimited in terms of sample number and economically advantageous due to lower costs.<sup>[174,175]</sup> Along with tools for data evaluation like MaxQuant<sup>[176]</sup> together



with the MaxLFQ algorithm<sup>[174]</sup> and stable as well as accurate protein quantification, LFQ methods became very popular and widespread.<sup>[177–179]</sup>

ABPP coupled with a LFQ method has surfaced as a powerful tool not only for studying enzymes in their native, complex environment or for identification of new enzymes but also for investigation of reversible and irreversible inhibitors through their ability to hinder probe labelling.<sup>[157,180]</sup> A competitive ABPP approach facilitates determination of both selectivity and potency of inhibitors by monitoring off-targets and differences in enrichment patterns.<sup>[158,181]</sup>

### 1.5.2 Competitive ABPP for Antibiotic Target Screening

Many advanced ABPP application strategies for drug development have been developed over the last decades.<sup>[175]</sup> In competitive ABPP, cells are first treated with an inhibitor or binder followed by an ABP, thus decreasing binding of the ABP to target enzymes by blocking the binding site (figure 1.10).<sup>[175]</sup> This method excludes unspecific binding, because only those enzymes are analysed, where the binder interacts with the enzymes active site. We were already able to apply this methodology to screen for DCS off-targets in *S. aureus*.<sup>[151]</sup> DCS is known to inhibit several **PLP**-DEs such as transaminases<sup>[92]</sup>, racemases<sup>[90]</sup> and decarboxylases<sup>[182]</sup>, causing severe side effects.<sup>[88,183]</sup> Here, we did not only find the known off-targets (*alr* and DAT), but also two previously undescribed **PLP**-DEs, ornithin decarboxylase (ODC) and diaminopimelate decarboxylase (DAPDC).<sup>[151]</sup> Moreover, we could show that *alr* is not the major target in a cellular context, which was recently suggested by metabolomics studies in mycobacteria, whereas *ddl* was described as the primary target.<sup>[184,185]</sup> Hence, competitive ABPP proved to be a comprehensive method to study off-targets of **PLP**-DE inhibitors.

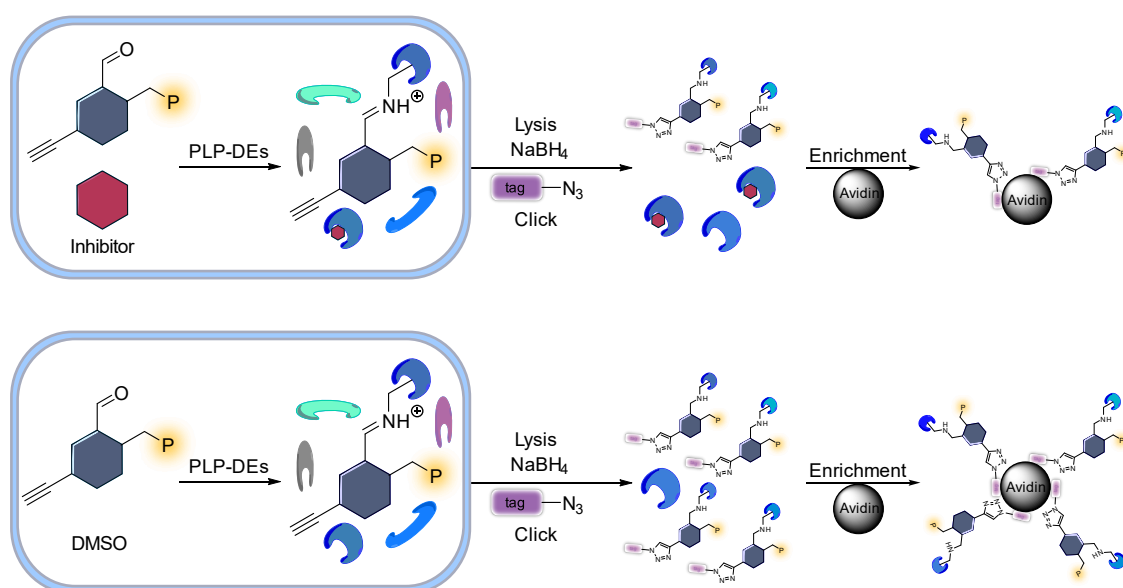


**Figure 1.10:** A competitive ABPP strategy to unravel binding of **PLP-DE** inhibitors, including off-targets. One sample is treated with the inhibitor compound and then with a suitable **PL**-probe. Here, some of the **PLP-DEs** get blocked by the inhibitor and the probe is therefore unable to bind. In parallel, a control sample is only treated with DMSO (or another solvent the inhibitor is soluble in) and the respective **PL**-probe. After lysis, reduction and enrichment, the inhibitor treated sample lacks **PLP-DEs**, which are not enriched in the downstream LFQ-MS analysis. In the end, data analysis and comparison of inhibitor treated cells against control samples gives information about possible target enzymes, here **PLP-DEs**.

In our competitive ABPP workflow, one sample is treated with the inhibitor compound followed by a suitable **PL**-probe. Some of the **PLP-DEs** get blocked by the inhibitor and the probe can therefore not bind. A further control sample is treated with DMSO only and the respective **PL**-probe. After lysis, reduction of imines, CuAAC and enrichment of labelled proteins, samples are processed as described in figure 1.9. The inhibitor treated sample lacks some of the **PLP-DEs**, which are not enriched due to their blocked active-site. A comparison of the data, in particular the LFQ-intensities of hit enzymes, allows the identification of significantly blocked and therefore inhibited **PLP-DEs**.

The competitive approach was already applied successfully in the target validation of electrophilic natural products such as **MICHAEL**-acceptors and epoxides, which mostly react with active-site cysteines.<sup>[186]</sup> Remarkably, recent studies by *Zanon et al.* showed a platform for screening electrophilic inhibitors proteome-wide, which target not only cysteines selectively but also tryptophans, histidines, arginines, methionines, aspartates and glutamates.<sup>[187]</sup> This tool will be instrumental to design novel covalent inhibitors targeting diverse amino acids.

## 1.6 Objectives

**PLP** is arguably the most versatile cofactor and is used by all forms of life. Bound to the active-site lysine it is involved in many different chemical transformations involving amino acid metabolism, regulation of immune function and biosynthesis of neurotransmitters. Some **PLP**-DEs are involved in diseases or represent druggable targets in pathogens. However, some of these enzymes lack a firm functional assignment. Due to the current antibiotic crisis, finding new antibiotic targets is becoming increasingly important. Along with their biological importance, the fact that bacteria share only about a third of their **PLP**-DEs with humans strengthen their role as druggable targets.<sup>[62]</sup> Therefore, a global overview of the **PLP**ome of pathogenic bacteria would support the process towards the discovery of selective inhibitors against crucial or essential **PLP**-DEs.

Based on former studies in our lab<sup>[151,152]</sup>, this thesis describes the synthesis of novel **PL**-probes for ABPP studies, among them a phosphoramidate pro-tide probe. The probes are derivatised at different ring positions, which will lead to an enhanced labelling coverage and give rise to a detailed map of binding preferences of certain structural motifs. Along with a refined labelling strategy, we will investigate the **PLP**ome of different bacterial organisms, including a *S. aureus* USA300 transposon mutant and a *E. coli* K12 knockout strain lacking **PLP** *de novo* biosynthesis as well as *P. aeruginosa* PAO1 wild type strain. This will lead to a labelling enhancement described in detail for *S. aureus*. Moreover, some uncharacterised or poorly characterised/putative **PLP**-DEs will be identified and validated using a series of different methods, among them metabolomics and different activity assays.

Until now, only a small number of clinically used drugs target enzymes involved in bacterial metabolism.<sup>[188]</sup> Since some **PLP**-DEs are druggable targets, competitive ABPP is a powerful method to screen compound libraries against this enzyme class with the aim of finding a selective inhibitor. For this, a small library consisting of 53 compounds will be screened against several pathogenic bacterial strains, spawning some hit molecules. Four compounds are then further investigated in *S. aureus* and *E. coli* using the described competitive approach. Indeed, **PLP**-dependent off-targets will be found, which are then further validated in activity and inhibition assays utilising purified enzymes.



# 2

## RESULTS AND DISCUSSION

---

*In this chapter, results of the thesis will be discussed including the synthesis of **PL**-probes and their application as **ABPP**-probes for enrichment and competitive studies in different bacterial strains. Moreover, insights into the catalysis of five poorly characterised **PLP**-DEs will be given. Finally, the antibiotic screen of a small compound library with subsequent off-target identification and in vitro validation experiments is presented as an application.*

### Contents

---

<b>2.1</b>	<b>Synthetic Strategy</b> . . . . .	<b>24</b>
<b>2.2</b>	<b>Biological Evaluation of the Probes</b> . . . . .	<b>41</b>
<b>2.3</b>	<b>PLPome Profiling</b> . . . . .	<b>51</b>
<b>2.4</b>	<b>Validation Experiments</b> . . . . .	<b>57</b>
<b>2.5</b>	<b>Application: Screening for Potential Inhibitors</b> . . . . .	<b>69</b>

---

A cofactor mimic capable of binding to its enzymes requires functionalisation with clickable handles but also the genuine integrity of the cofactor itself. This chapter will tell the story from synthetic design of probes, validation of hit enzymes found with several of these probes and finally their application in competitive ABPP screens for inhibitors against **PLP**-dependent enzymes. In the first part, synthetic strategies for **PL**-probes will be discussed. Here, three general types will be described as well as a novel, pro-tide based phosphoramidate probe. In the subsequent chapters, biological evaluation of the probes, followed by the profiling of bacterial **PLP**omes and some validation experiments will be presented. In the end, an *in vitro* compound screen of known and putative **PLP**-DE inhibitors will be performed and four hits will be further investigated by competitive ABPP and validation experiments by targeted metabolomics experiments.

## 2.1 Synthetic Strategy

**PL** is a highly reactive aldehyde compound, which needs to be protected appropriately for derivatisation. Many examples in literature describe different protecting strategies, mostly involving both alcohols and the aldehyde group. Several intermediates were further functionalised and studied in their capability of catalysing **PLP**-dependent reactions. Indeed, some of them were able to replace natural **PLP**, but often with lower reaction rates. On the other hand, a group of derivatives were not active at all in terms of catalysis, including some antivitamin, meaning that they inhibited function of some **PLP**-DEs.<sup>[189–206]</sup> In general, **PL** can be modified at all ring positions, the pyridine *N*, C2', C3, C4', the benzylic 5'-phosphate and last but not least, the aromatic C6 position. Of course, a minimal intervention in the cofactor's scaffold would be beneficial, since essential groups for catalysis like the aldehyde should not be modified. However, *Fonda et al.* and *Mechanik et al.* showed, that compound **42** and **43**, both modified at the C3, are unsuitable as cofactors for glutamate decarboxylase, despite binding to the enzyme.<sup>[207,208]</sup> Moreover, they tested the C5' derivative 5'-deoxy **PL** (**44**) and found insufficient binding of this mimic. However, *Schnackerz et al.* could reconstitute catalytically competent bacterial apo-*O*-acetylserine sulfhydrylase with **PL** 5'-deoxymethylphosphonate (**45**).<sup>[209]</sup> C4' derivatised compounds are often used as inhibitors, mimicking transition states, such as compound class **46**, which often bear the enzymes substrate bound as amine, e.g. pPTME, a human ornithine-decarboxylase inhibitor having a tryptophane bound to the **PLP** scaffold.<sup>[210]</sup> The aromatic C6 position was first derivatised by *Doktorova et al.* to 6-methyl **PLP** (**47**).<sup>[211]</sup> The compound showed aldimine formation suggesting toleration by the enzyme.<sup>[208]</sup> Of note, they synthesised the compound not by derivatisation of **PLP** itself but by a DIELS-ALDER reaction of oxazoles with dienophiles such as dimethyl maleate. **PLP**-6-phenylazo derivatives **48**, known from *Lambrecht et al.* as PPADS compounds and selective

inhibitors of P<sub>2</sub> receptors, were further investigated by *Kim et al.*<sup>[198,199,212]</sup> In addition, pyridine nitrogen derivatives such as deaza-PLP (**49**) or PLP-*N*-oxide (**50**) were shown to bind to certain PLP-DEs enabling a number of catalysed reactions.<sup>[207,213]</sup>

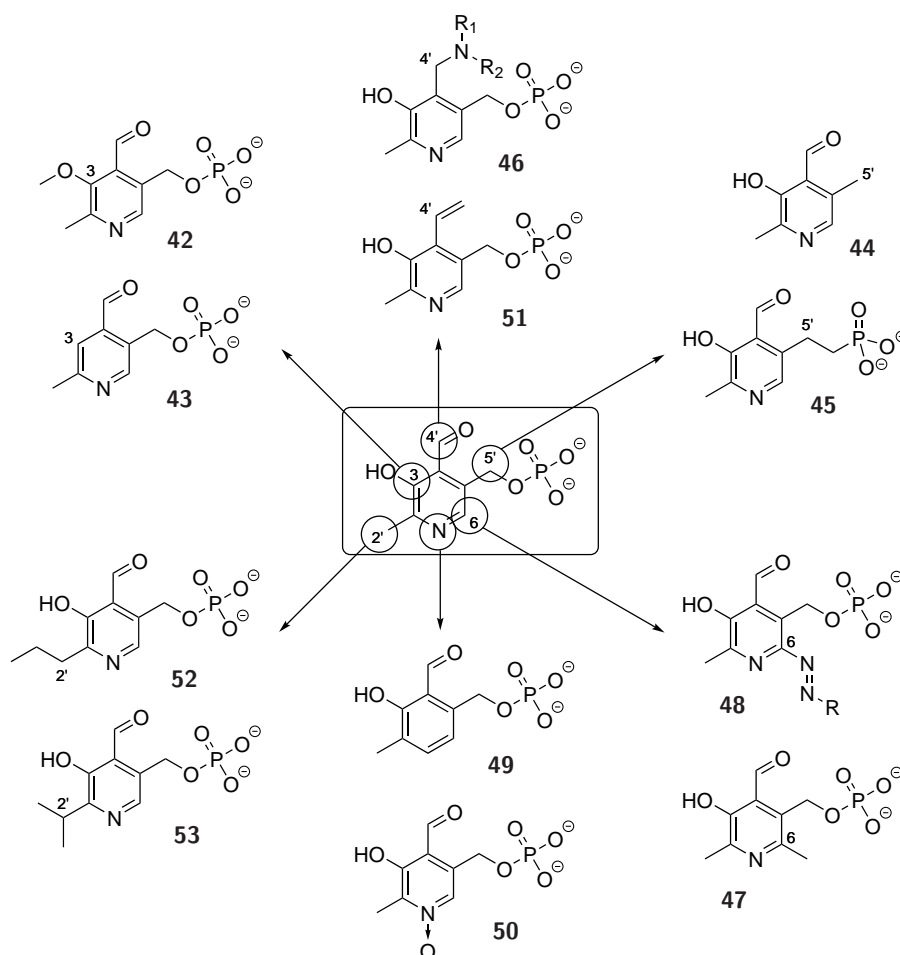
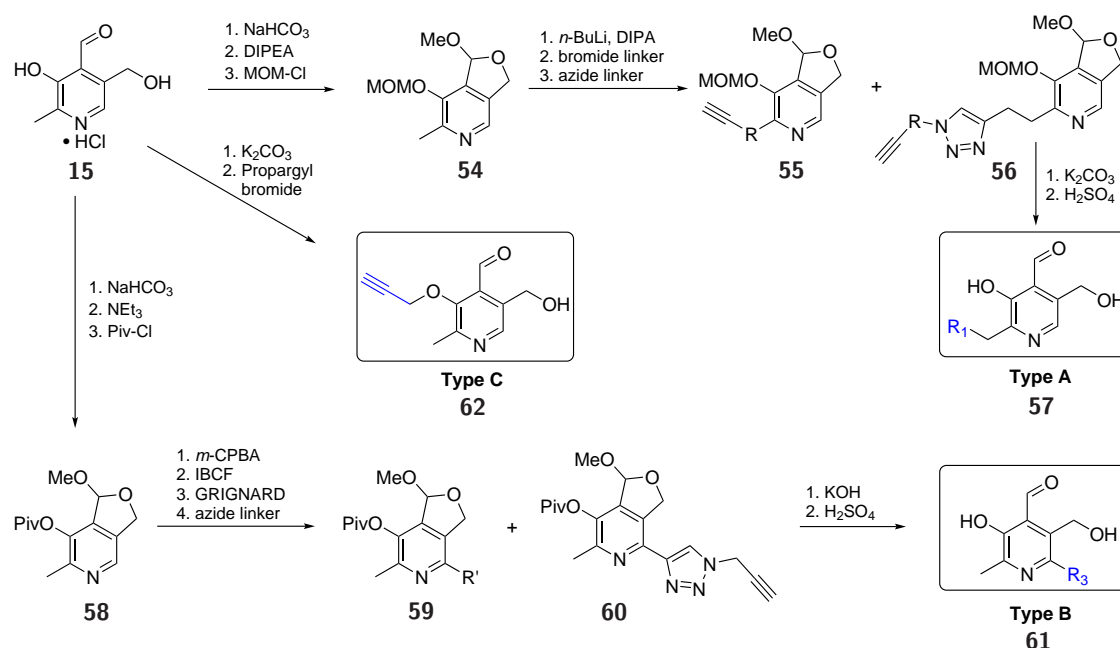


**Figure 2.1:** Different PLP derivatives at the C3 (**42**, **43**)<sup>[207,208]</sup>, C4' (**46**<sup>[210]</sup>, **51**<sup>[207]</sup>), C5' (**44**<sup>[207,208]</sup>, **45**<sup>[209]</sup>), C6 (**48**<sup>[198,199,212]</sup>, **47**<sup>[211]</sup>), the pyridine nitrogen (**49**<sup>[213]</sup>, **50**<sup>[207]</sup>) and the C2' (**52**, **53**)<sup>[34,203,209,214,215]</sup> were already synthesised and investigated regarding their suitability as cofactor substitute or inhibitor.

Finally, the C2' position was found to be unimportant for catalysis, since the methyl group is only a relic from its biosynthesis.<sup>[34]</sup> Moreover, several studies confirmed that some modifications, like an extended alkyl group (**52**) or a bulky dimethyl group (**53**), can be tolerated by certain enzymes to fulfil catalysis, despite lower kinetic parameters (all structures are shown in figure 2.1).<sup>[34,203,209,214,215]</sup> Furthermore, *Snell et al.* concluded, that some enzymes including asp-AT, tryptophanase, arg-decarboxylase and D-ser dehydratase, allow structural variety at the C2' position.<sup>[215]</sup> This fact was used by our group to design the first generation of PL-probes by *Hoegl et al.*, which were all derivatised at the C2'-position.<sup>[151]</sup>

### 2.1.1 PL-Derived Probes

For our proteomics approach, **PL**-probes bearing an alkyne or azide tag for subsequent attachment of a fluorescent or an enrichment handle are required. Because indispensable groups for binding to **PLP**-DEs should not be modified, we exploited the modification of the C6 (type B) and C3 (type C) sites of **PL** by the attachment of different alkyl and triazole moieties. Additionally, the scope of the **PL**-probe library has been extended by some more derivatives at the C2' (type A) (summary scheme 2.1).



**Scheme 2.1:** Synthetic overview of all different **PL**-probe types: type A (**57**), type B (**61**) and type C (**63**). Adapted from *Pfanzelt et al.*<sup>[170]</sup>

#### 2.1.1.1 Type A Probes

A library of five type A cofactor mimics was previously synthesised, termed **PL1-PL5** (figure 2.2).<sup>[151]</sup> The synthesis of **PL1** was inspired by *Korytnyk et al.*<sup>[190]</sup> Here, all the three alcohol groups of **PN** were protected with *tert*-butyldimethylsilyl (TBDMS) enabling selective hydroxylation of the C2'-methyl group *via* oxidation to the *N*-oxide and a subsequent BOEKELHEIDE-rearrangement.<sup>[216]</sup> The alcohol was then oxidised and transformed into a terminal alkyne using the OHIRA-BESTMANN-reagent.<sup>[217,218]</sup> Final deprotection led to the first **PL**-probe **PL1** (**64**).<sup>[151]</sup>



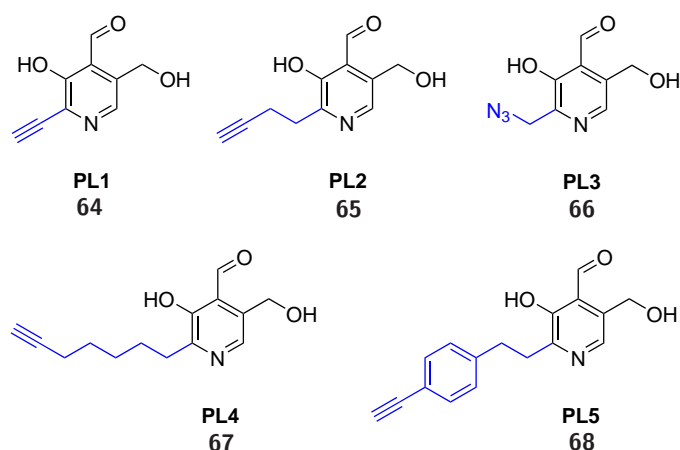


**Figure 2.2:** The first generation of PL-probes, **PL1-PL5**.<sup>[151]</sup>

**PL2** (65), **PL4** (67) and **PL5** (68) were synthesised utilising the same protected reactive intermediate. Here, **PL** is converted into a methylacetal and subsequent protection of the phenolic alcohol with methoxymethyl (MOM) chloride leads to the intermediate (54).<sup>[219]</sup> Then, an alkylation strategy inspired by *Kaiser et al.* utilising linkers with different chain lengths led to the protected precursors 55.<sup>[220]</sup> Final deprotection using potassium carbonate and sulfuric acid yielded the three type A probes **PL2**, **PL4** and **PL5**. This type A library was later completed by M. PFANZELT with **PL6**, **PL7**, **PL8** and **PL9** (figure 2.3).<sup>[221]</sup> Here, **PL8** and **PL9** were further functionalised by an azide linker *via* CuAAC (56). A different synthetic route was chosen for **PL3**. Again starting from **PN**, first the C3 and the C4' alcohol groups were protected as acetonide and the remaining 5' alcohol was protected as *para*-methoxybenzyl (PMB) ether using PMB chloride.<sup>[200,204,222]</sup> Same transformation steps as for **PL1** were applied to yield the C2' alcohol compound. Activation and substitution to the C2' azide followed by deprotection steps and final oxidation to the aldehyde led to the only azide PL-probe **PL3**.<sup>[151]</sup>

In total, nine type A probes were synthesised in order to maximize the labelling coverage of known and unknown **PLP-DEs** and reach sub-class specificity.

### 2.1.1.2 Type B Probes

Type B **PL**-probes were newly developed by M. PFANZELT utilising an appropriate protective group system originally used by *Kim et al.* for their synthesis of PPADS compounds.<sup>[198,221]</sup> First, **PL** was protected as methylacetal and subsequently reacted with pivaloyl (Piv) chloride, leading to intermediate 58.<sup>[198,221]</sup> The different phenolic alcohol protective group was chosen because it required oxidation stability, which could not be ensured with MOM. Oxidation with *meta*-chloroperbenzoic acid (*m*-CPBA)

and activation by *iso*-butyl chloroformate (IBCF) enhanced electrophilicity, which enabled nucleophilic substitution with different GRIGNARD-linkers (**59**). Again, one intermediate was further functionalised with an azide-alkyne linker, yielding the tetrazole compound **69**. Finally, basic deprotection followed by acetal deprotection in sulfuric acid led to type B probes **PL10**, **PL11** and **PL12**.

### **2.1.1.3** Type C Probe

---

To complete the library, one further compound, termed type C probe, was synthesised in 2018. Starting from **PL**, deprotonation of the phenolic proton by potassium carbonate and subsequent substitution with propargyl bromide led to **PL13** (**62**). Interestingly, the same probe, though for different applications, was synthesised by *Saha et al.* in 2021.<sup>[223]</sup> **PL13** was designed to show the extent to which the phenolic position is involved in labelling efficacy.

In summary, 13 different **PL**-probes bearing structural modifications at the C2', C3 or C6 position of the pyridine ring were synthesized (figures 2.2 and 2.3). These probes serve as chemical tools to access different binding sites of **PLP**-DEs in our proteomics methodology. Moreover, taken all probes together, a higher coverage of labelled enzymes was expected.

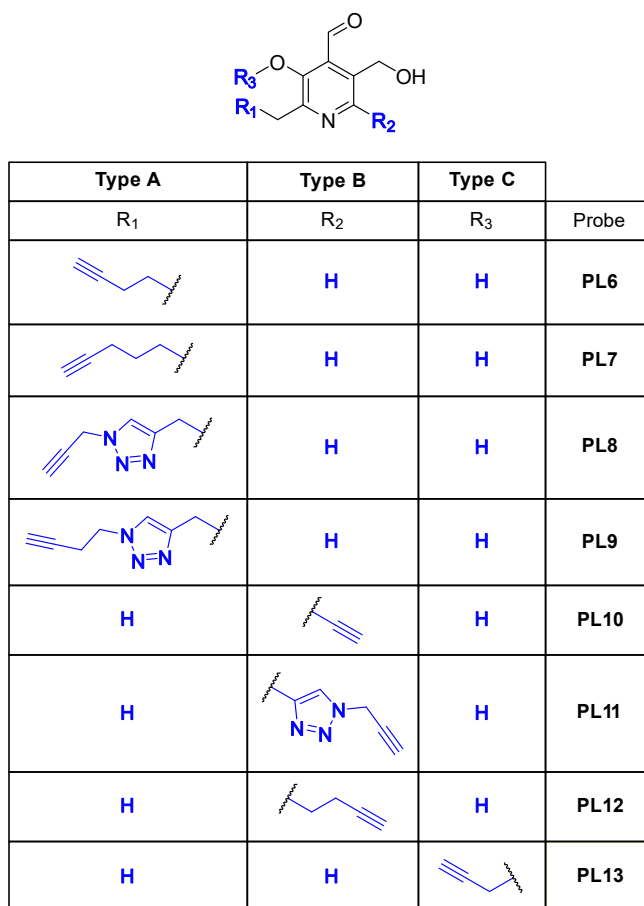


**Figure 2.3:** The second generation of **PL**-probes, **PL6-PL13**. Adapted from *Pfanzelt et al.*<sup>[170]</sup>

One of the most limiting steps in our labelling approach, especially in human cells, is the phosphorylation of our probes. *Fux et al.* could show, that only **PL1** is able to function as a cofactor mimic in certain cancer cell lines in contrast to **PL2**, because the human PLK is highly restricted in its substrate specificity.<sup>[152]</sup> Moreover, cultivation of cells in defined media lacking natural **PL** but containing 10  $\mu\text{M}$  **PL1** for 7 passages ( $\approx$  20 days) was required in order to reach accumulation of phosphorylated **PL1**, namely **PL1P**, in **PLP**-DEs. Due to this circumstance we conceptualized another strategy to bypass the rate limiting phosphorylation in order to obtain more beneficial probes with the potential of an enhanced labelling efficiency and enzyme coverage. A very well studied substance class, in which the phosphate group is first masked and then intracellularly cleaved by certain enzymes, are the phosphoramidates (PAs).<sup>[224]</sup> These moieties are frequently used as prodrugs, molecules with little or no pharmacological activity until their cleavage to the active, parent drug *in vivo*.<sup>[225]</sup> Especially many antivirals and anticancer-drugs contain phosphoramidate groups, because they are often derived from nucleosides, which need to be phosphorylated to triphosphates *in vivo* in order to be active.<sup>[226]</sup> The challenge in this case is, that the efficacy of human nucleoside/nucleotide kinases is often limited which would result in a restricted therapeutic use of non pro-tide (nucleoside phosphoramidate) masked drugs. As

another favorable effect, phosphoramidates improve the therapeutic potential by completely masking the charges of the phosphate group, since negatively charged molecules are unable to cross cell membranes.<sup>[227]</sup> The next subsection describes the general principle of phosphoramidates in biological systems and the development of a novel **PL3** derived phosphoramidate probe.

### 2.1.2 Pro-Tide Probe PL3PA

Initially, phosphoramidates were only used as pro-tides for antivirals or nucleoside-analogues in general. Recently, a lot of publications presented applications of phosphoramidates for different substance classes, e.g. phosphoserine<sup>[228]</sup> or fosfoxacin<sup>[229]</sup>. The phosphoramidate moiety protects phosphate groups until they are specifically cleaved *in situ*. Here, aryloxy (phenoxy, naphthoxy) and amino acid esters (i.a. L-alanine benzyl or isopropyl esters) are often used as masking groups, since they ensure high membrane permeability caused by increased lipophilicity.<sup>[225]</sup> *McGuigan et al.* showed in a study on 3'-azidothymidine (AZT), an anti-human immunodeficiency virus (HIV) agent, that L-alanine yielded the most potent phosphoramidate prodrug, compared to L-leucine or glycine.<sup>[230]</sup> Moreover, AZT phosphoramidates were even active in thymidine-kinase deficient cells, proving the ability of these compounds to deliver intact nucleoside analogue monophosphates into intact cells.<sup>[231]</sup> In consequence, many different drugs with clinical application, including sofosbuvir (**77**) and tenofovir (**78**), drugs against the hepatitis C virus (HCV) and HIV, respectively, were developed (figure 2.4 A).<sup>[225]</sup> The mechanism of phosphoramidate cleavage can be divided in four steps: two are enzyme-catalysed and the other two occur spontaneously. First, the amino acid ester **79** is cleaved by an esterase, which recognises the alanine functionality.<sup>[227]</sup> The resulting carboxylate **80** spontaneously attacks the phosphor intramolecularly leading to the heterocycle **81**. This cyclic anhydride undergoes hydrolysis to **82**, which is not enzymatically catalysed. Finally, the phosphoalanine is cleaved by cellular phosphoramidase to form the monophosphorylated compound **83** (figure 2.4 B). Generally, phosphoramidate compounds can be synthesised using a reactive phosphorochloridate agent, which is formed *in situ* from a phosphorodichloridate species, prior to the addition of the alcohol and a base (e.g. *N*-methyl imidazole), which is readily modified (figure 2.4 C). This powerful technology is not only applicable to drugs but also to cofactors, as *Kielkowski et al.* and *Rauh et al.* recently demonstrated in their studies on AMPylated proteins utilizing an adenosine monophosphate (AMP) phosphoramidate probe in ABPP experiments. This probe is cleaved *in situ* to the monophosphorylated AMP probe, which is further activated by cellular kinases to the active triphosphorylated probe.<sup>[232–234]</sup>

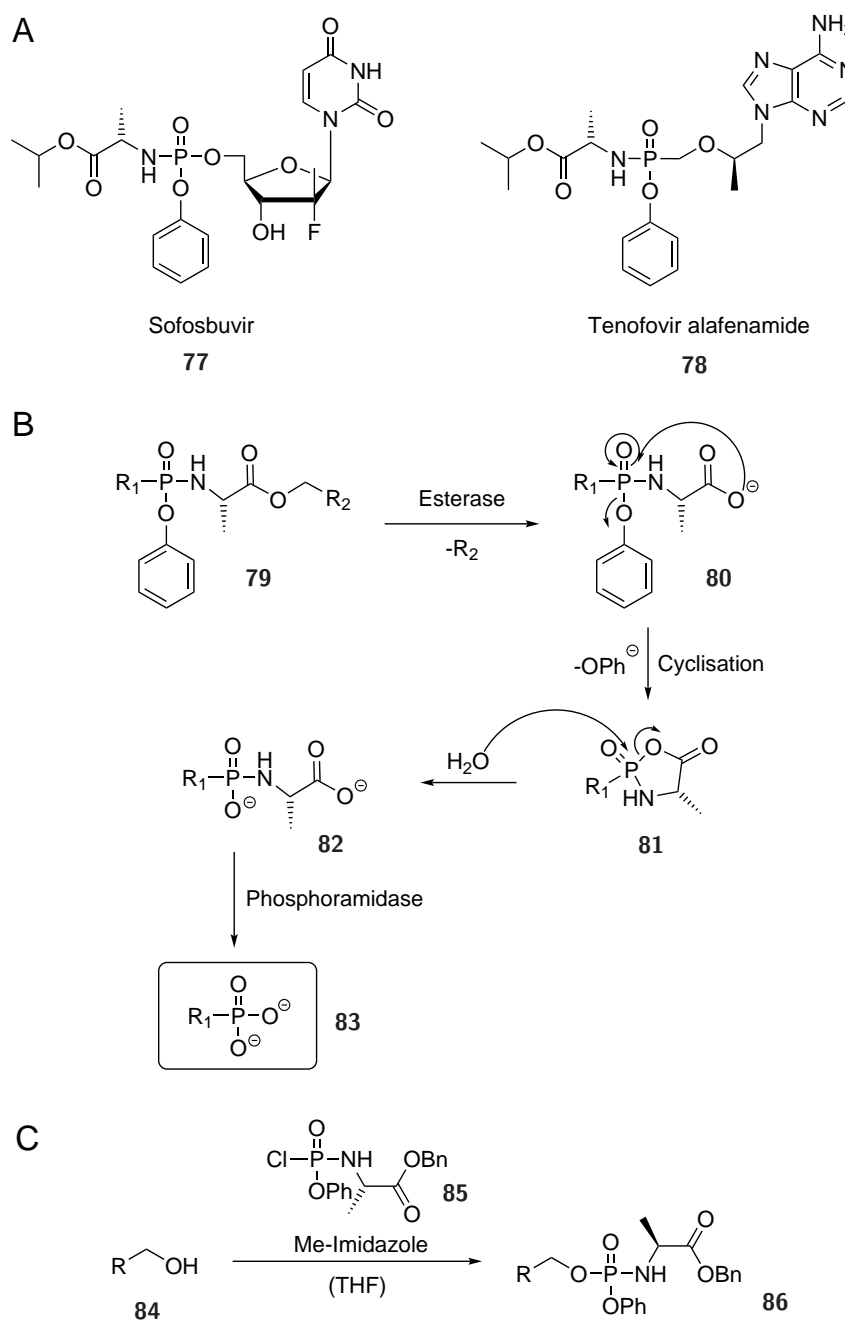
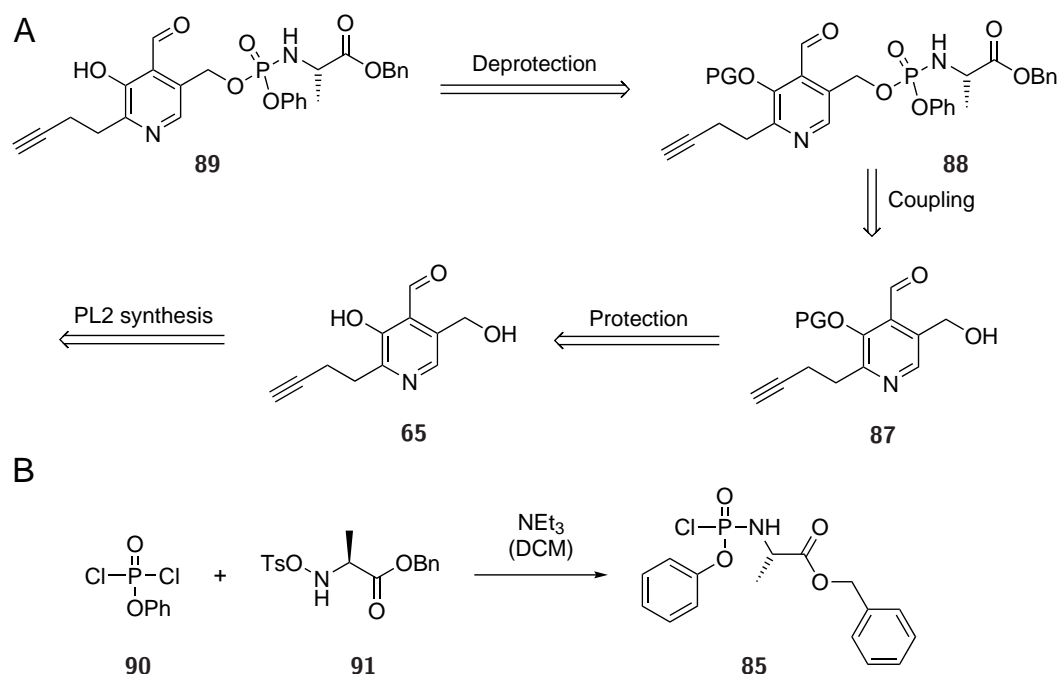


**Figure 2.4:** (A) The two phosphoramidate antivirals sofosbuvir (**77**) and tenofovir (**78**), which are in clinical use. (B) Mechanism of phosphoramidate cleavage. First, the ester is cleaved by an esterase. The generated carboxylate can then attack the phosphor leading to an intramolecular ringclosure. After hydrolysis, a phosphoramidase cleaves the amino acid leading to the monophosphorylated species.<sup>[227]</sup> (C) General synthesis of phosphoramidates (**86**) using a reactive phosphorochloridate species (**85**), which is formed *in situ*.

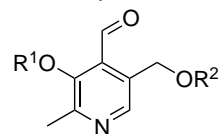
Based on this preliminary work, we wanted to design a **PL** phosphoramidate probe based on an already existing probe scaffold. Such a probe could make the **PLP**ome profiling independent of cellular **PLK** activation, making it easier to access **PLP**-DEs in human cells.

Initially, the plan was to synthesize a **PL2** derived phosphoramidate probe. The strategy was to first protect the phenolic alcohol at the C3-position of **PL2** (**65**) with an acidic cleavable protective group, yielding **87**, and then couple the benzylic alcohol with the phosphorochloridate to precursor **88**. After deprotection, **PL2** phosphoramidate **89** should be formed (scheme 2.2).



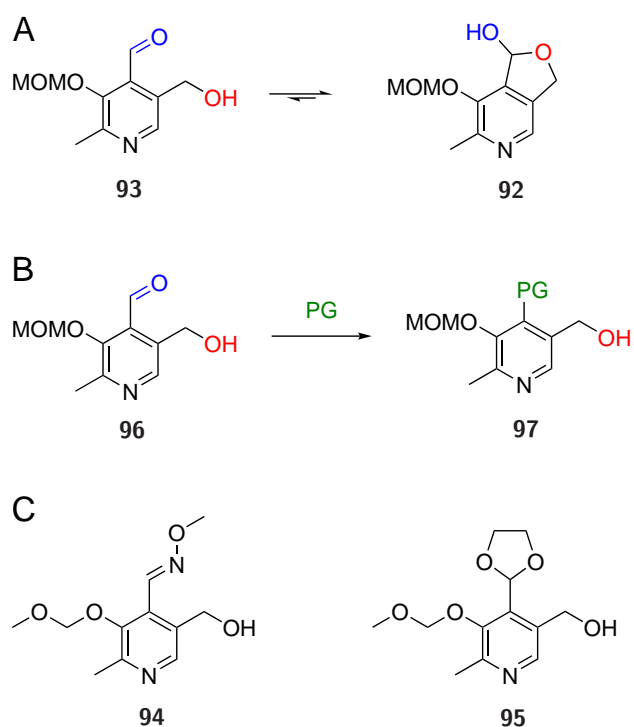
**Scheme 2.2:** (A) Retrosynthesis of the desired **PL2** phosphoramidate probe **PL2PA** (**89**). (B) Synthesis of the reactive phosphorochloridate species **85** from dichloridate **90** and protected L-alanine **91**.

For this approach, different protective groups (PGs) for the C3 alcohol and bases for prior deprotonation were elucidated directly on **PL** without any linker. Selectivity for the phenolic alcohol was shown for all investigated reaction conditions, except for MOM chloride and potassium carbonate. The latter reaction formed a bis-protected system. Table 2.1 summarises the tested conditions in this simplified setting.

**Table 2.1:** Protective Groups for C3' in **PL2PA** Synthesis.

Base	Reagent	C3'	C5'	Yield
K <sub>2</sub> CO <sub>3</sub>	MOMCl	MOM	OMOM	quant.
K <sub>2</sub> CO <sub>3</sub>	BnBr	Bn	OH	45%
NEt <sub>3</sub>	PivCl	Piv	OH	40%
NEt <sub>3</sub>	MOMCl	MOM	OH	20%
DIPEA	MOMCl	MOM	OH	49%

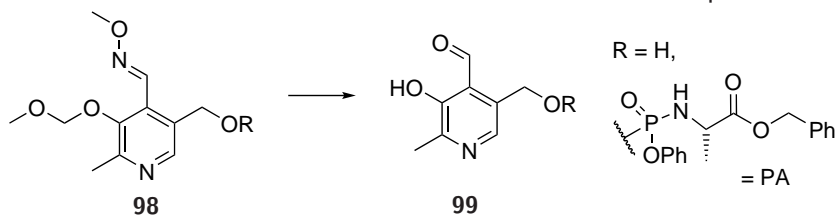
With *N,N*-diisopropylethylamine as base and MOM chloride as reagent, C3' protected **PL** was isolated in 49% yield. With this compound in hand, a first test reaction with the phosphorochloridate **85** was conducted leading to the formation of the desired product **86**. However, due to the low yield, no purification of the final product was feasible. A possible explanation for the low yield could be the formation of an acetal species (**92**), which could be verified by NMR. This observation is well known in literature: **PL** or **PLP** are not only present as hydroxyaldehydes **93** but are in an equilibrium with their corresponding hemiacetals (figure 2.5 A).<sup>[195]</sup> This was also the case for our **PL**-probes. For example, the NMR-signal of the aromatic proton in the hemiacetal-form of **PL6** appears at 7.96 ppm with an integral of 1. In contrast to that, the signal of the aromatic proton in the open form is visible at 8.15 ppm with an integral of 0.04.<sup>[221]</sup> The equilibrium clearly lies on the side of the hemiacetal. Consequently, the aldehyde moiety had to be protected, too, in order to achieve acceptable yields in the coupling reaction (figure 2.5 B). Two main PGs for the aldehyde were investigated, a methoxime (**94**) and an acetal (**95**) (figure 2.5 C).



**Figure 2.5:** (A) Equilibrium of open form **93** and hemiacetal form **92**. (B) Protection of the aldehyde could prevent intramolecular ring closure. (C) Structures of the two 4'-protected precursors **94** and **95**, which were further investigated.

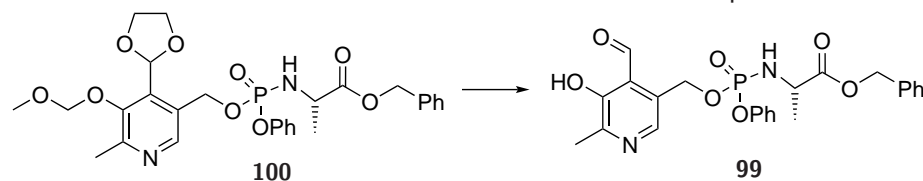
To yield the methoxime **94**, **PL** was first reacted with methoxyamine hydrochloride in ethanol at room temperature overnight.<sup>[219]</sup> Without purification, the methoxime was converted to the MOM protected compound **94** in 62% yield. Subsequently, **94** was converted with the phosphorochloridate **85** to result in the protected phosphoramidate **98**. With this compound and the precursor without the phosphoramidate moiety in hand, a series of test-deprotections was performed, summarised in table 2.2. Mild acidic deprotections did not work at all, not even with subsequent heating of the reaction mixture. Moreover, two mild deprotection reagents, 1,3-dibromo-5,5-dimethylhydantoin (DBDMH)<sup>[235]</sup>, and 1,4-diazobicyclo[2,2,2]octane (DABCO) bromine<sup>[236]</sup>, were applied without any detected conversion. Apparently, the methoxime is highly stable, possibly due to stabilisation effects within the extended  $\pi$ -system (figure 2.2). Only when using concentrated chloric acid and 37% paraformaldehyde (CHO) the m/z (mass to charge ratio) of the desired product found in the mass spectrum, but could not be isolated due to a very low yield.



**Table 2.2:** List of tested conditions for the methoxim deprotection.

Reagent	Temperature	Rest	Solvent	Yield
HCl 0.5 N	r.t., then reflux	PA	H <sub>2</sub> O	–
H <sub>2</sub> SO <sub>4</sub> 5%	r.t.	H	H <sub>2</sub> O/acetone	–
HCl 1.0 N	r.t.	H	THF	–
HCl 10%, 37% CHO	r.t.	PA	THF	–
K <sub>2</sub> CO <sub>3</sub>	r.t.	H	EtOH	–
DBDMH	r.t.	H	DCM/H <sub>2</sub> O	–
HCl <sub>conc</sub> , 37% CHO	r.t.	H	H <sub>2</sub> O	product detectable
DABCO-Br <sub>2</sub> , 37% CHO	r.t.	H	chloroform/H <sub>2</sub> O	–

Next, the acetal compound **95** was tested as a suitable substrate. First, **PL** was protected with 1,2-ethanediol and *p*-toluenesulfonic acid (*p*-TsOH). Then, reaction with MOM chloride resulted in the acetal **95** with a yield of 45% over two steps. Again, by conversion with the phosphorochloridate **85**, phosphoramidate **100** was obtained. For this compound, all deprotection reactions were conducted bearing the phosphoramidate moiety. Again, several acidic reagents were used in order to fully deprotect acetal and ether to the **PL**-phosphoramidate **PLPA** (**99**) (table 2.3)

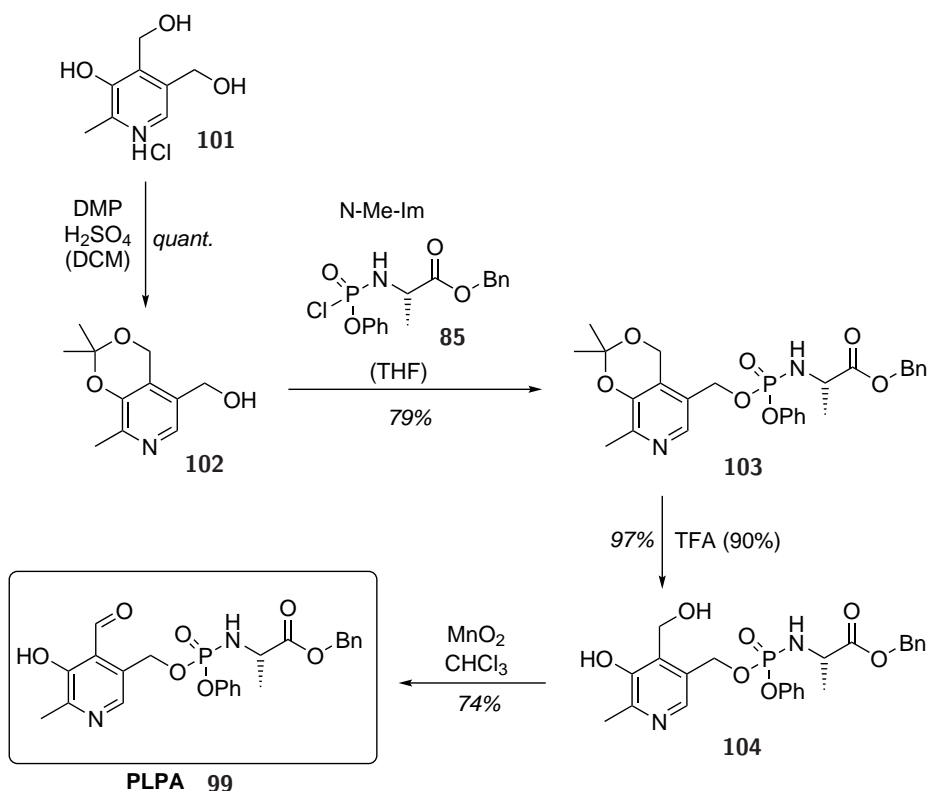
**Table 2.3:** List of tested conditions for the acetal deprotection.

Reagent	Temperature	Solvent	Yield
TFA 90%	r.t.	H <sub>2</sub> O	–
TFA 40%	r.t.	H <sub>2</sub> O	–
HCl 1.0 N	r.t. then reflux	H <sub>2</sub> O/acetone	–
HCl 6.0 N	r.t.	H <sub>2</sub> O	–
H <sub>2</sub> SO <sub>4</sub> 5%	r.t. then reflux	H <sub>2</sub> O/acetone	–
<i>p</i> -TsOH 25 mol%	r.t. then reflux	H <sub>2</sub> O/acetone	–
I <sub>2</sub> 10 mol%	r.t.	acetone	–

Different concentrations of trifluoro acetic acid (TFA) and HCl as well as sulfuric acid and *p*-TsOH<sup>[237]</sup> did not show any product formation. In addition, iodine in acetone<sup>[238]</sup> was also not able to cleave off both groups. Moreover, an open acetal, a semicarbazone in particular, and a 1,3-dioxane were synthesised with the corresponding MOM group at the C3'. While it was not possible to isolate the phosphoramidates of the open acetal and the semicarbazone, the 1,3-dioxane could be isolated in 55% yield. However, in accordance to all other investigated protective groups, final cleavage was also not possible for the 1,3-dioxane (data not shown).

Due to the failed test reactions with the discussed system, which would have been compatible with **PL2** synthesis, we focused on a different strategy. This approach is derived from the **PL3** synthesis and utilises adjusted protective groups. First, a minimal system without any tag was investigated. Therefore, **PN** hydrochloride (**101**) was stirred in 2,2-dimethoxypropane (DMP) and catalytic amounts of sulfuric acid to yield acetonide **102** quantitatively. Now, the 5' alcohol could react with the phosphorochloridate **85**. Luckily, phosphoramidate **103** could be isolated in 79% yield using the standard reaction conditions. Thereafter, the pure compound was stirred in 90% TFA and reaction controls were measured every 30 minutes. After 1.5 hours, an almost full conversion to diol **104** was detected. The last step, an oxidation to the 4'-aldehyde had to be optimised, since the first reaction using manganese(IV)-oxide in dichloromethane did not result in any product, even after addition of 12 equivalents MnO<sub>2</sub> in total and some methanol. Acetone as solvent did also not yield the desired product. DESS-MARTIN-periodinane as oxidising agent gave the acid instead of the aldehyde and was therefore not further investigated. As a last try, MnO<sub>2</sub> in chloroform without methanol, which was responsible for a methyl ester formation in prior experiments,

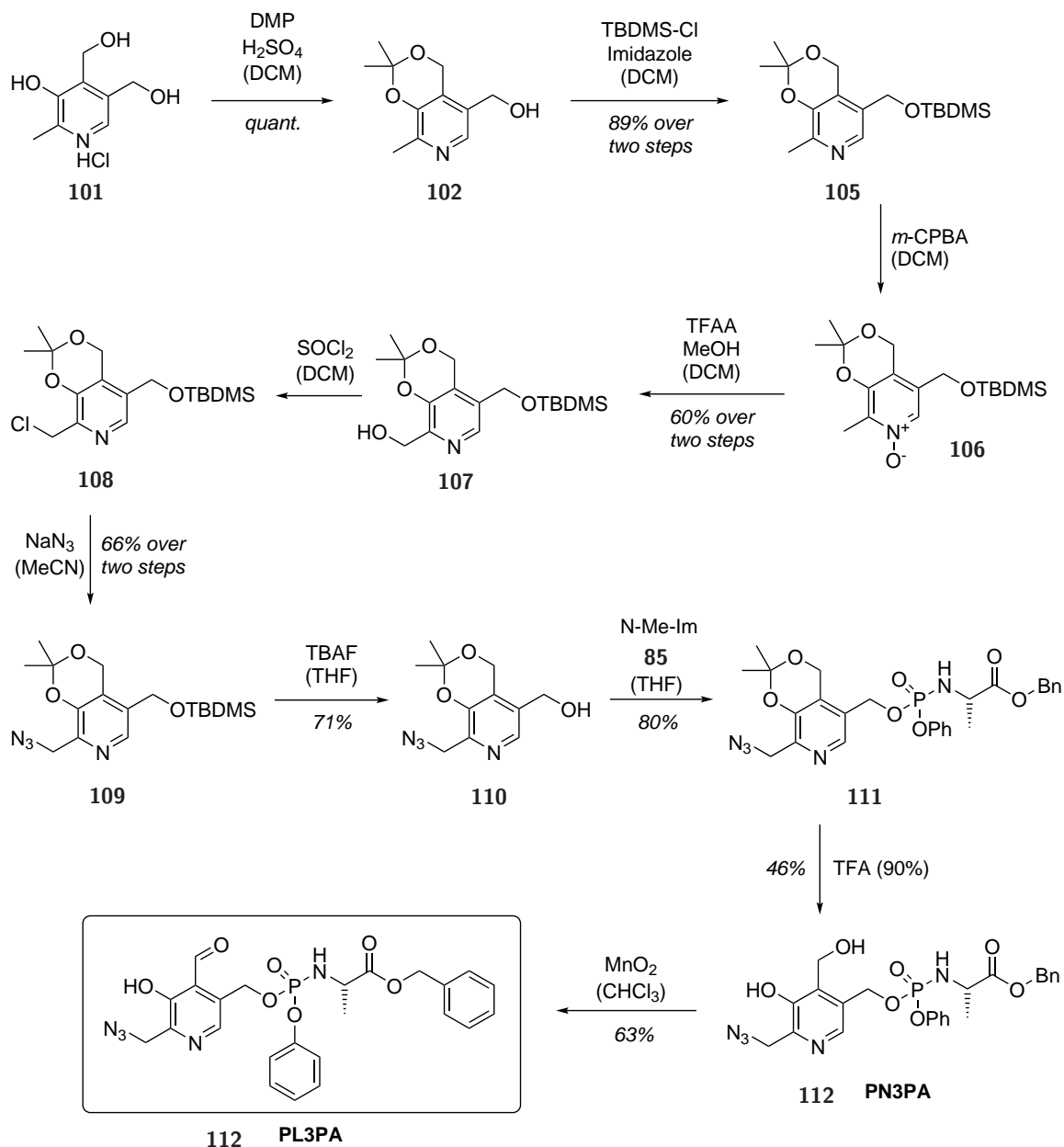
resulted in the phosphoramidate **PLPA** (**99**) in 74% yield (scheme 2.3).



**Scheme 2.3:** PN-HCl is protected as acetonide **102** and subsequently converted to the phosphoramidate species **103**. Deprotection to diol **104** using TFA and further oxidation with MnO<sub>2</sub> yields PL phosphoramidate **PLPA** (**99**).

With this optimised route, a **PL3** derived phosphoramidate synthesis was considered. For this, a different protective group was chosen, because during **PL3** synthesis, the 5'-alcohol protective group, a *para*-methoxybenzyl (PMB) ether, is deprotected in the very last step, which would be insufficient since this position has to be modified prior to re-oxidation of the aldehyde. Therefore, *tert*-butyldimethylsilyl protected acetal **105** was synthesised from alcohol **102** using imidazole as a base. Due to its stability to bases, nucleophiles and oxidation, the TBDMS-group suited perfectly for our purposes.<sup>[239]</sup> The next series of reactions were adapted from the **PL3** synthesis by Hoegl *et al.*<sup>[151]</sup> First, protected acetonide **105** was oxidised to the *N*-oxide **106** using *meta*-chloroperbenzoic acid (*m*-CPBA), which was used directly in the next step without further purification. Subsequently, trifluoroacetic anhydride (TFAA) and methanol were utilised in a BOEKELHEIDE-rearrangement<sup>[216]</sup> yielding 2'-alcohol **107** in 60% over two steps. Activation to the 2'-chloride **108** by thionyl chloride at 0 °C allowed substitution with sodium azide at 100 °C, yielding azide-tagged compound **109** in 66% over two steps. At this stage, the 5'-TBDMS protective group was removed by tetrabutylammonium fluoride (TBAF) giving alcohol **110** in 71% yield. Next, coupling with the reactive phosphorochloridate species **85** gave the protected, azide-tagged

phosphoramidate **111** in 80% yield after purification by flash chromatography. The critical next step was successful for the azide-tagged system, too. Here, diol **112**, termed **PN3PA**, was isolated in 46% yield after stirring acetone **111** in 90% TFA for 2 hours at room temperature. Finally, oxidation by  $\text{MnO}_2$  led to the final **PL**-phosphoramidate probe **PL3PA** (**113**) in a yield of 63% (scheme 2.4).



**Scheme 2.4:** **PN-HCl** (**101**) is first protected as acetone **102**, followed by its benzylic alcohol protection to silyl ether **105**. Oxidation to the *N*-oxide **106** with *m*-CPBA and subsequent BOEKELHEIDE-rearrangement leads to 2'-alcohol **107**. After activation to the chloride **108**, substitution with sodium azide leads to compound **109**. After removal of the TBDMS protective group using TBAF, reaction of alcohol **110** with the phosphorochloridate **85** leads to protected phosphoramidate **111**. Acetone cleavage to precursor **PN3PA** (**112**) and subsequent oxidation by  $\text{MnO}_2$  leads to the formation of final phosphoramidate probe **PL3PA** (**113**).

The  $^{31}\text{P}$ -NMR analysis indicated the presence of two diastereoisomers ( $\approx 1:1$ ) with the chiral center at the phosphorus atom. This is in accordance with other phosphoramidate syntheses.<sup>[231,232,240]</sup> In a total yield of 5.8% over 10 steps, the first described **PL**-phosphoramidate ABPP probe **PL3PA** was synthesised, derived from **PL3**. With the novel **PL3PA** probe, we hope to achieve more efficient enrichment of **PLP**-DEs, particularly in human cells, as we bypass the limitation of their **PLK**. Nevertheless, only a biological evaluation of this probe can reveal its suitability for our purposes, which will be discussed in the next section.

### 2.1.3 Synthesis of Phenelzine Analogues

---

For our screening and competitive labelling experiments, T. E. MAHER synthesised analogues of the hydrazine compound phenelzine, which was shown to be active against *S. aureus*.<sup>[170]</sup> We utilised a protocol by *Prusevich et al.* to synthesise the respective hydrazine compounds **114** from appropriate alkyl halides **115**.<sup>[241]</sup> Hydrazine monohydrate was added to the stirred solution of educt halide **115** in ethanol, and the reaction was refluxed overnight (figure 2.6 A). After purification by preparative reversed-phase high-performance liquid chromatography (HPLC), products were obtained as TFA salts (figure 2.6 B).

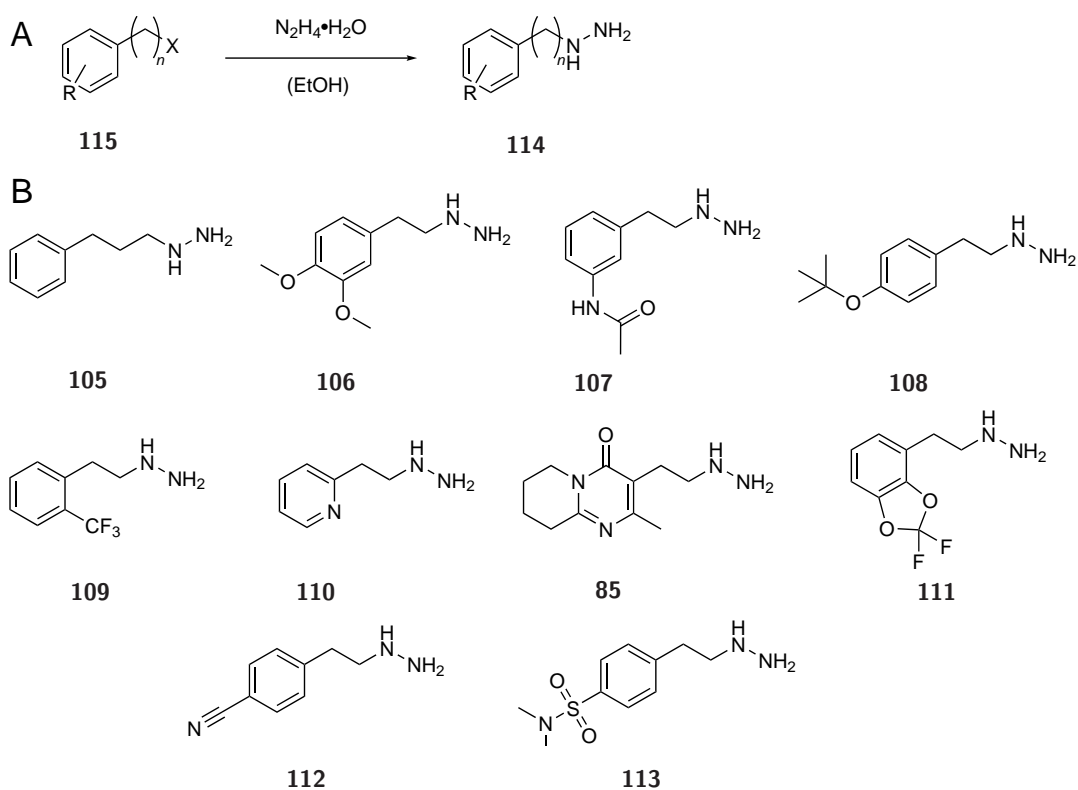


**Figure 2.6:** (A) General synthesis of phenelzine derivatives **114** by substitution of halides **115** by hydrazine.<sup>[241]</sup> (B) Structures of the 10 synthesized phenelzine derivatives.

With these derivatives in hand, the aim was to investigate the influence of structural modifications of phenelzine on the antibiotic activity.

## 2.2 Biological Evaluation of the Probes

The active form of vitamin B<sub>6</sub> is **PLP**, which is phosphorylated from precursors according to figure 1.2. For instance, **PL** is phosphorylated by cellular PLK. Since our **PL**-probes are derived from **PL**, we first investigated whether bacterial kinases are still able to phosphorylate our probes, bearing structural modifications at several sites, into their **PLP** derivatives.

### 2.2.1 Phosphorylation by *pdxK* and SaPLK

The probe phosphorylation was monitored *in vitro* by measuring the UV/Vis absorbance spectra of a mixture of the corresponding probe, the *S. aureus* PLK (*SaPLK*) or the *E. coli* PLK (*pdxK*) and adenosine triphosphate (ATP) in kinase buffer, which contained MgCl<sub>2</sub> for ATP complexation. *pdxK* was cloned and purified from *E. coli*, whereas *SaPLK* was purified from a vector, which was already used in previous studies.<sup>[242]</sup> The spectroscopic properties of **PL** and **PLP** derivatives, which absorb light at around 320 nm and 395 nm, respectively (figure 2.7 A), were already utilised in our earlier study in human cells in order to investigate the phosphorylation turnover of human PLK with **PL1**, **PL2** and **PL3**.<sup>[152]</sup> Similarly, we performed a phosphorylation assay using all 13 **PL**-probes with kinetic intervals of 40 minutes and 20 cycles in total. As an example, **PL2** phosphorylation by *SaPLK* and *pdxK* is depicted in figure 2.7 B and C (all other compounds are shown in figure A.1 and A.2). The absorbance of the unphosphorylated species decreased over time, while the absorbance of the phosphorylated species increased. This two-species state reached an equilibrium during the last few measurements. Probes with larger modifications at the C6-position, like **PL11** and **PL12**, were phosphorylated to a very low extent, as visible in figure 2.7 D, corresponding to *SaPLK* and *pdxK*, respectively. Moreover, *SaPLK* seemed to be less restricted in substrate specificity, as the overall phosphorylation efficiency was higher. Nevertheless, *pdxK* showed higher phosphorylation efficiency for **PL13** while **PL9** showed significantly different phosphorylation, too.

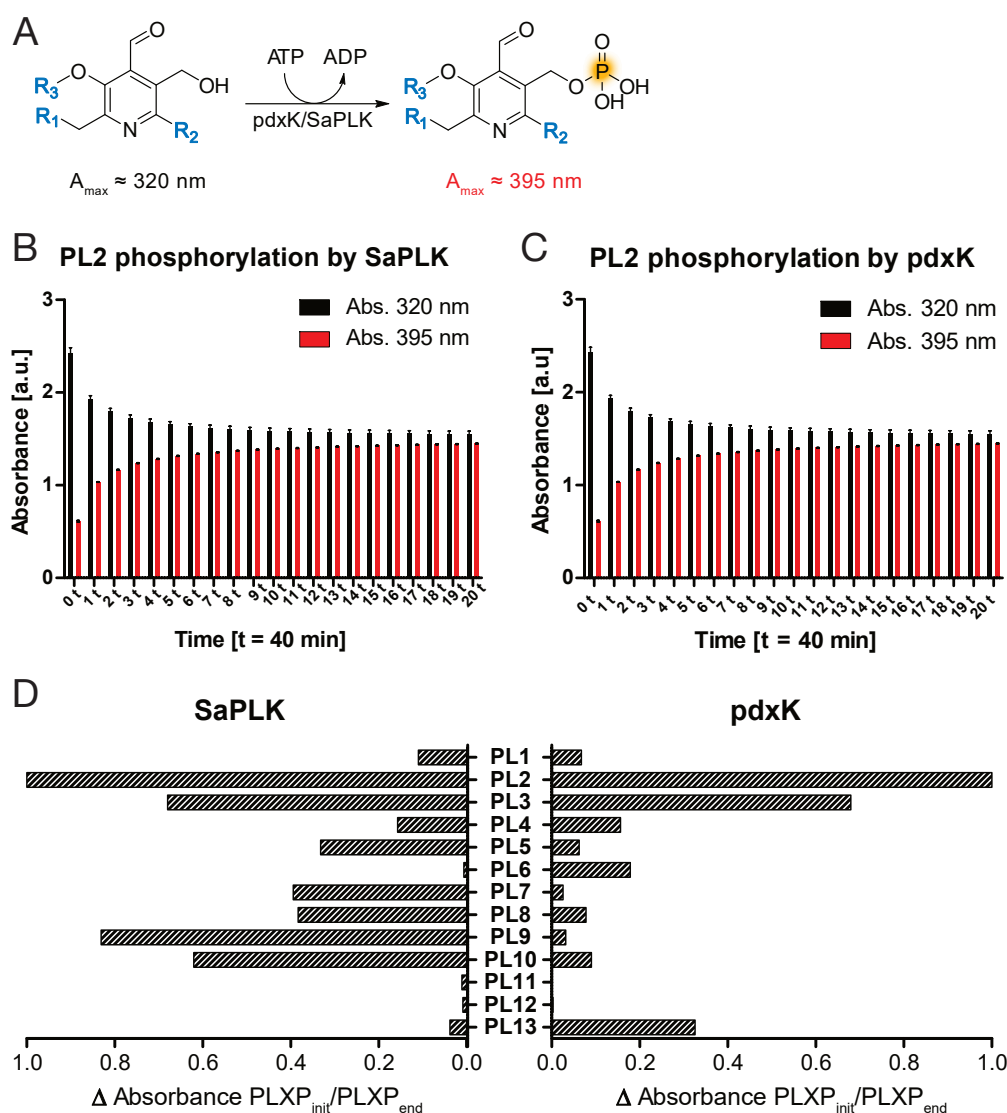


**Figure 2.7:** (A) Activation of **PL**-probes by pyridoxal kinases *pdxK* or *SaPLK* was monitored by measuring UV/Vis absorbance over time. (B) Phosphorylation of **PL2** by *SaPLK* (measurement every 40 min, 20 cycles,  $n = 3$ , mean  $\pm$  SEM). (C) Phosphorylation of **PL2** by *pdxK* (measurement every 40 min, 20 cycles,  $n = 3$ , mean  $\pm$  SEM). (D) Qualitative comparison of **PL** probe phosphorylation efficiency. Here, the difference of initial and final absorbance at wavelengths of the respective phosphorylated compound is depicted. For **PL6** *SaPLK* phosphorylation, the difference of initial and final absorbance at wavelengths of the unphosphorylated compound is depicted. For **PL13**, phosphorylated compound absorbed at 320 nm and unphosphorylated at wavelengths outside the measuring range. Adapted from *Pfanzelt et al.*<sup>[170]</sup>

We detected phosphorylation of most of our probes *in vitro*, which is a prerequisite for efficient labelling of **PLP**-DEs. The next evaluation step of our library was the supplementation of **PLP** by our probes in a **PLP** *de novo* synthesis knockout strain *E. coli* K12 in order to show, that our probes can function as cofactor surrogates.



### 2.2.2 Growth Studies

Similar to our previous study in *S. aureus*, we utilised a single-gene knockout mutant of *E. coli* K12, termed *E. coli* K12  $\Delta$ pdxJ, lacking **PLP** *de novo* synthesis. To generate this knockout mutant, the pyridoxine 5'-phosphate synthase *pdxJ* was disrupted by inserting a kanamycin cassette into the open-reading frame (ORF) of *pdxJ* (originated from the *Keio collection*, kindly provided by PROF. K. JUNG from the LMU, Munich).<sup>[243]</sup> This organism was chosen not only in order to apply our strategy to other bacteria, but especially to GRAM-negative ones, known to be challenging to address. Unlike GRAM-positive bacteria, GRAM-negatives possess a second membrane. These two membranes often block the uptake of small molecules.<sup>[244–246]</sup> Prior to growth experiments, the correct knockout insertion was verified by colony PCR, confirming the insertion of the kanamycin resistance cassette in the correct ORF (data not shown). For growth studies, bacteria were grown in chemically defined media (CDM)<sup>[247]</sup> lacking **PL** supplemented with certain concentrations of natural **PL** or probe in a 96-well plate. The absorbance was measured at 600 nm every 30 minutes for 24 hours. Probes **PL1**, **PL2**, **PL3**, **PL6**, **PL8**, **PL10** and **PL13** were tested (figure 2.8, figure A.3).

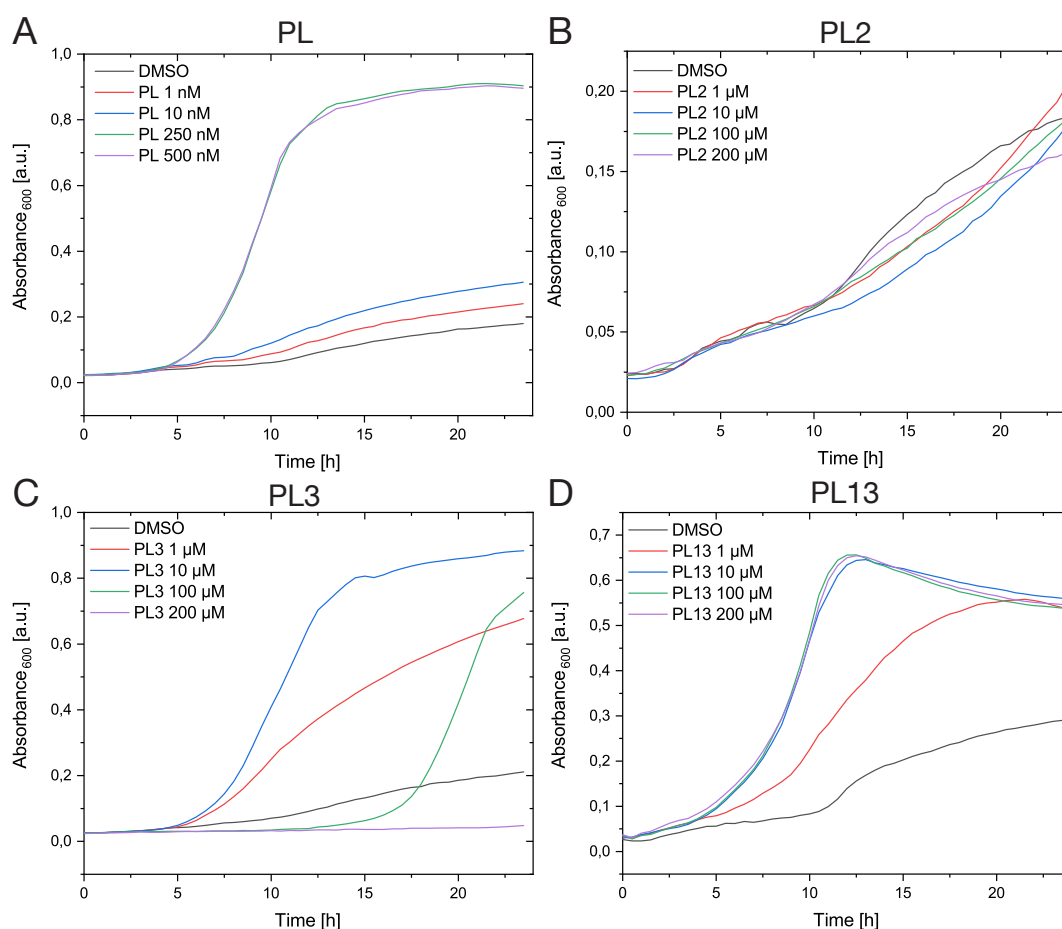


**Figure 2.8:** Growth of *E. coli* K12  $\Delta$ pdxJ in CDM supplemented with different concentrations of **PL** (A), **PL2** (B), **PL3** (C) and **PL13** (D). Adapted from Pfanzelt *et al.*<sup>[170]</sup>

Bacteria grew normally in CDM supplemented with natural **PL** at a concentration of 250 nM or more. On the contrary, they were not able to grow on **PL2** supplementation, a finding we also observed for the *S. aureus* transposon mutant in our previous studies.<sup>[151]</sup> While *E. coli* could grow on 10  $\mu$ M **PL3** to the same extent as with natural **PL**, higher concentrations (100 and 200  $\mu$ M) showed toxic effects. Surprisingly, **PL13** supplementation led to normal growth from 10  $\mu$ M or more. These results corroborate two important findings: First, the knockout mutant is clearly dependent on **PL** supplementation. Second, some of the probes are able to function as replacements for natural **PL**. Even though bacteria could not grow on some of the probes, they still fulfil their purpose as we already exemplified in previous *S. aureus* **PL2** labelling.<sup>[151]</sup> Some **PLP**-derivatives are unable to support enzymatic catalysis but are able to bind to certain **PLP**-DEs (see section 2.1).<sup>[34,203,209,214,215,248]</sup>

However, since the amount of probes needed for full growth are synthetically impractical, we decided to adopt the previously used strategy in which the bacteria are first grown to stationary phase in media containing **PL** and then transferred into media supplemented with the respective probe instead of **PL**.<sup>[151,248]</sup> Since full media, like

B-medium, contain yeast extract, a quantitative control of the vitamin B<sub>6</sub> amount is not feasible. In a summary table of dried yeast extract ingredients by *Tomé et al.*, 100 g of yeast extract is said to contain 8 mg of vitamin B<sub>6</sub>.<sup>[249]</sup> The B-medium used in this study contains 0.5% yeast extract, leading to an approximate vitamin B<sub>6</sub> concentration of 1.2  $\mu$ mol. This is almost 5 times higher than our obtained 250 nM **PL**-concentration, which was needed for full growth.

We therefore anticipated that lowering the concentration of endogenous **PL** in growth media would in turn maximize the incorporation of our **PL**-probes into **PLP**-DEs in our *in vivo* labelling setting. As we observed in growth studies, 250 nM of **PL** is the minimal concentration, which provided normal growth. We subsequently established growth conditions for all strains investigated in this study. For all strains, no matter if wild type or mutant, cultivation with a suitable CDM supplemented with 250 nM **PL** resulted in reliable growth and sufficient amount of bacteria for preparative labelling experiments (figure A.4).<sup>[170]</sup>

With the optimised growth conditions in hand, we first performed analytical labelling experiments in *E. coli* (**PL3** and **PL13**). Secondly, we optimised our previously published preparative labelling conditions in the *S. aureus* transposon mutant and compared different probe concentrations as well as two different media.

### 2.2.3 Analytical Labelling

---

As described in figure 1.8, fluorophores as reporter groups allow the visualisation of labelled proteins after SDS-PAGE.<sup>[250,251]</sup> To assess our experimental setup, we performed gel-based labelling in both *E. coli* K12 wild type (wt) and knockout strain. After growth of bacteria in CDM and labelling with probes **PL3** and **PL13** in **PL**-free CDM, bacteria were lysed and internal aldimines were reduced by NaBH<sub>4</sub>. Upon STAUDINGER-ligation with rhodamine phosphine (**PL3**) or CuAAC to rhodamine azide (**PL13**), several labelled proteins could be visualised by fluorescence scanning (figure 2.9).<sup>[170]</sup>

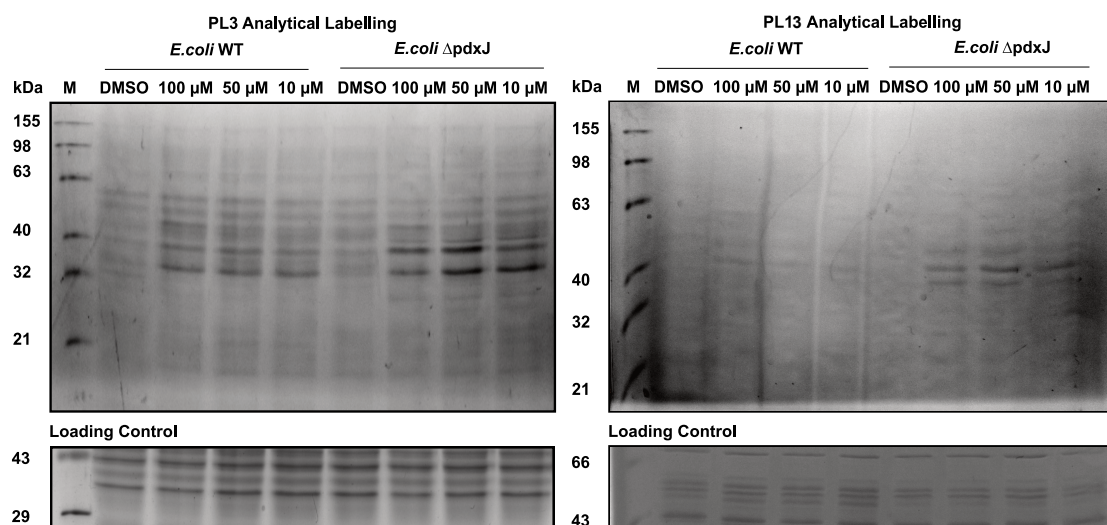


**Figure 2.9:** Analytical, gel-based labelling of **PLP**-DEs in *E. coli* wt and  $\Delta$ pdxJ at different **PL3** and **PL13** concentrations. Equal protein concentrations after gel loading was confirmed by Coomassie gel staining (Loading Control). Adapted from Pfanzelt *et al.*<sup>[170]</sup>

For both probes, bands are visible at probe concentrations of  $10 \mu\text{M}$  or more, at least in the knockout strain. Interestingly, **PL3** was able to compete with endogenous **PLP**, indicated by specific bands in the *E. coli* wt samples. In case of **PL13**, the probe did not seem to be able to replace natural **PLP**, resulting in no clearly visible fluorescent bands in the wt samples.

#### 2.2.4 A Refined Preparative Labelling Strategy

As our previous study concentrated on the *S. aureus* **PLP**ome, we wanted to optimise our previous labelling strategy regarding probe concentration and growth medium. Thus, we tested the effect of **PL2** concentration at 10 and  $100 \mu\text{M}$  and B-medium vs. CDM on the labelling efficiency in *S. aureus* USA300 TnpdxS. Interestingly, we could increase the number of significantly enriched **PLP**-DEs from 20 (B-medium,  $100 \mu\text{M}$  **PL2**)<sup>[151]</sup> to 27 in CDM with  $100 \mu\text{M}$  **PL2** (figure 2.10). This benchmark experiment confirmed  $100 \mu\text{M}$  as optimal probe concentration as well as growth of bacteria in CDM (the labelling time of 2 hours has not been changed, since it was shown, that almost 100% of **PL2** was metabolised into **PL2P** after this time<sup>[151]</sup>). Enrichment of more enzymes was even achieved with  $10 \mu\text{M}$  **PL2** in CDM compared to  $100 \mu\text{M}$  of the probe in B-medium. These optimised conditions will be adopted for all further labelling experiments.

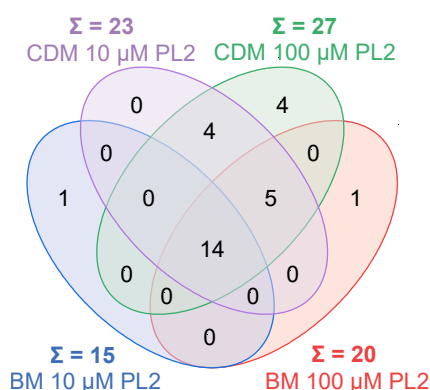


**Figure 2.10:** Comparison of enriched **PLP**-DEs in *S. aureus* using different media (B-medium, BM or chemically defined medium, CDM) and different **PL2** concentrations (10 and 100  $\mu\text{M}$ ). Enrichment compared to DMSO representing the  $t$ -test results [criteria:  $\log_2(\text{enrichment}) > 1$  and  $p$ -value  $< 0.05$ ,  $n = 3$ ]. Adapted from Pfanzelt et al.<sup>[170]</sup>

This observation confirmed our previous assumption, that lowering the **PL** amount in the growth phase has a positive impact on the later incorporation of cofactor mimics.

### 2.2.5 The Pro-Tide Probe PL3PA

The pro-tide probe **PL3PA** was primarily developed to tackle the phosphorylation issues in human cells. However, before applying the probe in HeLa cells, we investigated its ability to support bacterial growth, similar to other **PL**-probes as discussed before.

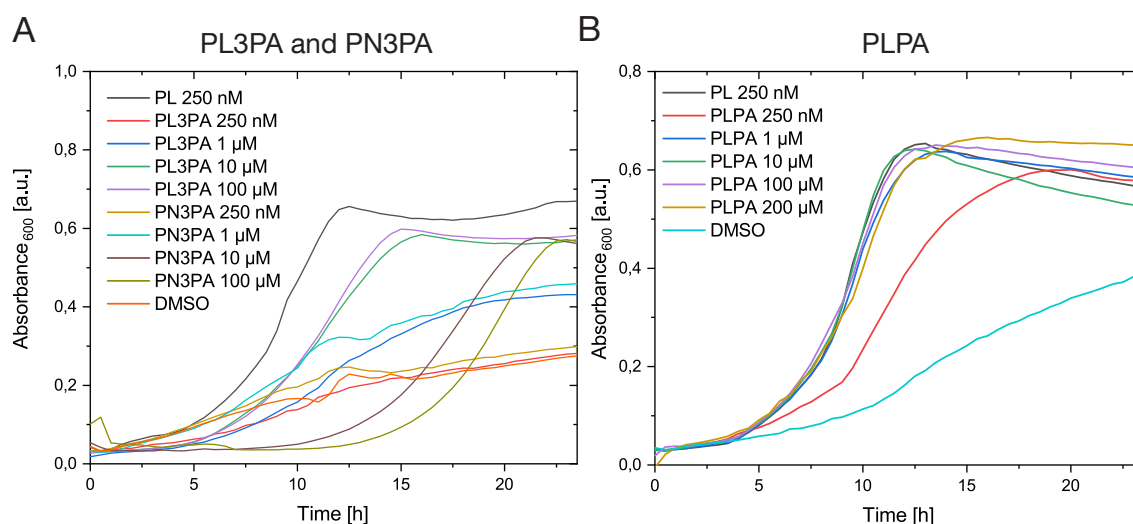


**Figure 2.11:** Growth of *E. coli* K12  $\Delta\text{pdxJ}$  in CDM supplemented with different concentrations of **PL3PA**, **PN3PA** (A) and **PLPA** (B).

We therefore supplemented *E. coli* K12  $\Delta\text{pdxJ}$  in CDM with various **PL3PA** con-

centrations. Simultaneously, we applied the precursor compound **PN3PA** and the minimal pro-tide **PLPA** to the bacteria for comparison (figure 2.11).

**PL3PA** at 10 and 100  $\mu\text{M}$  supports growth almost to the same extent as natural **PL**, though with a delay in time. Interestingly, at 10 and 100  $\mu\text{M}$  **PN3PA** supplementation there is a lag in bacterial growth, similar to the one at high **PL3** concentrations (figure 2.8 C). While in the case of **PL3** this effect is most likely due to toxic effects, in the case of **PN3PA** a lack of oxidation to the aldehyde could be responsible for the delayed growth. Nevertheless, this hypothesis was never proved. The **PL**-phosphoramidate without tag, **PLPA**, was able to support sufficient growth from 1  $\mu\text{M}$  or more, representing the four-fold concentration of natural **PL** needed for full growth. This fact could be explained by the cleavage of the phosphoramidate, which is a time consuming step.<sup>[252]</sup>

However, with this data in bacteria no conclusions could be drawn regarding the selectivity of the phosphoramidate cleavage, nor the fact, that those compounds get cleaved at all in bacteria.

As a next step, we performed gel-based analytical labelling in HeLa cells. For this experiment, confluent cells were treated with 10, 50 or 100  $\mu\text{M}$  **PL3PA** for 1.5 hours or overnight. Furthermore, labelling after various incubation times at 50  $\mu\text{M}$  **PL3PA** was conducted as well (0.5, 1.5, 3 and 6 hours), which is shown in figure 2.12.

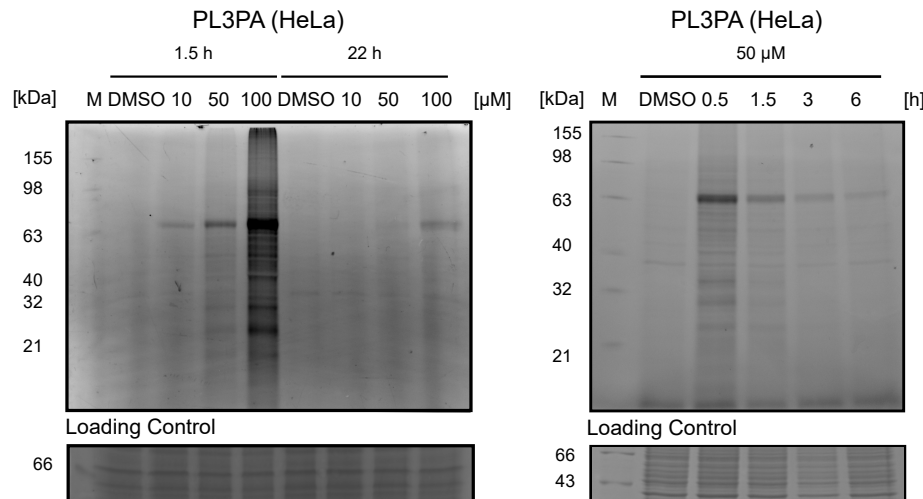
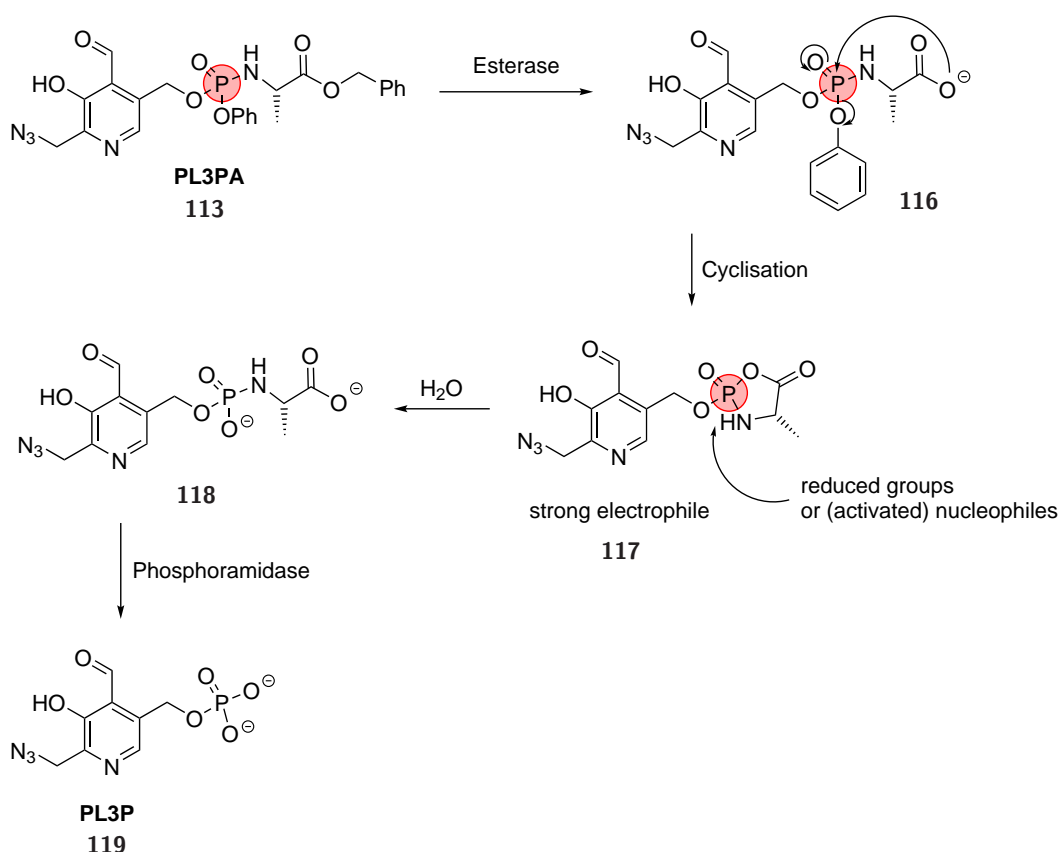


**Figure 2.12:** Analytical labelling of HeLa cells with **PL3PA** using different concentrations at 1.5 h and 22 h incubation time (left) or different incubation times (right) at 50  $\mu\text{M}$  probe. Equal protein concentrations after gel loading was confirmed by Coomassie gel staining (Loading Control).

Here, STAUDINGER-ligation with rhodamine-phosphine was performed after labelling, lysis and reduction with  $\text{NaBH}_4$ . Satisfyingly, in the negative control (DMSO), no band was visible, indicating low side reactivity. Moreover, increasing concentrations of **PL3PA** resulted in a higher intensity of labelled protein bands. Labelling time investigation revealed a decrease in labelling over time, whereas after 0.5 hours, most

intense labelling was observed. This unexpected observation is still not fully understood, but a possible explanation will be given after discussing the preparative labelling in HeLa cells with the pro-tide probe **PL3PA**. After labelling of confluent cells with  $50\ \mu\text{M}$  **PL3PA** for 30 minutes, we further followed the protocol by *Fux et al.* for the downstream processing of samples.<sup>[152]</sup> The MS analysis provided almost 1000 proteins, which were significantly enriched by **PL3PA**. However, a closer analysis of the enriched proteins is not meaningful due to the low selectivity of the probe. A possible explanation for the high number of enriched proteins is difficult, however, one property of the probe could cause an enrichment of many proteins within a certain time frame. As detected in the analytical labelling, the intensity of bands decreases over time. Since we added sodium borohydride immediately after labelling, there could have been an activation of several protein residues that could have nucleophilically attacked the still uncleaved phosphoramidate molecules, which would have resulted in an enrichment of a huge number of proteins (scheme 2.5). Especially the probe itself (**113**), the benzyl-ester cleaved intermediate **116** and the heterocycle **117** are highly electrophilic and presumably reactive towards nucleophiles.



**Scheme 2.5:** The three electrophilic species **113**, **116** and **117** could be responsible for side reactions with protein residues causing a high number of enriched proteins in our labelling experiment in HeLa cells. A short labelling time is therefore not sufficient for our purposes.

We did not test a different labelling time thus far, but the longer the probe is present in

the cells, the more active **PL3P** should be formed which in turn should result in more specific labelling. For future experiments, it would be reasonable to first investigate the **PL3PA**-cleavage with purified enzymes *in vitro* before improving the labelling conditions. Another possibility would be the metabolic quantification of **PL3P** (**119**) after certain dwell times of the parent probe **PL3PA** in the cells. Here, one could identify the appropriate time with the highest **PL3P** concentration.



## 2.3 PLPome Profiling

All synthesised **PL**-probes were evaluated regarding their suitability for *in vivo* proteomics experiments. *In vitro* phosphorylation studies revealed efficient phosphorylation of most of the probes by *S. aureus* and *E. coli* pyridoxal kinases. Moreover, applicability of **PL** probes as cofactor substitutes was elucidated *via* bacterial growth studies in the *E. coli* knockout mutant. Further, gel-based labelling experiments confirmed the ability of selected probes to function as **PLP**-DE detection handles *in situ*. With this evaluation data in hand, we followed up with MS-based proteomics in order to investigate **PLP**-DEs in *S. aureus* USA300 TnpdxS, *E. coli* K12  $\Delta$ pdxJ and *P. aeruginosa* PAO1 wt.

### 2.3.1 *S. aureus* PLPome

Following our chemical proteomic protocol<sup>[151]</sup> with the refined parameters, we first investigated the *S. aureus* USA300 TnpdxS **PLP**ome with all of our **PL**-probes. Cells were grown in CDM for 10 hours to stationary phase, incubated with 100  $\mu$ M probe for 2 hours, lysed using Lysostaphin and internal aldimins were reduced using NaBH<sub>4</sub>. Upon precipitation of proteins, CuAAC to biotin-azide or STAUDINGER-ligation to biotin-phosphine (in case of **PL3**) allowed enrichment of the labelled proteome *via* avidin-beads. Tryptic digest followed by LC-MS/MS analysis and subsequent LFQ-quantification<sup>[174]</sup> revealed characteristic patterns of significantly enriched **PLP**-DEs [cut-off criteria:  $\log_2 = 1$  (2-fold enrichment) and  $p$ -value  $< 0.05$ ] which are visualized in corresponding volcano plots individually (figure 2.13 A, figure A.5) as well as summarised in a heatmap (figure 2.13 B). Notably, we were able to significantly enrich 71% of the known and predicted **PLP**ome including 7 additional proteins representing a remarkable improvement by our refined strategy and extended probe library. Our expectations were exceeded by the fact that it was possible to achieve specific labelling of certain **PLP**-DEs with individual probes. Among the enriched enzymes was the cystein biosynthesis enzyme cystein synthase (*A0A0H2XG73*, *cysK*, 13)<sup>[253]</sup>, which was detected the first time with **PL10**. Moreover, enzymes such as the Cys/Met metabolism enzyme *A0A0H2XFH9* (7) or the essential *A0A0H2XGZ5* (16), a gluconate operon transcriptional repressor<sup>[254]</sup> were detected. Additionally, an uncharacterised helix-turn-helix (HTH) type transcriptional regulator<sup>[65]</sup> *A0A0H2XF80* (2), found by **PL12** and **PL13**, as well as *A0A0H2XHJ5* (21), an uncharacterised **PLP**-DE, found by **PL1**, **PL2**, **PL3** and **PL10**, which is essential for growth<sup>[254]</sup> were enriched with our **PL**-probes.

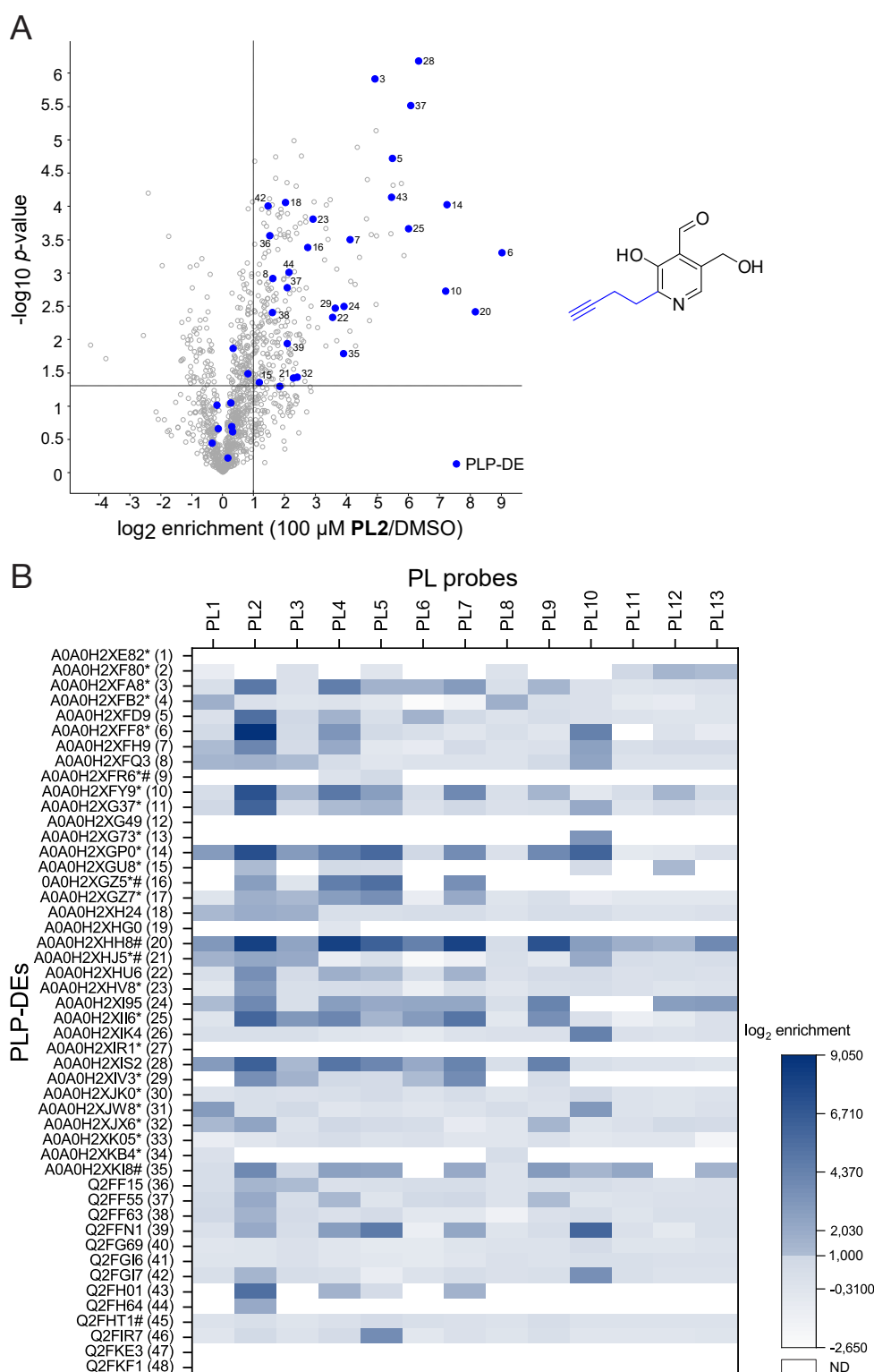


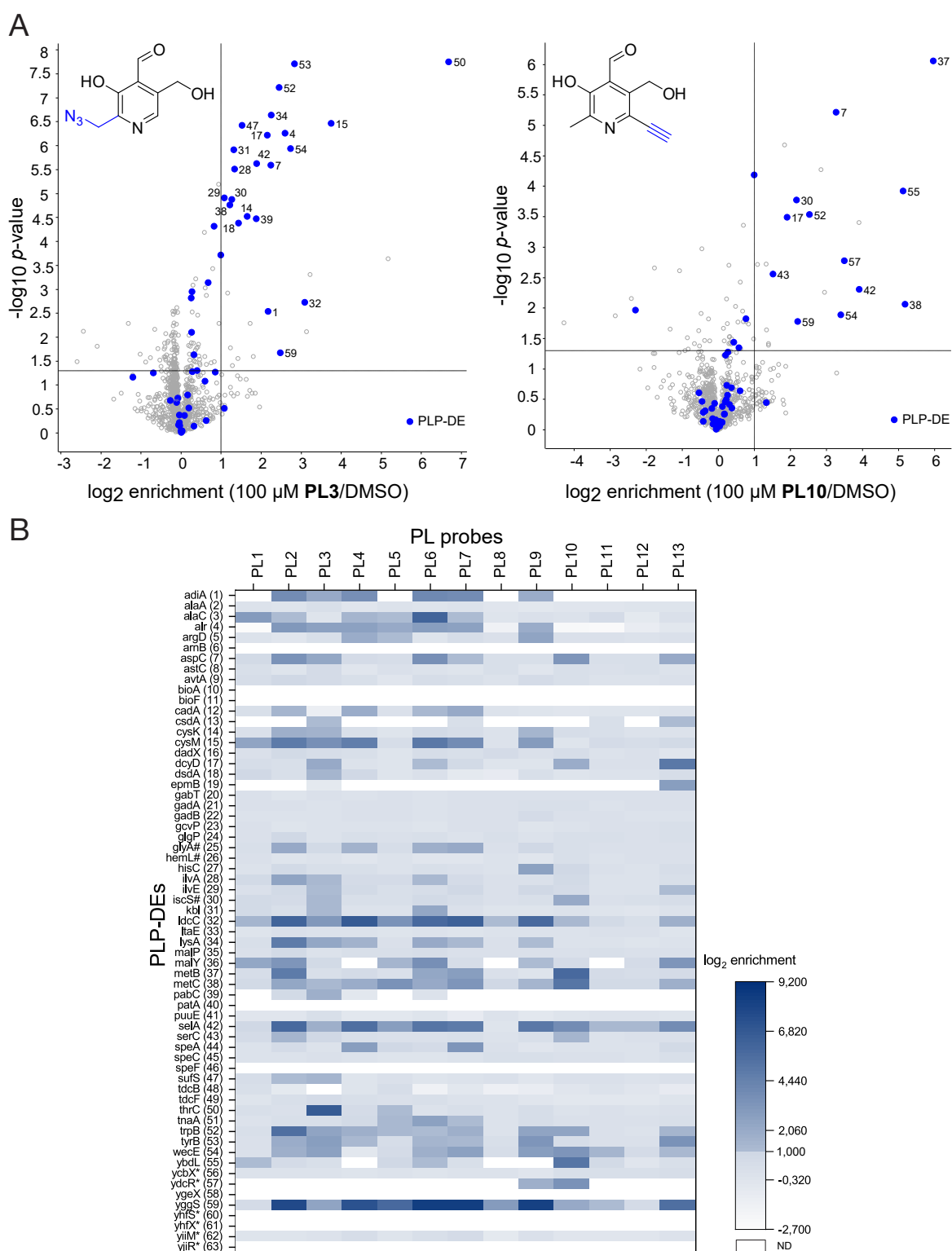
**Figure 2.13: (A)** Volcano plot of **PL2** enrichment at 100  $\mu\text{M}$  in *S. aureus* USA300 TnpdXS compared to DMSO representing the *t*-test results [criteria:  $\log_2(\text{enrichment}) > 1$  and  $p\text{-value} < 0.05$ ,  $n = 3$ ]. Blue colours depict **PLP**-DEs. Assigned numbers refer to table A.1. Remaining plots are shown in figure A.5 **(B)** Heatmap representing  $\log_2(\text{enrichment})$  values of all known or putative **PLP**-DEs in *S. aureus* for all 13 **PL**-probes ( $n = 3$ ). Enriched proteins have  $\log_2(\text{enrichment})$  values higher or equal 1. Not detected (ND) proteins are coloured white. **PLP**-DEs with a putative function or which are poorly characterised are marked with an asterisk. Essential enzymes are marked with a #.<sup>[254]</sup> This annotation is based on a recent literature research. Adapted from Pfanzelt *et al.*<sup>[170]</sup>

With the overall improvement of the **PLP**-DE detection in *S. aureus*, we next started to analyse the **PLP**ome of more challenging GRAM-negative bacteria. To face this challenge, we first utilised the *pdxJ* single-gene knockout mutant of *E. coli* K12.<sup>[243]</sup>

### 2.3.2 *E. coli* PLPome

Applying the same refined strategy in *E. coli* led to a significant enrichment of 38 **PLP**-DEs representing 61% of the known or predicted *E. coli* **PLP**ome for the first time (figure 2.14).<sup>[11,64]</sup> The overall coverage reflects the individual labelling preferences of our 13 **PL**-probes. This fact highlights that the structural variety of the probes is a prerequisite to address various binding sites of **PLP**-DEs. Similar to the *S. aureus* **PLP**ome profiling, relevant subclasses of **PLP**-DEs could be accessed with our new **PL**-probes, which would otherwise not have attracted our attention. Again, many newly detected **PLP**-DEs fulfil essential functions, such as *alaC* (3), an aminotransferase involved in alanine biosynthesis<sup>[255]</sup>, enriched by **PL6**, *iscS* (30), an essential cysteine desulfurase<sup>[256]</sup>, and *metB* (37), a cystathionine gamma-synthase involved in methionine biosynthesis<sup>[257]</sup>, both exclusively enriched by **PL10**. Again, structural modifications at the **PL** scaffold, such as the C6-derivative **PL10**, complement our detection mimics by satisfying structural preferences of certain **PLP**-DEs. Remarkably, this probe was also able to detect and enrich a putative HTH-transcriptional regulator, termed *ydcR* (57). Along with *yjiR* (63), *ydcR* is one of the two putative TR's in *E. coli*.<sup>[11]</sup> Since **PLP**-DEs in *E. coli* are quite well investigated, we focused on the characterisation of *ydcR*, which will be discussed later.

Overall, we managed to access the **PLP**ome of *E. coli* as a model GRAM-negative organism using our refined labelling protocol and the versatile **PL**-probe library. We not only covered a large number of **PLP**-DEs but could also show the added value of our method. Next, we tried to decipher whether our set of probes is able to compete with endogenous **PL** in an wild type strain without having its **PLP** *de novo* synthesis eliminated. Addressing this exciting question, we utilised *P. aeruginosa* PAO1, a critical pathogenic bacterial strain, causing many deaths mainly due to its antibiotic muliresistancy.<sup>[258,259]</sup> Especially in those strains, functional assignment of poorly characterised protein classes is urgently needed. The goal of this task is to find novel, unprecedented modes-of-action beyond the scope of well known drug targets.



**2.3.3** *P. aeruginosa* Wild Type PLPome

*P. aeruginosa* is one of the ESKAPE-pathogens, an acronym for multiresistant bacterial strains. The group includes *Enterococcus faecium*, *Staphylococcus aureus*, *Klebsiella pneumoniae*, *Acinetobacter baumannii*, *Pseudomonas aeruginosa* and *Enterobacter spp.*<sup>[258]</sup> Similar to *E. coli*, *P. aeruginosa* has two cell membranes, which hamper the uptake of small molecules tremendously.<sup>[244–246]</sup> Due to the lack of a suitable transposon mutant or knockout strain of *P. aeruginosa*, we deliberately utilised the wild type strain for our **PLP**ome profiling. Since most of the **PLP**-DEs we have investigated so far were detected by **PL1**, **PL2**, **PL3**, **PL6**, **PL10** and **PL13**, we used this set of six probes for mining the *P. aeruginosa* **PLP**ome. Satisfyingly, applying our refined labelling conditions enabled the enrichment of 51% of the known and predicted *P. aeruginosa* **PLP**ome (figure 2.15).<sup>[64]</sup> Here, **PL2**, **PL6** and **PL10** contributed the most to the overall coverage. Among the hits were *aruH* (4), an aminotransferase involved in arginine degradation<sup>[263]</sup>, enriched by **PL10** and *PA0394* (35), known as a **PLP** homeostasis protein<sup>[63]</sup>, which was enriched with **PL2** and **PL6** and homologue proteins were also highly enriched in *S. aureus* (*A0A0H2XHH8*) and *E. coli* (*yggs*). Moreover, *ilvA2* (24), a threonine dehydratase inferred from homology<sup>[66]</sup>, was highly enriched by **PL13** and *PA5313* (68), a putative **PLP**-dependent aminotransferase<sup>[65,66]</sup>, was only enriched by **PL10**. Interestingly, **PL10** attracted attention by its ability to enrich putative or known transcriptional regulators. Differing from *E. coli*, where only two TRs are known, *P. aeruginosa* has a lot more. Among them, **PL10** could detect *PA2032*, *PA2100*, *PA2897* and *PA5283*.<sup>[65]</sup> This obtained selectivity could be caused by extra space in the active site of this enzyme class, allowing C6-derivatives of **PL** to bind selectively.

All three **PLP**ome profiling experiments demonstrate that our **PL**-probes are able to enter both GRAM-positive and -negative bacteria, are then further activated by cellular PLKs to the active cofactor mimics, which can compete with endogenous **PLP** and finally bind to **PLP**-DEs. These internal aldimines can then be trapped by reduction and after enrichment, **PLP**-DEs can be analysed by LC-MS/MS. Having all these data in hand, we continued to pursue one of our main goals, the characterisation of unknown or poorly characterised/putative **PLP**-DEs, which will be the topic of the next section.

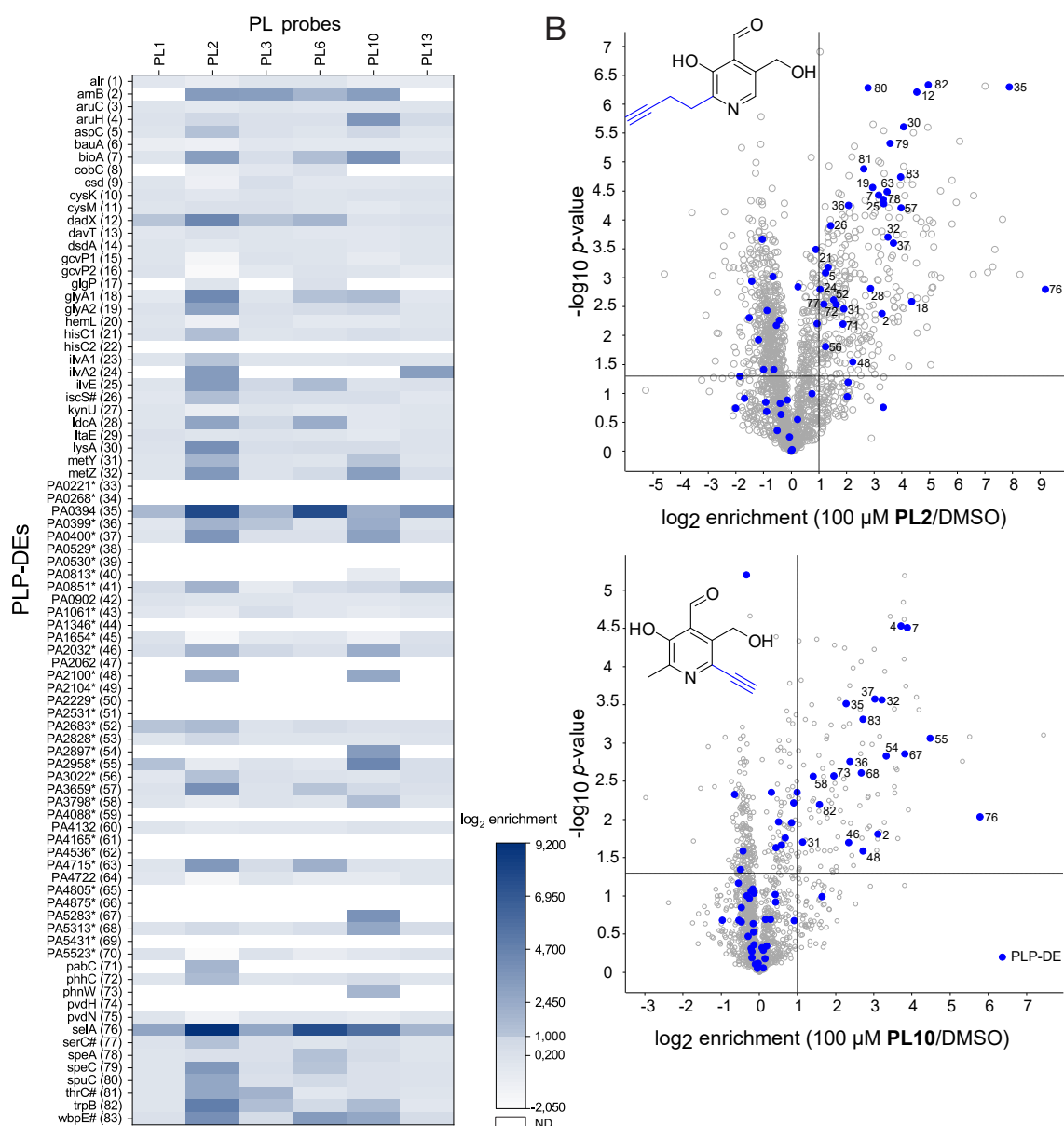


**Figure 2.15:** (A) Heatmap representing  $\log_2(\text{enrichment})$  values of all known or putative PLP-DEs in *P. aeruginosa* PAO1 for 6 selected PL-probes ( $n = 3$ ). Enriched proteins have  $\log_2(\text{enrichment})$  values higher or equal 1. Proteins not detected (ND) at all are coloured white. PLP-DEs with a putative function or which are poorly characterised are marked with an asterisk. Essential enzymes are marked with a #. This annotation is based on a recent literature research. (B) Volcano plot of PL2 and PL10 enrichment at 100  $\mu\text{M}$  in *P. aeruginosa* PAO1 compared to DMSO representing the  $t$ -test results [criteria:  $\log_2(\text{enrichment}) > 1$  and  $p\text{-value} < 0.05$ ,  $n = 3$ ]. Blue colours depict PLP-DEs. Assigned numbers refer to table A.3. Remaining plots are shown in figure A.7. Adapted from Pfanzelt *et al.*<sup>[170]</sup>

## 2.4 Validation Experiments

A large proportion (30-40%) of genes in all genomes lack functional assignment or is only poorly characterised.<sup>[264]</sup> This also applies to genes encoding **PLP**-DEs. Sequence-based classification of these enzymes has led to the fold-type classification without involving their catalytic function.<sup>[55]</sup> In contrast to this approach, *Perduciani and Peracchi* improved the functional assignment of **PLP**-DEs utilising reference search models, which resulted in a detailed genomic overview.<sup>[62]</sup> Their studies further resulted in the valuable vitamin B<sub>6</sub> database, which lists not only the current number of catalytic activities of **PLP**-DEs, but also their families, sequences and all corresponding references.<sup>[22]</sup> Furthermore, *Fleischman et al.* utilised different methods, including secondary structure matching (SSM) using the PDBeFold service in order to characterise three aminotransferases from the human microbiom.<sup>[147]</sup> This structural alignment again demonstrated the similarity of active sites of **PLP**-DEs, at least among same reaction type classes, such as aminotransferases. Among others, classical methods to study **PLP**-DEs include UV/Vis spectroscopy, since the enzymes show characteristic absorbance spectra depending on their binding mode. For instance, internal aldimines (330-360 nm; 420-430 nm) show different absorbance maxima in contrast to quinonoids ( $\approx$ 500 nm), external aldimines ( $\approx$ 430 nm) or **PMP** (330 nm).<sup>[213]</sup> Several studies could qualitatively show substrate specificities of aminotransferases by investigating changes in the UV/Vis spectrum after adding possible substrates.<sup>[147,151,213,265]</sup> Another possibility is the LC-MS(/MS) based determination of reaction products upon incubating unknown **PLP**-DEs with substrate libraries. A more complex *in vitro* method is named activity-based metabolomic profiling (ABMP), where the protein of interest is incubated with a metabolome extract.<sup>[248]</sup> Changes in metabolite levels can then be measured by LC-MS(/MS).<sup>[266]</sup> In 2017, *Sévin et al.* could characterise a unknown pyridoxine dehydrogenase (*pdxI*) from *E. coli* utilising ABMP.<sup>[267]</sup> Together with our **PLP**ome profiling tool, we attempt to verify **PLP** binding as well as catalytic insights of several putative **PLP**-DEs detected in our experiments.

A closer look at the enrichment data revealed a series of uncharacterised or poorly characterised proteins. All of them were at least annotated as putative **PLP**-binders (by *UniRule*<sup>[63]</sup>, *UniProt*<sup>[64]</sup>, *InterPro*<sup>[65]</sup> or *GO*<sup>[66]</sup>). We have then chosen proteins with the lowest annotation state on *UniProt*<sup>[64]</sup> and cloned and overexpressed these proteins in *E. coli* BL21 DE3 expression strains. After successful purification, proteins were first measured in an intact-protein mass spectrometry (IP-MS) experiment in order to confirm their identity as well as **PLP**-binding. For this, 10  $\mu$ M of the corresponding apo-enzyme was measured without and with additional NaBH<sub>4</sub>, in order to reduce the internal aldimine (figure 2.16).

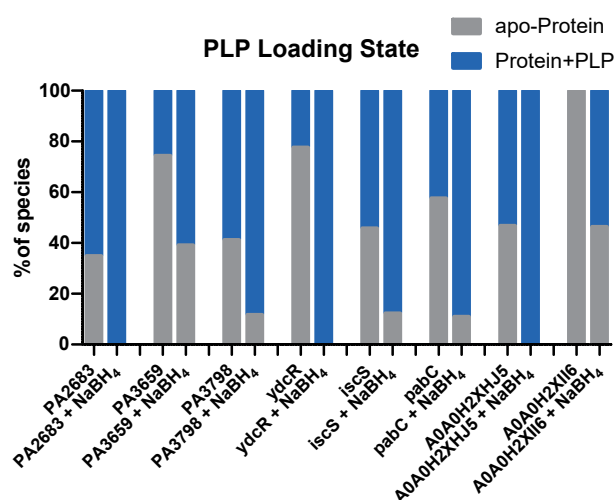


**Figure 2.16:** PLP loading states of overexpressed proteins were determined by intact protein MS (IP-MS). All proteins have **PLP** bound after purification (blue). This proportion can be increased by adding NaBH<sub>4</sub> due to reduction of the internal aldimine. Adapted from Pfanzelt et al.<sup>[170]</sup>

For further characterization, the proteins *PA3659* and *PA3798*, two putative aminotransferases and *PA2683*, a probable Ser/Thr dehydratase, all three from *P. aeruginosa* were selected. Additionally, *ydcR*, a putative HTH-type transcriptional regulator from *E. coli* as well as *A0A0H2XHJ5*, a putative cystein desulfurase from *S. aureus* were investigated in more detail.

### 2.4.1 The Aminotransferases *PA3659* and *PA3798*

Aminotransferases (ATs) belong either to the fold-type I or IV group and catalyse the stereoselective transfer of an amino group from an amine substrate to ketones, keto acids or aldehydes forming a chiral amine or amino acid and a new keto compound.<sup>[58]</sup> ATs have become very popular in biotechnology as they can be applied in the synthesis of optically pure amines, the production of polyamines ( $\beta$ , $\omega$ -amino acids) or the chemo-enzymatic synthesis of drugs.<sup>[58,268,269]</sup> Most ATs are able to transform a couple of substrate amines, such as the branched-chain L-amino acid ATs (BCATs). With decreasing activity, they can convert L-Leu, L-Glu, L-Met, L-Phe, L-Thr and L-Ala.<sup>[58]</sup> First insights into AT catalysis can be obtained by UV/Vis spectroscopy, as **PLP**-species absorb at different wavelengths during the transamination (figure 2.17 A).<sup>[270,271]</sup>

First, *PA3659* and *PA3798* were amplified by PCR from *P. aeruginosa* PAO1 genome using primers with Gateway<sup>®</sup> sequences. After cloning into the pET-55-DEST<sup>™</sup> expression vector bearing a N-terminal STREP-II purification tag, both proteins were



overexpressed and obtained in sufficient amounts. The catalytic activity of both enzymes was investigated in UV/Vis screens with 20 L- and a mixture of 11 selected D-amino acids (AAs). In figure 2.17 B, control samples and one example for a non-substrate or a preferred substrate are shown, respectively. Upon **PLP** addition, internal aldimine (red) peaks at around 400-430 nm increased in contrast to the corresponding unsaturated enzyme (grey). Enzymes treated with hydroxylamine (blue), which is able to replace **PLP**, were added as negative controls. The selected D-amino acids (green) also did not show any conversion for both enzymes. Gly (purple) turned out to be a non-substrate of *PA3659* and L-Trp (brown) as a highly preferred one. The same experiments were conducted for *PA3798*, hence with L-Ser as non-substrate and L-Gln as a preferred substrate (figure 2.17 C). For both D-AAs and non-substrates, no shifts of absorbance maxima were observed, meaning that no **PMP** was formed in the end. On the contrary, the preferred substrates showed a decrease in absorbance at around 400-430 nm and an increase at around 330 nm (**PMP**), confirming their conversion. The full screens of all 20 natural AAs as well as the D-AA mix against both enzymes are depicted in figure 2.17 D as individual heatmaps. Here, the relative absorbance difference between protein only and protein plus AA at 390 nm (*PA3659*) or 430 nm (*PA3798*) is depicted. If an AA can function as substrate, its internal aldimine peak decreases while the **PMP** absorbance peak increases.

Furthermore, preferred substrates of both enzymes were selected and transaminated products ( $\alpha$ -ketoacids) were quantified by LC-MS/MS. Therefore, *PA3659* and *PA3798* (5  $\mu$ M) were individually incubated with 10 mM L-Trp and L-Phe or L-Gln and L-Met, respectively. Additional **PLP** (100  $\mu$ M) for enzyme saturation and  $\alpha$ -ketoglutarate (5 mM) as amine acceptor were added to the reaction mixture. After incubation at 37 °C for 30 minutes, proteins were precipitated and then removed. The soluble fractions were evaporated and dissolved in LC-MS solvents. Positive controls showed signals during the applied parallel reaction monitoring (PRM) method. This MS/MS (MS<sup>2</sup>) method detects the product molecule, selects and fragments it resulting in a characteristic daughter ion spectrum. As expected, negative heat control (HC) samples did not show any product formation, confirming selective enzymatic turnover (figure 2.18).

In summary, we cloned and expressed two putative aminotransferases from *P. aeruginosa*, found by our **PLP**ome profiling, for which we confirmed **PLP**-binding by IP-MS and substrate specificity by UV/Vis-spectroscopy. Furthermore, we were able to confirm specific enzymatic turnover by a targeted metabolomics assay utilising a LC-MS/MS method.

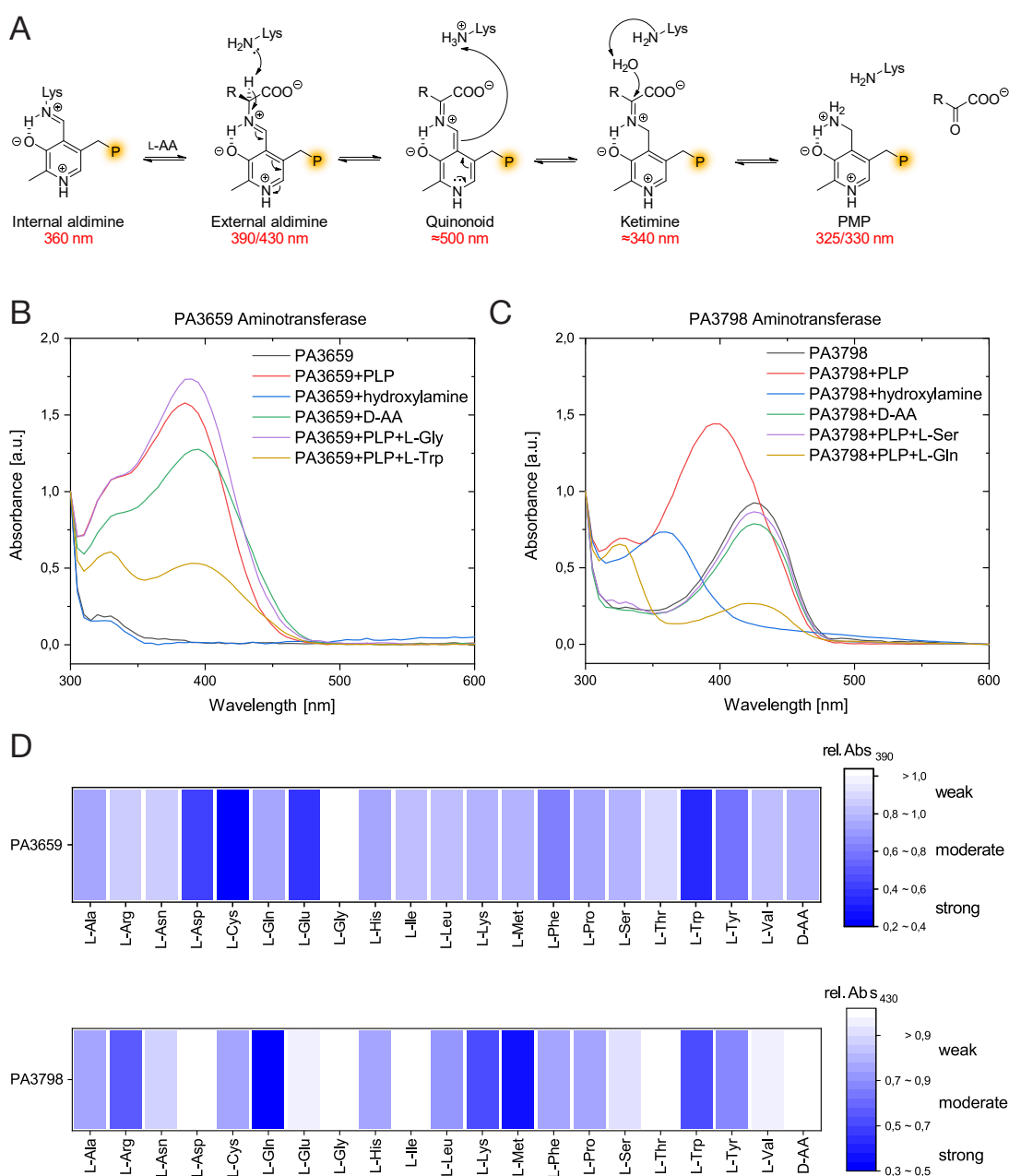


**Figure 2.17:** (A) Spectroscopic properties of PLP and substrate-complexes during transamination by aminotransferases.<sup>[213,270]</sup> (B) UV/Vis absorbance spectrum of PA3659 and different control samples as well as one non-substrate (L-Gly) and one preferred substrate (L-Trp). (C) UV/Vis absorbance spectrum of PA3798 and different control samples as well as one non-substrate (L-Ser) and one preferred substrate (L-Gln). (D) UV/Vis screening from 300 to 600 nm of aminotransferases PA3659 and PA3798 with 20 L-amino acids (AA) and a mixture of 11 D-amino acids (each 10 equivalents). Changes in absorbance at 390 or 430 nm, corresponding to the internal aldimines, were calculated and normalised. Adapted from Pfanzelt *et al.*<sup>[170]</sup>

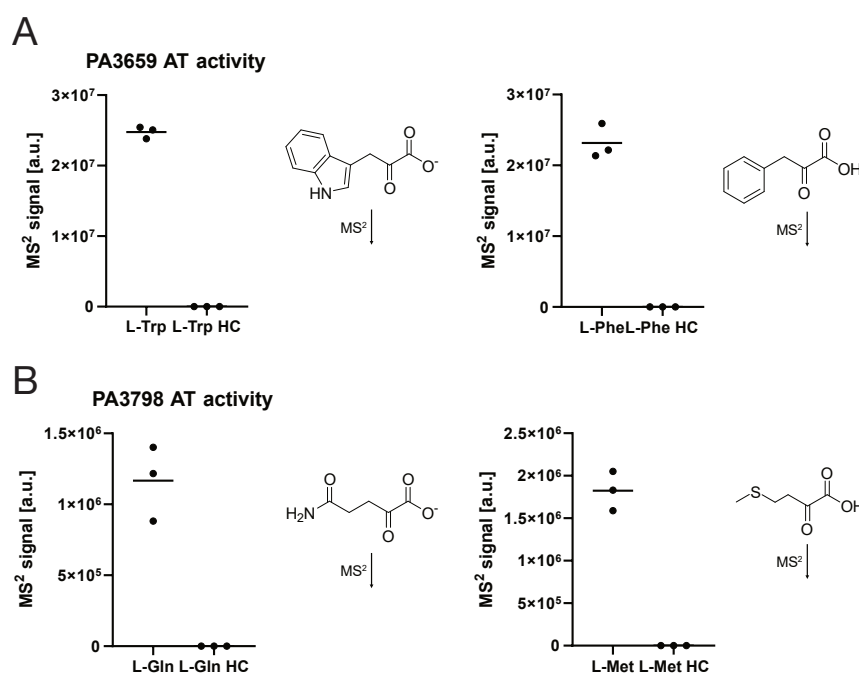
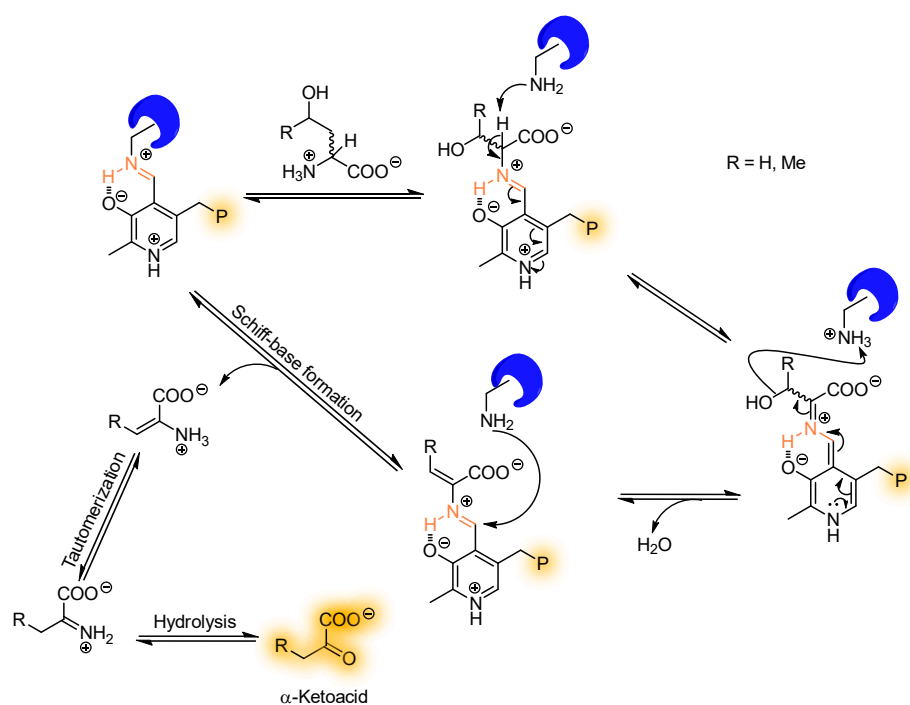


**Figure 2.18:** (A) LC-MS/MS analysis of transaminated products ( $\alpha$ -keto acids) after incubation of *PA3659* with L-Trp or L-Phe and (B) *PA3798* with L-Gln or L-Met ( $n = 3$ ). Heat control (HC) samples were treated equally except for incubating the protein for 5 min at 95 °C prior to addition of substrates. Adapted from *Pfanzelt et al.*<sup>[170]</sup>

### 2.4.2 The Serine/Threonine Dehydratase *PA2683*

The next *P. aeruginosa* protein for further characterisation was enriched by **PL1** and **PL2** and is annotated as probable serine/threonine dehydratase.<sup>[66]</sup> Just like both ATs, *PA2683* was cloned, overexpressed, purified and subsequently verified by IP-MS (figure 2.16). Serine dehydrates, often called serine deaminases, are able to dehydrate ( $-H_2O$ ) serine and often threonine. They thereby utilise **PLP** in a four step mechanism, leading to the formation of an  $\alpha, \beta$ -unsaturated amino acid. Upon tautomerisation to an imine, subsequent hydrolysis leads to the formation of either pyruvate (L-Ser) or oxobutanoate (L-Thr) (figure 2.6).<sup>[272,273]</sup> Of note, the internal **PLP** aldimine is reformed after catalysis and requires no regeneration.



**Scheme 2.6:** Catalytic mechanism for serine dehydratase/threonine deaminase forming pyruvate or oxobutanoate. [272,273] Adapted from Pfanzelt *et al.* [170]

First, a nicotinamide adenine dinucleotide (NADH)-coupled spectroscopic assay was utilised for calculation of kinetic parameters for L-Ser conversion. A lot of improvement steps were necessary to fulfil MICHAELIS-MENTEN kinetic prerequisites. Beside optimisation of enzyme and substrate concentrations, addition of AMP and  $Mg^{2+}$  showed acceleration of the reaction. Addition of ATP and  $Mg^{2+}$  was already known to enhance kinetics of serine dehydratases [274], however, AMP showed higher potency as an accelerator in this study. In the end, we found that  $2\ \mu M$  *PA2683*, 6 mM AMP and additional  $100\ \mu M$  **PLP** worked best for our experimental setup using L-Ser concentrations from 1 mM to 2.5 M. Moreover, parameters for the coupled assay were optimised. After the formation of pyruvate, lactate dehydrogenase (LDH) converts it to lactate, thereby consuming one equivalent NADH. The turnover of *PA2683* can therefore be measured by tracking the absorbance at 340 nm, the absorbance maximum of NADH. Hence, 2.5 mM NADH and  $25\ \mu g$  LDH were added per reaction as well. A series of negative controls was included, showing the integrity of the enzyme as serine dehydratase (figure 2.19 A). Moreover, a profiling of possible substrates (L-Ser, D-Ser, L-Thr and D-Thr) was conducted by a targeted metabolomics assay *via* LC-MS/MS. This experiment revealed both serine and threonine dehydratase activity, however, with preference of *PA2683* for the L-enantiomers (figure 2.19 B). Together with *PA2638*, a confirmed Ser/Thr dehydratase, we were able to give catalytic insights into three putative **PLP**-DEs from *P. aeruginosa*, which we detected with our refined labelling strategy.

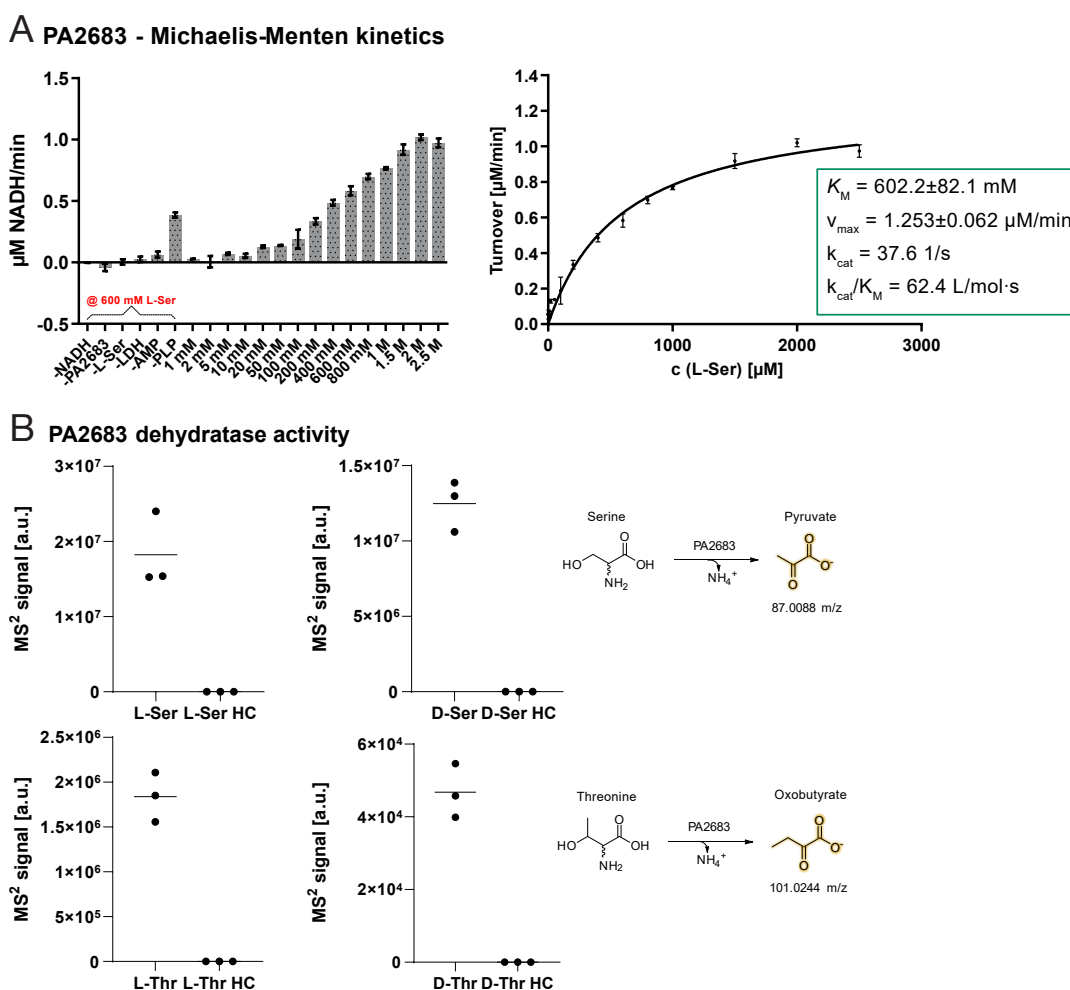


**Figure 2.19:** (A) MICHAELIS-MENTEN kinetics of *PA2683* ( $n = 3$ , mean  $\pm$  SEM) were calculated in *Graphpad Prism*. Control samples were conducted at 600 mM L-Ser. The enzyme contains endogenously bound **PLP** sufficient for catalysis. (B) LC-MS/MS analysis of products after incubation of *PA2683* with L-Ser, D-Ser, L-Thr or D-Thr and additional AMP and **PLP** at 37 °C. The  $\text{MS}^2$  signals of products (pyruvate or oxobutanoate) were integrated and plotted as individual values ( $n = 3$ ). Heat control (HC) samples were treated equally except for incubating the protein for 5 min at 95 °C prior to addition of substrates. Adapted from *Pfanzelt et al.*<sup>[170]</sup>

### 2.4.3 The Transcriptional Regulator *ydcR*

*E. coli ydcR* is described to be a *MocR*-like HTH-transcriptional regulator (TR)<sup>[65,66]</sup> and related proteins have been described before.<sup>[74,75,265,275–277]</sup> Together with *yjiR* they are the only two **PLP**-dependent *MocR* TRs in *E. coli* known so far.<sup>[276]</sup> These proteins bear a **PLP**-dependent domain of the fold type I **PLP**-DEs and a short N-terminal helix-turn-helix (HTH) domain which can bind to DNA.<sup>[277]</sup> **PLP**-dependent *MocR*-TRs are often involved in **PLP** metabolism as well as  $\gamma$ -amino

butyric acid (GABA) and taurine metabolism.<sup>[276]</sup> Moreover, genes encoding these TRs are often auto-repressors, meaning that their corresponding apo-TRs either repress expression of their own promoters, like apo-*GabR*, which needs **PLP** and GABA to activate expression<sup>[73,74,276]</sup>, or activate expression, like apo-*PdxR*, where **PLP** acts as a repressor of expression.<sup>[276,278–281]</sup> As mentioned before, such TRs are likely to bind to their own promoter regions.<sup>[276]</sup> Therefore, we had a closer look into the genome and the promoter regions around *ycdR* itself (figure 2.20 A). The *ycdQ/hicB* operon is located upstream of the ORF while the *ycdSTUV-patD* operon is located downstream. The latter encodes a putative ABC transporter system for the transport of putrescine.<sup>[282]</sup> *PatD* itself encodes a  $\gamma$ -amino butyraldehyde dehydrogenase.<sup>[283]</sup> Although no target gene is adjacent, in contrast to other *MocR*-TRs<sup>[72]</sup>, we thought an influence of putrescine could play a role in binding affinity of *ycdR*. Here, we tried to elucidate the binding region of *ycdR* experimentally utilizing an electrophoretic mobility shift assay (EMSA). Therefore, we first cloned and overexpressed *ycdR* with an attached maltose binding protein (MBP) due to solubility issues. Additionally, *yjiR*-MBP was overexpressed as negative control in order to confirm selectivity of *ycdR*. Thereafter, we generated fluorescent promoter regions of the *ycdR* promoter (PR<sub>ycdR</sub>) and the *ycdSTUV-patD* promoter (PR<sub>ycdR-ycdS</sub>) (figure 2.20 B). The latter was included as a negative control, since we did not expect binding to this fragment. We were able to show specific binding of *ycdR* to its own promoter region PR<sub>ycdR</sub> from 50 nM *ycdR* or more in this experimental setup (figure 2.20 C). Mixing *yjiR* instead of *ycdR* with PR<sub>ycdR</sub> exhibited no binding, which underlines the specificity of *ycdR* for PR<sub>ycdR</sub>. The second important negative control, the incubation of *ycdR* with PR<sub>ycdR-ycdS</sub> also did not show any significant binding at 200 nM *ycdR*. We further tested, if **PLP** or putrescine have an influence on DNA binding of *ycdR* (figure A.8). We could not observe any significant difference, suggesting that the promoter acts independently – at least in these *in vitro* assays.

We here elucidated the putative binding region of *ycdR*, a HTH-TR with a **PLP**-binding domain. We observed specific binding of *ycdR* for PR<sub>ycdR</sub> from 50 nM, while binding of *yjiR* to PR<sub>ycdR</sub> or binding of *ycdR* to PR<sub>ycdR-ycdS</sub> could be excluded. The final protein that we wanted to characterise further was *A0A0H2XHJ5*. This protein was detected in competitive ABPP experiments which are discussed in section 2.5.

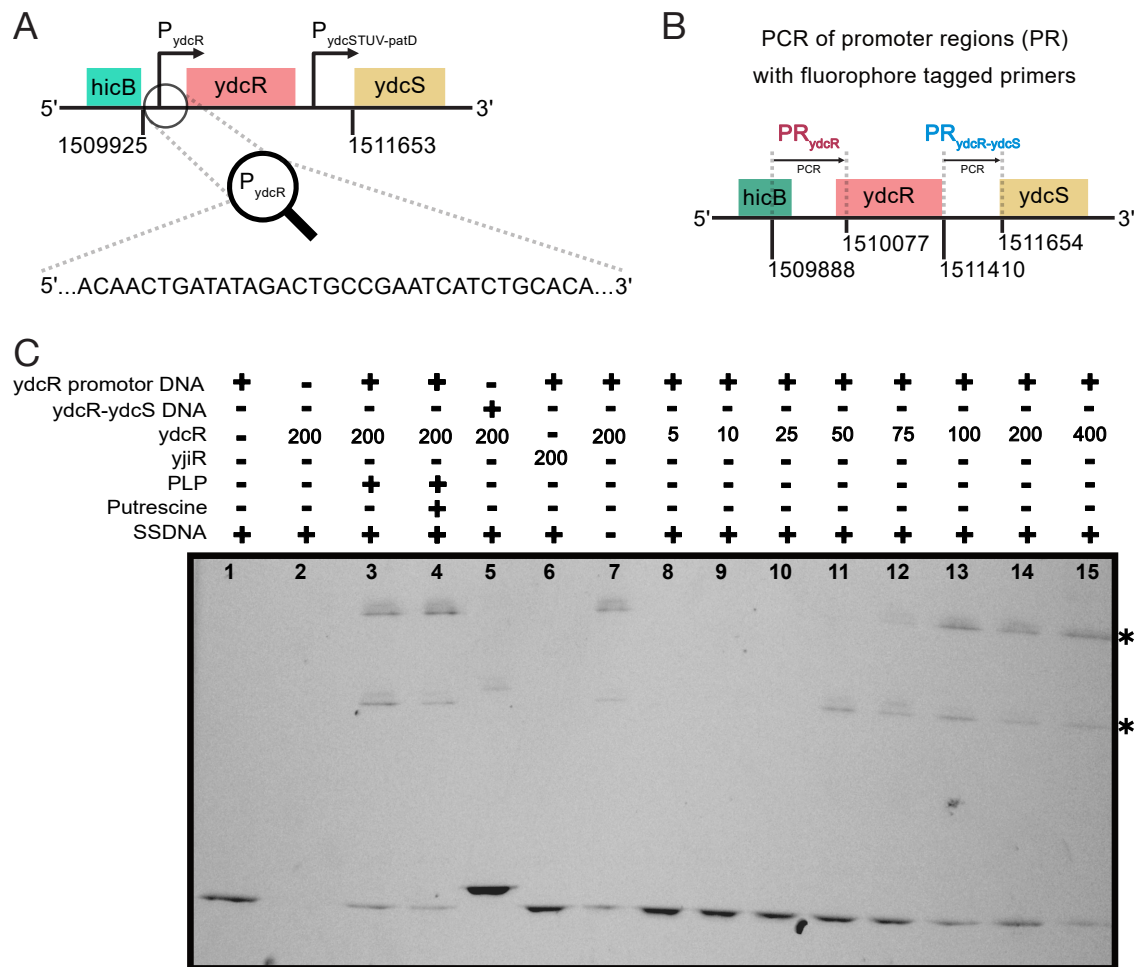
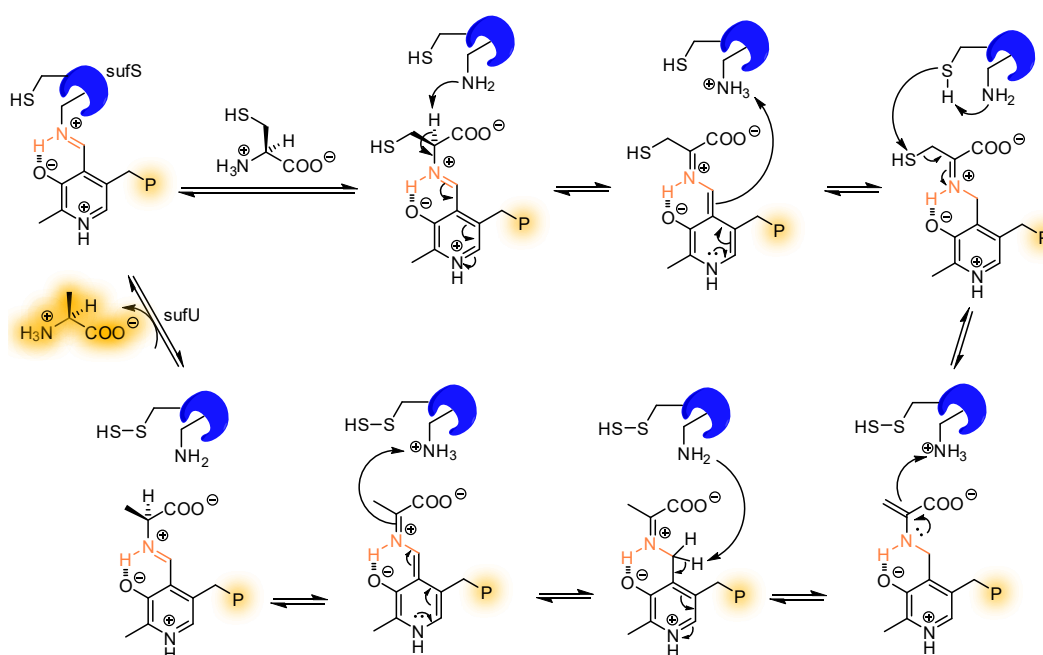


**Figure 2.20:** (A) Proposed binding site of *ydcR* between *hicB* and *ydcR*.<sup>[11]</sup> *ydcR* binds to its own promoter  $P_{ydcR}$ . Situated downstream is the *ydcSTUV-patD* operon with its own promoter  $P_{ydcR-ydcS}$ . (B) Fluorescent promoter regions  $PR_{ydcR}$  (189 bp containing a 5'-TAMRA) and  $PR_{ydcR-ydcS}$  (244 bp containing a 5'-TAMRA) were generated by PCR with corresponding primers listed in table 4.5. (C) EMSA gel under UV-illumination. Concentrations are given in nM. The interaction of *ydcR* with the *ydcR* promoter region fragment  $PR_{ydcR}$  is clearly visible starting at 50 nM *ydcR*. Fluorescent fragments were used at 10 ng. The two lines (\*) represent shifted DNA-protein complexes.<sup>[72]</sup> As negative controls, we included samples w/o *ydcR* (lane 1), w/o  $PR_{ydcR}$  (lane 2), w/  $PR_{ydcR-ydcS}$  instead of  $PR_{ydcR}$  (lane 5) and one sample with *yjiR* instead of *ydcR* (lane 6). To exclude unspecific DNA binding, we added  $2 \mu\text{g}/\mu\text{L}$  salmon sperm DNA (SSDNA) to each sample (except lane 7). Samples containing PLP (lane 3, 10 eq) and PLP and putrescine (lane 4, 10 eq PLP, 400 eq putrescine) were included (see also figure A.8). Adapted from Pfanzelt *et al.*<sup>[170]</sup>

#### 2.4.4 The Cysteine Desulfurase *A0A0H2XHJ5*

Cysteine desulfurases catalyse the  $\beta$ -elimination of L-Cys to L-Ala while forming an enzyme-bound persulfide, which is subsequently incorporated *via* an acceptor protein (FeS assembly protein, *iscU*, *sufU* or *nifU*) into many different biosynthesis pathways such as FeS cluster, thiamine, biotin, lipoic acid and NAD biosynthesis (figure 2.7).<sup>[20]</sup> There are two different groups of Cys desulfurases, based on sequence similarity: group I includes the *nifS* and *iscS* desulfurases, which contribute to minor pathways of FeS cluster biosynthesis by mobilising sulfur from L-Cys as a substrate.<sup>[20]</sup> Group II consists of the *sufS* desulfurase, which is mainly activated during stress.<sup>[20]</sup> Both systems are widely distributed among procaryotes and higher organisms. In particular, within bacterial species, group I systems are mainly found in GRAM-negative bacteria like *E. coli*, while group II system is mostly found in GRAM-positive bacteria such as *S. aureus* or *M. tuberculosis*.<sup>[284]</sup> For *B. subtilis* and *S. aureus*, the *suf*-system was shown to be essential for cell growth.<sup>[285,286]</sup> It was revealed that *A0A0H2XHJ5* exhibits homology to the very same group II protein, *sufS*.<sup>[66,286]</sup> The lack of a transposon mutant in the Nebraska transposon library of *S. aureus* suggests that this protein is essential for cell growth.<sup>[254]</sup> Moreover, the fact that it was one of the hit enzymes in our phenelzine target screen (subsection 2.5.1), we decided to confirm its function as cysteine desulfurase and therefore approve it as a member of the *suf*-family. Therefore, we cloned, expressed and purified the protein from *S. aureus* similar to the other proteins already discussed. After verification of the correct mass and **PLP**-binding, we tried to confirm its catalytic activity *via* a MS-based assay. For this, we optimised previously published conditions and found 5  $\mu$ M *A0A0H2XHJ5*, 10 mM L-Cys, 5 mM dithiothreitol (DTT), 100  $\mu$ M **PLP** and the FeS assembly protein *A0A0H2XJC0* (*sufU*) were sufficient and ideal for this experimental setup.<sup>[285,287]</sup>





**Scheme 2.7:** General cysteine desulfurase (*sufS*) catalytic reaction mechanism.<sup>[288,289]</sup> *SufU* is needed for the regeneration of the catalytic cysteine by transferring the thiol group to FeS-clusters.<sup>[284]</sup> Adapted from *Pfanzelt et al.*<sup>[170]</sup>

The formation of L-Ala after 40 minutes incubation at 37 °C was detected by a LC-MS method termed single reaction monitoring (SIM). Here, no MS<sup>2</sup> method could be applied due to the instability of alanine in the collision-induced dissociation (CID)-cell in the mass spectrometer. Nevertheless, product formation could be reliably quantified, which confirmed the activity of *A0A0H2XHJ5* as cysteine desulfurase (figure 2.21). Moreover, heat control samples (HC) did not show any product formation.

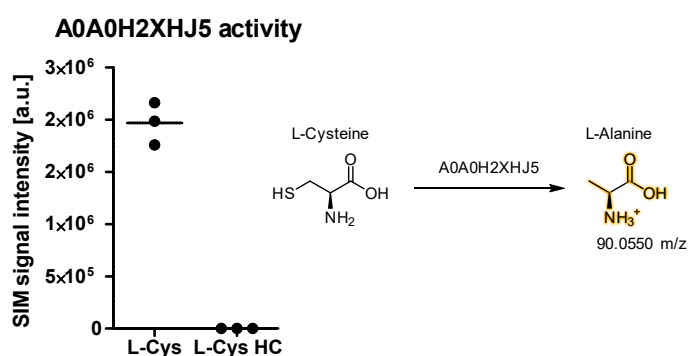


**Figure 2.21:** LC-MS analysis of alanine after incubation of *A0A0H2XHJ5* with L-Cys ( $n = 3$ ). Heat control (HC) samples were treated equally except for incubating the protein for 5 min at 95 °C prior to addition of substrates. Adapted from *Pfanzelt et al.*<sup>[170]</sup>

In summary, we were able to assign the function of five predicted PLP-DEs from all three studied organisms. We could confirm the aminotransferase activity and substrate selectivity of *P. aeruginosa* proteins *PA3659* and *PA3798*. Further, we

identified *PA2638* as a serine/threonine dehydratase utilising a spectroscopic assay, which revealed MICHAELIS-MENTEN kinetics, as well as a LC-MS/MS based detection of products. Next, we were able to show the binding site of *ydcR*, a putative HTH-transcriptional regulator in *E. coli* by an EMSA. We found, that it selectively binds to its own promoter region. Last but not least, *A0A0H2XHJ5* from *S. aureus* was confirmed to be a cysteine desulfurase *via* an LC-MS based metabolomics assay.

The second major goal of this work was to identify novel **PLP**-DE targets of antibacterial drugs using our **PL**-probes in a competitive ABPP approach.

## 2.5 Application: Screening for Potential Inhibitors

As discussed in the first chapter, a lot of inhibitors targeting **PLP**-DEs were developed so far. However, the number of *in vivo* applications is low due to their associated side effects. One marketed drug is DCS, which is used as second-line antibiotic against tuberculosis. DCS inhibits cellular alanine racemase by a mechanism-based inhibition. However, we were able to reveal three further **PLP**-DEs as major targets, DAT, DAPDC and ODC (see section 1.5.2).<sup>[151]</sup> A competitive approach of our methodology is therefore suitable to find antibacterial **PLP**-DE targets.

For our profiling, we first collected an inhibitor library consisting of 53 compounds, which are either already known *in vitro* **PLP**-DE inhibitors, binders of **PLP**, structurally related compounds to antibacterials or totally novel scaffolds (table 4.10), some of which were synthesised in our laboratory. First, we pre-screened this library at 500  $\mu\text{M}$  against the three bacterial strains used in this study for growth inhibition. Initial hit molecules were then further screened with a serial dilution down to 25  $\mu\text{M}$ . To our delight, we observed hits in all three bacterial strains (figure 2.22). Interestingly, all 14 molecules tested in the screen were active in *S. aureus*, five in *E. coli* and only three in *P. aeruginosa*. This confirms the assumption that GRAM-negative bacteria are generally more difficult to access with small molecule inhibitors. Compound CCG-50014, a mycobacterial alanine racemase inhibitor<sup>[101,103,104]</sup>, exhibited high activity in *S. aureus* as well as benserazide, a structurally related dihydroxyphenylalanine (DOPA)-decarboxylase inhibitor<sup>[9]</sup>, which was also active in *E. coli*. This compound is a prodrug, which forms a hydrazine upon hydrolysis, which is able to bind **PLP** as hydrazone within the DOPA-decarboxylase.<sup>[9,290–292]</sup> Carbidopa, a DOPA-decarboxylase inhibitor<sup>[9]</sup>, and phenelzine, a nonselective monoamine oxidase inhibitor<sup>[9]</sup>, are both hydrazine compounds, which are generally known to bind plasma **PLP** in the cell.<sup>[293]</sup> Both compounds were active down to 100  $\mu\text{M}$  in *S. aureus*. Moreover, MAC173979, an inhibitor of *para*-aminobenzoic acid (PABA) biosynthesis under nutrient limitation, was shown to exhibit moderate activity in *S. aureus*.<sup>[294,295]</sup> There are three enzymes involved in PABA biosynthesis from chorismic acid, *pabA*, *pabB* and *pabC*, of which *pabC* is a **PLP**-dependent aminodeoxychorismate lyase.<sup>[294]</sup> The remaining hit compounds are derivatives of phenelzine, which were synthesised by T. E. MAHER.<sup>[170]</sup>

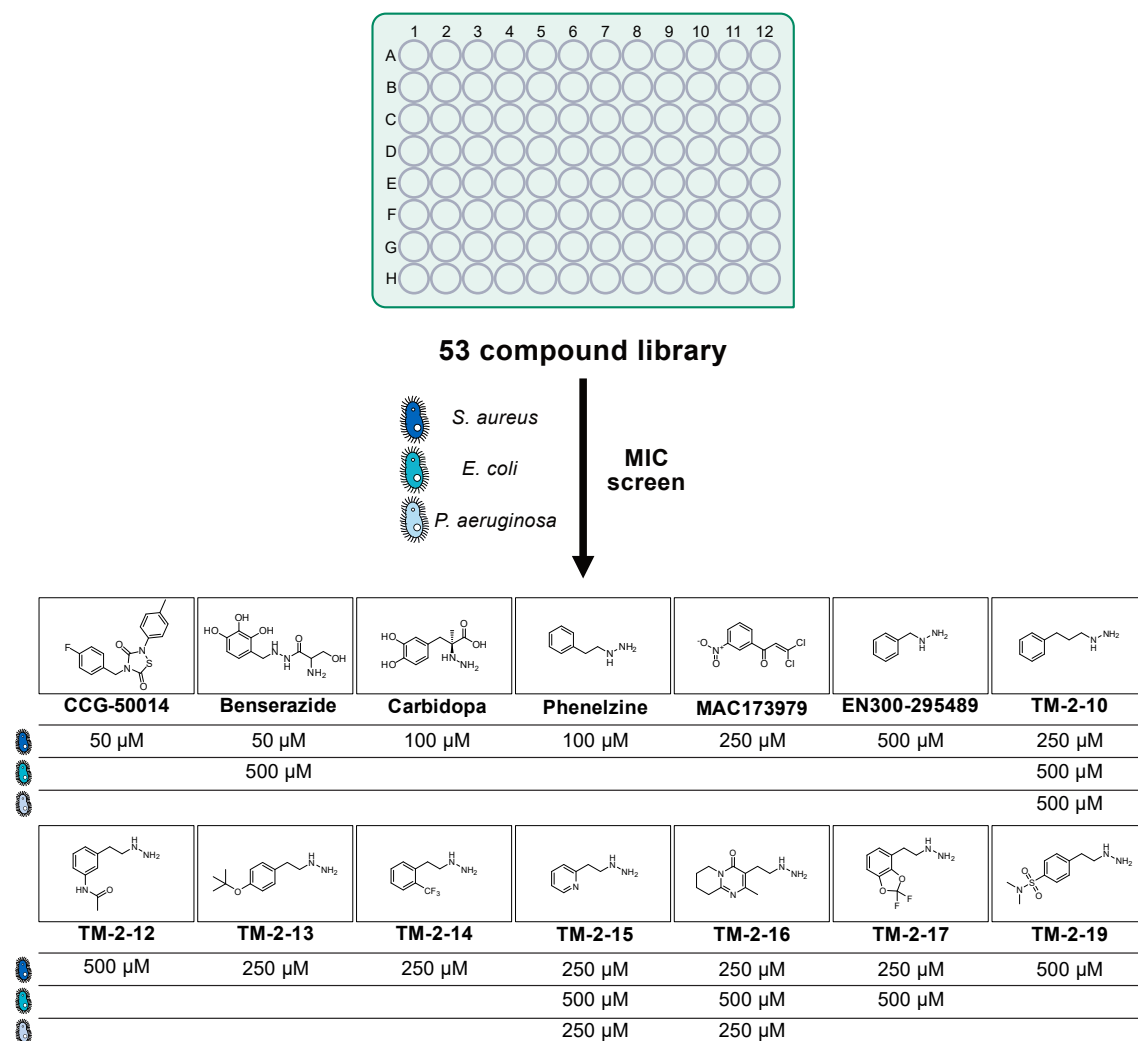


**Figure 2.22:** MIC-screen of a 53 compound library against *S. aureus* USA300, *E. coli* K12 and *P. aeruginosa*. Here, compound structures and corresponding MIC-values are shown. Adapted from Pfanzelt *et al.* [170]

As a first compound for competitive **PLP**-ome profiling in *S. aureus*, we have chosen the aromatic hydrazine phenelzine.

### 2.5.1 Phenelzine in *S. aureus*

Phenelzine is a marketed drug in the united states and used as non-selective, irreversible monoamine oxidase inhibitor for the treatment of depressions and panic attacks. [296] Often, patients resistant to other drug treatments, respond to phenelzine, making it a second-line antidepressant. [297] Unfortunately, phenelzine has a lot of side-effects due to its unselective target binding. Among MAO-A and MAO-B, the desired targets, it also inhibits alanine-transaminase and GABA-AT. [298,299] In addition, phenelzine

has the ability to bind free **PLP** in the plasma. *Malcolm et al.* found in a group of 19 patients treated with phenelzine, that **PLP** plasma levels were reduced on average to approximately 54% compared to a control group.<sup>[293]</sup> Nevertheless, due to its antibacterial potency, we set up a competitive labelling experiment utilising **PL2**, since this probe covers the majority of **PLP**-DEs in *S. aureus*. According to figure 1.10, we treated cells with three different molar ratios of phenelzine, 75  $\mu$ M, 100  $\mu$ M and 1 mM. Additionally, samples to which we first added methylhydrazine prior to probe treatment and samples with probe labelling prior to phenelzine addition, were included. With these control experiments, we aimed to exclude false positive hits. This resulted in several **PLP**-DEs, which were competed by phenelzine with high confidence (table 2.4, highlighted in green). These hit enzymes could be enriched by **PL2** and were competed by phenelzine at 1 mM. However, methylhydrazine did not show competition confirming a selective inhibition by phenelzine, suggesting that the structural features of phenelzine itself and not mere hydrazine reactivity are responsible for the inhibitory effect. We further anticipated that our probes could react directly with phenelzine in the bacterial cells or even in the reaction mixture. This is why we included the second control experiment, in which we first applied **PL2** and then phenelzine afterwards. We allowed **PL2** to enter the cells and get activated by *SaPLK* before phenelzine could be able to trap the probe. Since some enzymes, highlighted in orange, show competition with methylhydrazine but with phenelzine after **PL2** treatment as well, these **PLP**-DEs were added to the hit enzymes. These enzymes could be inhibited by phenelzine, but also show off reactivity towards hydrazines in general. Only one protein, *A0A0H2XI95* was not enriched by **PL2** but competed by phenelzine, which is why we labelled it as a false positive hit enzyme (table 2.4). Of note, only *A0A0H2XFB2* and *Q2FFN1* were found to be competed at 100 and 75  $\mu$ M phenelzine. This lack of competition at these concentrations could be due to the fact, that hydrazine compounds are highly reactive towards a series of compounds within the cell, which lowers their level of active species. These effects are also known as hydrazine poisoning in general.

**Table 2.4:** List of **PLP**-DEs, which were competed with phenelzine at 75  $\mu$ M, 100  $\mu$ M and 1 mM. As a control, bacteria were treated with methylhydrazine prior to **PL2** labelling. Proteins in green could be enriched as well as competed by phenelzine but not by methylhydrazine. Proteins highlighted in orange were both competed by phenelzine and methylhydrazine, indicating a possible unspecific inhibition by hydrazines. The red coloured protein could not be enriched and represents therefore a false positive hit. n.d. = not detected.

Uniprot ID	Enrichment PL2	Competition Phenelzine	Competition Methylhydrazine	Competition PL2 first	Essential
1 mM Phenelzine; 1 mM Methylhydrazine, 100 $\mu$ M PL2					
A0A0H2XFD9	+	+	-	+	-
A0A0H2XHH8	+	+	-	-	+
A0A0H2XII6	+	+	-	-	-
A0A0H2XIV3	+	+	-	-	-
Q2FF55	+	+	-	-	+
A0A0H2XFA8	+	+	+	+	-
A0A0H2XFB2	+	+	+	+	-
A0A0H2XFF8	+	+	+	+	-
A0A0H2XG37	+	+	+	+	-
A0A0H2XHJ5	+	+	+	+	+
A0A0H2XIS2	+	+	+	+	-
Q2FF63	+	+	+	+	-
Q2FFN1	+	+	+	+	-
A0A0H2XI95	-	+	-	-	-
100 $\mu$ M Phenelzine; 100 $\mu$ M Methylhydrazine, 100 $\mu$ M PL2					
A0A0H2XFB2	+	+	-	-	-
Q2FFN1	+	+	-	-	-
Q2FHT1	-	+	-	-	+
75 $\mu$ M Phenelzine; 75 $\mu$ M Methylhydrazine, 100 $\mu$ M PL2					
A0A0H2XFB2	+	+	n.d.	n.d.	-
Q2FFN1	+	+	n.d.	n.d.	-
Q2FHT1	-	+	n.d.	n.d.	+

A plot comparing the LFQ-intensities of DMSO control, **PL2** enrichment and the three different applied phenelzine concentrations for five representative **PLP**-DEs is depicted in figure 2.23. As *A0A0H2XII6*, a Orn/Lys/Arg decarboxylase, and *A0A0H2XHJ5*, an essential putative cysteine desulfurase, which we could confirm previously in this study were both out-competed by phenelzine we chose these two **PLP**-DEs for further target validation.

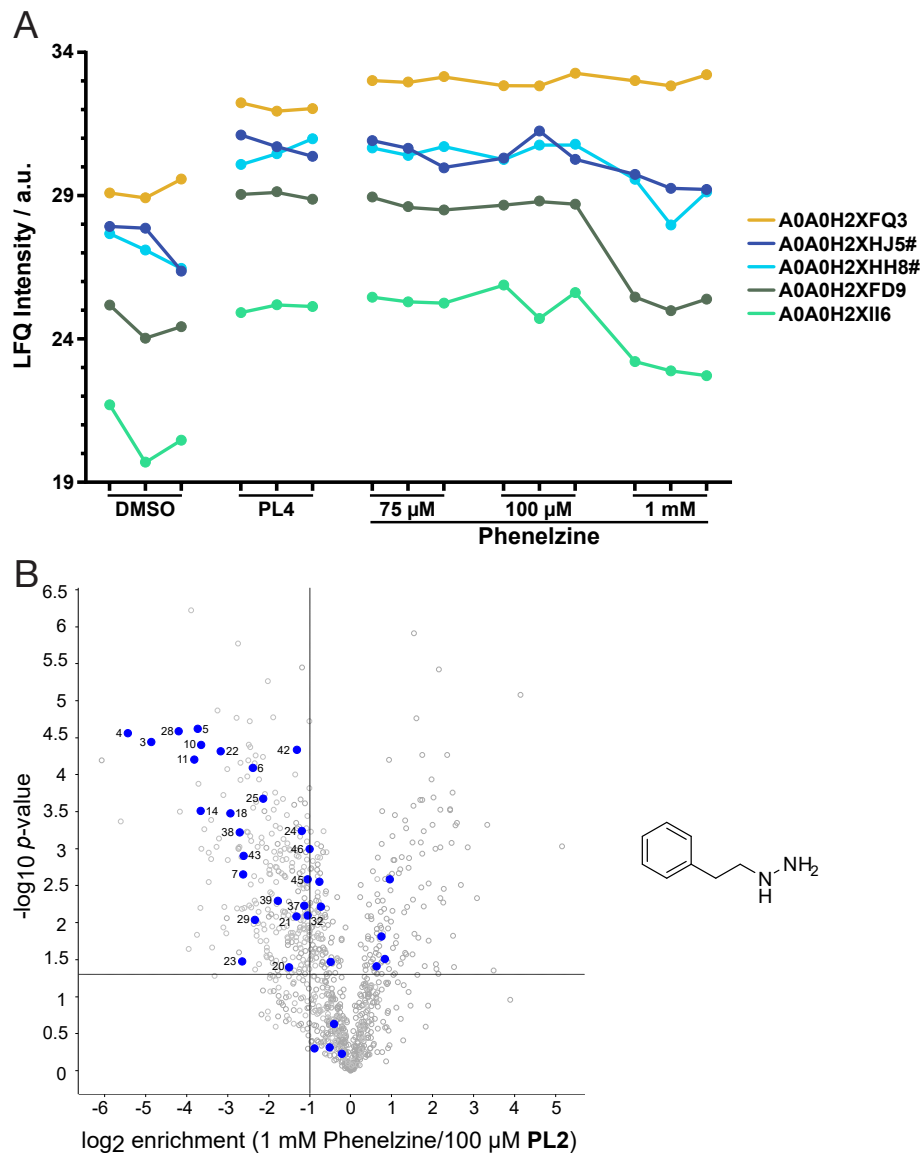


**Figure 2.23:** (A) Profile plot of selected proteins from Phenelzine competitive labelling in *S. aureus* USA300 TnpdXS. LFQ intensities of 3 individual replicates are depicted. Essential enzymes are marked with a #.<sup>[254]</sup> (B) Structure of Phenelzine and volcano plot of Phenelzine competitive labelling at 10 mM compared to 100  $\mu\text{M}$  **PL2** representing the *t*-test results [criteria:  $\log_2(\text{enrichment}) > 1$  and  $p\text{-value} < 0.05$ ,  $n = 3$ ]. Adapted from Pfanzelt *et al.*<sup>[170]</sup>

### 2.5.1.1 Target Verification by Mass Spectrometry

*A0A0H2XII6* is a poorly characterised **PLP**-DE with Orn/Lys/Arg decarboxylase function.<sup>[64]</sup> *A0A0H2XHJ5* is a cysteine desulfurase as discussed in section 2.4.4. Since both proteins were out-competed by phenelzine, we wanted to confirm that phenelzine is able to inhibit their function *in vitro*, too. For this, we utilised a targeted metabolomics assay similar to the one confirming the enzymes activity. First, the enzymes were cloned, overexpressed and purified. After confirming **PLP**-dependency and correct mass by IP-MS (figure 2.16), we performed an activity assay with 5  $\mu\text{M}$  protein, 10 mM L-lysine and 100  $\mu\text{M}$  **PLP** for 30 min at 37 °C in case of *A0A0H2XII6*. *A0A0H2XII6* catalyses the decarboxylation of L-lysine to cadaverine. For inhibition studies, *A0A0H2XII6* was preincubated with phenelzine at different concentrations (1 mM, 100  $\mu\text{M}$ , 50  $\mu\text{M}$ , 25  $\mu\text{M}$  or 12.5  $\mu\text{M}$ ) at 37 °C for 40 minutes. In case of *A0A0H2XHJ5*, we incubated 5  $\mu\text{M}$  protein with 2  $\mu\text{M}$  *A0A0H2XJC0*, 10 mM L-cysteine, 5 mM DTT and 100  $\mu\text{M}$  **PLP**. Here, *A0A0H2XHJ5* was preincubated with 10 mM, 1 mM, 100  $\mu\text{M}$ , 50  $\mu\text{M}$ , 10  $\mu\text{M}$  or 1  $\mu\text{M}$  phenelzine. After incubation, assays were terminated by adding cold acetone, causing protein precipitation. After the extraction of reaction products, analysis of cadaverine (*A0A0H2XII6*) by a PRM method and alanine (*A0A0H2XHJ5*) by a SIM method revealed inhibition for both enzymes by phenelzine (figure 2.24).

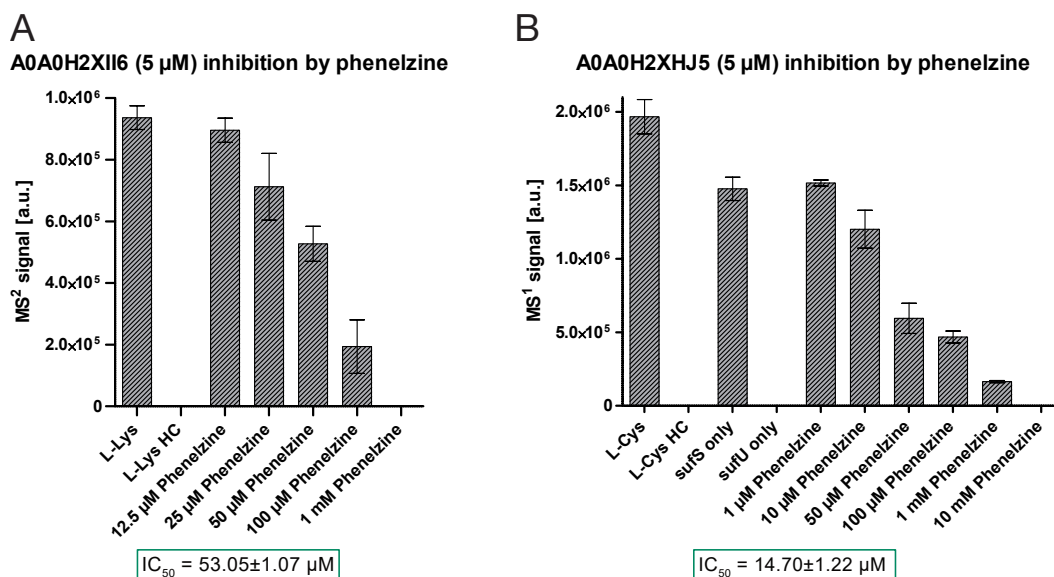


**Figure 2.24:** (A) Activity of *A0A0H2XII6* after incubation with different concentrations of phenelzine ( $n = 3$ ). Quantification of cadaverine was conducted by LC-MS/MS (MS<sup>2</sup> signal, PRM). IC<sub>50</sub> values were calculated in *Graphpad Prism 5.03* using the log(inhibitor) vs. response-variable slope function. Heat control (HC) samples were treated equally except for incubating the protein for 5 minutes at 95 °C prior to addition of substrates. (B) Activity of *A0A0H2XHJ5* (*sufS*) after incubation with different concentrations of phenelzine ( $n = 3$ ). Quantification of alanine was conducted by LC/MS (MS<sup>1</sup> signal, SIM). IC<sub>50</sub> values were calculated in *Graphpad Prism 5.03* using the log(inhibitor) vs. response-variable slope function. Adapted from *Pfanzelt et al.*<sup>[170]</sup>



Corresponding half maximal inhibitory concentrations ( $IC_{50}$ ) of phenelzine were calculated to be  $50.03 \pm 1.07 \mu\text{M}$  for *A0A0H2XII6* and  $14.70 \pm 1.22 \mu\text{M}$  for *A0A0H2XHJ5*.

In summary, we were able to apply our probe **PL2** in a competitive labelling experiment elucidating the **PLP**-DE targets of the hydrazine compound phenelzine in *S. aureus*. The profiling revealed a list of compounds, two of which we were able to further validate by MS-based assays. Since *A0A0H2XHJ5* is an essential **PLP**-DE, along with *Q2FF55* and *A0A0H2XHH8*, we assume that they contribute to the overall antibiotic activity of phenelzine *in vivo*.

### 2.5.2 Benserazide in *S. aureus*

The prodrug benserazide exhibits high antibacterial activity in *S. aureus* and low activity in *E. coli*. Benserazide is most likely cleaved hydrolytically to its respective hydrazine compound, which is able to bind to **PLP**.<sup>[9,290-292]</sup> Its best studied target is the **PLP**-DE DOPA-decarboxylase in humans.<sup>[9]</sup> Inhibiting DOPA-DC, which produces the important human neurotransmitters serotonin and dopamine, is clinically targeted to treat Parkinson's disease.<sup>[9]</sup> However, since benserazide is a hydrazine inhibitor, but bears structural modifications and a cleavage step before it is active in contrast to phenelzine, we similarly profiled the **PLP**-DE targets by a competitive approach. We therefore applied three different molar ratios (1:1, 1:10 and 1:100) of benserazide compared to **PL2** ( $100 \mu\text{M}$ ). Again, several **PLP**-DE target enzymes were found, two of which are essential and possibly contribute to the overall antibiotic effect of benserazide (table 2.5). Interestingly, phenelzine and benserazide share a majority of hit enzymes, possibly due to their hydrazine moiety and aromatic character. Nevertheless, benserazide has its own primary targets, such as the cysteine/methionine metabolism enzyme *A0A0H2XFH9*<sup>[63]</sup> or the threonine synthase *A0A0H2XH24*<sup>[63]</sup>. However, no competition was observed at a 1:1 ratio of benserazide and **PL2**. Figure 2.25 A depicts the LFQ-intensities in the DMSO, **PL2** and competitor treated samples of selected **PLP**-DEs. For example, the LFQ-intensity of *A0A0H2XH24* decreases almost to the level of the DMSO sample with higher benserazide concentrations, while *A0A0H2XFQ9* is not affected by high benserazide concentrations. Moreover, figure 2.25 B shows the plot for the 10 mM benserazide vs.  $100 \mu\text{M}$  **PL3** experiment. At the highest concentration, 22 **PLP**-DEs were out-competed whereas only 4 were out-competed at 1 mM, indicating the highest selectivity of benserazide for these 4 proteins.

As a last proof-of-concept competitive target validation in *S. aureus*, we picked CCG-50014 due to its absence of a hydrazine moiety and unprecedented binding mode.

**Table 2.5:** List of **PLP**-DEs, which were out-competed with benserazide at different molar ratios compared to **PL2**.

Uniprot ID	Enrichment PL2	Competition Benserazide 10 mM	Competition Benserazide 1 mM	Competition Benserazide 100 $\mu$ M	Essential
A0A0H2XFA8	+	+	+	-	-
A0A0H2XFB2	+	+	+	-	-
A0A0H2XFD9	+	+	-	-	-
A0A0H2XFF8	+	+	-	-	-
A0A0H2XFH9	+	+	-	-	-
A0A0H2XFY9	+	+	-	-	-
A0A0H2XGP0	+	+	-	-	-
A0A0H2XG37	+	+	-	-	-
A0A0H2XHU6	+	+	-	-	-
A0A0H2XHV8	+	+	-	-	-
A0A0H2XHJ5	+	+	-	-	+
A0A0H2XH24	+	+	+	-	-
A0A0H2XII6	+	+	-	-	-
A0A0H2XIS2	+	+	+	-	-
A0A0H2XIV3	+	+	-	-	-
A0A0H2XJX6	+	+	-	-	-
Q2FF55	+	+	-	-	+
Q2FF63	+	+	-	-	-
Q2FFN1	+	+	-	-	-
Q2FGI7	+	+	-	-	-
Q2FH01	+	+	-	-	-
Q2FIR7	+	+	-	-	-

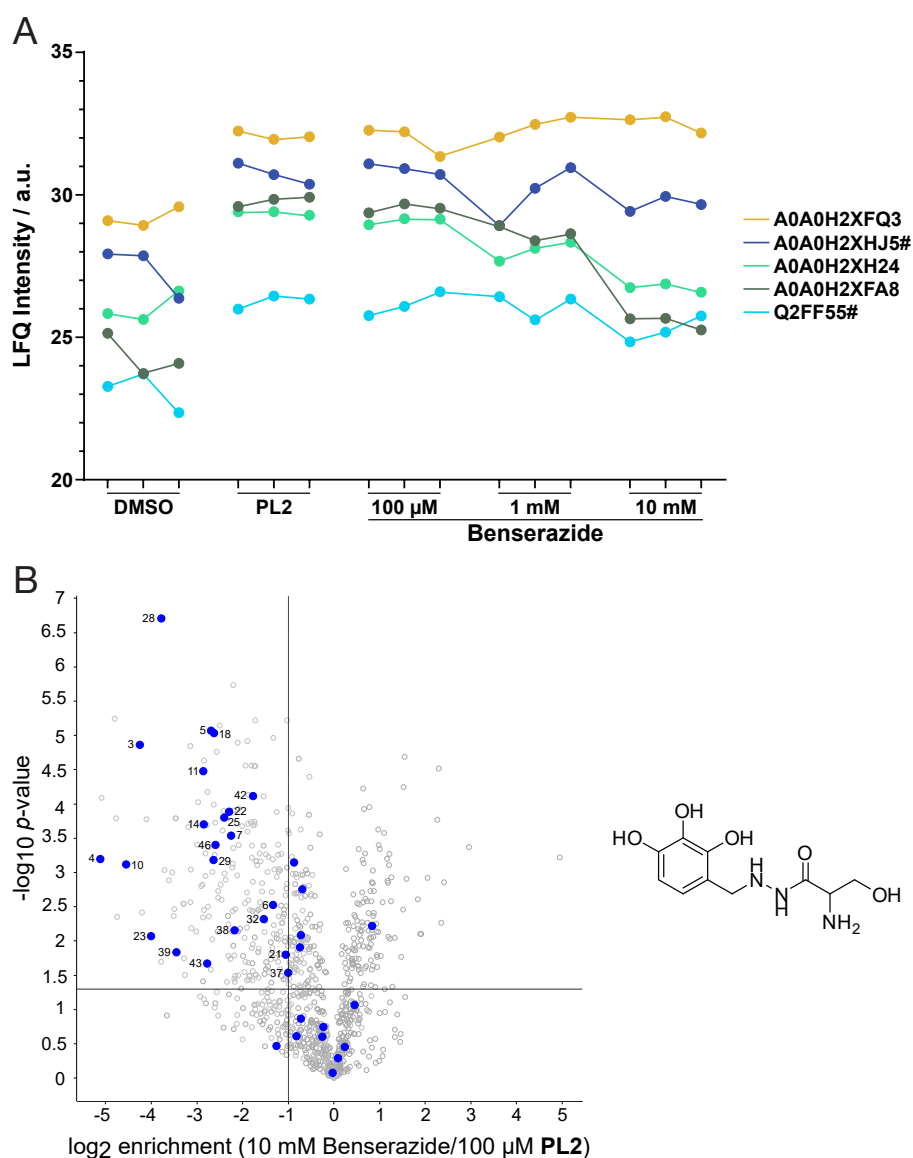


**Figure 2.25:** (A) Profile plot of selected proteins from Benserazide competitive labelling in *S. aureus* USA300 TnpdXS. LFQ intensities of 3 individual replicates are depicted. Essential enzymes are marked with a #.<sup>[254]</sup> (B) Structure of Benserazide and volcano plot of Benserazide competitive labelling at 10 mM compared to 100  $\mu$ M **PL2** representing the *t*-test results [criteria:  $\log_2(\text{enrichment}) > 1$  and  $p\text{-value} < 0.05$ ,  $n = 3$ ]. Adapted from Pfanzelt *et al.*<sup>[170]</sup>

### 2.5.3 CCG-50014 in *S. aureus*

The thiadiazolidinone CCG-50014 was initially found as an inhibitor of regulator G-protein signaling (RGS) proteins and is still one of the most potent inhibitors of this protein class to date.<sup>[300,301]</sup> Prior to this finding, studies on thiadiazolidinones in general revealed them as potent dihydroorotate dehydrogenase (DHODase) inhibitors of

both GRAM-positive and GRAM-negative enzymes but not the human homologue.<sup>[302]</sup> Later, *Citustea et al.* and *Lee et al.* screened compounds against alanine racemases of methicillin resistant *S. aureus* and the mycobacteria *M. tuberculosis* and *M. smegmatis*.<sup>[103,104]</sup> CCG-50014 showed not only an *in vitro* *alr* inhibition activity but also an MIC, which was shown to be twice as high than the IC<sub>50</sub> in HeLa cells, making the compound a potential antibacterial drug candidate, although with a tight therapeutic window.<sup>[103]</sup> Therefore, the question of how the compound binds to **PLP**-DEs arises. Previous studies claim that there is a covalent interaction between the RGS-proteins and CCG-50014 *via* the attack of cysteine residues in proximity.<sup>[301,303,304]</sup> However, the *alr* inhibition studies conclude that the compound is unlikely to interact with the internal **PLP**-aldimine or to occupy the substrate binding-site due to spatial constraints.<sup>[103]</sup> Based on mass spectrometry results, they further claimed that the interaction with *alr* is non-covalent.

In this study, we utilised **PL2** to identify **PLP**-DE off-targets by applying CCG-50014 at three different concentrations (2.5 mM, 500  $\mu$ M and 100  $\mu$ M) with **PL2** at a constant concentration of 100  $\mu$ M. The evaluation of competitive labelling data revealed several **PLP**-DEs, which were competed at 2.5 mM (9 proteins) and 500  $\mu$ M (1 protein) (table 2.6).

**Table 2.6:** List of **PLP**-DEs, which were out-competed with CCG-50014 at different molar ratios compared to **PL2**.

Uniprot ID	Enrichment <b>PL2</b>	Competition CCG-50014 2.5 mM	Competition CCG-50014 500 $\mu$ M	Competition CCG-50014 100 $\mu$ M	Essential
A0A0H2XFD9	+	+	-	-	-
A0A0H2XFH9	+	+	+	-	-
A0A0H2XFY9	+	+	-	-	-
A0A0H2XGP0	+	+	-	-	-
A0A0H2XHH8	+	+	-	-	+
A0A0H2XHJ5	+	+	-	-	+
A0A0H2XIS2	+	+	-	-	-
A0A0H2XKI8	+	+	-	-	+
Q2FIR7	+	+	-	-	-

*A0A0H2XFH9*, a cysteine/methionine metabolism enzyme with predicted cystathionine- $\beta$ -lyase activity<sup>[64]</sup>, was the only **PLP**-DE, which we found to be concentration dependently competed (figure 2.26). Interestingly, three of the out-competed proteins were essential: the already discussed cystein desulfurase *A0A0H2XHJ5*, the **PLP**-homeostasis protein *A0A0H2XHH8* and the *nifS*-type

cysteine desulfurase *A0A0H2XKI8*<sup>[64]</sup>. While the competitive ABPP experiment indicates direct binding to these proteins, they do not reveal the mode of binding of CCG-5001. As cysteine desulfurases contain a catalytically essential cysteine in proximity to their active lysine<sup>[289]</sup>, there is the possibility that the inhibitor binds covalently to this cysteine within the active pocket. This hypothesis for the mode of binding can only be confirmed by direct binding site studies. Of note, the overall depletion of **PLP**-DEs is lower in comparison to both hydrazine compounds phenelzine and benserazide. This is due to a higher reactivity of hydrazines but could also be explained by a higher selectivity of CCG-50014 due to its unprecedented binding mode. Figure 2.26 shows a selection of **PLP**-DEs, some of which were out-competed by CCG-50014. Moreover, the volcano-plot of the 2.5 mM CCG-50014 competition against **PL2** is depicted.

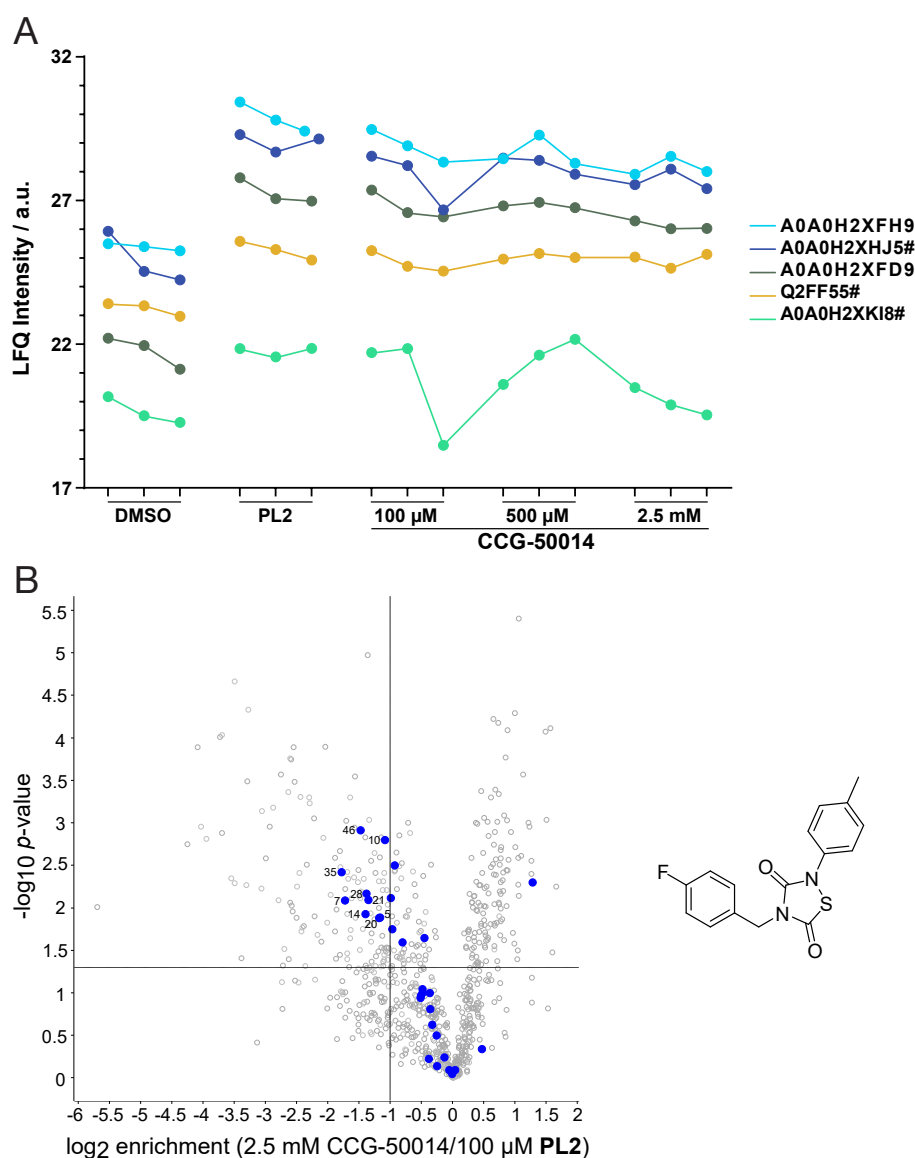
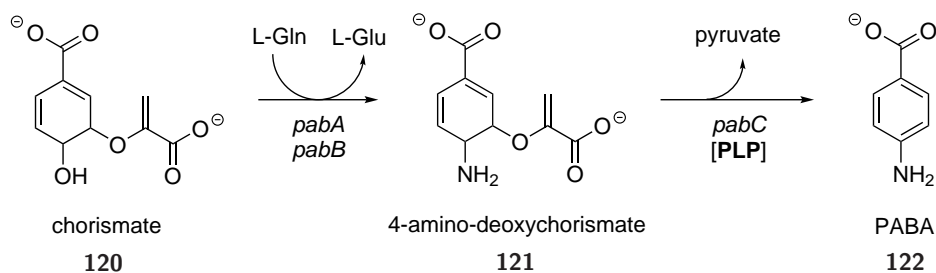


**Figure 2.26:** (A) Profile plot of selected proteins from CCG-50014 competitive labelling in *S. aureus* USA300 TnpdXS. LFQ intensities of 3 individual replicates are shown. Essential enzymes are marked with a #.<sup>[254]</sup> (B) Structure of CCG-50014 and volcano plot of CCG-50014 competitive labelling at 2.5 mM compared to 100  $\mu$ M PL2 representing the *t*-test results [criteria:  $\log_2(\text{enrichment}) > 1$  and  $p\text{-value} < 0.05$ ,  $n = 3$ ]. Adapted from Pfanzelt *et al.*<sup>[170]</sup>

As a final proof-of-concept experiment, we applied our strategy in *E. coli* to analyse the targets of MAC173979 by using our PL3 probe.

2.5.4 MAC173979 in *E. coli*

MAC173979, a dichloronitrophenyl propenone, was found to inhibit *E. coli* growth under nutrient limitation.<sup>[294]</sup> Utilising a metabolite suppression approach, *Zlitni et al.* further proved that MAC173979 inhibits PABA biosynthesis. Unfortunately, they were not able to determine the specific enzyme target. Nevertheless, kinetic evaluation of MAC173979 inhibition of the *pabA-pabB-pabC* system (scheme 2.8) suggested that it acts as an irreversible, time-dependent inhibitor.



**Scheme 2.8:** First, chorismate (**120**) is converted into its 4-amino derivative 4-amino-4-deoxychorismate (**121**) by *pabA* and *pabB*. L-glutamine functions as amino-donor. *PabC*, a PLP-DE, then catalyses the release of pyruvate and formation of PABA (**122**).<sup>[305]</sup>

Since MAC173979 contains a MICHAEL-acceptor system (figure 2.22), it could be susceptible to an attack by nucleophilic residues while one chlorine functions as leaving group. However, synthesis of an analogue lacking the MICHAEL-acceptor system showed similar  $IC_{50}$  values, invalidating a covalent mode of action of the inhibitor. The authors claimed, that, although a covalent interaction cannot be excluded, MAC173979 acts as a noncovalent, time-dependent inhibitor with a very low dissociation constant.<sup>[294]</sup> A more recent study by *Thiede et al.* utilised MAC173979 as an agent which potentiates the tuberculocidal activity of *p*-aminosalicylic acid (PAS) by inhibiting PABA biosynthesis.<sup>[295]</sup> In gene disruption experiments, the authors showed that a *pabB* disruption leads to a more severe defect of *M. tuberculosis* than disruption of *pabC*, which converts 4-amino-4-deoxychorismate (ADC, **121**) to PABA (**122**). They conclude that *pabB* disruption generates stronger auxotrophic phenotypes, since the conversion of ADC to PABA could occur spontaneously, which *Wright et al.* were able to show for chorismate.<sup>[295,306]</sup> In summary, MAC173979 inhibits bacterial PABA biosynthesis, which either led to cell death in PABA lacking media or to enhancement of antituberculocidal activity of PAS. Nevertheless, a specific enzyme target was not determined. Therefore, we wanted to address this question by using our competitive ABPP approach in *E. coli*. For this we used **PL3**, since *pabC*, a potential target enzyme, was detected with this probe only. We applied three different concentrations of MAC173979, 10 mM, 1 mM and 100  $\mu$ M. After data analysis, we found a series of PLP-DEs to be out-competed (table 2.7). Among them were two essential PLP-DEs,

*glyA*, the *E. coli* SHMT<sup>[307]</sup>, and *iscS*, a cysteine desulfurase<sup>[308]</sup>. Many **PLP**-DEs with various functions were out-competed at 1 mM MAC173979 or more. Of note, some proteins were only out-competed at 1 mM, but not at 10 mM, such as *glyA* or *serC*, a phosphoserine aminotransferase. However, due to the fact that *glyA* and *serC* were not enriched by **PL3**, they are most likely false positive hits in this experiment. Moreover, *pabC* was competed at 1 mM and 10 mM MAC173979, a finding we wanted to further investigate *in vitro*.



**Table 2.7:** List of **PLP**-DEs, which were out-competed with MAC173979 at different molar ratios compared to **PL3**.

Gene Name	Enrichment PL3	Competition MAC173979 10 mM	Competition MAC173979 1 mM	Competition MAC173979 100 $\mu$ M	Essential
adiA	+	+	+	-	-
alaC	-	+	-	-	-
alr	+	+	-	-	-
aspC	+	+	+	-	-
avtA	-	+	+	-	-
cysK	+	+	-	-	-
cysM	+	+	-	-	-
dcyD	+	+	+	-	-
dsdA	+	+	+	-	-
glyA	-	-	+	-	+
ilvA	+	+	+	-	-
ilvE	+	+	+	-	-
iscS	+	+	+	-	+
kbl	+	-	+	-	-
ldcC	+	+	+	-	-
lysA	+	+	+	-	-
metC	+	-	+	-	-
pabC	+	+	+	-	-
selA	+	+	+	-	-
serC	-	-	+	-	-
sufS	+	+	+	-	-
thrC	+	+	+	-	-
trpB	+	+	+	-	-
tyrB	+	+	+	-	-
wecE	+	+	+	-	-

As shown in figure 2.27 A, some enzymes were more effectively out-competed than others. *ThrC*, a threonine synthase<sup>[309]</sup>, exhibited the highest decrease in LFQ-intensity, while *pabC* was only weakly affected. Furthermore, the competition experiment at 10 mM MAC173979 is depicted in figure 2.27 B.

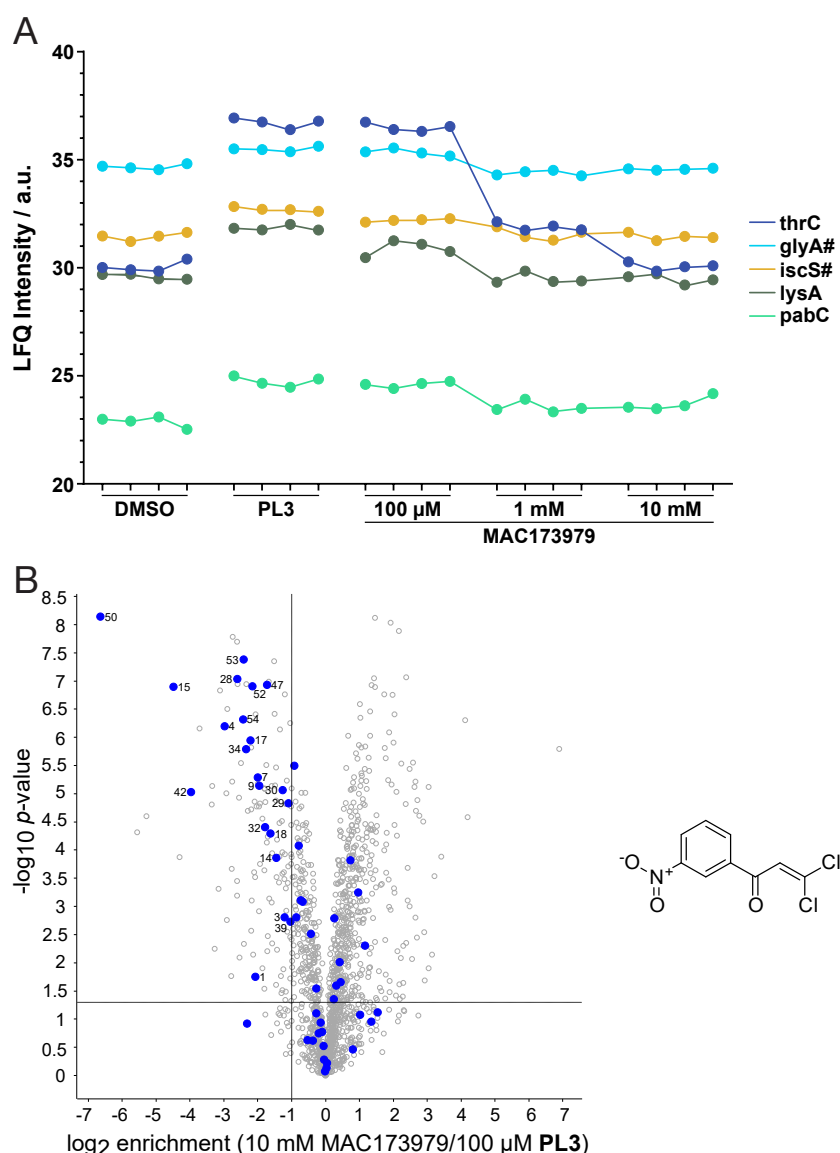
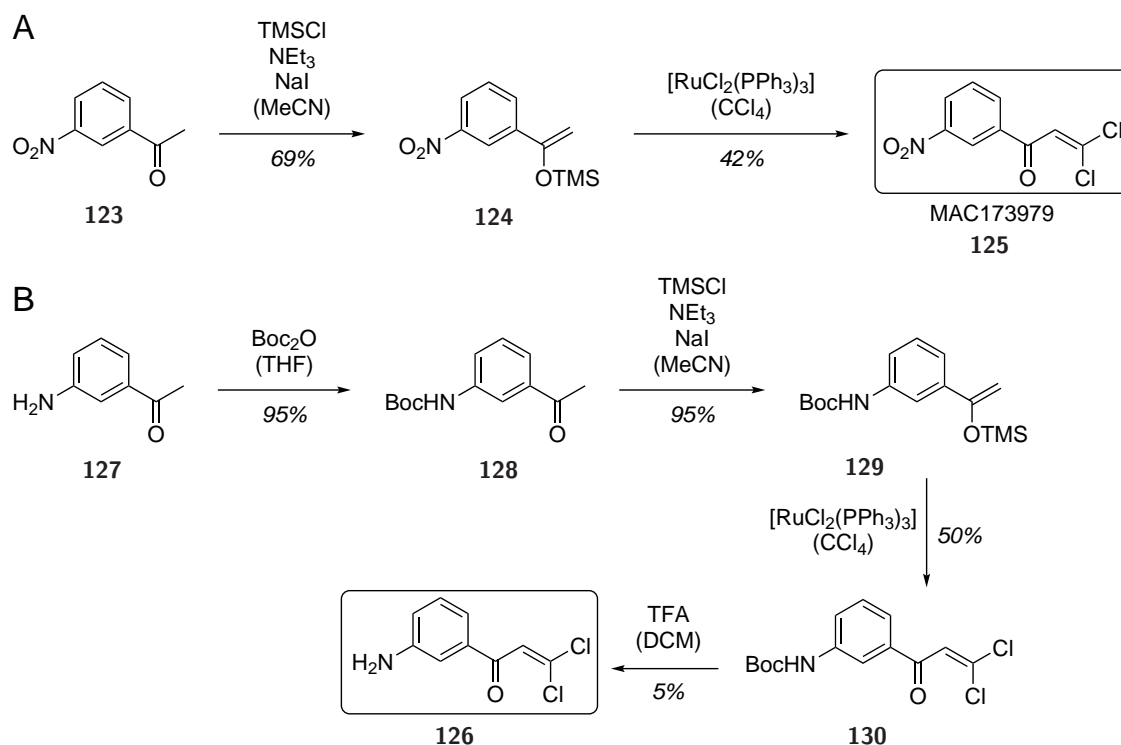


**Figure 2.27:** (A) Profile plot of selected proteins from MAC173979 competitive labelling in *E. coli* K12  $\Delta$ pdxJ. LFQ intensities of 4 individual replicates are depicted. Essential enzymes are marked with a #.<sup>[260–262]</sup> (B) Structure of MAC173979 and volcano plot of MAC173979 competitive labelling at 10 mM compared to 100  $\mu$ M PL3 representing the *t*-test results [criteria:  $\log_2(\text{enrichment}) > 1$  and  $p\text{-value} < 0.05$ ,  $n = 4$ ].

Due to the overwhelming evidence for the inhibition of PABA biosynthesis by MAC173979, but the lack of a clear mechanism of action, we decided to synthesise MAC173979 and its amine derivative in order to study their activity as possible *pabC* inhibitors. We reasoned that MAC173979 could be reduced by nitroreductases within living cells, like other nitro-compounds, to its respective amine.<sup>[310]</sup> This compound could then further bind to PLP-DEs as an external aldimine and function as a transition state mimic.

## 2.5.4.1 Synthesis of MAC173979 and its Amine Derivative

MAC173979 was previously synthesised by *Thiede et al.* from *m*-nitroacetophenone (**123**).<sup>[295]</sup> After conversion of **123** into its silylvinyl ether **124**, reaction with carbon tetrachloride and catalytic  $[\text{RuCl}_2(\text{PPh}_3)_3]$ , MAC173979 (**125**) was yielded as a white powder (scheme 2.9 A). Based on this synthesis, we developed a synthetic route for the MAC173979 amine derivative **126**. We started with *m*-aminoacetophenone (**127**), which was first *tert*-butyloxycarbonyl (Boc) protected using Boc anhydride ( $\text{Boc}_2\text{O}$ ). Then, Boc protected amine **128** was converted into the silylvinyl ether **129** in 95% yield. Fortunately, reaction to the dichlorovinylketon **130** worked for this system as well. The last step, the Boc deprotection, proved to be more difficult, since we did not receive any product after TFA addition. We therefore diluted the reaction upon completion with dichloromethane and first washed the phase with saturated sodium bicarbonate solution<sup>[311]</sup>, which in the end resulted in 5% yield of the MAC173979 amine **126**, which was enough compound for further experiments.



**Scheme 2.9:** (A) Synthesis of MAC173979 (**125**) following a published procedure.<sup>[295]</sup> (B) Synthesis of the MAC173979 amine derivative **126** from *m*-aminoacetophenone (**127**) in four steps.

### 2.5.4.2 Target Validation

In order to study the potency of both MAC compounds, we utilised a coupled, NADH-dependent spectroscopic assay which we have already used in our previous studies on *S. aureus pabC*.<sup>[151,312]</sup> Here, chorismic acid is converted by *pabB* into ADC using  $(\text{NH}_4)_2\text{SO}_4$  as amine source. This is the reason for the absence of *pabA*, the glutamine amidotransferase, which normally generates ammonia, which *pabB* can incorporate into chorismate.<sup>[313]</sup> Due to the release of pyruvate, the reaction can be tracked utilising LDH. LDH converts pyruvate to lactate while generating  $\text{NAD}^+$  from NADH, which we monitored spectroscopically at 340 nm. First, conditions were set as following:  $1\ \mu\text{M}$  *pabC* from *E. coli* was first incubated with different molar ratios of MAC173979 or the MAC173979 amine (1:1, 1:10, 1:100, 1:500, 1:1000) for 30 minutes at  $37^\circ\text{C}$ . Then  $5\ \mu\text{M}$  *pabB* from *E. coli*,  $0.75\ \text{mM}$  NADH,  $1\ \text{mM}$  chorismate and  $25\ \mu\text{g}$  LDH were added to the wells and the reaction was monitored by measuring the absorbance at 340 nm every minute (figure 2.28). Unfortunately, addition of high concentrations of both compounds led to inconclusive curves, probably due to the insolubility of those compounds at high concentrations. Nevertheless, MAC173979 at a 1:1 ratio did not affect the reaction rate, while a ratio of 1:10 and 1:100 seemed to lower the conversion. On the other side, the MAC173979 amine did not lead to a significant decrease in *pabC* activity. Several control experiments proved the integrity of the assay itself. However, these data are not convincing enough in order to conclude any inhibitory activity of MAC173979 or its amine derivative against *pabC*.

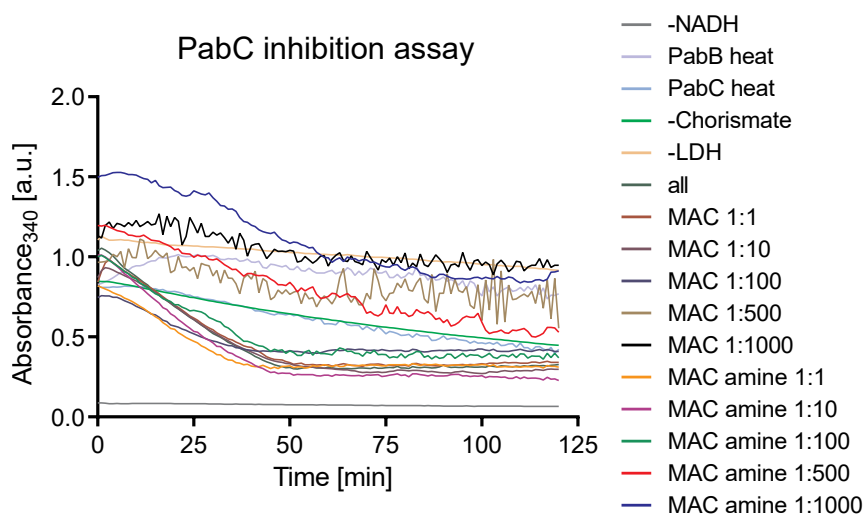


**Figure 2.28:** The aminodeoxychorismate lyase *pabC* catalyses the last step of the PABA biosynthesis, while pyruvate is formed as a side product. Therefore, the reaction rate can be monitored by a coupled, NADH-dependent spectroscopic assay, where pyruvate is converted to lactate by LDH, which consumes one equivalent of NADH per turnover.<sup>[151,312]</sup>

# 3

## SUMMARY AND OUTLOOK

---

*In this chapter, a summary of the results achieved in this thesis as well as an outlook on possible developments of the project in the future will be discussed.*

### Contents

---

<b>3.1</b>	<b>Summary . . . . .</b>	<b>88</b>
<b>3.2</b>	<b>Outlook . . . . .</b>	<b>91</b>

---

## 3.1 Summary

To overcome the antibiotic resistance crisis, ways to go beyond the classical scope of bacterial targets are urgently needed. One possible solution is to mine the cellular inventory of cofactor-dependent proteins for novel targets exhibiting an essential role for viability. This approach bears several advantages including the focus on an enzyme class often involved in crucial cellular processes, the druggability due to confirmed small molecule (cofactor) binding and the uptake of cofactors into challenging GRAM-negative cells.

Pyridoxal phosphate-dependent enzymes (**PLP**-DEs) play a crucial role in basic metabolic processes in all living organisms. Accordingly, some drugs were developed against promising **PLP**-DEs, among them antibiotics like D-cycloserine. Investigating this enzyme class is urgently needed to not only understand their catalytic scope but also to screen inhibitors off-targets in a competitive approach.

This thesis covers the synthesis and evaluation of pyridoxal derived ABPP probes for the global profiling of **PLP**-dependent enzymes in *S. aureus*, *E. coli* and *P. aeruginosa*. Besides the functional investigation of putative or poorly characterised **PLP**-DEs, we screened a small library of putative **PLP**-DE inhibitors against these strains and validated target enzymes *in vitro*, which were out-competed in competitive ABPP experiments.

In literature, many examples of modified **PL(P)** scaffolds were shown to exhibit catalytic activity in some **PLP**-DEs similar to **PLP**. We therefore adapted protocols by Hoegl *et al.*<sup>[151]</sup>, Kim *et al.*<sup>[198]</sup> and Saha *et al.*<sup>[223]</sup> and designed synthetic routes for C2'-, C3'- and C6-derivatised **PL** ABP's. Our current **PL**-probe library consists of 13 derivatives, which bear either an alkyne or an azide tag for ABPP. First, we investigated the ability of *S. aureus* (SaPLK) and *E. coli* (*pdxK*) pyridoxal kinases (PLKs) to convert our probes into biological active cofactor mimics. Except for the bulky, C6-modified probes **PL11** and **PL12**, which were only poorly phosphorylated, we could show that all other probes were efficiently activated. Next, we utilized an *E. coli* K12 pyridoxine 5'-phosphate synthase knockout strain, termed  $\Delta$ pdxJ, for growth experiments in chemically defined media (CDM) lacking **PL**. This strain is unable to synthesise **PLP** *de novo* and therefore perfectly suitable to show that our probes can function as cofactor surrogates. Indeed, growth was observed for some tested probes. This finding underlines the ability of some of our probes to substitute the natural cofactor. Moreover, we elucidated the minimal amount of **PL** supplemented to CDM, which is necessary to support normal growth. All strains investigated were supplemented with 250 nM **PL** during growth, no matter if wild type strains or **PLP** *de novo* synthesis mutants. Additional analytical labelling experiments in *E. coli* K12 wild type and  $\Delta$ pdxJ with **PL3** and **PL13** revealed specific labelling of proteins in both strains. However, signals of bands were more intense in the knockout strain.

Prior to our **PLP**ome profiling, we tested the influence of probe concentration and medium on the labelling efficiency. Therefore, we utilised the *S. aureus* USA300 transposon mutant TnpdxS from our previous study and benchmarked the labelling efficiency at 10 and 100  $\mu\text{M}$  **PL2** using full medium (B-medium) or CDM. The number of enzymes could be increased from 20 (100  $\mu\text{M}$  **PL2**, B-medium) to 27 (100  $\mu\text{M}$  **PL2**, CDM), demonstrating a huge increase in efficiency when using CDM for bacterial growth. We anticipate, that a lower amount of **PL** in the media in turn maximises the incorporation of our probes into **PLP**-DEs. With the refined labelling protocol in hand, we investigated the **PLP**omes of *S. aureus* USA300 TnpdxS and *E. coli* K12  $\Delta\text{pdxJ}$  with our complete set of probes. We were able to enrich 71% (*S. aureus*) and 61% (*E. coli*) of the predicted or confirmed **PLP**ome. For the first time, we were able to show, that our chemical proteomic strategy is transferable to GRAM-negative bacteria. With an optimised set of probes, we managed to mine the *P. aeruginosa* wild type strain for **PLP**-DEs, most likely enabled by a sufficient competition of the probes with endogenous **PLP**. Here, we received a coverage of 51% of all known or predicted **PLP**-DEs. This showcases, that our methodology is not constrained to the use of knockout or transposon strains, which are devoid of **PLP** *de novo* synthesis.

The high structural diversity of our **PL**-probe library enabled specific labelling of certain **PLP**-DEs with individual probes in all three strains. We found some **PLP**-DEs specifically with the new generation of probes, which would otherwise have escaped our attention. Among them was an uncharacterised HTH-type transcriptional regulator (*ydcR*) from *E. coli*, whose DNA binding site we were able to resolve *via* electrophoretic mobility shift assays. We further investigated three putative **PLP**-binders from *P. aeruginosa* and could give insights into the catalytic mechanisms of *PA2683*, a serine/threonine dehydratase, as well as the two aminotransferases *PA3659* and *PA3798*. Third, *A0A0H2XHJ5*, a putative cysteine desulfurase from *S. aureus*, was confirmed to produce alanine from cysteine by a targeted metabolomics assay. Our methodology proved to be a powerful tool to detect novel or poorly characterised **PLP**-DEs in GRAM-positive and -negative bacteria.

As an application, we collected a library of 53 putative **PLP**-DE binders and screened them against the strains investigated in this thesis. Indeed, 14 compounds were active in at least one of the three strains. Interestingly, phenelzine, a human non-selective monoamine oxidase inhibitor, showed high activity in *S. aureus*. Since the only chemically reactive group in phenelzine is its hydrazine moiety, we wanted to further investigate the influence of structural modifications on the antibiotic activity. We therefore synthesised 10 phenelzine derivatives bearing modifications either at the phenyl or the aliphatic residue. However, we could not observe a lower minimal inhibitory concentration in *S. aureus*, but three of the derivatives were active in *P. aeruginosa*, which is generally hard to address with drugs. For our proof-of-concept experiments, we choose phenelzine, benserazide, CCG-50014 (all in *S. aureus*) and MAC173979 (*E. coli*). Here, we studied the **PLP**-dependent protein targets in

competitive ABPP approaches utilising **PL2** or **PL3**. We could show not only that the compounds inhibit certain **PLP**-DEs concentration dependently, but were also able to confirm two enzyme targets of phenelzine, *A0A0H2XHJ5* and *A0A0H2XII6*. Using targeted metabolomic assays, we showed that phenelzine inhibits *A0A0H2XHJ5* cysteine desulfurase and *A0A0H2XII6* lysine decarboxylase activity with  $IC_{50}$  values of  $14.70 \pm 1.22 \mu\text{M}$  and  $50.03 \pm 1.07 \mu\text{M}$ , respectively. In summary, our chemical proteomic approach provides the possibility to screen potential drugs for new **PLP**-dependent antibacterial targets in diverse pathogenic bacteria.

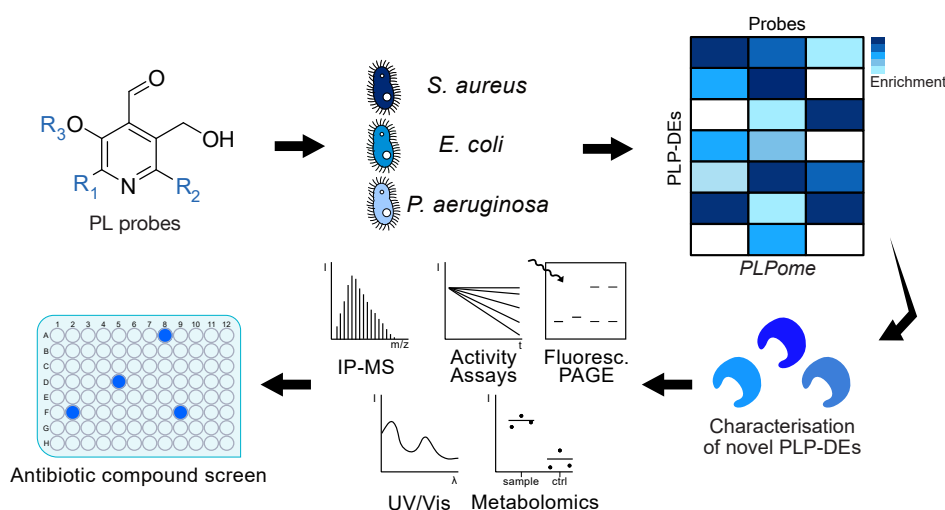


**Figure 3.1:** Graphical summary of the work. Functionalised **PL**-derivatives were utilised to study the **PLP**ome of three pathogenic bacteria. Interestingly, certain probes exhibited specific labelling and showed preferences in their target enzymes. We selected five putative **PLP**-binders from all three organisms and were able to give insights into their catalysis by using several different biochemical methods. In the end, we screened potential **PLP**-DE inhibitors and could verify two **PLP**-dependent protein targets of phenelzine *via* targeted metabolomics. Adapted from Pfanzelt *et al.*<sup>[170]</sup>

In a side project, a novel, pro-tide-based phosphoramidate probe, **PL3PA**, was synthesised in order to circumvent the limiting phosphorylation of certain PLKs. Especially the human PLK is highly restricted with respect to its substrates. A phosphoramidate probe could be activated PLK independently *in situ* and could give access to organisms, which are more difficult to mine with our classical **PL**-probes. First experiments showed, that the kinetics of **PL3PA** cleavage are not yet ideal for its application in human cells. Nevertheless, optimising the phosphoramidate moiety for enhanced kinetics could solve the activation issue and could help us to profile the human **PLP**ome faster and with a higher coverage, compared to our previous studies using the unphosphorylated probe **PL1**.<sup>[152]</sup>



## 3.2 Outlook

The wealth of uncharacterised proteins represents an untapped source for novel drug targets. However, tools to decipher their function are largely lacking. Hence, strategies which allow the number of possible enzymatic transformations to be narrowed down are ideal starting points for functional annotations. Our methodology to mine a druggable class of enzymes helps to increase our understanding of this diverse, versatile enzyme family and is able to provide valuable data for inhibitor screening approaches. Nevertheless, full enzyme characterisation is only possible by combining different biochemical and microbiological strategies.

In order to increase labelling efficiency and to address different organisms, we synthesised a phosphoramidate **PL3** derived probe which is independent from activation by PLK. With a refined pro-tide-based **PL**-probe, one could not only perform **PLP**ome profiling in many different bacterial strains and human cells, but could also utilise the phosphoramidate for the design of specific inhibitors of **PLP**-DEs. Many **PL**-derived inhibitors, often transition-state mimics, need to be phosphorylated in order to be active *in vivo*. For example, the plasmodial ornithine decarboxylase inhibitor PT3 is a cyclised conjugate of **PL** and tryptophane, which gets phosphorylated by cellular PLK enhancing its inhibitory effect drastically.<sup>[210]</sup> A phosphoramidate transition-state mimic would logically be more active than its unphosphorylated form in most cases, since substrate specificity of PLKs are often the restricting factor. In future, phosphoramidate transition-state mimics could enhance the inhibitory effect of **PL**-derived drugs. For both labelling and inhibitor design with phosphoramidates, it could be necessary to adjust the reaction kinetics by modulating the residues. Interestingly, recent studies on kinetics of enzyme-free hydrolysis of phosphoramidates revealed that substitution of alanine to proline-derivatives enhanced cleavage 45-fold.<sup>[252]</sup> Moreover, *Procházková et al.* demonstrated photoinducible phosphoramidate systems for studying the self-immolation process of this compound class.<sup>[314]</sup> They concluded that the kinetics of cleavage highly depends on the amino acid and its sterical demand. Therefore, adjusting the **PL3PA** phosphoramidates residues can lead to an increase of its cleavage rates, which would be beneficial for future **PLP**ome profiling experiments in different organisms.

Another approach could be the screening of more diverse compound libraries against their activity on **PLP**-DEs. As we demonstrated in this study, a proteome-wide profiling of (off)-targets is possible by a competitive ABPP approach with our **PL**-probes. Once we are able to address large parts of the human **PLP**ome with our phosphoramidate probe, the screening could then be extended in order to find inhibitors against **PLP**-DEs, which are involved in the development of human diseases. For example, serine hydroxymethyltransferase and ornithine aminotransferase are key target enzymes, since they are involved in cell proliferation and cancer development.<sup>[315,316]</sup>

Bacterial resistances are becoming more and more common among pathogenic strains, leading to a limitation in treatability of their infections. Novel antibiotics are therefore urgently needed. Modern perspectives suggest to re-utilise validated antibacterial targets and associated lead molecules.<sup>[317]</sup> One of these studies led to the development of an antibiotic, which is active against drug-resistant *S. aureus*, persists and biofilms.<sup>[318]</sup> The original structure, sorafenib, a human kinase inhibitor, was structurally derivatised leading to a potent polypharmacological antibiotic. Especially unprecedented targets like **PLP**-DEs are attractive clinically druggable targets, since bacteria only share one third of their **PLP**ome with humans.<sup>[62]</sup> For instance, several **PLP**-dependent bacterial peptidoglycan synthesis enzyme inhibitors were developed, including D-cycloserine (DCS).<sup>[93]</sup> However, severe side-effects limit their clinical use. Since most of the known **PLP**-DE inhibitors are mechanism-based, refining of their structure could lead to more selective candidates with less off-targets. Good examples of this strategy are represented by the cyclic, fluorinated inhibitors developed by *Silverman et al.*<sup>[116,134,135,319–326]</sup> A similar strategy towards refining the chemical structures would be transferable to the alanine racemase inhibitor DCS. Along with combined modern techniques like mass spectrometry approaches and computational docking studies, our chemical proteomic tool could help to determine both selectivity and potency of novel **PLP**-DE inhibitors in the future.

# 4

## MATERIAL AND METHODS

---

*Chemical synthesis and biochemical procedures are described in this chapter. Most experiments were adapted from Pfanzelt et al.<sup>[170,221]</sup> and Hoegl et al.<sup>[151,248]</sup>*

### Contents

---

4.1	Chemistry . . . . .	94
4.2	Biochemistry . . . . .	162
4.3	Proteomics . . . . .	173
4.4	Targeted Metabolomics Assays . . . . .	179
4.5	Compound Screen . . . . .	183

---

## 4.1 Chemistry

### 4.1.1 General Methods

All air or water sensitive reactions were carried out under argon atmosphere in dried reaction flasks. Anhydrous solvents and water-sensitive liquid chemicals were transferred using argon flushed syringes.

Commercially available starting materials, reagents and anhydrous solvents were obtained from *Sigma Aldrich*, *TCI Europe*, *VWR*, *Roth*, and *Alfa Aesar*, and used without further purification. Percent values (%) refer to mass percent values. The solutions used are aqueous solutions, unless otherwise stated.

#### Analytical thin layer chromatography

Qualitative thin layer chromatography was recorded on silica gel plates (aluminum) from *Merck* (0.25 mm silica 60, F254). For visualization, TLC plates were observed under UV-light ( $\lambda = 254$  nm and  $\lambda = 366$  nm), and/or stained with  $\text{KMnO}_4$  (3.00 g  $\text{KMnO}_4$ , 20.0 g  $\text{K}_2\text{CO}_3$  and 5.00 mL 5%  $\text{NaOH}$  in 300 mL water), CAM (5.00 g Cer-(IV)-sulfate, 25.0 g ammoniummolybdate and 50.0 mL conc. sulphuric acid in 450 mL water) or PMA (5 g phosphomolybdic acid in 100 mL ethanol) with subsequent heat treatment (ca. 250 °C). Column chromatography was carried out using silica gel [40-63  $\mu\text{m}$  (Si 60)] from *Merck*.

#### NMR-Spectroscopy

NMR spectra were recorded on *Bruker* AVHD-400 and AVHD-500 instruments. The chemical shifts ( $\delta$ ) are reported in parts per million (ppm) and spectra are referenced to residual proton and carbon signals of the deuterated solvents:<sup>[327]</sup>

$\text{CDCl}_3$ :  $\delta$  ( $^1\text{H}$ ) = 7.26 ppm,  $\delta$  ( $^{13}\text{C}$ ) = 77.16 ppm

$d^6$ -DMSO:  $\delta$  ( $^1\text{H}$ ) = 2.50 ppm,  $\delta$  ( $^{13}\text{C}$ ) = 39.52 ppm

$\text{CD}_3\text{CN}$ :  $\delta$  ( $^1\text{H}$ ) = 1.94 ppm,  $\delta$  ( $^{13}\text{C}$ ) = 1.32, 118.26 ppm

The following abbreviations are used to describe NMR coupling patterns: s – singlet; d – doublet; t – triplet; q – quartet; p – quintet; dd – doublet of doublet; m – multiplet; br – broad. The coupling constants,  $J$ , are reported in Hertz (Hz).

#### Mass-Spectrometry

HRMS spectra were acquired by ESI using a LTQ-FT Ultra or a LTQ-Orbitrap XL mass spectrometer (*Thermo Fisher Scientific*). LC-MS measurements were conducted on a MSQ Plus mass spectrometer (*Thermo Fisher Scientific*). Processing of mass spectrometry data was performed using Xcalibur 2.2 (*Thermo Fisher Scientific*).

### High Pressure Liquid Chromatography

Compounds were purified by preparative, reversed-phase HPLC using a *Waters* 2545 quaternary gradient module equipped with a *Waters* 2998 photodiode array detector and fraction collector on a *YMC* Triart C18 column (250×10 mm, 5  $\mu$ m). Gradients are listed in table 4.1, using ddH<sub>2</sub>O and HPLC-grade acetonitrile (no TFA) as the mobile phase.

Method A		Method B		Method C		
t[min]	%-H <sub>2</sub> O +0.1% TFA	%-MeCN +0.1% TFA	%-H <sub>2</sub> O	%-MeCN	%-H <sub>2</sub> O	%-MeCN
0	98	2	98	2	98	2
1	98	2	90	10	98	2
12	50	50	50	50	70	30
13	2	98	2	98	2	98
14	2	98	2	98	2	98
15	98	2	98	2	98	2
17	98	2	98	2	98	2

Method D		Method E		
t[min]	%-H <sub>2</sub> O	%-MeCN	%-H <sub>2</sub> O +0.1% TFA	%-MeCN +0.1% TFA
0	98	2	98	2
1	60	40	80	20
12	2	98	40	60
13	2	98	2	98
14	2	98	2	98
15	98	2	98	2
17	98	2	98	2

**Table 4.1:** List of used HPLC-gradients.

## 4.1.2 Synthesis

### 4.1.2.1 General Procedures (GP)

#### Alkylation (GP1) <sup>[151,220]</sup>

To a dry flask containing anhydrous tetrahydrofuran at 0 °C were added diisopropylamine (2.4 eq) and *n*-butyllithium (2.5 M in hexanes, 2.2 eq), and the reaction mixture was stirred for 20 min. Upon cooling to −78 °C, the corresponding protected intermediate (1.0 eq) dissolved in anhydrous tetrahydrofuran was added dropwise. After stirring the reaction for 1 h, propargyl bromide (3.0 eq) was added at −78 °C and the reaction was allowed to warm to room temperature overnight. The reaction was quenched by adding satd. ammonium chloride solution (50 mL) at −78 °C and water (50 mL). The aqueous layer was extracted with ethyl acetate (4×60 mL), and the combined organic phases were washed with satd. sodium chloride solution (60 mL), dried over sodium sulfate and concentrated under reduced pressure. The crude product was purified by flash chromatography.

#### TMS-Protection of Alkynes (GP2) <sup>[328,329]</sup>

Corresponding alkyne (1.0 eq) was added to a solution of *n*-butyllithium (2.5 M in hexanes, 2.2 eq) in anhydrous tetrahydrofuran at −78 °C. The solution was then allowed to warm to 20 °C and was stirred for 30 min. Subsequently, trimethylsilyl chloride (2.5 eq) was added slowly at −78 °C and the reaction was allowed to warm to room temperature overnight. 5% acetic acid (60 mL) was then added and the mixture was stirred for 2 h at room temperature, concentrated and extracted with diethyl ether (3×50 mL). The combined organic phases were washed with satd. sodium chloride solution (150 mL), dried over sodium sulfate, filtered and concentrated. The crude product was purified by flash chromatography.

#### Mesylation of Alcohols (GP3) <sup>[328,330–332]</sup>

To a solution of corresponding alcohol (1.0 eq) in anhydrous dichloromethane was added triethylamine (2.0 eq). Methanesulfonyl chloride (1.2 eq) was added dropwise at −10 °C or −15 °C and the reaction was stirred for 2 h. The reaction mixture was then poured into 0.5 M hydrochloric acid (20 mL), the organic layer was separated and washed with a satd. sodium bicarbonate solution and satd. sodium chloride solution (each 30 mL). The organic phase was dried over sodium sulfate, filtered and concentrated to yield the corresponding mesylate which was used for the next reaction step without any further purification.

**Bromination of Mesylates (GP4)** [328,331]

To a solution of corresponding mesylate (1.0 eq) in anhydrous acetone was added lithium bromide (4.8 eq). The reaction was then stirred at 40 °C for 72 h. Upon completion, most of the solvent was removed *in vacuo* and diethyl ether (200 mL) and water (20 mL) were added. The organic layer was washed with satd. sodium sulfate solution, satd. sodium bicarbonate solution and water (each 50 mL) and subsequently dried over sodium sulfate, filtered and concentrated *in vacuo*. The crude product was purified by flash chromatography.

**Substitution with Sodium Azide (GP5)** [332,333]

To a solution of corresponding mesylate (1.0 eq) in anhydrous dimethyl formamide was added sodium azide (1.1 eq), and the suspension was heated to 65 °C with vigorous stirring for 3 h under argon. Then, water (20 mL) was added, the suspension was filtered through a plug of Celite<sup>®</sup>, and the Celite<sup>®</sup> was washed with diethyl ether (100 mL). The water dimethyl formamide mixture was extracted with diethyl ether (3×30 mL), and the combined organic layers were washed with water (2×50 mL) and satd. sodium chloride solution (60 mL). The organic phase was then dried over sodium sulfate, filtered and concentrated *in vacuo*. The crude product was purified by flash chromatography.

**Nucleophilic Substitution (GP6)** [198,199]

Protected *N*-oxide (1.0 eq) was added to a dry flask containing anhydrous tetrahydrofuran and the solution was cooled to −78 °C. Subsequently, *iso*-butylchloroformate (1.0 eq) was added dropwise. The reaction was stirred for 30 min, upon which corresponding alkyne (2.0 eq) was rapidly added. The reaction was stirred at −78 °C for 1 h upon which the ice bath was removed and the reaction was allowed to warm to room temperature for 1 h. The reaction was quenched by adding satd. sodium bicarbonate solution (30 mL) at −78 °C. The aqueous layer was extracted with diethyl ether (3×30 mL). The combined organic phases were dried over sodium sulfate and concentrated under reduced pressure. The crude product was purified by flash chromatography.

**Click-Reaction (GP7)** [334]

To a solution of corresponding alkyne (1.0 eq) in acetonitrile/dimethyl sulfoxide (4:1) were added sodium ascorbate (0.20 eq) and copper sulfate pentahydrate (0.20 eq). Subsequently, corresponding azide (1.0 eq) was added to the reaction mixture dropwise under vigorous stirring and the reaction was stirred overnight at room temperature. Upon completion, the reaction was quenched with satd. ammonium chloride solution (10 mL), forming a white precipitate. After separation, the aqueous layer was extracted with ethyl acetate (3×30 mL). The combined organic phases were washed with satd. ammonium chloride solution (50 mL) and dried over sodium sulfate. Upon concentra-

tion under reduced pressure, the residue was purified by flash chromatography.

#### **TMS Deprotection (GP8)** [329]

To a solution of corresponding TMS-protected alkyne (1.0 eq) dissolved in anhydrous methanol was added potassium carbonate (1.0-5.0 eq) and the reaction was stirred overnight at room temperature. Upon completion, diethyl ether and water were added (each 20 mL) and the aqueous layer was extracted with diethyl ether (3×40 mL). After concentration under reduced pressure, the residue was purified by flash chromatography.

#### **Acetal and Ether Deprotection (GP9)** [151,198]

Corresponding MOM-protected acetal (1.0 eq) was dissolved in a mixture of acetone/water (1:1) containing 5% sulfuric acid and refluxed at 85 °C for 1 h. The reaction was allowed to cool to room temperature and was then concentrated under reduced pressure. The product was purified by HPLC using the given method.

#### **TMS, Acetal and Ester Deprotection (GP10)** [198]

Corresponding Piv-protected alkyne (1.0 eq) was dissolved in 2% potassium hydroxide in methanol and stirred at room temperature for 2 h. The reaction was diluted with dichloromethane (10 mL), passed through silica gel and washed with a mixture of dichloromethane/methanol (1:1). The filtrate was concentrated to dryness and the resulting brown solid was dissolved in 5% sulfuric acid in acetone/water (1:1). The mixture was heated at 85 °C for 1 h and then the reaction was allowed to cool down and acetone was removed under reduced pressure. The product was purified by HPLC using the given method.

#### **Phenelzine Derivatisation (GP11)** [241]

Procedure adapted from a previously published protocol by *Prusevich et al.* Hydrazine monohydrate (10 eq)<sup>†</sup> was added to a stirred solution of the appropriate alkyl halide (1.0 eq) in ethanol (3 mL). The reaction mixture was refluxed for overnight, after which the mixture was concentrated to dryness *in vacuo*. The crude residue was dissolved in a minimum volume of acetonitrile/water and purified by preparative reversed phase HPLC. Unless otherwise stated, the eluents as given in table 4.1 (method A). The fractions containing the product were combined and dried by lyophilisation.

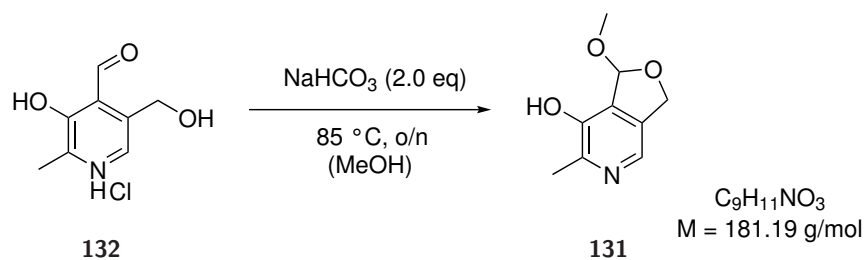
<sup>†</sup>CAUTION: Hydrazine monohydrate is highly toxic.



**4.1.2.2** Probe Synthesis

PL1, PL2, PL3, PL4 and PL5 were synthesized as described previously.<sup>[151,152]</sup>

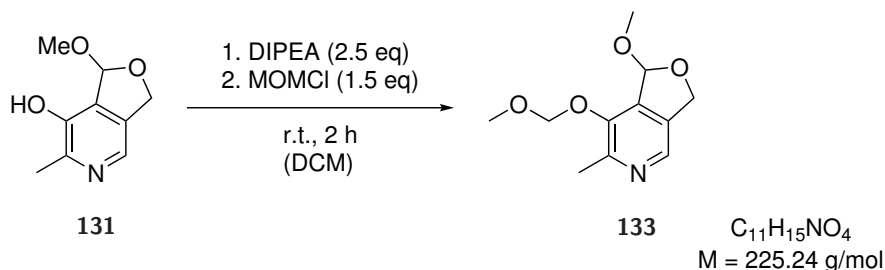
**1-Methoxy-6-methyl-1,3-dihydrofuro[3,4-*c*]pyridin-7-ol (131)**<sup>[151,198]</sup>



Pyridoxal hydrochloride (7.00 g, 34.4 mmol, 1.0 eq) was suspended in anhydrous methanol (70 mL) and refluxed at 85 °C for 1 h. After cooling to room temperature, sodium bicarbonate (2.89 g, 34.4 mmol, 1.0 eq) was added. The reaction was stirred at 85 °C overnight. The obtained white mixture was filtered three times to remove precipitated sodium chloride and washed with dichloromethane (1 × 50 mL). Removal of the solvents caused crystallization of intermediate acetal **131**, which was used in the following reaction without further purification.

**TLC:**  $R_f = 0.50$  (10% MeOH/DCM) [UV/ $KMnO_4$ ].

**HRMS** (ESI) ( $C_9H_{11}NO_3$   $[M+H]^+$ ) calcd.: 182.0817  
found: 182.0811.

**1-Methoxy-7-(methoxymethoxy)-6-methyl-1,3-dihydrofuro[3,4-c]pyridine (133)** <sup>[151,335]</sup> pyri-

1-Methoxy-6-methyl-1,3-dihydrofuro[3,4-c]pyridin-7-ol (5.49 g, 30.3 mmol, 1.0 eq) was dissolved in anhydrous dichloromethane (55 mL) and diisopropylethylamine (13.2 mL, 9.72 g, 75.8 mmol, 2.5 eq) was added while stirring. Chloromethyl methyl ether (3.45 mL, 3.66 g, 45.4 mmol, 1.5 eq) was then added dropwise at 0 °C and the reaction mixture was stirred for 2 h at room temperature. After removal of the solvent and purification by flash chromatography (MeOH/DCM, 1-4%), compound **133** (6.16 g, 27.3 mmol, 80% over 2 steps) was obtained as a yellow oil.

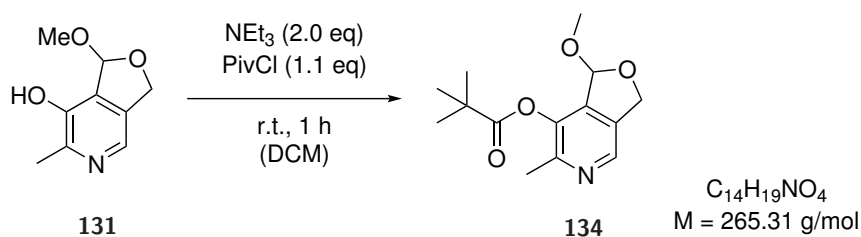
**TLC:**  $R_f = 0.49$  (80% EtOAc/hexanes) [UV/CAM].

**$^1H$ -NMR** (400 MHz,  $CDCl_3$ ):  $\delta$ [ppm] = 8.15 (s, 1 H), 6.26 (s, 1 H), 5.43 (d,  $^4J = 6.5$  Hz, 1 H), 5.18 (d,  $^2J = 12.7$  Hz, 1 H), 5.08 (d,  $^4J = 6.5$  Hz, 1 H), 5.03 (d,  $^2J = 12.7$  Hz, 1 H), 3.51 (s, 3 H), 3.46 (s, 3 H), 2.56 (s, 3 H).

**$^{13}C$ -NMR** (100 MHz,  $CDCl_3$ ):  $\delta$ [ppm] = 150.2, 146.5, 136.0, 135.0, 134.2, 106.2, 96.3, 70.2, 56.9, 54.9, 19.4.

**HRMS** (ESI) ( $C_{11}H_{15}NO_4$  [M+H]<sup>+</sup>) calcd.: 226.1079  
found: 226.1072.

The analytical data are in accordance with previous literature reports.<sup>[151]</sup>

1-Methoxy-6-methyl-1,3-dihydrofuro[3,4-*c*]pyridin-7-yl pivalate (**134**)<sup>[198]</sup>

To a solution of 1-methoxy-6-methyl-1,3-dihydrofuro[3,4-*c*]pyridin-7-ol (3.64 g, 20.1 mmol, 1.0 eq) in anhydrous dichloromethane (60 mL) was added triethylamine (5.26 mL, 3.87 g, 38.2 mmol, 1.9 eq). Subsequently, pivaloyl chloride (2.75 mL, 2.71 g, 22.5 mmol, 1.1 eq) was added at 0 °C and the reaction mixture was stirred for 2 h at room temperature. Upon completion, the solution was concentrated under reduced pressure to yield compound **134** as a pale yellow oil, which did not require further purification.

**TLC:**  $R_f = 0.56$  (50% EtOAc/hexanes) [UV/ $KMnO_4$ ].

**$^1H$ -NMR** (400 MHz,  $CDCl_3$ ):  $\delta$ [ppm] = 8.35 (s, 1 H), 6.09 (s, 1 H), 5.23 (d,  $^2J = 12.8$  Hz, 1 H), 5.10 (d,  $^2J = 12.8$  Hz, 1 H), 3.37 (s, 3 H), 2.45 (s, 3 H), 1.40 (s, 9 H).

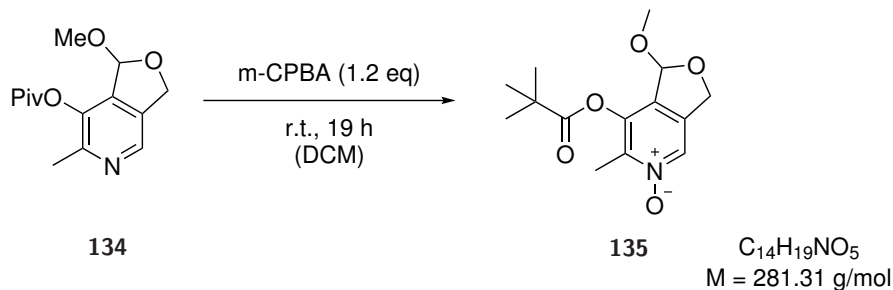
**$^{13}C$ -NMR** (100 MHz,  $CDCl_3$ ):  $\delta$ [ppm] = 175.5, 150.9, 141.2, 139.6, 138.4, 135.8, 106.1, 70.8, 54.6, 39.4, 27.2, 18.9.

**HRMS** (ESI) ( $C_{11}H_{15}NO_4$   $[M+H]^+$ ) calcd.: 266.1392

found: 266.1385.

The analytical data are in accordance with previous literature reports.<sup>[198]</sup>

1-Methoxy-6-methyl-7-(pivaloyloxy)-1,3-dihydrofuro[3,4-*c*]pyridine-*N*-oxide (**135**)<sup>[198]</sup>



*Meta*-chloro perbenzoic acid (77%, 9.15 g, 23.0 mmol, 1.2 eq) was added to a solution of acetal **134** (5.23 g, 19.7 mmol, 1.0 eq) in anhydrous dichloromethane (100 mL) in five portions. After addition, the reaction was stirred overnight at room temperature. Then, the reaction mixture was quenched with satd. sodium thiosulfate solution (100 mL) and diluted with dichloromethane (80 mL). After separation of the phases, the organic layer was washed with satd. sodium bicarbonate and satd. sodium chloride solutions (each 100 mL), dried over sodium sulfate and concentrated to yield the intermediate *N*-oxide **135** as a pale yellow solid, which was used directly in the next step.

**TLC:**  $R_f = 0.44$  (5% MeOH/DCM) [UV/KMnO<sub>4</sub>].

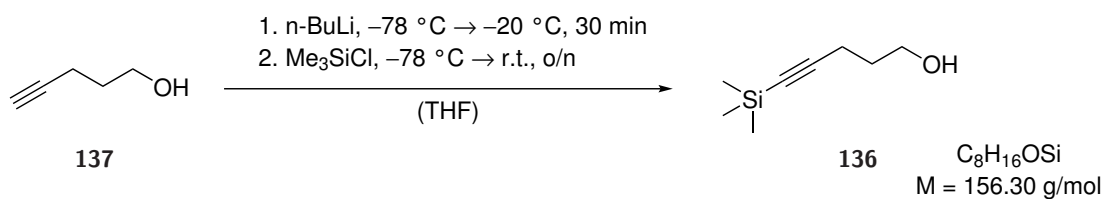
**<sup>1</sup>H-NMR** (400 MHz, CDCl<sub>3</sub>):  $\delta[\text{ppm}] = 8.19$  (s, 1 H), 6.03 (s, 1 H), 5.18 (d,  $^2J = 13.3$  Hz, 1 H), 5.05 (d,  $^2J = 13.3$  Hz, 1 H), 3.38 (s, 3 H), 2.37 (s, 3 H), 1.40 (s, 9 H).

**<sup>13</sup>C-NMR** (100 MHz, CDCl<sub>3</sub>):  $\delta[\text{ppm}] = 174.9, 160.7, 145.0, 142.8, 140.6, 136.3, 106.1, 70.5, 54.7, 39.5, 27.1, 11.6$ .

**HRMS** (ESI) (C<sub>11</sub>H<sub>15</sub>NO<sub>4</sub> [M+H]<sup>+</sup>) calcd.: 282.1336

found: 282.1333.

The analytical data are in accordance with previous literature reports.<sup>[198]</sup>

**4.1.2.3** Linker Synthesis5-(Trimethylsilyl)pent-4-yn-1-ol (**136**) [328,336]

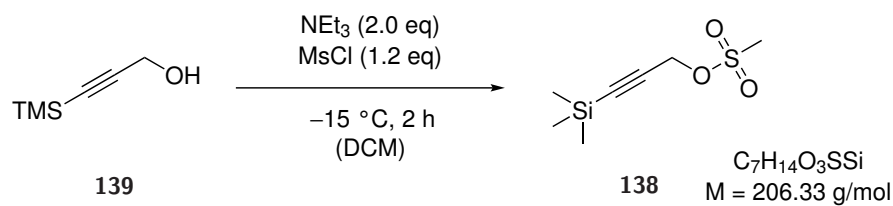
Following GP2, alkyne **137** (2.00 g, 23.8 mmol, 1.0 eq) was converted with *n*-butyllithium (2.5 M in hexanes; 21.0 mL, 2.2 eq) and trimethylsilyl chloride (7.54 mL, 6.46 g, 59.4 mmol, 2.5 eq) in anhydrous tetrahydrofuran (40 mL). After purification by column chromatography (EtOAc/hexanes, 20-60%), TMS protected compound **136** (3.32 g, 21.3 mmol, 90%) was obtained as a pale yellow oil.

**TLC:**  $R_f = 0.76$  (50% EtOAc/hexanes) [CAM].

**$^1\text{H-NMR}$**  (400 MHz,  $\text{CDCl}_3$ ):  $\delta$ [ppm] = 3.76 (t,  $^3J = 6.5\text{ Hz}$ , 2 H), 2.35 (t,  $^3J = 6.5\text{ Hz}$ , 2 H), 1.77 (p,  $^3J = 6.5\text{ Hz}$ , 2 H), 0.14 (s, 9 H).

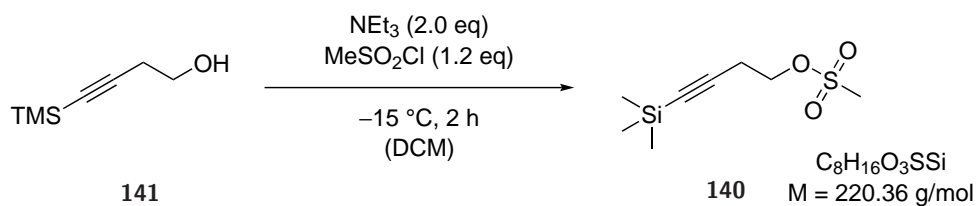
**$^{13}\text{C-NMR}$**  (100 MHz,  $\text{CDCl}_3$ ):  $\delta$ [ppm] = 106.6, 85.3, 62.0, 31.2, 16.6, 0.10.

The analytical data are in accordance with previous literature reports. [328]

**3-(Trimethylsilyl)prop-2-yn-1-yl methanesulfonate (138)** <sup>[330]</sup>

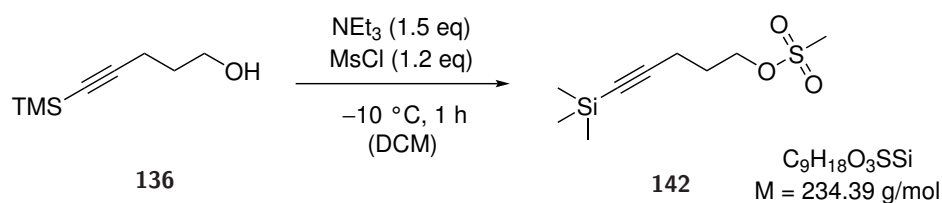
Following GP3, alcohol **139** (1.16 mL, 1.00 g, 7.98 mmol, 1.0 eq) was converted with triethylamine (2.16 mL, 1.58 g, 15.6 mmol, 2.0 eq) and methanesulfonyl chloride (6.48 mL, 5.53 g, 50.9 mmol, 2.5 eq) in anhydrous dichloromethane (40 mL). After concentration *in vacuo*, mesylate **138** (1.23 g, 5.96 mmol, 75%) was obtained and used for the next reaction step without any further purification.

**TLC:**  $R_f = 0.67$  (20% EtOAc/hexanes) [ $\text{KMnO}_4$ ].

4-(Trimethylsilyl)but-3-yn-1-yl methanesulfonate (**140**)<sup>[328,331,332]</sup>

Following GP3, alcohol **141** (2.34 mL, 2.00 g, 14.1 mmol, 1.0 eq) was converted with triethylamine (3.91 mL, 2.85 g, 28.1 mmol, 2.0 eq) and methanesulfonyl chloride (1.31 mL, 1.93 g, 16.9 mmol, 1.2 eq) in anhydrous dichloromethane (50 mL). After concentration *in vacuo*, mesylate **140** (3.12 g, 14.1 mmol, 100%) was obtained and used for the next reaction step without any further purification.

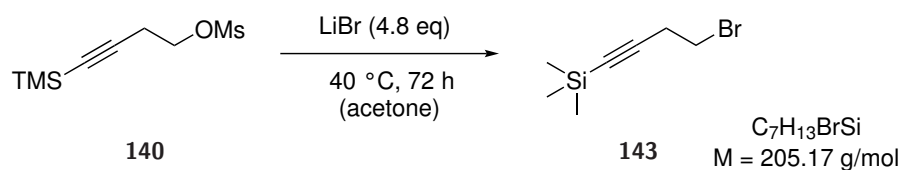
**TLC:**  $R_f = 0.83$  (50% EtOAc/hexanes) [CAM].

5-(Trimethylsilyl)pent-4-yn-1-yl methanesulfonate (**142**)<sup>[328,331]</sup>

Following GP3, alcohol **136** (3.48 mL, 3.00 g, 19.2 mmol, 1.0 eq) was converted with triethylamine (3.99 mL, 2.91 g, 28.8 mmol, 1.5 eq) and methanesulfonyl chloride (1.78 mL, 2.64 g, 23.0 mmol, 1.2 eq) in anhydrous dichloromethane (50 mL) at  $-10\text{ }^\circ\text{C}$ . After concentration *in vacuo*, mesylate **142** (4.41 g, 18.8 mmol, 98%) was obtained and used for the next reaction step without any further purification.

**TLC:**  $R_f = 0.87$  (50% EtOAc/hexanes) [CAM].



(4-Bromobut-1-yn-1-yl)trimethylsilane (**143**)<sup>[328]</sup>

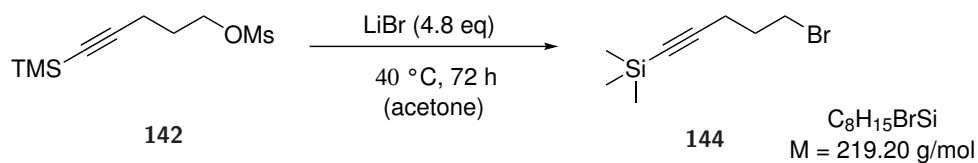
Following GP4, mesylate **138** (3.12 g, 14.1 mmol, 1.0 eq) was converted with lithium bromide (5.87 g, 67.7 mmol, 4.8 eq) in anhydrous acetone (30 mL). The crude product was purified by flash chromatography (hexanes) to yield bromide **143** (2.69 g, 13.1 mmol, 93%) as a clear oil.

**TLC:**  $R_f = 0.58$  (hexanes) [CAM].

**$^1\text{H-NMR}$**  (400 MHz,  $\text{CDCl}_3$ ):  $\delta[\text{ppm}] = 3.34$  (t,  $^3J = 7.5$  Hz, 2 H), 2.77 (t,  $^3J = 7.5$  Hz, 2 H), 0.16 (s, 9 H).

**$^{13}\text{C-NMR}$**  (100 MHz,  $\text{CDCl}_3$ ):  $\delta[\text{ppm}] = 103.3, 87.2, 29.3, 24.5, 0.1$ .

The analytical data are in accordance with previous literature reports.<sup>[328]</sup>

**(5-Bromopent-1-yn-1-yl)trimethylsilane (144)** <sup>[328,331]</sup>

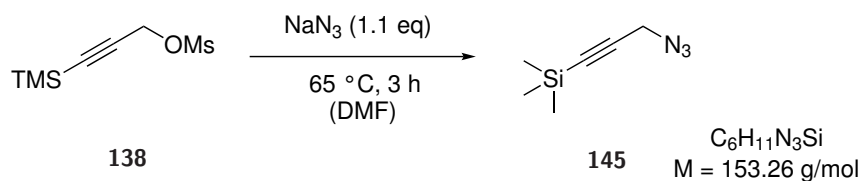
Following GP4, mesylate **142** (4.40 g, 18.8 mmol, 1.0 eq) was converted with lithium bromide (7.83 g, 90.2 mmol, 4.8 eq) in anhydrous acetone (50 mL). The crude product was purified by flash chromatography (hexanes) to yield bromide **144** (3.46 g, 15.8 mmol, 85%) as a clear oil.

**TLC:**  $R_f = 0.42$  (hexanes) [CAM].

**$^1\text{H-NMR}$**  (400 MHz,  $\text{CDCl}_3$ ):  $\delta$ [ppm] = 3.51 (t,  $^3J = 6.7$  Hz, 2 H), 2.41 (t,  $^3J = 6.7$  Hz, 2 H), 2.04 (p,  $^3J = 6.7$  Hz, 2 H), 0.15 (s, 9 H).

**$^{13}\text{C-NMR}$**  (100 MHz,  $\text{CDCl}_3$ ):  $\delta$ [ppm] = 105.2, 85.9, 32.4, 31.6, 18.8, 0.24.

The analytical data are in accordance with previous literature reports. <sup>[328]</sup>

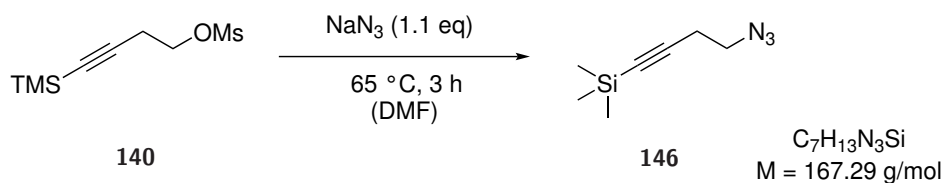
**(3-Azidoprop-1-yn-1-yl)trimethylsilane (145)** [333]

Following GP5, mesylate **138** (1.23 g, 5.96 mmol, 1.0 eq) was converted with sodium azide (426 mg, 6.56 mmol, 1.1 eq) in anhydrous dimethyl formamide (20 mL). The crude product was purified by flash chromatography (EtOAc/hexanes, 5-30%) to yield azide **145** (366 mg, 2.39 mmol, 41%) as a clear oil.

**TLC:**  $R_f = 0.80$  (10% EtOAc/hexanes) [ $\text{KMnO}_4$ ].

**$^1\text{H-NMR}$**  (400 MHz,  $\text{CDCl}_3$ ):  $\delta[\text{ppm}] = 3.92$  (s, 2 H), 0.20 (s, 9 H).

**$^{13}\text{C-NMR}$**  (100 MHz,  $\text{CDCl}_3$ ):  $\delta[\text{ppm}] = 97.1, 93.2, 40.8, -0.1$ .

**(4-Azidobut-1-yn-1-yl)trimethylsilane (146)** <sup>[332,333]</sup>

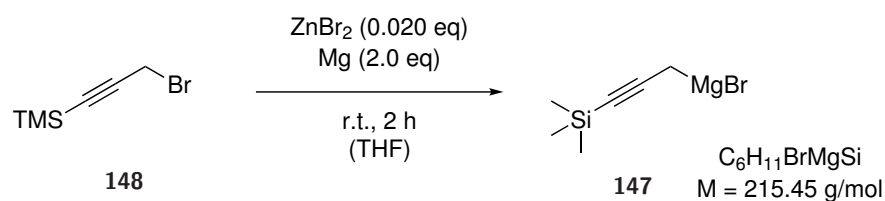
Following GP5, mesylate **140** (3.41 g, 15.5 mmol, 1.0 eq) was converted with sodium azide (1.11 g, 17.0 mmol, 1.1 eq) in anhydrous dimethyl formamide (40 mL). The crude product was purified by flash chromatography (EtOAc/hexanes, 0-30%) to yield azide **146** (1.89 g, 11.3 mmol, 73%) as a clear oil.

**TLC:**  $R_f = 0.88$  (10% EtOAc/hexanes) [ $\text{KMnO}_4$ ].

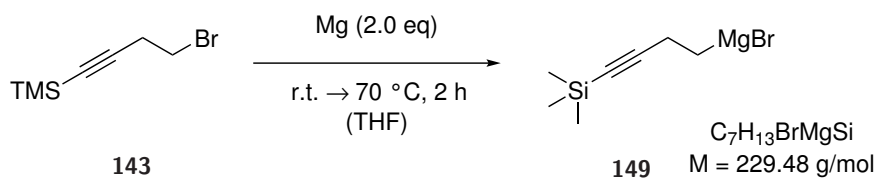
**$^1\text{H-NMR}$**  (400 MHz,  $\text{CDCl}_3$ ):  $\delta$ [ppm] = 3.38 (t,  $^3J = 6.9\text{ Hz}$ , 2 H), 2.52 (t,  $^3J = 6.9\text{ Hz}$ , 2 H), 0.16 (s, 9 H).

**$^{13}\text{C-NMR}$**  (100 MHz,  $\text{CDCl}_3$ ):  $\delta$ [ppm] = 102.8, 87.4, 49.9, 21.1, 0.04.

The analytical data are in accordance with previous literature reports. <sup>[332]</sup>

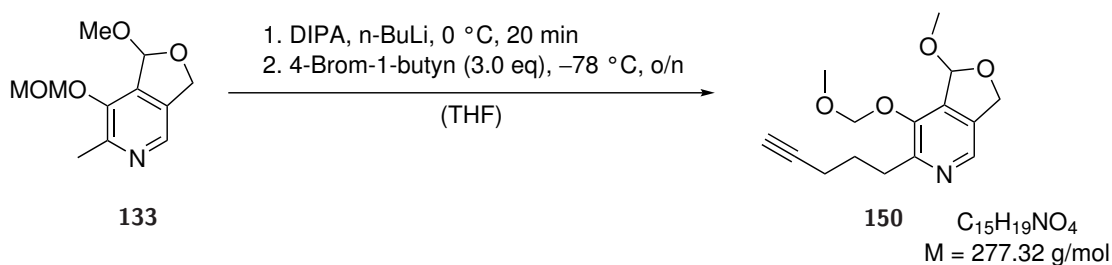
**3-(Trimethylsilyl)prop-2-yn-1 magnesium bromide (147)** <sup>[337]</sup>

To a dry three-necked flask (100 mL) equipped with a condenser and a dropping funnel were added zinc(II)bromide (100 mg, 442  $\mu\text{mol}$ , 2 mol%), magnesium (977 mg, 40.2 mmol, 2.0 eq) and anhydrous diethyl ether (12 mL). Then, (3-bromoprop-1-yn-1-yl)trimethylsilane (3.40 mL, 4.00 g, 20.1 mmol, 1.0 eq) in anhydrous diethyl ether (15 mL) was added dropwise using a dropping funnel. The addition began at room temperature and continued for 30 min until an exothermic reaction was observed. Following this observation, the mixture was cooled to 0 °C and stirred at this temperature for an additional 2 h. The freshly generated reagent was directly used in the following GRIGNARD-reaction.

4-(Trimethylsilyl)but-3-yn-1 magnesium bromide (149) <sup>[338]</sup>

To a dry three-necked flask (100 mL) equipped with a condenser and a dropping funnel, were added magnesium (391 mg, 16.1 mmol, 1.5 eq) and anhydrous tetrahydrofuran (6 mL). Then (4-bromobut-1-yn-1-yl)trimethylsilane (2.20 g, 10.7 mmol, 1.0 eq) in anhydrous tetrahydrofuran (8 mL) was added dropwise using a dropping funnel. The addition began at room temperature and continued under reflux at 70 °C for 1 h until an exothermic reaction was observed. Following this observation, the mixture was stirred for an additional 1 h. The freshly generated reagent was directly used in the following GRIGNARD-reaction.

## 4.1.2.4 Alkylations

1-Methoxy-7-(methoxymethoxy)-6-(pent-4-yn-1-yl)-1,3-dihydrofuro[3,4-*c*]-pyridine (**150**)<sup>[151]</sup>

Following GP1, protected pyridoxal **133** (300 mg, 1.33 mmol, 1.0 eq) was converted with diisopropylamine (451  $\mu$ L, 323 mg, 3.19 mmol, 2.4 eq), *n*-butyllithium (2.5 M in hexanes; 1.17 mL, 188 mg, 2.93 mmol, 2.2 eq) and 4-bromobut-1-yne (375  $\mu$ L, 531 mg, 3.99 mmol, 3.0 eq) in anhydrous tetrahydrofuran (9 mL). The crude product was purified by flash chromatography (EtOAc/hexanes, 20-60%) to yield alkylated compound **150** (48.0 mg, 173  $\mu$ mol, 14%) as a pale yellow oil.

**TLC:**  $R_f$  = 0.66 (50% EtOAc/hexanes) [UV/ $KMnO_4$ ].

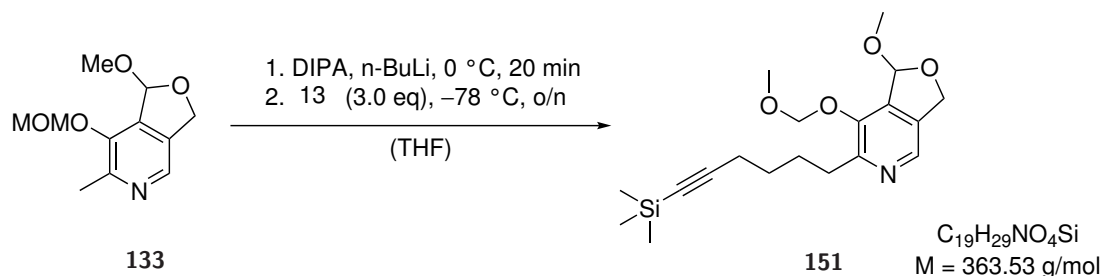
**$^1H$ -NMR** (400 MHz,  $CDCl_3$ ):  $\delta$ [ppm] = 8.18 (s, 1 H), 6.26 (s, 1 H), 5.44 (d,  $^4J$  = 6.5 Hz, 1 H), 5.19 (d,  $^2J$  = 12.8 Hz, 1 H), 5.08 (d,  $^4J$  = 6.5 Hz, 1 H), 5.02 (d,  $^2J$  = 12.8 Hz, 1 H), 3.52 (s, 3 H), 3.47 (s, 3 H), 3.00 (t,  $^3J$  = 7.3 Hz, 2 H), 2.29 (td,  $^{3,4}J$  = 7.3, 2.5 Hz, 2 H), 1.97 (p,  $^3J$  = 7.3 Hz, 2 H), 1.96 (t,  $^4J$  = 2.5 Hz, 1 H).

**$^{13}C$ -NMR** (100 MHz,  $CDCl_3$ ):  $\delta$ [ppm] = 152.8, 146.3, 135.9, 135.7, 133.8, 106.3, 96.4, 84.5, 70.1, 68.6, 57.0, 55.0, 31.7, 27.5, 18.5.

**HRMS** (ESI) ( $C_{13}H_{15}NO_3$  [M+H]<sup>+</sup>) calcd.: 278.1387

found: 278.1382.

1-Methoxy-7-(methoxymethoxy)-6-[6-(trimethylsilyl)hex-5-yn-1-yl]-1,3-dihydrofuro[3,4-*c*]pyridine (**151**)<sup>[151]</sup>



Following GP1, protected pyridocal **133** (300 mg, 1.33 mmol, 1.0 eq) was converted with diisopropylamine (451  $\mu$ L, 323 mg, 3.19 mmol, 2.4 eq), *n*-butyllithium (2.5 M in hexanes; 1.17 mL, 188 mg, 2.93 mmol, 2.2 eq) and (5-bromopent-1-yn-1-yl)trimethylsilane (875 mg, 3.99 mmol, 3.0 eq) in anhydrous tetrahydrofuran (9 mL). The crude product was purified by flash chromatography (EtOAc/hexanes, 20-60%) to yield alkylated compound **151** (265 mg, 729  $\mu$ mol, 55%) as a pale yellow oil.

**TLC:**  $R_f$  = 0.61 (50% EtOAc/hexanes) [UV/ $KMnO_4$ ].

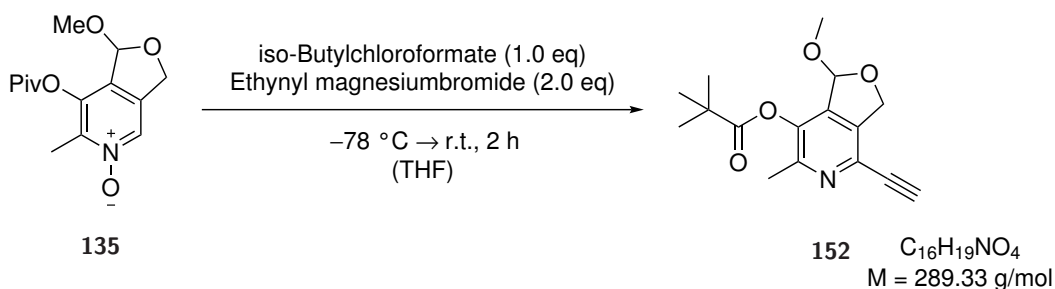
**$^1H$ -NMR** (400 MHz,  $CDCl_3$ ):  $\delta$ [ppm] = 8.19 (s, 1 H), 6.28 (s, 1 H), 5.48 (d,  $^4J$  = 6.4 Hz, 1 H), 5.20 (d,  $^2J$  = 13.5 Hz, 1 H), 5.09 (d,  $^4J$  = 6.4 Hz, 1 H), 5.05 (d,  $^2J$  = 13.5 Hz, 1 H), 3.52 (s, 3 H), 3.48 (s, 3 H), 2.99 (t,  $^3J$  = 7.5 Hz, 2 H), 2.27 (t,  $^3J$  = 7.5 Hz, 2 H), 1.83 (p,  $^3J$  = 7.5 Hz, 2 H), 1.62 (p,  $^3J$  = 7.5 Hz, 2 H), 0.13 (s, 9 H).

**$^{13}C$ -NMR** (100 MHz,  $CDCl_3$ ):  $\delta$ [ppm] = 153.1, 146.8, 136.3, 134.5, 106.2, 96.4, 84.6, 77.4, 70.0, 68.3, 57.1, 54.9, 34.5, 28.7, 28.2, 19.9, 0.32.

**HRMS** (ESI) ( $C_{19}H_{29}NO_4Si$  [ $M+H$ ] $^+$ ) calcd.: 364.1944  
found: 364.1936.



## 4.1.2.5 Nucleophilic Substitution

4-Ethynyl-1-methoxy-6-methyl-1,3-dihydrofuro[3,4-*c*]-pyridin-7-ylpivalate (**152**)<sup>[198]</sup>

Following GP6, protected *N*-oxide **135** (619 mg, 2.20 mmol, 1.0 eq) was converted with *iso*-butylchloroformate (286  $\mu$ L, 301 mg, 2.20 mmol, 1.0 eq) and ethynyl magnesiumbromide (0.5 M in tetrahydrofuran; 8.80 mL, 569 mg, 4.40 mmol, 2.0 eq) in anhydrous tetrahydrofuran (7 mL). The crude product was purified by flash chromatography (EtOAc/hexanes, 10-40%) to yield alkylated compound **152** (184 mg, 636  $\mu$ mol, 29%) as a brown yellow solid.

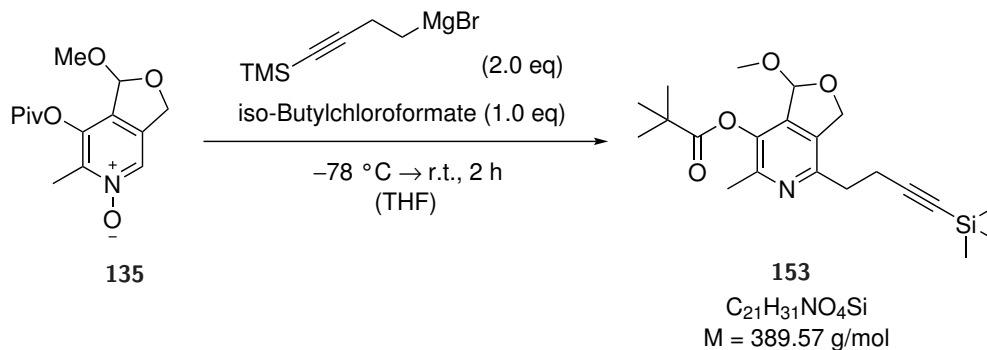
**TLC:**  $R_f = 0.58$  (20% EtOAc/hexanes) [UV/ $KMnO_4$ ].

**$^1H$ -NMR** (400 MHz,  $CDCl_3$ ):  $\delta$ [ppm] = 6.09 (d,  $^4J = 1.8$  Hz, 1 H), 5.22 (dd,  $^{2,4}J = 13.7$ , 1.8 Hz, 1 H), 5.10 (d,  $^2J = 13.7$  Hz, 1 H), 3.36 (s, 3 H), 3.31 (s, 1 H), 2.44 (s, 3 H), 1.38 (s, 9 H).

**$^{13}C$ -NMR** (100 MHz,  $CDCl_3$ ):  $\delta$ [ppm] = 175.3, 152.1, 141.2, 139.2, 138.4, 132.2, 106.6, 81.0, 80.0, 71.4, 54.6, 39.4, 27.1, 19.0.

**HRMS** (ESI) ( $C_{16}H_{19}NO_4$  [M+H]<sup>+</sup>) calcd.: 290.1387

found: 290.1380.

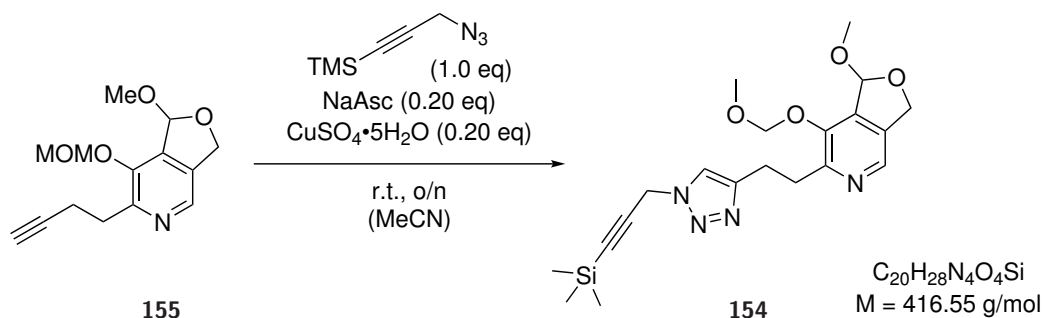
**1-Methoxy-6-methyl-4-[4-(trimethylsilyl)but-3-yn-1-yl]-1,3-dihydrofuro-[3,4-*c*]pyridin-7-yl pivalate (**153**)**<sup>[198]</sup>

Following GP6, protected *N*-oxide **135** (700 mg, 2.49 mmol, 1.0 eq) was converted with *iso*-butylchloroformate (323  $\mu$ L, 340 mg, 2.49 mmol, 1.0 eq) and freshly prepared 4-(trimethylsilyl)but-3-yn-1-magnesiumbromide in anhydrous tetrahydrofuran (7 mL). The crude product was purified by flash chromatography (EtOAc/hexanes, 5-40%) to yield a brown yellow solid containing compound among a mixture of products that could not be separated.

**TLC:**  $R_f$  = 0.51 (20% EtOAc/hexanes) [UV/KMnO<sub>4</sub>].

**HRMS** (ESI) (C<sub>21</sub>H<sub>31</sub>NO<sub>4</sub>Si [M+H]<sup>+</sup>) calcd.: 390.2095  
found: 390.2093.

## 4.1.2.6 Click Reactions

1-Methoxy-7-(methoxymethoxy)-6-2-1-[3-(trimethylsilyl)prop-2-yn-1-yl]-1*H*-1,2,3-triazol-4-ylethyl-1,3-dihydrofuro[3,4-*c*]pyridine (**154**)<sup>[334]</sup>

Following GP7, protected alkyne from **PL2** synthesis **155** (220 mg, 836  $\mu$ mol, 1.0 eq) was converted with sodium ascorbate (33.1 mg, 167  $\mu$ mol, 0.20 eq), copper sulfate pentahydrate (41.8 mg, 167  $\mu$ mol, 0.20 eq) and (3-azidoprop-1-yn-1-yl)trimethylsilane (128 mg, 836  $\mu$ mol, 1.0 eq) in acetonitrile/dimethyl sulfoxide (4:1, 10 mL). The crude product was purified by flash chromatography (MeOH/DCM, 2-6%) to yield **154** (232 mg, 558  $\mu$ mol, 67%) as a yellow oil.

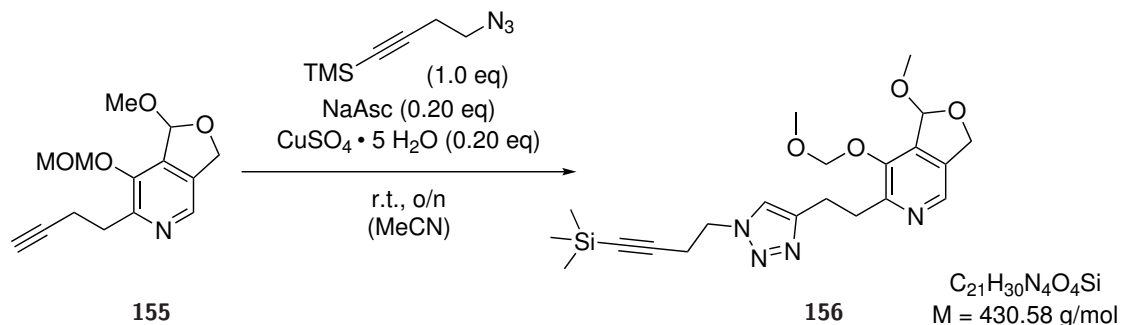
**TLC:**  $R_f$  = 0.61 (10% MeOH/DCM) [UV/ $KMnO_4$ ].

**$^1H$ -NMR** (400 MHz,  $CDCl_3$ ):  $\delta$ [ppm] = 8.18 (s, 1 H), 7.50 (s, 1 H), 6.24 (d,  $^4J$  = 1.6 Hz, 1 H), 5.42 (d,  $^4J$  = 6.6 Hz, 1 H), 5.17 (d,  $^2J$  = 13.3 Hz, 1 H), 5.10 (s, 2 H), 5.04 (d,  $^4J$  = 6.6 Hz, 1 H), 5.01 (d,  $^2J$  = 13.3 Hz, 1 H), 3.48 (s, 3 H), 3.46 (s, 3 H), 3.31-3.22 (m, 2 H), 3.22-3.14 (m, 2 H), 0.18 (s, 9 H).

**$^{13}C$ -NMR** (100 MHz,  $CDCl_3$ ):  $\delta$ [ppm] = 152.0, 148.0, 146.3, 136.1, 135.5, 133.7, 120.8, 106.3, 96.5, 96.1, 92.8, 70.0, 57.0, 54.9, 40.7, 32.2, 24.4, -0.30.

**HRMS** (ESI) ( $C_{20}H_{28}N_4O_4Si$  [ $M+H$ ] $^+$ ) calcd.: 417.1953  
found: 417.1943.

1-Methoxy-7-(methoxymethoxy)-6-2-1-[4-(trimethylsilyl)but-3-yn-1-yl]-1*H*-1,2,3-triazol-4-ylethyl-1,3-dihydrofuro[3,4-*c*]pyridine (**156**)<sup>[334]</sup>



Following GP7, protected alkyne from **PL2** synthesis **155** (210 mg, 798  $\mu\text{mol}$ , 1.0 eq) was converted with sodium ascorbate (31.6 mg, 0.160 mmol, 0.20 eq), copper sulfate pentahydrate (39.8 mg, 160  $\mu\text{mol}$ , 0.20 eq) and (4-azidobut-1-yn-1-yl)trimethylsilane (133 mg, 798  $\mu\text{mol}$ , 1.0 eq) in acetonitrile/dimethyl sulfoxide (4:1, 10 mL). The crude product was purified by flash chromatography (MeOH/DCM, 2-6%) to yield **156** (229 mg, 532  $\mu\text{mol}$ , 67%) as a yellow oil.

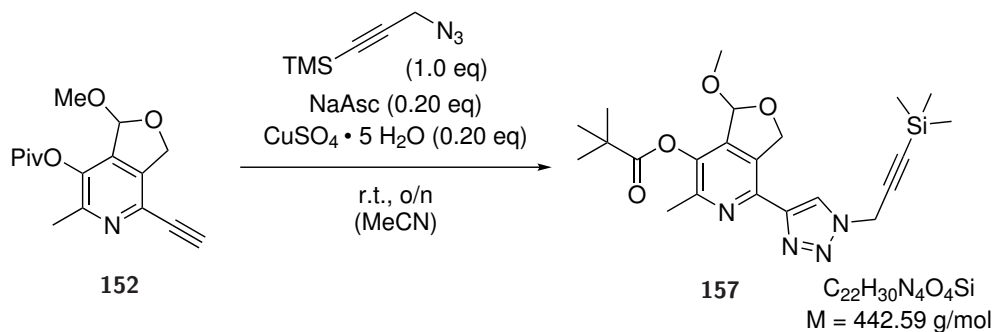
**TLC:**  $R_f = 0.34$  (EtOAc) [UV/KMnO<sub>4</sub>].

**<sup>1</sup>H-NMR** (400 MHz, CDCl<sub>3</sub>):  $\delta$ [ppm] = 8.18 (s, 1 H), 7.39 (s, 1 H), 6.25 (d, <sup>4</sup>*J* = 1.6 Hz, 1 H), 5.42 (d, <sup>4</sup>*J* = 6.6 Hz, 1 H), 5.18 (d, <sup>2</sup>*J* = 12.7 Hz, 1 H), 5.04 (d, <sup>4</sup>*J* = 6.6 Hz, 1 H), 5.02 (d, <sup>2</sup>*J* = 12.7 Hz, 1 H), 4.44 (t, <sup>3</sup>*J* = 6.9 Hz, 2 H), 3.48 (s, 3 H), 3.46 (s, 3 H), 3.30-3.23 (m, 2 H), 3.21-3.13 (m, 2 H), 2.77 (t, <sup>3</sup>*J* = 6.9 Hz, 2 H), 0.13 (s, 9 H).

**<sup>13</sup>C-NMR** (100 MHz, CDCl<sub>3</sub>):  $\delta$ [ppm] = 152.1, 147.7, 146.3, 136.1, 135.5, 133.6, 121.5, 106.3, 102.1, 96.1, 88.2, 70.1, 57.0, 55.0, 48.8, 32.2, 24.5, 22.2, 0.03.

**HRMS** (ESI) (C<sub>21</sub>H<sub>30</sub>N<sub>4</sub>O<sub>4</sub>Si [M+H]<sup>+</sup>) calcd.: 431.2109

found: 431.2103.

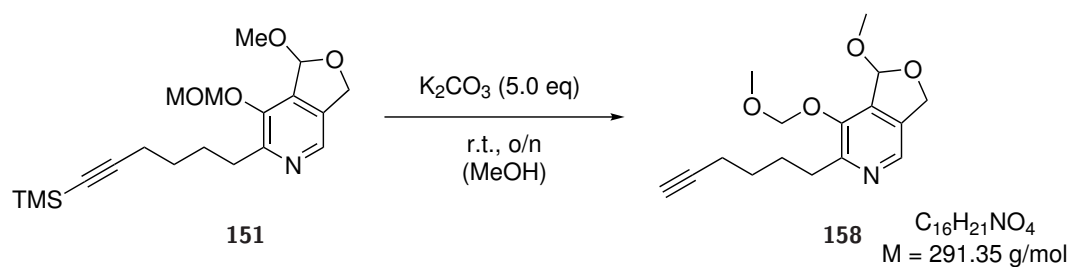
**1-Methoxy-6-methyl-4-1-[3-(trimethylsilyl)prop-2-yn-1-yl]-1*H*-1,2,3-triazol-4-yl-1,3-dihydrofuro[3,4-*c*]pyridin-7-yl pivalate (157)** <sup>[334]</sup>

Following GP7, protected alkyne **152** (100 mg, 346  $\mu\text{mol}$ , 1.0 eq) was converted with sodium ascorbate (13.7 mg, 69.1  $\mu\text{mol}$ , 0.20 eq), copper sulfate pentahydrate (17.3 mg, 69.1  $\mu\text{mol}$ , 0.20 eq) and (3-azidoprop-1-yn-1-yl)trimethylsilane (53.0 mg, 346  $\mu\text{mol}$ , 1.0 eq) in acetonitrile/dimethyl sulfoxide (4:1, 5 mL). The crude product was purified by flash chromatography (MeOH/DCM, 2-6%) to yield a yellow oil containing compound among a mixture of products that could not be separated.

**TLC:**  $R_f = 0.49$  (20% EtOAc/hexanes) [UV/ $\text{KMnO}_4$ ].

**HRMS** (ESI) ( $\text{C}_{22}\text{H}_{30}\text{N}_4\text{O}_4\text{Si}$   $[\text{M}+\text{H}]^+$ ) calcd.: 443.2109  
found: 443.2108.

## 4.1.2.7 TMS Deprotection

6-(Hex-5-yn-1-yl)-1-methoxy-7-(methoxymethoxy)-1,3-dihydrofuro[3,4c]-pyridine (**158**)<sup>[329]</sup>

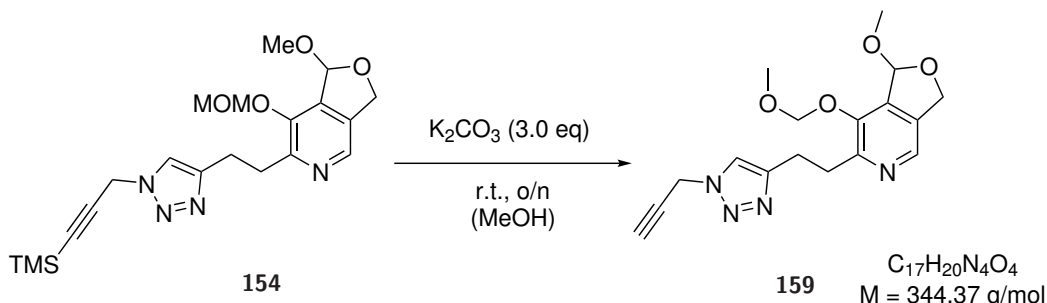
Following GP8, TMS-protected alkyne **151** (207 mg, 569  $\mu\text{mol}$ , 1.0 eq) was converted with potassium carbonate (388 mg, 2.85 mmol, 5.0 eq) in anhydrous methanol (15 mL). The crude product was purified by flash chromatography (EtOAc/hexanes, 30-70%) to yield **158** (154 mg, 529  $\mu\text{mol}$ , 93%) as a yellow oil.

**TLC:**  $R_f = 0.56$  (50% EtOAc/hexanes) [UV/CAM].

**$^1\text{H-NMR}$**  (400 MHz,  $\text{CDCl}_3$ ):  $\delta$ [ppm] = 8.18 (s, 1 H), 6.27 (s, 1 H), 5.46 (d,  $^4J = 6.5$  Hz, 1 H), 5.19 (d,  $^2J = 12.9$  Hz, 1 H), 5.09 (d,  $^4J = 6.5$  Hz, 1 H), 5.03 (d,  $^2J = 12.9$  Hz, 1 H), 3.52 (s, 3 H), 3.47 (s, 3 H), 2.95 (t,  $^3J = 7.6$  Hz, 2 H), 2.24 (td,  $^3,4J = 7.6, 2.7$  Hz, 2 H), 1.92 (t,  $^4J = 2.7$  Hz, 1 H), 1.84 (p,  $^3J = 7.6$  Hz, 2 H), 1.63 (p,  $^3J = 7.6$  Hz, 2 H).

**$^{13}\text{C-NMR}$**  (100 MHz,  $\text{CDCl}_3$ ):  $\delta$ [ppm] = 153.1, 146.5, 136.3, 134.5, 106.3, 96.4, 84.6, 77.4, 70.1, 68.4, 57.1, 55.0, 31.8, 28.5, 28.0, 18.5.

**HRMS** (ESI) ( $\text{C}_{16}\text{H}_{21}\text{NO}_4$   $[\text{M}+\text{H}]^+$ ) calcd.: 292.1549  
found: 292.1542.

**1-Methoxy-7-(methoxymethoxy)-6-2-[1-(prop-2-yn-1-yl)-1*H*-1,2,3-triazol-4-yl]ethyl-1,3-dihydrofuro[3,4-*c*]pyridine (159)** <sup>[329]</sup>

Following GP8, TMS-protected alkyne **154** (210 mg, 504  $\mu\text{mol}$ , 1.0 eq) was converted with potassium carbonate (210 mg, 1.52 mmol, 3.0 eq) in anhydrous methanol (20 mL). The crude product was purified by flash chromatography (MeOH/DCM, 2-6%) to yield **159** (169 mg, 491  $\mu\text{mol}$ , 98%) as a yellow oil.

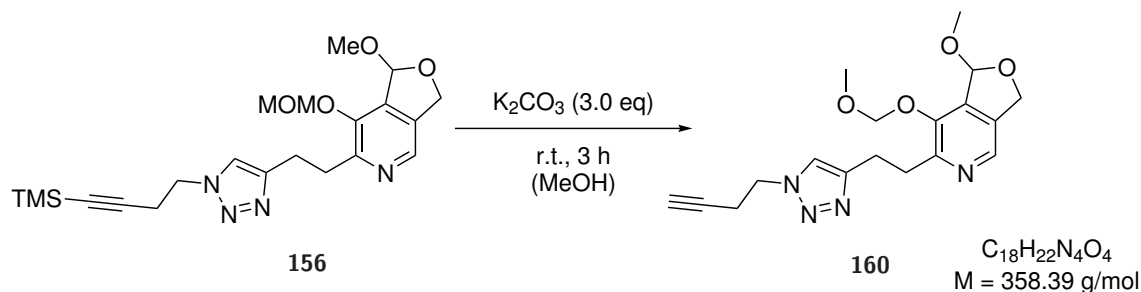
**TLC:**  $R_f = 0.51$  (EtOAc) [UV/ $\text{KMnO}_4$ ].

**$^1\text{H-NMR}$**  (400 MHz,  $\text{CDCl}_3$ ):  $\delta[\text{ppm}] = 8.18$  (s, 1 H), 7.49-7.41 (m, 1 H), 6.26 (d,  $^4J = 1.7 \text{ Hz}$ , 1 H), 5.65 (d,  $^4J = 6.6 \text{ Hz}$ , 1 H), 5.43 (d,  $^3J = 6.6 \text{ Hz}$ , 1 H), 5.19 (d,  $^2J = 13.3 \text{ Hz}$ , 1 H), 5.12 (s, 2 H), 5.05 (d,  $^4J = 6.6 \text{ Hz}$ , 1 H), 5.03 (d,  $^2J = 13.3 \text{ Hz}$ , 1 H), 3.49 (s, 3 H), 3.47 (s, 3 H), 3.31-3.25 (m, 2 H), 3.23-3.15 (m, 2 H).

**$^{13}\text{C-NMR}$**  (100 MHz,  $\text{CDCl}_3$ ):  $\delta[\text{ppm}] = 201.6, 152.0, 148.5, 146.4, 136.2, 135.5, 133.7, 118.9, 106.3, 98.7, 96.2, 88.8, 70.1, 57.0, 55.0, 32.1, 24.4$ .

**HRMS** (ESI) ( $\text{C}_{17}\text{H}_{20}\text{N}_4\text{O}_4$  [ $\text{M}+\text{H}$ ] $^+$ ) calcd.: 345.1557  
found: 345.1551.

**6-2-[1-(But-3-yn-1-yl)-1*H*-1,2,3-triazol-4-yl]ethyl-1-methoxy-7(methoxy-methoxy)-1,3-dihydrofuro[3,4-*c*]pyridine (**160**)** <sup>[329]</sup>



Following GP8, TMS-protected alkyne **156** (200 mg, 464  $\mu\text{mol}$ , 1.0 eq) was converted with potassium carbonate (190 mg, 1.39 mmol, 3.0 eq) in anhydrous methanol (20 mL). The crude product was purified by flash chromatography (MeOH/DCM, 2-6%) to yield **160** (155 mg, 433  $\mu\text{mol}$ , 93%) as a yellow oil.

**TLC:**  $R_f = 0.25$  (EtOAc) [UV/ $\text{KMnO}_4$ ].

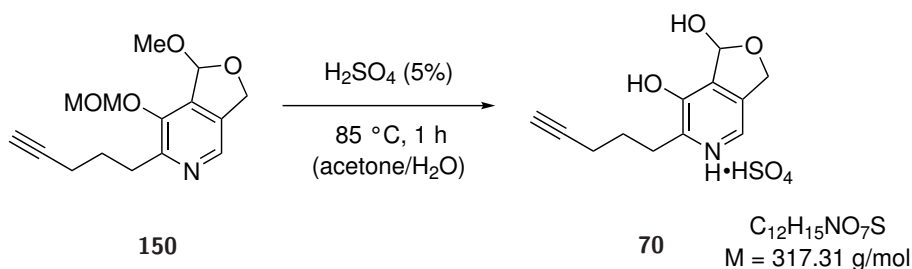
**$^1\text{H-NMR}$**  (400 MHz,  $\text{CDCl}_3$ ):  $\delta$ [ppm] = 8.19 (s, 1 H), 7.38 (s, 1 H), 6.25 (d,  $^4J = 1.6$  Hz, 1 H), 5.41 (d,  $^4J = 6.6$  Hz, 1 H), 5.19 (d,  $^2J = 12.8$  Hz, 1 H), 5.05 (d,  $^4J = 6.6$  Hz, 1 H), 5.03 (d,  $^2J = 12.8$  Hz, 1 H), 4.45 (t,  $^3J = 6.8$  Hz, 2 H), 3.49 (s, 3 H), 3.47 (s, 3 H), 3.31-3.23 (m, 2 H), 3.23-3.15 (m, 2 H), 2.75 (td,  $^3,^4J = 6.8, 2.7$  Hz, 2 H), 2.05 (t,  $^4J = 2.7$  Hz, 1 H).

**$^{13}\text{C-NMR}$**  (100 MHz,  $\text{CDCl}_3$ ):  $\delta$ [ppm] = 152.2, 147.8, 146.4, 136.1, 135.6, 133.7, 121.6, 106.3, 96.2, 79.8, 71.5, 70.1, 57.0, 55.0, 48.7, 32.2, 24.5, 20.8.

**HRMS** (ESI) ( $\text{C}_{18}\text{H}_{22}\text{N}_4\text{O}_4$  [ $\text{M}+\text{H}$ ] $^+$ ) calcd.: 359.1719

found: 359.1710.



**4.1.2.8** Acetal and Ether Deprotection, Final Probes**3-Hydroxy-5-(hydroxymethyl)-2-(pent-4-yn-1-yl)isonicotinaldehyde bisulfate (PL6,70)** [198]

Following GP9, MOM-protected acetal **150** (48.0 mg, 173  $\mu\text{mol}$ , 1.0 eq) was deprotected in acetone/water (1:1; 5 mL) containing 5% sulfuric acid. After purification by HPLC (method B), probe **PL6** (10.0 mg, 31.5  $\mu\text{mol}$ , 19%) was obtained as a fluffy white solid.

**TLC:**  $R_f = 0.12$  (50% EtOAc/hexanes) [UV/ $\text{KMnO}_4$ ].

**HPLC:**  $t_R = 8.3$  min (method B).

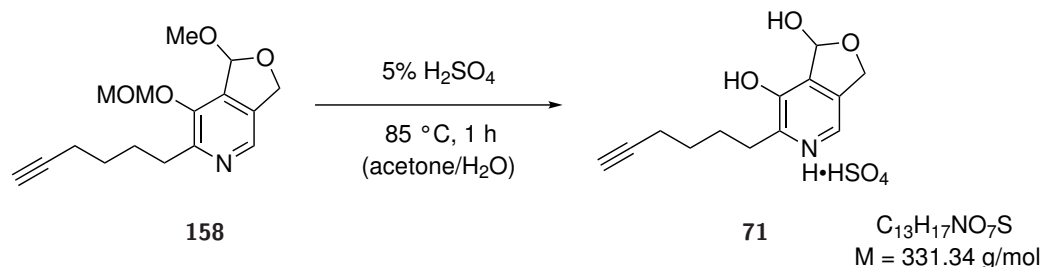
**$^1\text{H-NMR}$**  (400 MHz,  $\text{d}^6\text{-DMSO}$ ):  $\delta$ [ppm] = 9.60 (s, 1 H), 7.96 (s, 1 H), 6.64 (d,  $^3J = 7.8$  Hz, 1 H), 6.41 (d,  $^3J = 7.8$  Hz, 1 H), 5.04 (d,  $^2J = 12.9$  Hz, 1 H), 4.86 (d,  $^2J = 12.9$  Hz, 1 H), 2.81 (t,  $^3J = 7.1$  Hz, 2 H), 2.77 (t,  $^4J = 2.6$  Hz, 1 H), 2.21 (td,  $^3,4J = 7.1, 2.6$  Hz, 2 H), 1.81 (p,  $^3J = 7.1$  Hz, 2 H).

**$^{13}\text{C-NMR}$**  (100 MHz,  $\text{d}^6\text{-DMSO}$ ):  $\delta$ [ppm] = 148.0, 145.7, 135.1, 133.7, 132.5, 98.5, 84.5, 71.3, 68.8, 30.3, 26.8, 17.6.

**HRMS** (ESI) ( $\text{C}_{12}\text{H}_{13}\text{NO}_3$   $[\text{M}+\text{H}]^+$ ) calcd.: 220.0974

found: 220.0967.

**2-(hex-5-yn-1-yl)-3-hydroxy-5-(hydroxymethyl)isonicotinaldehyde bisulfate (PL7,71)** <sup>[198]</sup>



Following GP9, MOM-protected acetal **158** (50.0 mg, 172  $\mu\text{mol}$ , 1.0 eq) was deprotected in acetone/water (1:1; 10 mL) containing 5% sulfuric acid. After purification by HPLC (method B), probe **PL7** (30.0 mg, 90.5  $\mu\text{mol}$ , 55%) was obtained as a fluffy white solid.

**TLC:**  $R_f = 0.13$  (50% EtOAc/hexanes) [UV/CAM].

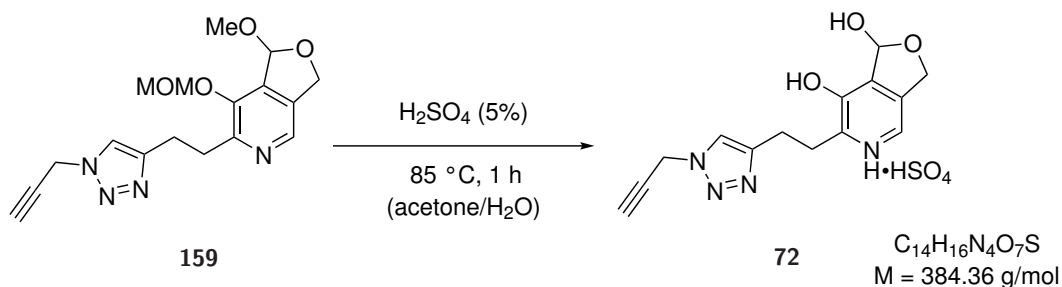
**HPLC:**  $t_R = 6.0$  min (method B).

**$^1\text{H-NMR}$**  (400 MHz,  $d^6$ -DMSO):  $\delta$ [ppm] = 10.4 (s, 1 H), 8.03 (s, 1 H), 6.77 (br. s, 1 H), 6.45 (s, 1 H), 5.07 (d,  $^2J = 13.0$  Hz, 1 H), 4.89 (d,  $^2J = 13.0$  Hz, 1 H), 2.79 (t,  $^3J = 7.4$  Hz, 2 H), 2.73 (t,  $^4J = 2.7$  Hz, 1 H), 2.18 (td,  $^3,^4J = 7.4, 2.7$  Hz, 2 H), 1.71 (p,  $^3J = 7.4$  Hz, 2 H), 1.48 (p,  $^3J = 7.4$  Hz, 2 H).

**$^{13}\text{C-NMR}$**  (100 MHz,  $d^6$ -DMSO):  $\delta$ [ppm] = 148.0, 146.3, 135.8, 135.3, 131.1, 98.4, 84.5, 71.2, 68.9, 30.1, 27.8, 27.1, 17.6.

**HRMS** (ESI) ( $\text{C}_{13}\text{H}_{15}\text{NO}_3$   $[\text{M}+\text{H}]^+$ ) calcd.: 234.1125

found: 234.1121.

**3-Hydroxy-5-(hydroxymethyl)-2-2-[1-(prop-2-yn-1-yl)-1*H*-1,2,3-triazol-4-yl]ethyl isonicotinaldehyde bisulfate (PL8,72)**<sup>[198]</sup>

Following GP9, MOM-protected acetal **159** (160 mg, 465  $\mu$ mol, 1.0 eq) was deprotected in acetone/water (1:1; 10 mL) containing 5% sulfuric acid. After purification by HPLC (method C), probe **PL8** (100 mg, 260  $\mu$ mol, 56%) was obtained as a fluffy white solid.

**TLC:**  $R_f = 0.10$  (EtOAc) [UV/CAM].

**HPLC:**  $t_R = 8.4$  min (method C).

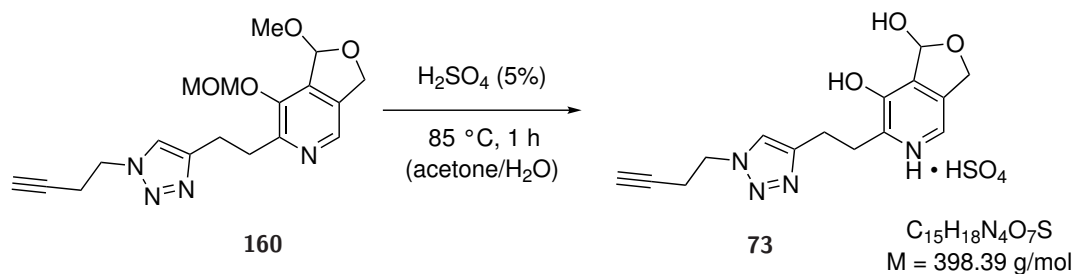
**<sup>1</sup>H-NMR** (400 MHz,  $d^6$ -DMSO):  $\delta$ [ppm] = 9.70 (s, 1 H), 7.98 (s, 1 H), 7.91 (s, 1 H), 7.77 (t,  $^3J = 6.5$  Hz, 1 H), 6.67 (d,  $^3J = 7.7$  Hz, 1 H), 6.42 (dd,  $^{3,4}J = 7.7, 1.7$  Hz, 1 H), 5.84 (d,  $^3J = 6.5$  Hz, 2 H), 5.05 (d,  $^2J = 13.0$  Hz, 1 H), 4.87 (d,  $^2J = 13.0$  Hz, 1 H), 3.10-3.05 (m, 2 H), 3.05-2.97 (m, 2 H).

**<sup>13</sup>C-NMR** (100 MHz,  $d^6$ -DMSO):  $\delta$ [ppm] = 201.3, 147.7, 147.5, 145.8, 135.3, 133.8, 132.5, 120.0, 98.5, 97.6, 88.9, 68.8, 30.9, 23.6.

**HRMS** (ESI) ( $C_{14}H_{14}N_4O_3$  [ $M+H$ ]<sup>+</sup>) calcd.: 287.1144

found: 287.1136.

2-2-[1-(but-3-yn-1-yl)-1*H*-1,2,3-triazol-4-yl]ethyl-3-hydroxy-5(hydroxy-methyl) isonicotinaldehyde bisulfate (**PL9,73**)<sup>[198]</sup>



Following GP9, MOM-protected acetal **160** (150 mg, 419  $\mu\text{mol}$ , 1.0 eq) was deprotected in acetone/water (1:1; 10 mL) containing 5% sulfuric acid. After purification by HPLC (method C), probe **PL9** (86.0 mg, 216  $\mu\text{mol}$ , 52%) was obtained as a fluffy white solid.

**TLC:**  $R_f = 0.10$  (EtOAc) [UV/ $\text{KMnO}_4$ ].

**HPLC:**  $t_R = 8.3$  min (method C).

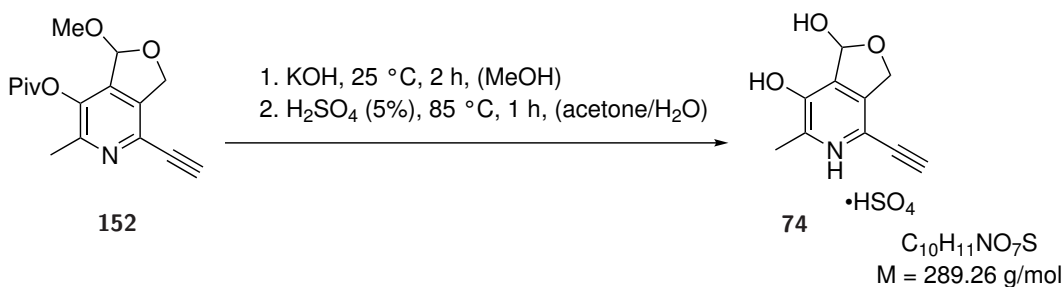
**$^1\text{H-NMR}$**  (400 MHz,  $\text{d}^6$ -DMSO):  $\delta$ [ppm] = 9.70 (s, 1 H), 7.99 (s, 1 H), 7.88 (s, 1 H), 6.67 (d,  $^3J = 6.9$  Hz, 1 H), 6.42 (d,  $^3J = 6.9$  Hz, 1 H), 5.05 (d,  $^2J = 12.9$  Hz, 1 H), 4.87 (d,  $^2J = 12.9$  Hz, 1 H), 4.42 (t,  $^3J = 6.8$  Hz, 2 H), 3.13-3.02 (m, 2 H), 3.02-2.05 (m, 2 H), 2.90 (t,  $^4J = 2.7$  Hz, 1 H), 2.75 (td,  $^3,4J = 6.8, 2.7$  Hz, 2 H).

**$^{13}\text{C-NMR}$**  (100 MHz,  $\text{d}^6$ -DMSO):  $\delta$ [ppm] = 147.6, 146.6, 145.7, 135.3, 133.8, 132.6, 122.0, 98.5, 80.7, 73.3, 68.8, 47.8, 31.2, 23.8, 19.2.

**HRMS** (ESI) ( $\text{C}_{15}\text{H}_{16}\text{N}_4\text{O}_3$  [ $\text{M}+\text{H}$ ] $^+$ ) calcd.: 301.1301

found: 301.1293.

## 4.1.2.9 Acetal and Ester Deprotection, Final Probes

2-Ethynyl-5-hydroxy-3-(hydroxymethyl)-6-methyl isonicotinaldehyde bisulfate (PL10,74)<sup>[198]</sup>

Following GP10, Piv protected acetal **152** (169 mg, 584  $\mu$ mol, 1.0 eq) was deprotected first in 2% potassium hydroxide in methanol (5 mL) followed by deprotection in acetone/water (1:1; 10 mL) containing 5% sulfuric acid. After purification by HPLC (method C), probe **PL10** (78.0 mg, 270  $\mu$ mol, 47%) was obtained as a fluffy white solid.

**TLC:**  $R_f = 0.16$  (10% MeOH/DCM) [UV/KMnO<sub>4</sub>].

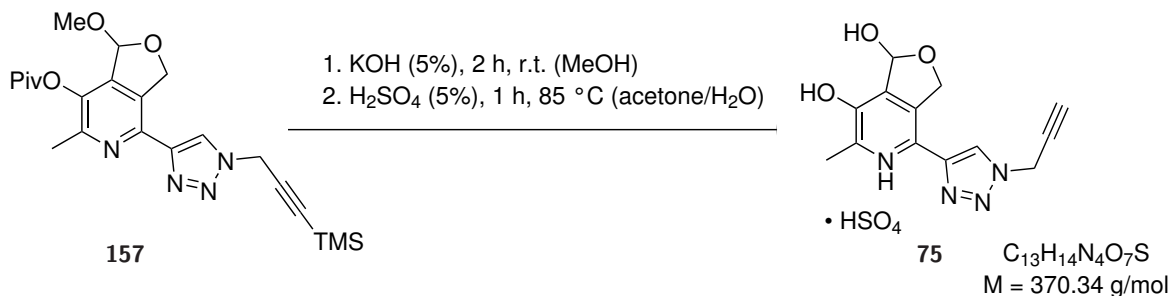
**HPLC:**  $t_R = 6.3$  min (method C).

**<sup>1</sup>H-NMR** (400 MHz, d<sup>6</sup>-DMSO):  $\delta$ [ppm] = 10.2 (br. s, 1 H), 6.76 (br. s, 1 H), 6.42 (s, 1 H), 5.03 (d,  $^2J = 13.4$  Hz, 1 H), 4.85 (d,  $^2J = 13.4$  Hz, 1 H), 4.27 (s, 1 H), 2.35 (s, 3 H).

**<sup>13</sup>C-NMR** (100 MHz, d<sup>6</sup>-DMSO):  $\delta$ [ppm] = 147.0, 146.6, 138.7, 133.3, 124.1, 99.1, 81.4, 81.0, 69.2, 18.9.

**HRMS** (ESI) (C<sub>10</sub>H<sub>9</sub>NO<sub>3</sub> [M+H]<sup>+</sup>) calcd.: 192.0661  
found: 192.0654.

**3-Hydroxy-5-(hydroxymethyl)-2-methyl-6-[1-(prop-2-yn-1-yl)-1*H*-1,2,3-triazol-4-yl] isonicotinaldehyde bisulfate (PL11,75)** <sup>[198]</sup>



Following GP10, crude Piv protected acetal **157** (1.0 eq) was deprotected first in 5% potassium hydroxide in methanol (7 mL) followed by deprotection in acetone/water (1:1; 8 mL) containing 5% sulfuric acid. After purification by HPLC (method B), probe **PL11** (17.0 mg, 45.9  $\mu\text{mol}$ , 14% over 2 steps) was obtained as a fluffy white solid.

**TLC:**  $R_f = 0.39$  (50% EtOAc/hexanes) [UV/KMnO<sub>4</sub>].

**HPLC:**  $t_R = 9.6$  min (method B).

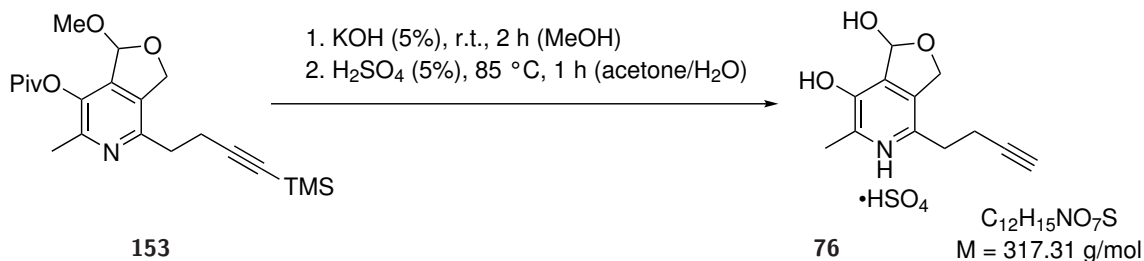
**<sup>1</sup>H-NMR** (400 MHz, d<sup>6</sup>-DMSO):  $\delta$ [ppm] = 9.84 (s, 1 H), 8.42 (s, 1 H), 7.84 (t, <sup>4</sup> $J = 5.2$  Hz, 1 H), 6.69 (d, <sup>3</sup> $J = 8.0$  Hz, 1 H), 6.45 (dd, <sup>3,4</sup> $J = 8.0, 1.7$  Hz, 1 H), 5.92 (d, <sup>3</sup> $J = 5.2$  Hz, 2 H), 5.33 (d, <sup>2</sup> $J = 13.8$  Hz, 1 H), 5.18 (d, <sup>2</sup> $J = 13.8$  Hz, 1 H), 2.42 (s, 3 H).

**<sup>13</sup>C-NMR** (100 MHz, d<sup>6</sup>-DMSO):  $\delta$ [ppm] = 201.7, 148.0, 145.9, 145.8, 134.6, 132.8, 131.9, 119.9, 98.1, 97.5, 89.3, 70.7, 18.9.

**HRMS** (ESI) (C<sub>13</sub>H<sub>12</sub>N<sub>4</sub>O<sub>3</sub> [M+H]<sup>+</sup>) calcd.: 273.0988

found: 273.0980.

2-(But-3-yn-1-yl)-5-hydroxy-3-(hydroxymethyl)-6-methylisonicotinaldehyde bisulfate (**PL12,76**)<sup>[198]</sup>



Following GP10, Piv protected acetal **153** (400 mg, 1.03 mmol, 1.0 eq) was deprotected first in 2% potassium hydroxide in methanol (8 mL) followed by deprotection in acetone/water (1:1; 10 mL) containing 5% sulfuric acid. After purification by HPLC (method B), probe **PL12** (78.0 mg, 246  $\mu$ mol, 24%) was obtained as a fluffy white solid.

**TLC:**  $R_f$  = 0.08 (20% EtOAc/hexanes) [UV/KMnO<sub>4</sub>].

**HPLC:**  $t_R$  = 5.5 min (method B).

**<sup>1</sup>H-NMR** (400 MHz, d<sup>6</sup>-DMSO):  $\delta$ [ppm] = 9.42 (s, 1 H), 6.68 (d, <sup>3</sup> $J$  = 6.7 Hz, 1 H), 6.41 (d, <sup>3</sup> $J$  = 6.7 Hz, 1 H), 5.07 (d, <sup>2</sup> $J$  = 12.8 Hz, 1 H), 4.90 (d, <sup>2</sup> $J$  = 12.8 Hz, 1 H), 2.74 (t, <sup>4</sup> $J$  = 2.6 Hz, 1 H), 2.69 (t, <sup>3</sup> $J$  = 7.4 Hz, 2 H), 2.49-2.44 (m, 2 H), 2.35 (s, 3 H).

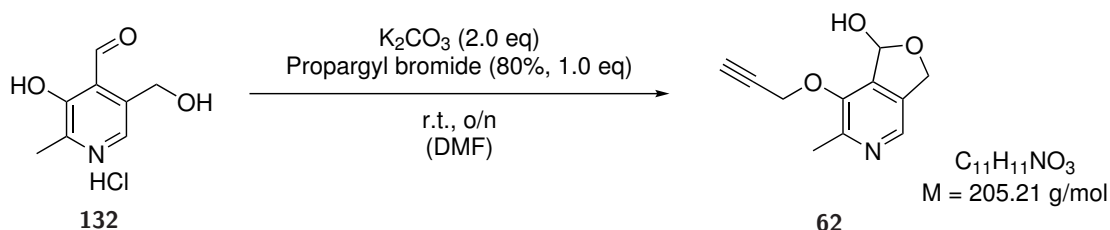
**<sup>13</sup>C-NMR** (100 MHz, d<sup>6</sup>-DMSO):  $\delta$ [ppm] = 144.9, 144.7, 141.6, 134.0, 133.0, 98.8, 84.2, 71.4, 68.9, 33.1, 18.7, 17.3.

**HRMS** (ESI) (C<sub>12</sub>H<sub>13</sub>NO<sub>3</sub> [M+H]<sup>+</sup>) calcd.: 220.0974

found: 220.0967.

## 4.1.2.10 PL13 Synthesis

6-methyl-7-(prop-2-yn-1-yloxy)-1,3-dihydrofuro[3,4-c]pyridin-1-ole (PL13, 62)<sup>[223]</sup>



Pyridoxal hydrochloride (500 mg, 2.46 mmol, 1.0 eq) was dissolved in anhydrous dimethyl formamide (25 mL). Then, potassium carbonate (635 mg, 4.91 mmol, 2.0 eq) was added and the mixture was stirred for 15 min prior to the addition of propargyl bromide (80% in hexanes, 274  $\mu$ L, 365 mg, 2.46 mmol, 1.0 eq). After stirring the reaction overnight, the solvent was evaporated under reduced pressure and the crude mixture was purified by column chromatography (MeOH/DCM, 5-10%) to yield **PL13** (126 mg, 614  $\mu$ mol, 25%) as an off-white solid.

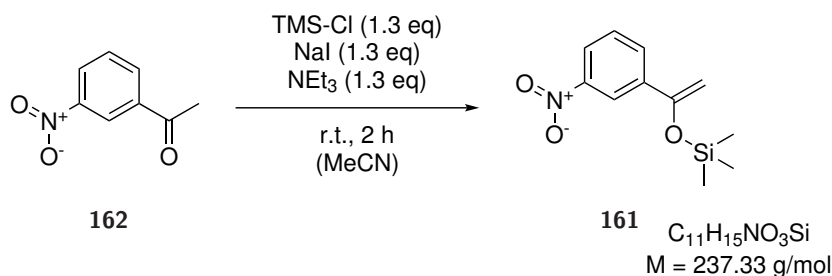
**TLC:**  $R_f = 0.44$  (10% MeOH/DCM) [UV/CAM].

**$^1H$ -NMR** (400 MHz,  $d^6$ -DMSO):  $\delta$ [ppm] = 8.15 (s, 1 H), 7.10 (d,  $^3J = 7.7$  Hz, 1 H), 6.58 (dd,  $^3,4J = 7.7, 1.7$  Hz, 1 H), 5.07 (d,  $^2J = 13.0$  Hz, 1 H), 4.95 (dd,  $^4,4J = 2.4, 1.1$  Hz, 2 H), 4.92 (d,  $^2J = 13.0$  Hz, 1 H), 3.62 (t,  $^4J = 2.4$  Hz, 1 H).

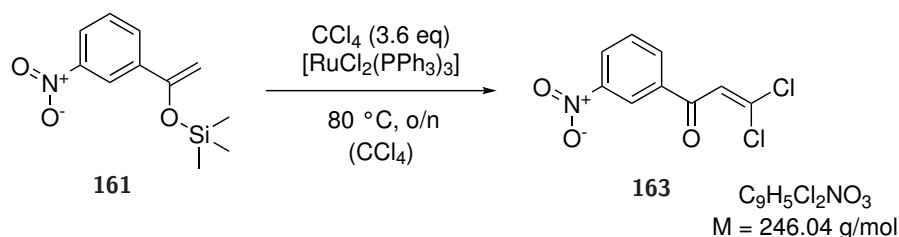
**$^{13}C$ -NMR** (100 MHz,  $d^6$ -DMSO):  $\delta$ [ppm] = 149.1, 146.5, 136.5, 136.0, 135.7, 98.9, 79.1, 78.8, 68.6, 58.9, 19.3.

**HRMS** (ESI) ( $C_{11}H_{12}NO_3$  [ $M+H$ ] $^+$ ) calcd.: 206.0812  
found: 206.0811.



**4.1.2.11** Synthesis of Screening CompoundsTrimethyl[1-(3-nitrophenyl)vinyl]oxysilane (**161**)<sup>[295]</sup>

*m*-Nitroacetophenone (991 mg, 6.00 mmol, 1.0 eq), trimethylsilyl chloride (951  $\mu$ L, 7.50 mmol, 1.3 eq), and triethylamine (1.05 mL, 7.50 mmol, 1.3 eq) were added to a flame dried flask. The mixture was stirred at room temperature and a solution of sodium iodide (1.12 g, 7.50 mmol, 1.3 eq) in acetonitrile (7.50 mL, 1.0 M) was added dropwise. After stirring the reaction for 2 h, it was cooled to 0 °C and hexanes (6 mL) was added. After adding water (6 mL) the phases were separated, and the aqueous layer was extracted with hexanes (2 $\times$ 6 mL). The combined organic phases were washed with water (2 $\times$ 6 mL), dried over magnesium sulfate and concentrated under reduced pressure. The intermediate trimethylsilyl enol ether **161** (973 mg, 4.10 mmol, 69%) was obtained as a yellow oil that was used without further purification.

3,3-Dichloro-1-(3-nitrophenyl)prop-2-en-1-one (**163**)<sup>[295]</sup>

Carbon tetrachloride (1.40 mL, 14.5 mmol, 3.6 eq) was added to a flame-dried pressure tube, and the vessel was sealed with a silicon septum. The solvent was frozen at  $-78^\circ\text{C}$  and vacuum was applied to 0.3 mbar. The solvent was then allowed to thaw under vacuum before the vessel was filled with argon. This freeze-pump thaw process was repeated twice. Ruthenium(II)-tris-triphenylphosphine dichloride (46.0 mg, 480  $\mu\text{mol}$ , 1 mol%) and crude trimethyl[1-(3-nitrophenyl)vinyl]oxysilane (973 mg, 4.10 mmol, 1.0 eq) were added. The vessel was sealed and heated at  $80^\circ\text{C}$  for 17 h while stirring. Upon completion, the reaction was cooled down and directly purified by column chromatography (EtOAc/hexanes, 5-20%) to yield dichlorovinyl **163** (415 mg, 1.69 mmol, 42%) as a white powder.

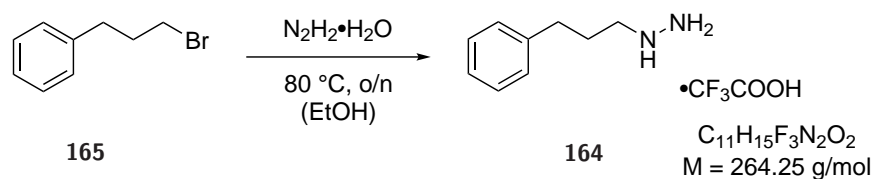
**TLC:**  $R_f = 0.54$  (20% EtOAc/hexanes) [UV/ $\text{KMnO}_4$ ].

**$^1\text{H-NMR}$**  (400 MHz,  $d^6$ -DMSO):  $\delta$ [ppm] = 7.83-7.89 (m, 1 H), 8.03 (s, 1 H), 8.44 (ddd,  $^{3,4,4}J = 7.8, 1.7, 1.1 \text{ Hz}$ , 3 H), 8.50 (ddd,  $^{3,4,4}J = 8.2, 2.3, 1.0 \text{ Hz}$ , 1 H), 8.70 (*virt. t*,  $^3J \approx ^3J = 1.9 \text{ Hz}$ , 1 H).

**$^{13}\text{C-NMR}$**  (100 MHz,  $d^6$ -DMSO):  $\delta$ [ppm] = 184.6, 148.1, 137.6, 134.7, 134.6, 130.7, 128.0, 124.7, 122.9.

**HRMS** (ESI) ( $\text{C}_{11}\text{H}_{12}\text{NO}_3$  [ $\text{M}+\text{H}$ ] $^+$ ) calcd.: 206.0812  
found: 206.0811.

The analytical data are in accordance with previous literature reports.<sup>[295]</sup>

**(3-Phenylpropyl)hydrazine trifluoroacetate salt (TM-2-10,164)** <sup>[241]</sup>

The title compound was synthesized from 3-phenylpropyl bromide (76.0  $\mu\text{L}$ , 99.5 mg, 500  $\mu\text{mol}$ , 1.0 eq) according to GP11. The crude product was purified by preparative reversed-phase HPLC, with an applied gradient as following: 2% MeCN (+0.1% TFA) to 98% in 12 min, 98% MeCN (+0.1% TFA) for 2 min, to 2% MeCN (+0.1% TFA) in 1 min, 2% MeCN (+0.1% TFA) for 2 min yielding **164** (32.6 mg, 123  $\mu\text{mol}$ , 25%) as an off-white solid.

**HPLC:**  $t_{\text{R}} = 5.5$  min (method A modified).

**$^1\text{H-NMR}$**  (300 MHz,  $\text{CD}_3\text{OD}$ ):  $\delta[\text{ppm}] = 7.31\text{-}7.27$  (m, 2 H), 7.23-7.17 (m, 3 H), 3.03 (t,  $^3J = 7.8$  Hz, 2 H), 2.71 (t,  $^3J = 7.6$  Hz, 2 H), 1.96 (q,  $^3J = 7.8$  Hz, 2 H).

**$^{13}\text{C-NMR}$**  (125 MHz,  $\text{CD}_3\text{OD}$ ):  $\delta[\text{ppm}] = 161.6$  (q,  $J = 34$  Hz,  $\text{CF}_3\text{CO}_2\text{H}$ ) $\dagger$ , 140.5, 128.2, 128.0, 125.9, 116.8 (q,  $J = 290$  Hz,  $\text{CF}_3\text{CO}_2\text{H}$ ) $\dagger$ , 50.6, 32.2, 26.5.

**$^{19}\text{F-NMR}$**  (377 MHz,  $\text{CD}_3\text{OD}$ ):  $\delta[\text{ppm}] = -76.9$  (s,  $\text{CF}_3\text{CO}_2\text{H}$ ).

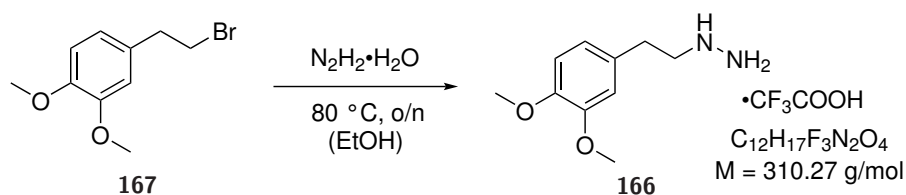
**HRMS** (ESI) ( $\text{C}_9\text{H}_{15}\text{N}_2$   $[\text{M}+\text{H}]^+$ ) calcd.: 151.1230

found: 151.1232.

The analytical data are in accordance with previous literature reports. <sup>[241]</sup>

$\dagger\text{CF}_3\text{CO}_2\text{H}$  peaks poorly characterised due to low signal intensity

(3,4-Dimethoxyphenethyl)hydrazine trifluoroacetate salt (TM-2-11,166) [241]



The title compound was synthesized from 4-(2-bromoethyl)-1,2-dimethoxybenzene (40.0 mg, 163  $\mu\text{mol}$ , 1.0 eq) according to GP11. Purification by preparative reversed-phase HPLC yielded **166** (16.5 mg, 53.0  $\mu\text{mol}$ , 33%) as an off-white solid.

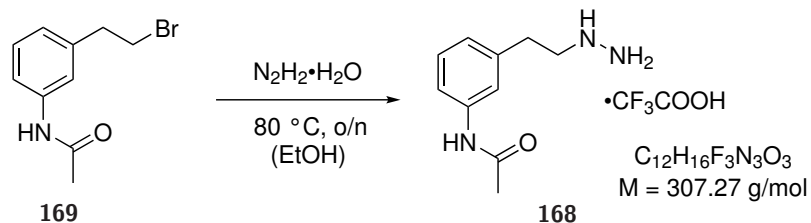
**HPLC:**  $t_{\text{R}} = 5.5\text{ min}$  (method A).

**$^1\text{H-NMR}$**  (300 MHz,  $\text{CD}_3\text{OD}$ ):  $\delta[\text{ppm}] = 8.29\text{ (s, 1 H)}$ ,  $7.92\text{ (s, 1 H)}$ ,  $6.82\text{-}6.79\text{ (m, 1 H)}$ ,  $6.66\text{-}6.59\text{ (m, 2 H)}$ ,  $4.51\text{ (d, }^3J = 6.9\text{ Hz, 2 H)}$ ,  $3.77\text{ (s, 3 H)}$ ,  $3.73\text{ (s, 3 H)}$ ,  $3.11\text{ (d, }^3J = 6.9\text{ Hz, 2 H)}$ .

**$^{13}\text{C-NMR}$**  (125 MHz,  $\text{CD}_3\text{OD}$ ):  $\delta[\text{ppm}] = 149.1$ ,  $148.1$ ,  $130.0$ ,  $120.9$ ,  $112.1$ ,  $111.6$ ,  $55.0$ ,  $54.9$ ,  $45.4$ ,  $35.0$ .

**$^{19}\text{F-NMR}$**  (377 MHz,  $\text{CD}_3\text{OD}$ ):  $\delta[\text{ppm}] = -76.9\text{ (s, CF}_3\text{CO}_2\text{H)}$ .

*N*-[3-(2-Hydrazineylethyl)phenyl]acetamide ditrifluoroacetate salt (TM-2-12,168)<sup>[241]</sup>



The title compound was synthesized from *N*-(3-(2-bromoethyl)phenyl)acetamide (40.0 mg, 165  $\mu\text{mol}$ , 1.0 eq) according to GP11. Purification by preparative reversed-phase HPLC yielded **168** (19.8 mg, 64.0  $\mu\text{mol}$ , 39%) as a yellow oil.

**HPLC:**  $t_{\text{R}} = 5.5\text{ min}$  (method A).

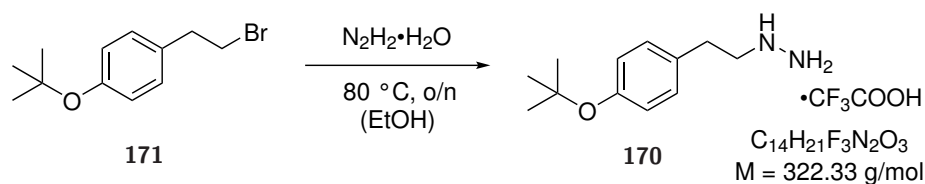
**$^1\text{H-NMR}$**  (400 MHz,  $\text{CD}_3\text{OD}$ ):  $\delta[\text{ppm}] = 7.58\text{ (s, 1 H)}$ ,  $7.33\text{--}7.24\text{ (m, 2 H)}$ ,  $7.03\text{--}7.00\text{ (m, 1 H)}$ ,  $3.27\text{ (t, }^3J = 7.6\text{ Hz, 2 H)}$ ,  $2.93\text{ (t, }^3J = 7.6\text{ Hz, 2 H)}$ ,  $2.12\text{ (s, 3 H)}$ .

**$^{13}\text{C-NMR}$**  (125 MHz,  $\text{CD}_3\text{OD}$ ):  $\delta[\text{ppm}] = 170.4$ ,  $138.9$ ,  $137.7$ ,  $128.9$ ,  $124.1$ ,  $120.2$ ,  $118.5$ ,  $52.0$ ,  $31.4$ ,  $22.4$ .

**$^{19}\text{F-NMR}$**  (377 MHz,  $\text{CD}_3\text{OD}$ ):  $\delta[\text{ppm}] = -76.9\text{ (s, CF}_3\text{CO}_2\text{H)}$ .

**HRMS** (ESI) ( $\text{C}_{10}\text{H}_{16}\text{N}_3\text{O} [\text{M}+\text{H}]^+$ ) calcd.: 194.1288  
found: 194.1294.

[4-(*tert*-Butoxy)phenethyl]hydrazine trifluoroacetate salt (TM-2-13,170)<sup>[241]</sup>



The title compound was synthesized from 1-(2-bromoethyl)-4-(*tert*-butoxy)-benzene (40.0 mg, 156  $\mu\text{mol}$ , 1.0 eq) according to GP11. Purification by preparative reversed-phase HPLC yielded **170** (36.1 mg, 112  $\mu\text{mol}$ , 72%) as a white solid.

**HPLC:**  $t_{\text{R}} = 5.5\text{ min}$  (method A).

**$^1\text{H-NMR}$**  (400 MHz,  $\text{CD}_3\text{OD}$ ):  $\delta[\text{ppm}] = 7.19\text{ (m, 2 H)}$ ,  $6.98\text{-}6.95\text{ (m, 2 H)}$ ,  $3.24\text{ (t, }^3J = 8.0\text{ Hz, 2 H)}$ ,  $2.91\text{ (t, }^3J = 8.0\text{ Hz, 2 H)}$ ,  $1.32\text{ (s, 9 H)}$ .

**$^{13}\text{C-NMR}$**  (125 MHz,  $\text{CD}_3\text{OD}$ ):  $\delta[\text{ppm}] = 161.3\text{-}162.1\text{ (q, } J = 35\text{ Hz, CF}_3\text{CO}_2\text{H)}^\dagger$ ,  $154.1$ ,  $132.0$ ,  $128.9$ ,  $124.3$ ,  $113.3\text{-}120.3\text{ (q, } J = 290\text{ Hz, CF}_3\text{CO}_2\text{H)}^\dagger$ ,  $78.2$ ,  $52.2$ ,  $30.5$ ,  $27.8$ .

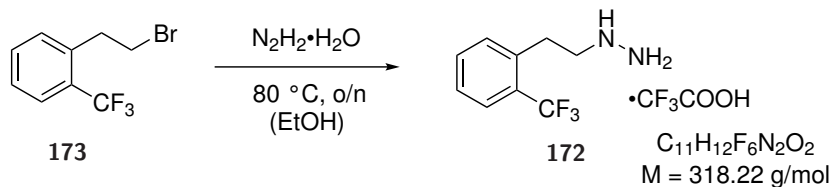
**$^{19}\text{F-NMR}$**  (377 MHz,  $\text{CD}_3\text{OD}$ ):  $\delta[\text{ppm}] = -77.0\text{ (s, CF}_3\text{CO}_2\text{H)}$ .

**HRMS** (ESI) ( $\text{C}_{12}\text{H}_{21}\text{N}_2\text{O}$   $[\text{M}+\text{H}]^+$ ) calcd.: 209.1648

found: 209.1654.

$^\dagger\text{CF}_3\text{CO}_2\text{H}$  peaks poorly characterised due to low signal intensity

[2-(Trifluoromethyl)phenethyl]hydrazine trifluoroacetate salt (TM-2-14,172)<sup>[241]</sup>



The title compound was synthesized from 1-(2-bromoethyl)-2-(trifluoromethyl)benzene (40.0 mg, 158  $\mu\text{mol}$ , 1.0 eq) according to GP11. Purification by preparative reversed-phase HPLC yielded **172** (27.2 mg, 86.0  $\mu\text{mol}$ , 54%) as a white solid.

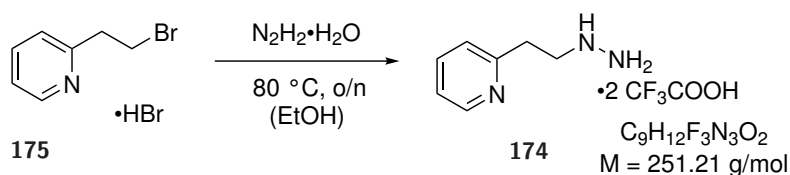
**HPLC:**  $t_{\text{R}} = 5.5\text{ min}$  (method A).

**$^1\text{H-NMR}$**  (400 MHz,  $\text{CD}_3\text{OD}$ ):  $\delta[\text{ppm}] = 7.72\text{-}7.70$  (m, 1 H), 7.63-7.59 (m, 1 H), 7.51-7.43 (m, 2 H), 3.26-3.22 (m, 2 H), 3.15-3.11 (m, 2 H).

**$^{13}\text{C-NMR}$**  (125 MHz,  $\text{CD}_3\text{OD}$ ):  $\delta[\text{ppm}] = 161.5$  (q,  $J = 35\text{ Hz}$ ,  $\text{CF}_3\text{CO}_2\text{H}$ ), 135.8, 132.3, 131.5, 128.4 (q,  $J = 30\text{ Hz}$ ,  $\text{CF}_3$ ), 127.1, 125.8 (q,  $J = 5\text{ Hz}$ ,  $\text{CF}_3$ ), 124.7 (q,  $J = 270\text{ Hz}$ ,  $\text{CF}_3$ ), 116.7 (q,  $J = 289\text{ Hz}$ ,  $\text{CF}_3\text{CO}_2\text{H}$ ), 51.5, 28.6.

**$^{19}\text{F-NMR}$**  (377 MHz,  $\text{CD}_3\text{OD}$ ):  $\delta[\text{ppm}] = -60.9, -77.0$ .

**HRMS** (ESI) ( $\text{C}_9\text{H}_{12}\text{F}_3\text{N}_2$   $[\text{M}+\text{H}]^+$ ) calcd.: 205.0947  
found: 205.0952.

2-(2-Hydrazineylethyl)pyridine ditrifluoroacetate salt (TM-2-15,174)<sup>[241]</sup>

The title compound was synthesized from 2-(2-bromoethyl)pyridine hydrogenbromide (40.0 mg, 150  $\mu\text{mol}$ , 1.0 eq) according to GP11. Purification by preparative reversed-phase HPLC yielded **174** (46.1 mg, 126  $\mu\text{mol}$ , 84%) as a red solid.

**HPLC:**  $t_{\text{R}} = 5.5$  min (method A).

**$^1\text{H-NMR}$**  (400 MHz,  $\text{CD}_3\text{OD}$ ):  $\delta$ [ppm] = 8.72 (d,  $^3J = 5.6$  Hz, 1 H), 8.32 (td,  $^{3,4}J = 8.0$ , 1.6 Hz, 1 H), 7.87 (d,  $^3J = 8.0$  Hz, 1 H), 7.77 (t,  $^3J = 5.6$  Hz, 1 H), 3.49 (t,  $^3J = 6.8$  Hz, 2 H), 3.35 (t,  $^3J = 6.8$  Hz, 2 H)†.

**$^{13}\text{C-NMR}$**  (125 MHz,  $\text{CD}_3\text{OD}$ ):  $\delta$ [ppm] = 161.7 (q,  $J = 34$  Hz,  $\text{CF}_3\text{CO}_2\text{H}$ ), 155.6, 144.2, 143.0, 126.2, 124.1, 115.6 (q,  $J = 291$  Hz,  $\text{CF}_3\text{CO}_2\text{H}$ ), 48.7, 31.2.

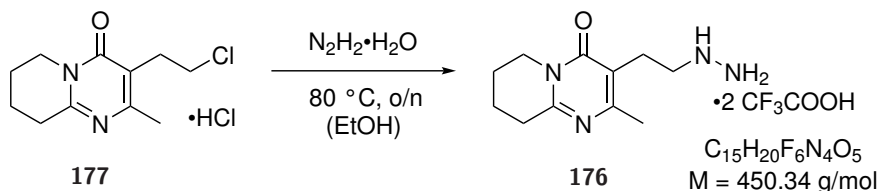
**$^{19}\text{F-NMR}$**  (377 MHz,  $\text{CD}_3\text{OD}$ ):  $\delta$ [ppm] =  $-76.9$  (s,  $\text{CF}_3\text{CO}_2\text{H}$ ).

**HRMS** (ESI) ( $\text{C}_7\text{H}_{12}\text{N}_3$  [ $\text{M}+\text{H}$ ] $^+$ ) calcd.: 138.1026

found: 138.1021.

†Overlap of compound peak with  $\text{CD}_3\text{OD}$  reference quintet prevents solvent peak from being observed



**3-(2-Hydrazineylethyl)-2-methyl-6,7,8,9-tetrahydro-4*H*-pyrido[1,2-*a*]-pyrimidin-4-one ditrifluoroacetate salt (TM-2-16,176)**<sup>[241]</sup>

The title compound was synthesized from pyrimidinone hydrogenchloride **177** (40.0 mg, 152  $\mu\text{mol}$ , 1.0 eq) according to GP11. Purification by preparative reversed-phase HPLC, with fraction collection utilising the 275 nm trace, yielded **176** (58.3 mg, 130  $\mu\text{mol}$ , 85%) as a pale yellow oily residue.

**HPLC:**  $t_{\text{R}} = 5.5 \text{ min}$  (method A).

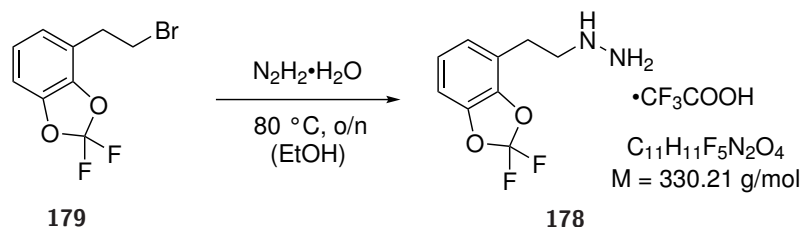
**$^1\text{H-NMR}$**  (400 MHz,  $\text{CD}_3\text{OD}$ ):  $\delta[\text{ppm}] = 3.98$  (t,  $^3J = 6.0 \text{ Hz}$ , 2 H), 3.25 (t,  $^3J = 6.8 \text{ Hz}$ , 2 H), 3.10 (t,  $^3J = 6.8 \text{ Hz}$ , 2 H), 2.92 (t,  $^3J = 6.8 \text{ Hz}$ , 2 H), 2.08-2.02 (m, 2 H), 1.99-1.92 (m, 2 H).  **$^{13}\text{C-NMR}$**  (125 MHz,  $\text{CD}_3\text{OD}$ ):  $\delta[\text{ppm}] = 161.6$  (q,  $J = 34 \text{ Hz}$ ,  $\text{CF}_3\text{CO}_2\text{H}$ ), 161.2, 160.6, 152.8, 117.8, 116.8 (q,  $J = 290 \text{ Hz}$ ,  $\text{CF}_3\text{CO}_2\text{H}$ ), 48.6, 43.6, 21.9, 20.5, 17.1, 17.0, 16.8

**$^{19}\text{F-NMR}$**  (377 MHz,  $\text{CD}_3\text{OD}$ ):  $\delta[\text{ppm}] = -76.9$ - $-76.8$  (m,  $\text{CF}_3\text{CO}_2\text{H}$ ).

**HRMS** (ESI) ( $\text{C}_{11}\text{H}_{19}\text{N}_4\text{O}$   $[\text{M}+\text{H}]^+$ ) calcd.: 223.1553

found: 223.1561.

[2-(2,2-Difluorobenzo[*d*][1,3]dioxol-4-yl)ethyl]hydrazine trifluoroacetate salt (TM-2-17,178)<sup>[241]</sup>



The title compound was synthesized from 4-(2-bromoethyl)-2,2-difluoro-1,3-dioxolane (40.0 mg, 151  $\mu$ mol, 1.0 eq) according to GP11. Purification by preparative reversed-phase HPLC yielded **178** (33.3 mg, 101  $\mu$ mol, 67%) as a white solid.

**HPLC:**  $t_R = 5.5$  min (method A).

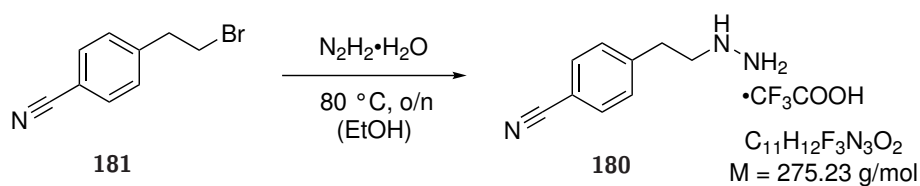
**<sup>1</sup>H-NMR** (400 MHz, CD<sub>3</sub>OD):  $\delta$ [ppm] = 7.16-7.04 (m, 3H), 3.29 (t,  $^3J = 7$  Hz, 2H), 3.02 (t,  $^3J = 7.6$  Hz, 2H).

**<sup>13</sup>C-NMR** (125 MHz, CD<sub>3</sub>OD):  $\delta$ [ppm] = 161.7 (q,  $J = 35$  Hz, CF<sub>3</sub>CO<sub>2</sub>H), 143.4, 142.0, 131.4 (t,  $J = 251$  Hz, CF<sub>3</sub>), 124.7, 124.0, 120.2, 116.8 (q,  $J = 290$  Hz, CF<sub>3</sub>CO<sub>2</sub>H), 108.0, 49.5, 26.4.

**<sup>19</sup>F-NMR** (377 MHz, CD<sub>3</sub>OD):  $\delta$ [ppm] = -52.0 (s, 2F), -77.0 (s, 3F).

**HRMS** (ESI) (C<sub>9</sub>H<sub>11</sub>F<sub>2</sub>N<sub>2</sub>O<sub>2</sub> [M+H]<sup>+</sup>) calcd.: 217.0783

found: 217.0788.

4-(2-Hydrazineylethyl)benzonitrile trifluoroacetate salt (TM-2-18,180)<sup>[241]</sup>

The title compound was synthesized from 4-(2-bromoethyl)benzonitrile (40.0 mg, 190  $\mu\text{mol}$ , 1.0 eq) according to GP11. Purification by preparative reversed-phase HPLC yielded **180** (20.1 mg, 73.0  $\mu\text{mol}$ , 38%) as an off-white, yellow solid.

**HPLC:**  $t_R = 5.5\text{ min}$  (method A).

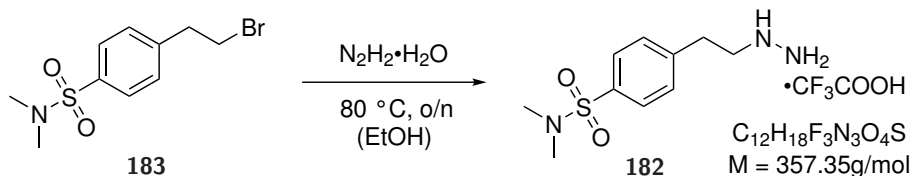
**$^1\text{H-NMR}$**  (300 MHz,  $\text{CD}_3\text{OD}$ ):  $\delta[\text{ppm}] = 7.72\text{-}7.69\text{ (m, 2 H)}$ ,  $7.48\text{-}7.45\text{ (m, 2 H)}$ ,  $3.27\text{ (t, }^3J = 7.8\text{ Hz, 2 H)}$ ,  $3.02\text{ (t, }^3J = 7.8\text{ Hz, 2 H)}$ .

**$^{13}\text{C-NMR}$**  (125 MHz,  $\text{CD}_3\text{OD}$ ):  $\delta[\text{ppm}] = 132.2, 129.5, 125.4, 118.2, 110.5, 50.9, 33.1$ .

**$^{19}\text{F-NMR}$**  (377 MHz,  $\text{CD}_3\text{OD}$ ):  $\delta[\text{ppm}] = -76.9\text{ (s, CF}_3\text{CO}_2\text{H)}$ .

**HRMS** (ESI) ( $\text{C}_9\text{H}_{12}\text{N}_3\text{ [M+H]}^+$ ) calcd.: 162.1026

found: 162.1025.

**4-(2-Hydrazineylethyl)-*N,N*-dimethylbenzenesulfonamide trifluoroacetate salt (TM-2-19,182)**<sup>[241]</sup>

The title compound was synthesized from 4-(2-bromoethyl)-*N,N*-dimethylbenzene-1-sulfonamide (40.0 mg, 137  $\mu\text{mol}$ , 1.0 eq) according to GP11. Purification by preparative reversed-phase HPLC yielded **182** (36.3 mg, 102  $\mu\text{mol}$ , 74%) as a white solid.

**HPLC:**  $t_{\text{R}} = 5.5$  min (method A).

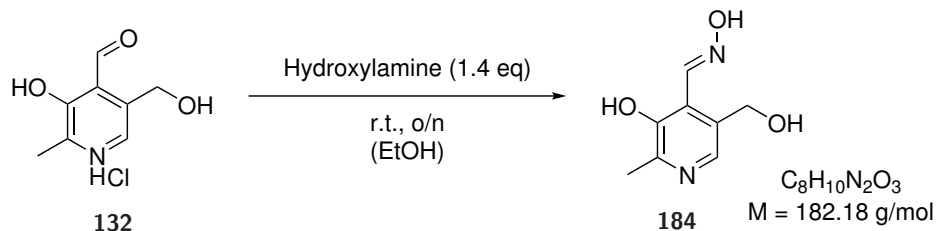
**$^1\text{H-NMR}$**  (300 MHz,  $\text{CD}_3\text{OD}$ ):  $\delta[\text{ppm}] = 7.75$  (d,  $^3J = 8.0$  Hz, 2 H), 7.53 (d,  $^3J = 8.0$  Hz, 2 H), 3.29 (t,  $^3J = 7.6$  Hz, 2 H), 3.04 (t,  $^3J = 7.6$  Hz, 2 H), 2.68 (s, 6 H).

**$^{13}\text{C-NMR}$**  (125 MHz,  $\text{CD}_3\text{OD}$ ):  $\delta[\text{ppm}] = 1616$  (q,  $J = 35$  Hz,  $\text{CF}_3\text{CO}_2\text{H}$ ), 143.2, 133.7, 129.3, 128.0, 116.7 (q,  $J = 289$  Hz,  $\text{CF}_3\text{CO}_2\text{H}$ ), 108.0, 51.1, 36.9, 31.4.

**$^{19}\text{F-NMR}$**  (377 MHz,  $\text{CD}_3\text{OD}$ ):  $\delta[\text{ppm}] = -77.0$  (s,  $\text{CF}_3\text{CO}_2\text{H}$ ).

**HRMS** (ESI) ( $\text{C}_{10}\text{H}_{18}\text{N}_3\text{O}_2\text{S}$   $[\text{M}+\text{H}]^+$ ) calcd.: 244.1114  
found: 244.1122.

(*E*)-3-hydroxy-5-(hydroxymethyl)-2-methylisonicotinaldehyde O-methyl oxime (**184**)<sup>[339]</sup>



Hydroxylamine hydrochloride (478 mg, 6.88 mmol, 1.4 eq) was added to a stirred solution of pyridoxal hydrochloride (1.00 g, 4.91 mmol, 1.0 eq) in ethanol (100 mL). The reaction was stirred at room temperature overnight. Upon completion, the solvent was removed under reduced pressure and the residue was purified by HPLC (method C) to yield methoxim **184** (508 mg, 2.79 mmol, 57%) as a white solid.

**TLC:**  $R_f = 0.69$  (10% MeOH/DCM) [UV/CAM].

**HPLC:**  $t_R = 1.6$  min (method C).

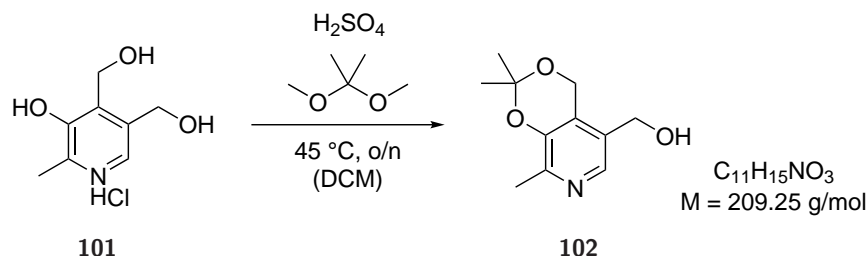
**<sup>1</sup>H-NMR** (400 MHz, d<sup>6</sup>-DMSO):  $\delta$ [ppm] = 8.64 (s, 1 H), 8.20 (s, 1 H), 4.73 (s, 2 H), 4.06 (s, 3 H), 3.78 (s, 1 H), 2.62 (s, 3 H).

**HRMS** (ESI) (C<sub>8</sub>H<sub>11</sub>N<sub>2</sub>O<sub>3</sub> [M+H]<sup>+</sup>) calcd.: 183.0765

found: 183.0763.

**4.1.2.12** Synthesis of Pro-Tide Probes PLPA and PL3PA

{2,2,8-Trimethyl-4*H*-[1,3]dioxino[4,5-*c*]pyridin-5-yl}methanol (**102**)<sup>[206]</sup>



Pyridoxal hydrochloride (5.00 g, 24.3 mmol, 1.0 eq) was dissolved in anhydrous dichloromethane (100 mL). Then, 2,2-dimethoxypropane (25.0 mL, 21.0 g, 202 mmol, 8.3 eq) and sulfuric acid (96%, 1.80 mL) were added and the reaction was stirred at 45 °C overnight. Upon completion and cooling down to room temperature, the mixture was diluted with dichloromethane (50 mL) and washed with satd. sodium bicarbonate solution (2×50 mL). The aqueous layer was further extracted with dichloromethane (4×30 mL) and the combined organic phase was dried over sodium sulfate, filtered and concentrated under reduced pressure. The crude product was recrystallised from ether/pentane (2:1) to yield the acetal **102** quantitatively as a white solid.

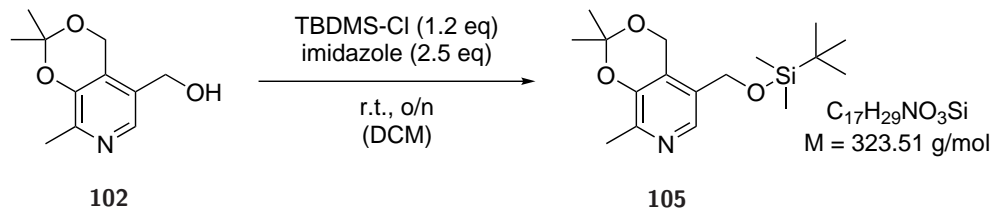
**TLC:**  $R_f = 0.76$  (50% EtOAc/hexanes) [UV/PMA].

**<sup>1</sup>H-NMR** (400 MHz, CDCl<sub>3</sub>):  $\delta$ [ppm] = 8.14 (s, 1 H), 4.95 (s, 2 H), 4.66 (s, 2 H), 2.56 (s, 3 H), 1.58 (s, 6 H).

**<sup>13</sup>C-NMR** (100 MHz, CDCl<sub>3</sub>):  $\delta$ [ppm] = 148.2, 146.3, 138.9, 129.1, 126.0, 100.0, 60.7, 58.7, 24.9, 18.6.

**HRMS** (ESI) (C<sub>11</sub>H<sub>16</sub>NO<sub>3</sub> [M+H]<sup>+</sup>) calcd.: 210.1125  
found: 210.1124.

The analytical data are in accordance with previous literature reports.<sup>[206]</sup>

5-[[*tert*-Butyldimethylsilyl]oxy]methyl}-2,2,8-trimethyl-4*H*-[1,3]dioxino-[4,5-*c*]pyridine (**105**)<sup>[151]</sup>

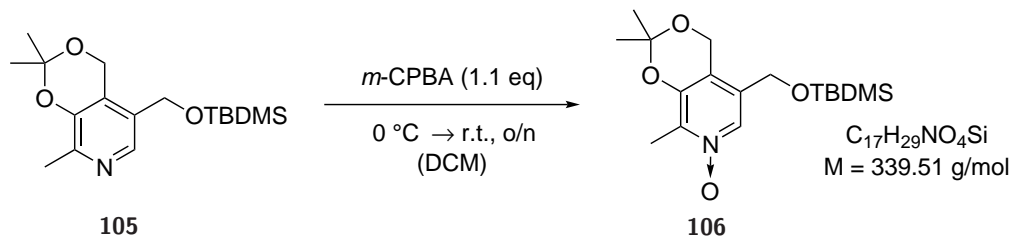
Acetal **102** (2.00 g, 9.56 mmol, 1.0 eq) was dissolved in anhydrous dichloromethane (30 mL) and imidazole (1.63 g, 23.9 mmol, 2.5 eq) was added while stirring. In parallel, *tert*-butyldimethylsilyl chloride (1.73 g, 11.5 mmol, 1.2 eq) was dissolved in anhydrous dichloromethane (30 mL) and subsequently added to the reaction mixture. After stirring at room temperature overnight the reaction was quenched by adding satd. sodium bicarbonate solution (50 mL) and the aqueous layer was extracted with dichloromethane (4×50 mL). The combined organic phase was dried over sodium sulfate, filtered and concentrated under reduced pressure. The crude product was purified by flash chromatography (EtOH/hexanes, 20-80%) to yield the protected alcohol **105** (2.73 g, 8.44 mmol, 89%) as a clear oil.

**TLC:**  $R_f = 0.64$  (5% MeOH/DCM) [UV/CAM].

**<sup>1</sup>H-NMR** (400 MHz,  $CDCl_3$ ):  $\delta$ [ppm] = 7.94 (s, 1 H), 4.88 (s, 2 H), 4.58 (s, 2 H), 2.40 (s, 3 H), 1.55 (s, 6 H), 0.89 (s, 9 H), 0.07 (s, 6 H).

**<sup>13</sup>C-NMR** (100 MHz,  $CD_3OD$ ):  $\delta$ [ppm] = 147.7, 146.1, 138.6, 129.4, 125.6, 99.7, 61.3, 58.9, 26.0, 24.9, 18.7, 18.4, -5.2.

**HRMS** (ESI) ( $C_{17}H_{30}NO_3Si$  [M+H]<sup>+</sup>) calcd.: 324.1989  
found: 324.1990.

5-[[*tert*-Butyldimethylsilyl]oxy]methyl]-2,2,8-trimethyl-4*H*-[1,3]dioxino-[4,5-*c*]pyridine 7-oxide (**106**)<sup>[190,198]</sup>

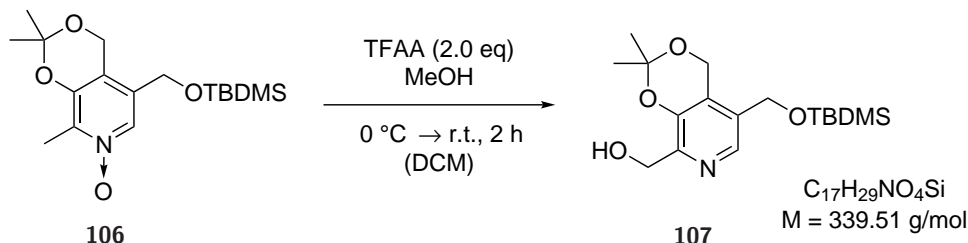
Protected pyridoxine **105** (2.73 g, 8.44 mmol, 1.0 eq) was dissolved in anhydrous dichloromethane (50 mL) and *meta*-chloroperbenzoic acid (77%, 2.08 g, 9.28 mmol, 1.1 eq) was added in portions over 15 min at 0 °C. The reaction was allowed to warm up and stirred overnight at room temperature. Upon completion, satd. sodium bicarbonate solution (20 mL) was added and the aqueous layer was extracted with dichloromethane (3×30 mL). The organic layer was dried over sodium sulfate and concentrated *in vacuo* to yield *N*-oxide **106**, which did not require further purification.

**TLC:**  $R_f = 0.11$  (50% EtOAc/hexanes) [UV/CAM].

**HRMS** (ESI) (C<sub>17</sub>H<sub>30</sub>NO<sub>4</sub>Si [M+H]<sup>+</sup>) calcd.: 340.1939  
found: 340.1940.



5-[[*tert*-Butyldimethylsilyl]oxy]methyl]-2,2-dimethyl-4*H*-[1,3]dioxino[4,5-*c*]pyridin-8-yl)methanol (**107**)<sup>[151,190,216]</sup>



Trifluoroacetic acid (2.31 mL, 3.48 g, 16.6 mmol, 2.0 eq) was added to a solution of crude *N*-oxide **106** (2.81 g, 8.28 mmol, 1.0 eq) in anhydrous dichloromethane (50 mL) *via* syringe at 0 °C in two batches. The ice bath was then removed and the reaction was stirred for 2 h. Anhydrous methanol (10 mL) was slowly added at 0 °C and the reaction was stirred for 20 min and subsequently allowed to warm to room temperature while stirring for another 20 min. The mixture was diluted with dichloromethane (150 mL) and extracted with satd. sodium bicarbonate solution (50 mL). The organic phase was dried over sodium sulfate, filtered and concentrated under reduced pressure. The crude product was purified by flash chromatography (EtOAc/hexanes, 20-60%) to yield the alcohol **107** (1.66 g, 4.89 mmol, 60%) as a yellow solid.

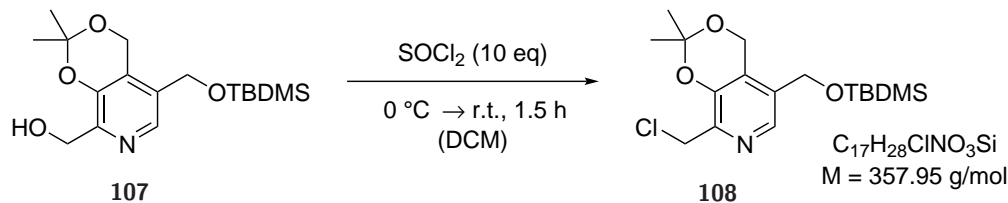
**TLC:**  $R_f = 0.57$  (50% EtOAc/hexanes) [UV/CAM].

**$^1H$ -NMR** (400 MHz,  $d^6$ -DMSO):  $\delta$ [ppm] = 8.04 (s, 1 H), 4.89 (s, 2 H), 4.82 (t, benzyl (chloro(phenoxy)phosphoryl)-L-alaninate 1 H), 4.67 (s, 2 H), 4.46 (d,  $^3J = 5.8$  Hz, 2 H), 1.48 (s, 6 H), 0.88 (s, 9 H), 0.07 (s, 6 H).

**$^{13}C$ -NMR** (100 MHz,  $d^6$ -DMSO):  $\delta$ [ppm] = 148.2, 145.2, 138.2, 131.3, 126.2, 100.0, 60.5, 59.6, 58.3, 26.2, 24.8, 18.3, -4.9.

**HRMS** (ESI) ( $C_{17}H_{30}NO_4Si$  [M+H]<sup>+</sup>) calcd.: 340.1939  
found: 340.1939.

5-[[*tert*-Butyldimethylsilyloxy]methyl]-8-(chloromethyl)-2,2-dimethyl-4*H*-[1,3]dioxino[4,5-*c*]pyridine (**108**)<sup>[151]</sup>



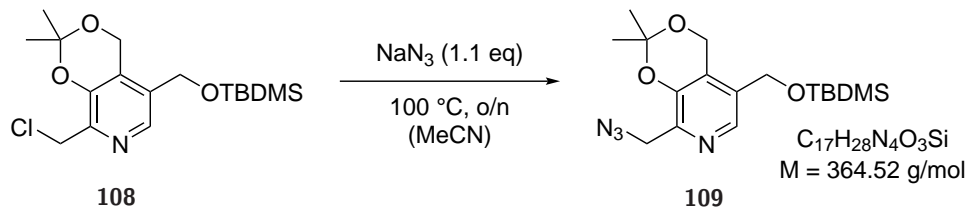
Alcohol **107** (1.66 g, 4.89 mmol, 1.0 eq) was dissolved in anhydrous dichloromethane (80 mL) and cooled to 0 °C prior to the slow addition of thionyl chloride (3.54 mL, 5.81 g, 48.8 mmol, 10 eq) *via* syringe over 30 min. The reaction was stirred for 20 min at 0 °C and additional 30 min at room temperature. After cooling the reaction to 0 °C, satd. sodium bicarbonate solution was added until the mixture was basic ( $\approx 100$  mL). The phases were separated and the organic layer was washed with satd. sodium bicarbonate and satd. sodium chloride solution (each 20 mL), dried over sodium sulfate and concentrated under reduced pressure to yield crude chloride **108** as a pale yellow oil, which was used directly in the next step without further purification.

**TLC:**  $R_f = 0.58$  (5% EtOAc/DCM) [UV/CAM].

**$^1\text{H-NMR}$**  (400 MHz,  $d^6$ -DMSO):  $\delta$ [ppm] = 8.09 (s, 1 H), 4.92 (s, 2 H), 4.70 (s, 1 H), 4.67 (s, 2 H), 1.52 (s, 6 H), 0.89 (s, 9 H), 0.09 (s, 6 H).

**$^{13}\text{C-NMR}$**  (100 MHz,  $d^6$ -DMSO):  $\delta$ [ppm] = 146.1, 143.7, 138.6, 133.2, 127.4, 100.6, 60.3, 58.3, 42.3, 26.3, 26.2, 24.9, 24.8, 18.3, 18.3, -2.7, -4.9.

**HRMS** (ESI) ( $\text{C}_{17}\text{H}_{29}\text{ClNO}_3\text{Si}$   $[\text{M}+\text{H}]^+$ ) calcd.: 358.1600  
 found: 358.1601.

**8-(Azidomethyl)-5-[[*tert*-butyldimethylsilyl]oxy]methyl]-2,2-dimethyl-4*H*-[1,3]dioxino[4,5-*c*]pyridine (**109**)<sup>[151]</sup>**

To a solution of crude chloride **108** (1.72 g, 4.80 mmol, 1.0 eq) in anhydrous acetonitrile (70 mL), sodium azide (343 mg, 5.28 mmol, 1.1 eq) was added and refluxed at 100 °C overnight. Upon completion, the reaction was washed with satd. sodium chloride solution (50 mL), dried over sodium sulfate and concentrated under reduced pressure. The crude product was purified by flash chromatography (EtOAc/hexanes, 20-70%) to yield azide **109** (1.17 g, 3.20 mmol, 66% over two steps) as a brown oil.

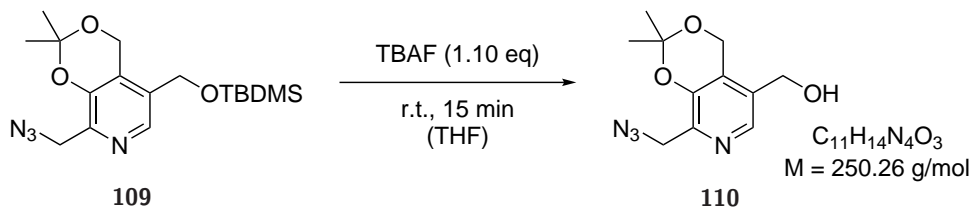
**TLC:**  $R_f = 0.60$  (5% EtOAc/DCM) [UV/CAM].

**<sup>1</sup>H-NMR** (400 MHz, CDCl<sub>3</sub>):  $\delta$ [ppm] = 8.07 (s, 1 H), 4.90 (s, 2 H), 4.62 (s, 2 H), 4.44 (s, 2 H), 1.58 (s, 6 H), 0.91 (s, 9 H), 0.09 (s, 6 H).

**<sup>13</sup>C-NMR** (100 MHz, CDCl<sub>3</sub>):  $\delta$ [ppm] = 146.4, 143.6, 138.7, 131.9, 126.9, 100.4, 60.9, 58.7, 50.7, 25.8, 24.7, 18.2, -5.4.

**HRMS** (ESI) (C<sub>17</sub>H<sub>29</sub>N<sub>4</sub>O<sub>3</sub>Si [M+H]<sup>+</sup>) calcd.: 365.2003  
found: 365.2006.

[8-(Azidomethyl)-2,2-dimethyl-4*H*-[1,3]dioxino[4,5-*c*]pyridin-5-yl] methanol (**110**)<sup>[340]</sup> -



Azide **109** (358 mg, 1.17 mmol, 1.0 eq) was dissolved in anhydrous tetrahydrofuran (20 mL) and tetrabutylammonium fluoride (1 M, 1.17 mL, 1.17 mmol, 1.0 eq) was added slowly. After stirring for 15 min solvent was evaporated under reduced pressure and the crude product was purified by flash chromatography (MeOH/DCM, 5-10%) to yield alcohol **110** (204 mg, 815  $\mu\text{mol}$ , 71%) as a pale pink oil.

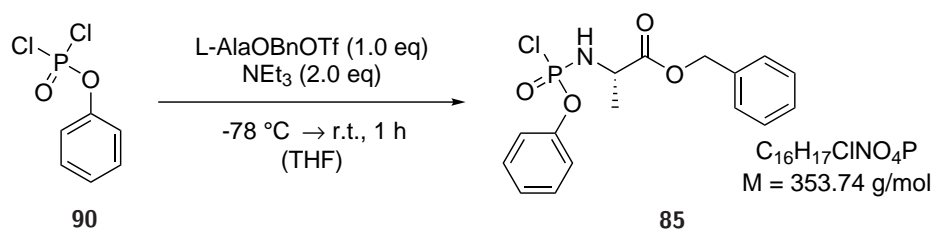
**TLC:**  $R_f = 0.49$  (10% MeOH/DCM) [UV/CAM].

**$^1\text{H-NMR}$**  (400 MHz,  $\text{CDCl}_3$ ):  $\delta[\text{ppm}] = 8.06$  (s, 1 H), 4.99 (s, 2 H), 4.65 (s, 2 H), 4.46 (s, 2 H), 3.13 (s, 1 H), 1.60 (s, 6 H).

**$^{13}\text{C-NMR}$**  (100 MHz,  $\text{CDCl}_3$ ):  $\delta[\text{ppm}] = 146.7, 143.7, 138.7, 131.9, 127.7, 100.8, 60.2, 58.6, 50.5, 24.7$ .

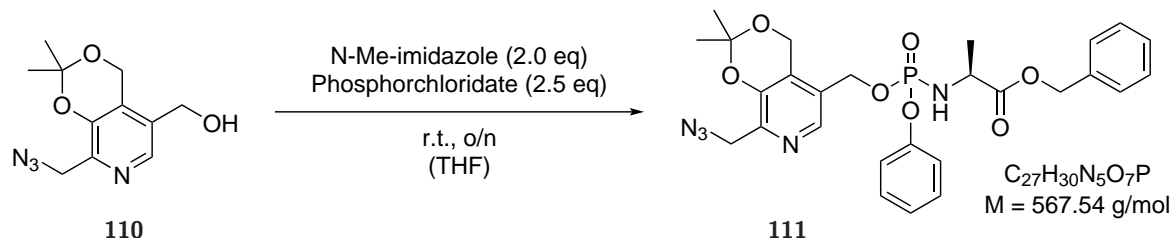
**HRMS** (ESI) ( $\text{C}_{11}\text{H}_{15}\text{N}_4\text{O}_3$   $[\text{M}+\text{H}]^+$ ) calcd.: 251.1139

found: 251.1138.

Benzyl [chloro(phenoxy)phosphoryl]-L-alaninate (**185**)<sup>[341]</sup>

To a flame dried two-necked flask containing anhydrous dichloromethane (16 mL), phenyl-dichlorophosphate (493  $\mu$ L, 696 mg, 3.30 mmol, 1.0 eq) and *O*-benzyl-L-alaninetoluol-*p*-sulfonate (1.16 g, 3.30 mmol, 1.0 eq) at  $-78^\circ\text{C}$ , triethylamine (915  $\mu$ L, 668 mg, 6.60 mmol, 2.0 eq) was slowly added. The reaction was stirred for 30 min at  $-78^\circ\text{C}$  and then allowed to warm up to room temperature, where it was stirred for another 30 min. After removal of the solvent *in situ* formed phosphorochloridate **85** was used directly in the next step.

Benzyl {[8-(azidomethyl)-2,2-dimethyl-4*H*-[1,3]dioxino[4,5-*c*]pyridin-5-yl]methoxy}(phenoxy)phosphoryl-L-alaninate (**111**)<sup>[341]</sup>



To a dry flask containing alcohol **110** (200 mg, 799  $\mu\text{mol}$ , 1.0 eq) in anhydrous tetrahydrofuran (10 mL) was added *N*-methyl imidazole (129  $\mu\text{L}$ , 131 mg, 1.60 mmol, 2.0 eq). Then, reactive chlorophosphate **85** ( $\approx 2.00$  mmol, 2.5 eq) dissolved in anhydrous tetrahydrofuran (10 mL) was slowly added and the mixture was stirred at room temperature overnight. Upon completion, the reaction was quenched by adding satd. ammonium chloride solution (20 mL) and extracted with ethylacetate (3  $\times$  30 mL). The combined organic phase was dried over sodium sulfate, filtrated and concentrated *in vacuo*. The crude product was purified by flash chromatography (MeOH/DCM, 2-6%) to yield protected phosphoramidate **111** (361 mg, 631  $\mu\text{mol}$ , 80%) as a colorless, viscous oil.

**TLC:**  $R_f = 0.49$  (10% MeOH/DCM) [UV/CAM].

**<sup>1</sup>H-NMR** (400 MHz,  $\text{CDCl}_3$ ):  $\delta$ [ppm] = 7.98 (s, 1 H), 7.34-7.27 (m, 7 H), 7.18-7.14 (m, 3 H), 5.15-5.06 (m, 2 H), 4.99-4.97 (m, 2 H), 4.83-4.69 (m, 2 H), 4.12-3.97 (m, 1 H), 3.68-3.60 (m, 1 H), 2.42 (s, 3 H), 1.52-1.49 (m, 6 H), 1.37 (d,  $^3J = 10.4$  Hz, 3 H).

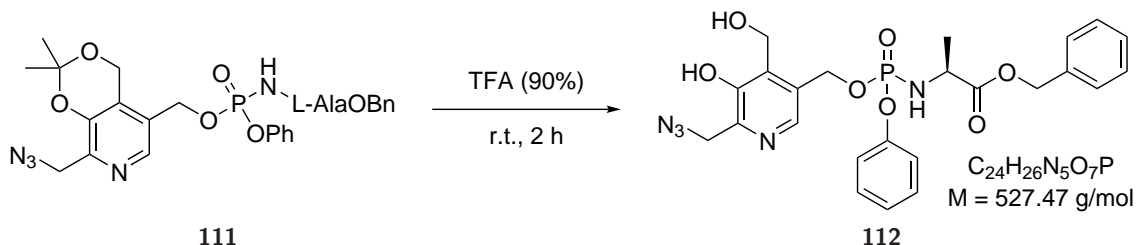
**<sup>13</sup>C-NMR** (100 MHz,  $\text{CDCl}_3$ ):  $\delta$ [ppm] = 173.2, 150.6, 148.8, 146.2, 139.3, 135.2, 129.7, 128.6, 128.5, 128.2, 125.1, 120.2, 100.1, 67.3, 63.6, 58.3, 50.4, 50.3, 25.0, 24.5, 20.9, 18.3.

**<sup>31</sup>P-NMR** (160 MHz,  $\text{CDCl}_3$ ):  $\delta$ [ppm] = 2.33.

**HRMS** (ESI) ( $\text{C}_{27}\text{H}_{31}\text{N}_5\text{O}_7\text{P}$  [M+H]<sup>+</sup>) calcd.: 568.1956

found: 568.1954.

Benzyl {[6-(azidomethyl)-5-hydroxy-4-(hydroxymethyl)pyridin-3-yl]-methoxy}(phenoxy)phosphoryl-L-alaninate (**112**)<sup>[232]</sup>



Acetal **111** (349 mg, 645  $\mu$ mol, 1.0 eq) was dissolved in aqueous trifluoroacetic acid (90%, 7.5 mL) and stirred at room temperature for 2 h. Upon completion, the reaction was quenched by adding methanol (20 mL) which was subsequently removed azeotropically together with trifluoroacetic acid under reduced pressure. The crude product was purified by flash chromatography (MeOH/DCM, 2-10%) to yield the diol **112** (148 mg, 281  $\mu$ mol, 46%) as a clear, viscous oil.

**TLC:**  $R_f$  = 0.11 (5% MeOH/DCM) [UV/CAM].

**$^1H$ -NMR** (400 MHz,  $CDCl_3$ ):  $\delta$ [ppm] = 8.03 (s, 1 H), 7.33-7.28 (m, 7 H), 7.18-7.08 (m, 3 H), 5.14-4.85 (m, 7 H), 4.53 (s, 2 H), 4.06-3.94 (m, 2 H), 1.38-1.32 (m, 3 H).

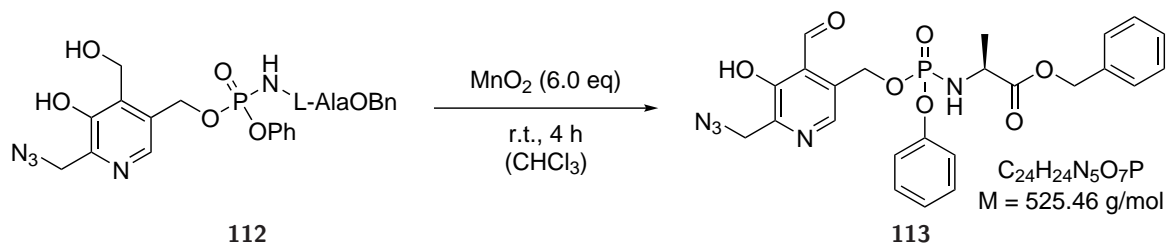
**$^{13}C$ -NMR** (100 MHz,  $CDCl_3$ ):  $\delta$ [ppm] = 173.6, 151.1, 150.2, 144.9, 140.6, 136.4, 133.9, 130.9, 130.0, 128.9, 128.5, 128.3, 125.1, 120.6, 66.5, 63.6, 56.4, 50.8, 50.4, 20.1.

**$^{31}P$ -NMR** (160 MHz,  $CDCl_3$ ):  $\delta$ [ppm] = 2.06.

**HRMS** (ESI) ( $C_{24}H_{27}N_5O_7P$   $[M+H]^+$ ) calcd.: 528.1643

found: 528.1639.

Benzyl {[6-(azidomethyl)-4-formyl-5-hydroxypyridin-3-yl]methoxy}-  
(phenoxy)phosphoryl-L-alaninate (**113**)



To a solution of diol **112** (45.0 mg, 85.3  $\mu$ mol, 1.0 eq) in anhydrous chloroform (5 mL) was added manganese(IV)-oxide (44.5 mg, 512  $\mu$ mol, 6.0 eq) and further 4 equivalents every hour (133 mg, 1.54 mmol, 18 eq in total). Upon completion, the suspension was filtered, the residue washed with chloroform and the filtrate was then concentrated under reduced pressure. The crude product was purified by HPLC using method D ( $t_R = 5.5$  min) and lyophilised to generate final probe **PL3PA** (**113**) (23.5 mg, 44.7  $\mu$ mol, 52%) as a pale brown, viscous oil.

**TLC:**  $R_f = 0.78$  (10% MeOH/DCM) [UV/CAM].

**HPLC:**  $t_R = 5.5$  min (method D).

**$^1H$ -NMR** (400 MHz,  $CDCl_3$ ):  $\delta$ [ppm] = 11.50 (br s, 1 H), 10.28 (s, 1 H), 8.19 (s, 1 H), 7.37-7.28 (m, 7 H), 7.17-7.09 (m, 3 H), 5.40-5.24 (m, 2 H), 5.16-5.08 (m, 2 H), 4.54 (s, 2 H), 4.11-3.99 (m, 1 H), 3.88-3.67 (m, 1 H), 1.38 (d,  $^3J = 7.1$  Hz, 3 H).

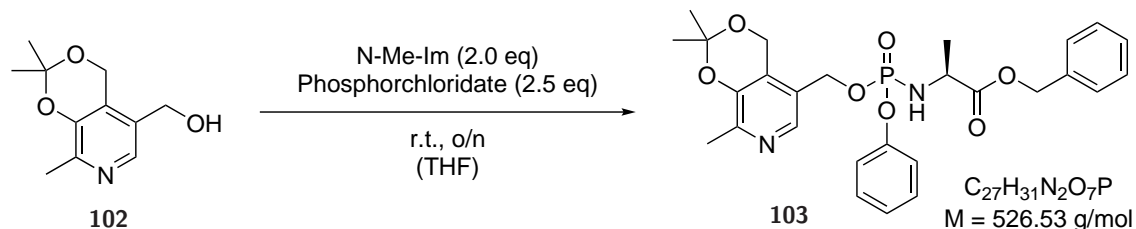
**$^{13}C$ -NMR** (100 MHz,  $CDCl_3$ ):  $\delta$ [ppm] = 196.1, 173.4, 153.7, 150.3, 149.7, 140.7, 135.2, 129.9, 128.8, 128.7, 128.4, 125.5, 121.1, 120.3, 67.6, 62.9, 62.1, 50.6, 50.4, 21.0.

**$^{31}P$ -NMR** (160 MHz,  $CDCl_3$ ):  $\delta$ [ppm] = 2.34.

**HRMS** (ESI) ( $C_{24}H_{25}N_5O_7P$  [ $M+H$ ] $^+$ ) calcd.: 526.1486  
found: 526.1482.



Benzyl {phenoxy[(2,2,8-trimethyl-4*H*-[1,3]dioxino[4,5-*c*]pyridin-5-yl)-methoxy]phosphoryl}-*L*-alaninate (**103**)<sup>[341]</sup>



To a dry flask containing alcohol **102** (314 mg, 1.50 mmol, 1.0 eq) in anhydrous tetrahydrofuran (12 mL) was added *N*-methyl imidazole (241  $\mu\text{L}$ , 246 mg, 3.00 mmol, 2.0 eq). Then, reactive chlorophosphate **85** ( $\approx 4.00$  mmol, 2.5 eq) dissolved in anhydrous tetrahydrofuran (12 mL) was slowly added and the mixture was stirred at room temperature overnight. Upon completion, the reaction was quenched by adding satd. ammonium chloride solution (20 mL) and extracted with ethylacetate ( $3 \times 40$  mL). The combined organic phase was dried over sodium sulfate, filtrated and concentrated *in vacuo*. The crude product was purified by flash chromatography (MeOH/DCM, 2-6%) to yield protected phosphoramidate **111** (621 mg, 1.18 mmol, 79%) as a colorless, viscous oil.

**TLC:**  $R_f = 0.53$  (10% MeOH/DCM) [UV/CAM].

**$^1\text{H-NMR}$**  (400 MHz,  $d^6$ -DMSO):  $\delta[\text{ppm}] = 7.96$  (s, 1 H), 7.36-7.28 (m, 7 H), 7.20-7.10 (m, 3 H), 6.23-6.08 (m, 1 H), 5.14-5.04 (m, 2 H), 5.03-4.92 (m, 2 H), 4.89-4.74 (m, 2 H), 3.98-3.87 (m, 1 H), 2.29 (s, 3 H), 1.52-1.40 (m, 6 H), 1.25 (t,  $^3J = 7.5$  Hz, 3 H).

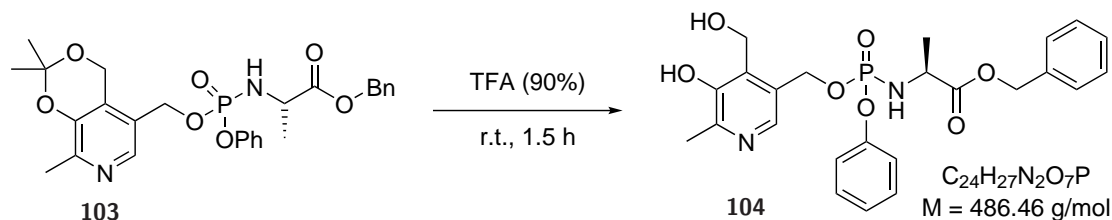
**$^{13}\text{C-NMR}$**  (100 MHz,  $d^6$ -DMSO):  $\delta[\text{ppm}] = 173.1, 150.7, 147.2, 145.2, 139.6, 135.9, 129.6, 128.4, 128.0, 127.8, 125.9, 123.8, 120.2, 99.6, 66.0, 62.8, 57.7, 50.0, 48.6, 26.6, 19.6, 18.3$ .

**$^{31}\text{P-NMR}$**  (160 MHz,  $d^6$ -DMSO):  $\delta[\text{ppm}] = 3.67$ .

**HRMS** (ESI) ( $\text{C}_{27}\text{H}_{32}\text{N}_2\text{O}_7\text{P}$   $[\text{M}+\text{H}]^+$ ) calcd.: 527.1942

found: 527.1942.

Benzyl {[5-hydroxy-4-(hydroxymethyl)-6-methylpyridin-3-yl]methoxy}-  
(phenoxy)phosphoryl-L-alaninate (**104**)<sup>[232]</sup>



Acetal **103** (621 mg, 1.18 mmol, 1.0 eq) was dissolved in aqueous trifluoroacetic acid (90%, 10 mL) and stirred at room temperature for 1.5 h. Upon completion, the reaction was quenched by adding methanol (20 mL) at 0 °C which was subsequently removed azeotropically together with trifluoroacetic acid under reduced pressure. The crude product was purified by flash chromatography (MeOH/DCM, 5-10%) to yield diol **104** (554 mg, 1.38 mmol, 97%) as a clear, viscous oil.

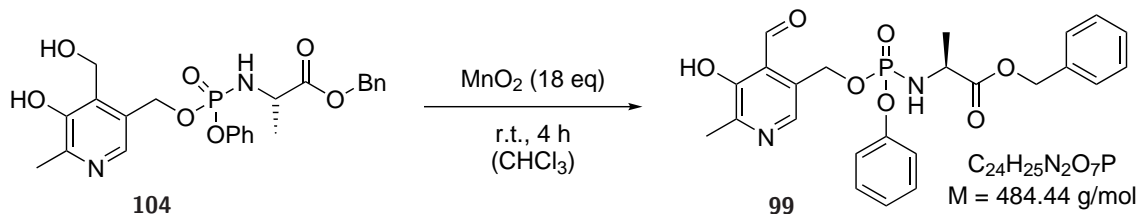
**TLC:**  $R_f = 0.48$  (10% MeOH/DCM) [UV/CAM].

**<sup>1</sup>H-NMR** (400 MHz,  $d^6$ -DMSO):  $\delta$ [ppm] = 9.26 (br s, 1 H), 7.90 (s, 1 H), 7.39-7.26 (m, 7 H), 6.19-6.06 (m, 3 H), 5.76 (br s, 1 H), 5.13-4.99 (m, 4 H), 4.69 (s, 2 H), 3.97-3.84 (m, 1 H), 2.35 (s, 3 H), 1.26-1.18 (m, 3 H).

**<sup>13</sup>C-NMR** (100 MHz,  $d^6$ -DMSO):  $\delta$ [ppm] = 173.1, 150.9, 149.5, 147.5, 139.8, 139.7, 135.9, 131.9, 129.6, 128.4, 128.0, 127.8, 124.5, 120.2, 65.1, 63.3, 56.0, 49.9, 48.5, 19.5.

**<sup>31</sup>P-NMR** (160 MHz,  $d^6$ -DMSO):  $\delta$ [ppm] = 3.58.

**HRMS** (ESI) ( $\text{C}_{24}\text{H}_{28}\text{N}_2\text{O}_7\text{P}$   $[\text{M}+\text{H}]^+$ ) calcd.: 487.1629  
found: 487.1628.

Benzyl {[[(4-formyl-5-hydroxy-6-methylpyridin-3-yl)methoxy](phenoxy)}-phosphoryl-L-alaninate (**99**)

To a solution of diol **104** (58.0 mg, 119  $\mu$ mol, 1.0 eq) in anhydrous chloroform (10 mL) was added manganese(IV)-oxide (62.0 mg, 715  $\mu$ mol, 6.0 eq) and further 4 equivalents every hour (186 mg, 2.14 mmol, 18 eq in total). Upon completion, the suspension was filtered, the residue washed with chloroform and the filtrate was then concentrated under reduced pressure. The crude product was purified by HPLC using method D ( $t_R$  = 5.8 min) and lyophilised to generate final probe **PLPA** (**99**) (42.6 mg, 87.9  $\mu$ mol, 74%) as a pale brown, viscous oil.

**TLC:**  $R_f$  = 0.78 (10% MeOH/DCM) [UV/CAM].

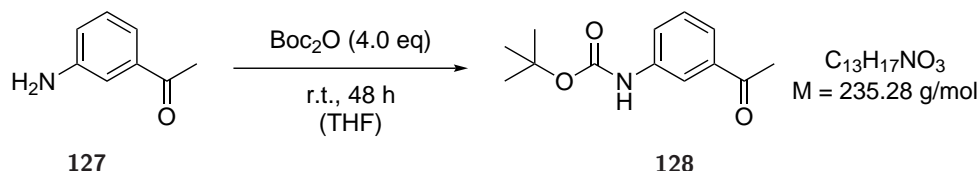
**HPLC:**  $t_R$  = 5.8 min (method D).

**$^1H$ -NMR** (400 MHz,  $d^6$ -DMSO):  $\delta$ [ppm] = 11.93 (br s, 1 H), 10.36 (s, 1 H), 8.12 (s, 1 H), 7.40-7.26 (m, 7 H), 7.21-7.10 (m, 3 H), 6.29-6.14 (m, 1 H), 5.46-5.28 (m, 2 H), 5.14-5.00 (m, 2 H), 4.03-3.86 (m, 1 H), 2.48-2.40 (m, 3 H), 1.31-1.20 (m, 3 H).

**$^{31}P$ -NMR** (160 MHz,  $d^6$ -DMSO):  $\delta$ [ppm] = 3.74.

**HRMS** (ESI) ( $C_{24}H_{26}N_2O_7P$  [M+H] $^+$ ) calcd.: 485.1473

found: 485.1473.

**4.1.2.13** Synthesis of the MAC173979 Amine*tert*-Butyl (3-acetylphenyl)carbamate (**128**)<sup>[311]</sup>

To a solution of *m*-aminoacetophenone **127** (1.35 g, 10.0 mmol, 1.0 eq) in anhydrous tetrahydrofuran (15 mL) was added di-*tert*-butyl dicarbonate (8.72 g, 40.0 mmol, 4.0 eq) and the reaction was stirred for 48 h. Upon completion, the mixture was concentrated under reduced pressure and the residue was extracted with ethyl acetate and water. Organic layers were then washed with satd. sodium chloride solution and dried over sodium sulfate. The crude product was purified by flash chromatography (EtOAc/hexanes, 20%) to yield **128** (2.23 g, 9.48 mmol, 95%) as a white solid.

**TLC:**  $R_f = 0.45$  (20% EtOAc/hexanes) [UV].

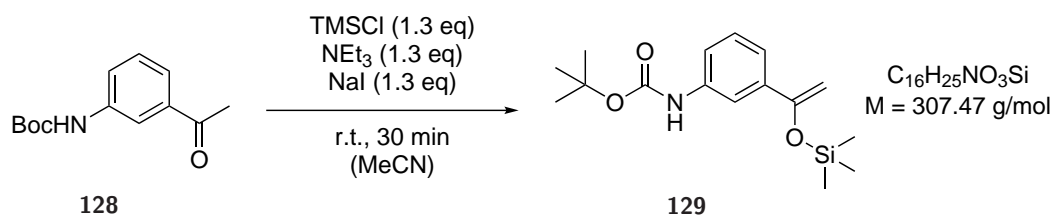
**<sup>1</sup>H-NMR** (400 MHz, CDCl<sub>3</sub>):  $\delta$ [ppm] = 7.95-7.89 (m, 1 H), 7.67-7.58 (m, 2 H), 7.38 (t,  $^3J = 7.9 \text{ Hz}$ , 1 H), 6.67 (s, 1 H), 2.59 (s, 3 H), 1.53 (s, 9 H).

**<sup>13</sup>C-NMR** (100 MHz, CDCl<sub>3</sub>):  $\delta$ [ppm] = 198.1, 152.8, 139.0, 138.0, 129.4, 123.1, 123.0, 118.2, 81.1, 28.5, 26.9.

**HRMS** (ESI) ( $\text{C}_{13}\text{H}_{18}\text{NO}_3$  [M+H]<sup>+</sup>) calcd.: 236.1282

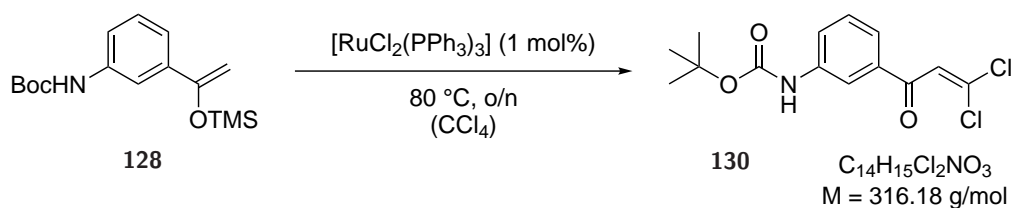
found: 236.1282.

The analytical data are in accordance with previous literature reports.<sup>[311]</sup>

*tert*-Butyl {3-[1-(trimethylsilyl)oxy]vinyl}phenylcarbamate (**129**)<sup>[295]</sup>

Compound **128** (2.23 g, 9.48 mmol, 1.0 eq), trimethylsilyl chloride (1.50 mL, 1.29 g, 11.9 mmol, 1.3 eq), and triethylamine (1.64 mL, 1.20 g, 11.9 mmol, 1.3 eq) were added to a flame dried flask. The mixture was stirred at room temperature and a solution of sodium iodide (1.78 g, 11.9 mmol, 1.3 eq) in acetonitrile (12 mL, 1.0 M) was added dropwise. After stirring the reaction for 30 min, it was cooled to 0 °C and hexanes (6 mL) was added. After adding water (6 mL) the phases were separated, and the aqueous layer was extracted with hexanes (2×6 mL). The combined organic phases were washed with water (2×6 mL), dried over sodium sulfate and concentrated under reduced pressure. The intermediate trimethylsilyl enol ether **129** (2.77 g, 8.96 mmol, 95%) was obtained and was used without further purification.

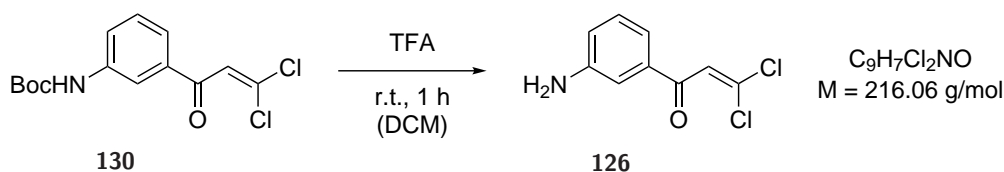
**HRMS** (ESI) (C<sub>16</sub>H<sub>26</sub>NO<sub>3</sub>Si [M+H]<sup>+</sup>) calcd.: 308.1677  
found: 308.1674.

*tert*-Butyl [3-(3,3-dichloroacryloyl)phenyl]carbamate (**130**)<sup>[295]</sup>

Carbon tetrachloride (3.11 mL, 32.3 mmol, 3.6 eq) was added to a flame-dried pressure tube, and the vessel was sealed with a silicon septum. The solvent was frozen at  $-78^\circ\text{C}$  and vacuum was applied to 0.3 mbar. The solvent was then allowed to thaw under vacuum before the vessel was filled with argon. This freeze-pump thaw process was repeated twice. Ruthenium(II)-tris-triphenylphosphine dichloride (86.0 mg, 896  $\mu\text{mol}$ , 1 mol%) and crude trimethylsilyl enol ether **129** (2.77 g, 8.96 mmol, 1.0 eq) were added. The vessel was sealed and heated at  $80^\circ\text{C}$  for 17 h while stirring. Upon completion, the reaction was cooled down and directly purified by column chromatography (EtOAc/hexanes, 3-15%) to yield dichlorovinyl **130** (1.41 g, 4.46 mmol, 50%) as a white powder.

**TLC:**  $R_f = 0.36$  (10% EtOAc/hexanes) [UV].

**HRMS** (ESI) ( $\text{C}_{14}\text{H}_{16}\text{Cl}_2\text{NO}_3$   $[\text{M}+\text{H}]^+$ ) calcd.: 316.0502  
found: 316.0503.

1-(3-Aminophenyl)-3,3-dichloroprop-2-en-1-one (**126**)<sup>[311]</sup>

Boc-protected amine **130** (700 mg, 2.21 mmol, 1.0 eq) was dissolved in dichloromethane (15 mL) and trifluoroacetic acid (6 mL) was added. After stirring the reaction for 1 h at room temperature, dichloromethane (30 mL) was added and the solution was washed with satd. sodium bicarbonate solution (30 mL). After separation, the organic phase was dried over sodium sulfate and solvents were removed *in vacuo*. The crude product was purified by HPLC using method E ( $t_R = 4.5$  min) and lyophilised to generate final MAC173979 amine (**126**) (21.1 mg, 9.77  $\mu$ mol, 5%) as a brown oil.

**HPLC:**  $t_R = 4.5$  min (method E).

**<sup>1</sup>H-NMR** (400 MHz, CD<sub>3</sub>CN):  $\delta$ [ppm] = 7.40 (s, 1 H), 7.29-7.24 (m, 3 H), 7.00-6.95 (m, 1 H).

**<sup>13</sup>C-NMR** (100 MHz, CD<sub>3</sub>CN):  $\delta$ [ppm] = 186.8, 154.8, 137.8, 129.7, 125.5, 120.7, 118.6, 114.8, 114.4.

**HRMS** (ESI) (C<sub>9</sub>H<sub>8</sub>Cl<sub>2</sub>NO [M+H]<sup>+</sup>) calcd.: 215.9978  
found: 215.9978.

## 4.2 Biochemistry

### 4.2.1 Culture Media

**Table 4.2:** List of used buffers and media.

Buffer/Medium	Ingredients
LB-medium	Peptone (10 g), NaCl (5 g), yeast extract (5 g) in 1 L ddH <sub>2</sub> O, pH = 7.5
B-medium	Peptone (10 g), NaCl (5 g), yeast extract (5 g), K <sub>2</sub> PO <sub>4</sub> (1 g) in 1 L ddH <sub>2</sub> O, pH = 7.5
CDM <sub>SA</sub>	Adapted from <sup>[342]</sup>
CDM <sub>EC</sub>	Adapted from <sup>[247]</sup>
CDM <sub>PA</sub>	Adapted from <sup>[343]</sup>

### 4.2.2 Cloning and Expression of Proteins

#### 4.2.2.1 PCR and Gene Purification

*S. aureus*, *E. coli* and *P. aeruginosa* genes were amplified by polymerase chain reaction (PCR) according to table 4.3 and table 4.4. Primers and their annealing temperatures are given in table 4.5. After verification of the reactions by an 1% agarose gel, PCR products were purified using a E.Z.N.A.<sup>®</sup> MicroElute Cycle Pure Kit (*Omega*) according to the manufacturers protocol.



**Table 4.3:** PCR conditions.

Buffer/Medium	Ingredients
Forward primer (10 $\mu$ M)	2.5 $\mu$ L
Reverse primer (10 $\mu$ M)	2.5 $\mu$ L
dNTPs (10 mM)	1 $\mu$ L
Genomic DNA (150 $\frac{ng}{\mu L}$ )	1 $\mu$ L
5 $\times$ Phusion HF buffer	10 $\mu$ L
DMSO	(1.5 $\mu$ L if necessary)
ddH <sub>2</sub> O	fill up to 50 $\mu$ L

**Table 4.4:** Thermocyclic conditions.

Step	Temperature [ $^{\circ}$ C]	Time [s]	Cycles
Initial denaturation	98	30	1
Denaturation	98	10	35
Annealing	see table 4.5	30	
Extension	72	30	
Final extension	72	10 min	1
Hold	4	$\infty$	

Table 4.5: Primer list.

Primer	Gene	Organism	Sequence	Annealing Temp. [°C]	Company
Gateway pdxK fwd	<i>pdxK</i>	<i>E. coli</i>	ggggacaagttgtacaaaaaagcaggcttt AGTAGTTTGTGTT GTTTAACGATAAG	61	<i>Eurofins</i>
Gateway pdxK rev			ggggaccactttgtacaagaaagctgggtg TTATGCTTCCGCCAGCG		
Gateway ydcR fwd	<i>ydcR</i>	<i>E. coli</i>	ggggacaagttgtacaaaaaagcaggcttt AAAAAATACCAGCAGCTTGC	60	<i>Eurofins</i>
Gateway ydcR rev			ggggaccactttgtacaagaaagctgggtg TTACAGCCGTTCTTGAATAAG		
Gateway yjiR fwd	<i>yjiR</i>	<i>E. coli</i>	ggggacaagttgtacaaaaaagcaggcttt TACGCGTTATCAACATCTGG	59	<i>Eurofins</i>
Gateway yjiR rev			ggggaccactttgtacaagaaagctgggtg TTATTCCATTGCCGATACAC		
SLIM MBP tailed			GCCCTGAAAAT AAAGATTCTCGCC AGAAGTCTGCGGTCTTTCAG	68	<i>Sigma Aldrich</i>
SLIM MBP short			AGTCTGCGGTCTTTCAGGGCTTC		
SLIM ydcR tailed	<i>ydcR</i>	<i>E. coli</i>	TCTGGCGAGAATCT TTATTTTCAGGG CAAAAAATACCAGCAGCTTGC	68	<i>Sigma Aldrich</i>
SLIM ydcR short			AAAAAATACCAGCAGCTTGC		
PR <sub>ydcR-ydcS</sub> fwd	<i>ydcR-ydcS</i> intergenic region	<i>E. coli</i>	[TAMRA] TAGCGTTTAATTTAATTCCTCTTAG	59	<i>Sigma Aldrich</i>
PR <sub>ydcR-ydcS</sub> rev			[TAMRA] TAAGGTCTTACTCCTGTCTG		

Primer	Gene	Organism	Sequence	Annealing Temp. [°C]	Company
PR <sub>ydcR</sub> fwd	<i>ydcR</i> promotor region	<i>E. coli</i>	[TAMRA] GGCGCTTGGCAAAGAGTTATC	59	<i>Sigma Aldrich</i>
PR <sub>ydcR</sub> rev			[TAMRA] GCAACGAAGGCAAACGATCG		
Gateway iscS fwd	<i>iscS</i>	<i>E. coli</i>	ggggacaagtttgtaaaaaagcaggcttt AAATTACCGATTTATCTCGACTACTC	61	<i>Sigma Aldrich</i>
Gateway iscS rev			ggggaccactttgtacaagaagctgggtg TTAATGATGAGCCCATTCGATG		
Gateway iscU fwd	<i>iscU</i>	<i>E. coli</i>	ggggacaagtttgtaaaaaagcaggcttt GCTTACAGCGAAAAAGTTATC	59	<i>Sigma Aldrich</i>
Gateway iscU rev			ggggaccactttgtacaagaagctgggtg TTATTTTGCTTCACGTTTGC		
Gateway pabC fwd	<i>pabC</i>	<i>E. coli</i>	ggggacaagtttgtaaaaaagcaggcttt TTCTTAATTAACGGTCATAAGCAGG	61	<i>Sigma Aldrich</i>
Gateway pabC rev			ggggaccactttgtacaagaagctgggtg CTAATTCGGGCGCTCAC		

Primer	Gene	Organism	Sequence	Annealing Temp. [°C]	Company
Gateway A0A0H2XHJ5 fwd	<i>A0A0H2XHJ5</i>	<i>S. aureus</i>	ggggacaagtttgtaaaaaagcaggcttt GCCGAACACTCATTTGAC	61	<i>Sigma Aldrich</i>
Gateway A0A0H2XHJ5 rev			ggggaccactttgtacaagaaagctgggtg TTAAAATTCATAAGAGAAAACTCCTTC		
Gateway sufU fwd	<i>sufU</i>	<i>S. aureus</i>	ggggacaagtttgtaaaaaagcaggcttt AATTTTAATAATCTAGA TCAATTATATAGATCTG	59	<i>Sigma Aldrich</i>
Gateway sufU rev			ggggaccactttgtacaagaaagctgggtg CTATTCTTCTTCAGTCGTACC		
Gateway A0A0H2XII6 fwd	<i>A0A0H2XII6</i>	<i>S. aureus</i>	ggggacaagtttgtaaaaaagcaggcttt AAGCAACCTATTTT AAATAAATTAGAAAG	55	<i>Sigma Aldrich</i>
Gateway A0A0H2XII6 rev			ggggaccactttgtacaagaaagctgggtg TTATTCATCCTCAACT AAAATTTTATTATTTT		
Gateway PA2683 fwd	<i>PA2683</i>	<i>P. aeruginosa</i>	ggggacaagtttgtaaaaaagcaggcttt CACGACCTGCCTACCTACGACG	68	<i>Sigma Aldrich</i>
Gateway PA2683 rev			ggggaccactttgtacaagaaagctgggtg CTAGCCGCCGAGCAAGGC		
Gateway PA3659 fwd	<i>PA3659</i>	<i>P. aeruginosa</i>	ggggacaagtttgtaaaaaagcaggcttt AATACCGCACTCGACAACCTGC	68	<i>Sigma Aldrich</i>
Gateway PA3659 rev			ggggaccactttgtacaagaaagctgggtg TCAGCGCGCCGCAG		
Gateway PA3798 fwd	<i>PA3798</i>	<i>P. aeruginosa</i>	ggggacaagtttgtaaaaaagcaggcttt ATTCAGAGCAAGCTGCCGAATG	66	<i>Sigma Aldrich</i>
Gateway PA3798 rev			ggggaccactttgtacaagaaagctgggtg TCAGATCGCGCATAGCTTTTCC		

#### 4.2.2.2 Gateway Cloning

Cloning was performed using the *Invitrogen* Gateway<sup>®</sup> cloning system with pDONR<sup>™</sup>201<sub>Kan</sub> (*Invitrogen*) or pDONR<sup>™</sup>207<sub>Gen</sub> (*Invitrogen*) as the donor vectors and pET-55-DEST<sup>™</sup><sub>Amp</sub> (*Invitrogen*), pETG-41K<sub>Kan</sub> (*EMBL*) or pDEST007<sub>Amp</sub> (custom made) as the destination vectors. Protocols were adopted from *Invitrogen*<sup>[344]</sup>. Expression vectors were transformed into *E. coli* BL21 (DE3).

#### 4.2.2.3 Site-directed and Ligation Independent Mutagenesis (SLIM)

SLIM was chosen to introduce a TEV (Tobacco Etch Virus) protease cleavage site between the maltose binding protein (MBP) and the protein *ydcR*. For this, two PCR reactions were performed: one with a tailed MBP primer (SLIM MBP tailed) and the short one for *ydcR* (SLIM *ydcR* short) and one PCR with the short MBP primer (SLIM MBP short) and the long one for *ydcR* (SLIM *ydcR* tailed). PCR reactions were conducted as discussed before with additional DMSO (3%), an annealing temperature of 68 °C and an elongated extension time of 2.5 min. PCR products were verified by 1% agarose gels and sequencing (*Genewiz*) and purified as described in section 4.2.2.1. The destination vector was digested with 1  $\mu$ L Dpn I in 5  $\mu$ L of CutSmart<sup>®</sup> buffer (*NEB*) at 37 °C for 1 h. Then, complementary TEV sites were hybridized by taking 20  $\mu$ L of the respective two PCR fragments and 10  $\mu$ L of H buffer (750 mM NaCl, 125 mM TRIS, 100 mM EDTA, pH = 9.0). The reaction was conducted at 99 °C for 3 min and two cycles at 65 °C for 5 min, followed by 30 °C for 40 min. The final vector was transformed into *E. coli* BL21 (DE3).

#### 4.2.2.4 Protein Overexpression

LB-media containing 0.1 mg/mL ampicillin (100 mg/mL stock in ethanol/ddH<sub>2</sub>O = 1/1) or 25  $\mu$ g/mL kanamycin (25 mg/mL stock in ddH<sub>2</sub>O) was inoculated with 1:100 overnight culture of the corresponding vector containing *E. coli* BL21 (DE3) strain. After growth at 37 °C to an OD<sub>600</sub> of 0.5-0.6, 1 mM *iso*-propyl-1-thio-galactopyranoside (IPTG, 1 M stock in ddH<sub>2</sub>O) except otherwise stated for pET-55-DEST<sup>™</sup><sub>Amp</sub> and pETG-41K<sub>Kan</sub> or 2  $\mu$ g/mL anhydrotetracycline (aTet, 2 mg/mL stock in ddH<sub>2</sub>O) for pDEST007<sub>Amp</sub> were added and the protein expression was carried out at the temperature corresponding to table 4.6. Bacteria were then harvested (6000 rpm, 10 min, 4 °C, rotor SLA-3000; Sorvall RC 6+, *Thermo Scientific*) and washed with 30 mL PBS once prior to cell lysis and protein purification.

**Table 4.6:** Proteinexpression conditions.

Protein Name	Gene Name	Uniprot ID	Overexpression	MW [Da]	Tags
Pyridoxine/pyridoxal/pyridoxamine kinase	<i>pdxK</i>	P40191	18 °C, o/n	33,137.0	N-STREP-II
Uncharacterized HTH-type transcriptional regulator	<i>ydcR</i>	P77730	18 °C, o/n 0.25 mM IPTG	95,690.5	ydcR-TEV-MBP-C-His
Uncharacterized HTH-type transcriptional regulator	<i>yjiR</i>	P39389	18 °C, o/n 0.25 mM IPTG	95,942.0	yjiR-MBP-C-His
Cysteine desulfurase	<i>iscS</i>	P0A6B7	18 °C, o/n	47,422.5	N-STREP-II
Iron-sulfur cluster assembly scaffold protein	<i>iscU</i>	P0ACD4	18 °C, o/n 2 µg/mL aTet	16,126.0	N-STREP-II
Aminodeoxychorismate lyase	<i>pabC</i>	P28305	18 °C, o/n	32,005.0	N-STREP-II
Probable cysteine desulfurase	<i>sufS</i>	A0A0H2XHJ5	18 °C, o/n	48,565.0	N-STREP-II
NifU family SUF system FeS assembly protein	<i>SAUSA300_0821</i>	A0A0H2XJC0	18 °C, o/n 2 µg/mL aTet	19,294.5	N-STREP-II
Orn/Lys/Arg decarboxylase	<i>SAUSA300_0458</i>	A0A0H2XII6	18 °C, o/n	53,370.5	N-STREP-II
Probable serine/threonine dehydratase, degradative	<i>PA2683</i>	Q9I0F5	18 °C, o/n	37,099.0	N-STREP-II
Probable aminotransferase	<i>PA3659</i>	Q9HXY0	25 °C, o/n	47,685.0	N-STREP-II
Probable aminotransferase	<i>PA3798</i>	Q9HXJ9	18 °C, o/n	45,736.0	N-STREP-II

### 4.2.3 Protein Purification of STREP Tagged Proteins

Cell pellets from 2 L culture were resuspended in 20 mL STREP binding buffer (50 mM  $\text{NaH}_2\text{PO}_4$ , 300 mM NaCl, pH = 7.9) and lysed by sonication (7 min 30%, 3 min 70%, 2 cycles; *Bandelin* Sonolus HD 2070). The lysate was clarified by centrifugation (18000 rpm, 45 min, 4 °C, SLA-3000) and loaded onto a StrepTrap column (*GE Healthcare*) pre-equilibrated with STREP binding buffer integrated into a Äkta purifier10 FPLC system (*GE Healthcare*). Untagged proteins were removed by washing the column with 10 column volumes STREP binding buffer at a flow rate of 3 mL/min. Elution of STREP-tagged proteins was conducted by applying 5 column volumes STREP elution buffer (STREP binding buffer, 2.5 mM desthiobiotin, pH = 7.9). The eluted fractions were collected, concentrated with a suitable centrifugal mass filter (MWCO: 3/10/30/50 kDa, *Millipore*) and desalted into STREP binding buffer by loading the proteins onto a HiTrap Desalting column (*GE Healthcare*) at a flow rate of 3 mL/min. Eluates were combined, concentrated and protein aliquots were snap frozen in liquid nitrogen and stored at  $-80^\circ\text{C}$ . Protein concentrations were measured at 280 nm on a *Tecan Infinite*<sup>®</sup> M Nano plate reader in a NanoQuant plate<sup>™</sup>.

### 4.2.4 Purification of His Tagged Proteins *ydcR* and *yjiR*

Protein purification of recombinant *ydcR* and *yjiR* using a HisTrap HP 5 ml column (*GE Healthcare*) for Ni-NTA affinity purification and a HiTrap Desalting 5 ml column (*GE Healthcare*) for desalting. First, the HisTrap HP 5 mL column was equilibrated with His-Tag purification buffer A (50 mM  $\text{NaH}_2\text{PO}_4$ , 300 mM NaCl, 5 mM DTT, 20 mM imidazole, pH = 8.0). Non-specifically bound proteins were removed by washing with 14 column volumes buffer A. The tagged proteins were eluted with 4 column volumes 100% His-Tag purification buffer B (50 mM  $\text{NaH}_2\text{PO}_4$ , 300 mM NaCl, 5 mM DTT, 300 mM Imidazole, pH = 8.0). The protein containing elution fractions were concentrated (MWCO: 50 kDa) and loaded onto HiTrap Desalting (5 mL) column equilibrated with buffer C (50 mM  $\text{NaH}_2\text{PO}_4$ , 300 mM NaCl, 5 mM DTT, pH = 8.0). Proteins were eluted with five column volumes of desalting buffer. Eluates were combined, concentrated and protein aliquots were snap frozen in liquid nitrogen and stored at  $-80^\circ\text{C}$ . Protein concentrations were measured at 280 nm on a *Tecan Infinite*<sup>®</sup> M Nano plate reader in a NanoQuant plate<sup>™</sup>.

### 4.2.5 UV/Vis Measurements

---

**PLP**-dependent enzymes bound to **PLP** absorb at wavelengths which depend on the protonation state of the internal imine.<sup>[151,213,248,270]</sup> First, the enzymes were diluted to 100  $\mu\text{M}$  in PBS and their absorption was recorded at room temperature on an Infinite<sup>®</sup> M Nano by *Tecan* Trading AG from 300 to 600 nm with 5 nm increments. To determine possible substrates such as amino acids, proteins were incubated with 500  $\mu\text{M}$  of **PLP** and 1 mM of substrate for 15 min prior to the measurement. Additionally, control samples containing 25 mM hydroxylamine for generation of the apo-enzymes were performed.

### 4.2.6 Probe Phosphorylation Studies with *pdxK* and SaPLK

---

Qualitative phosphorylation of probes by *pdxK* and SaPLK was determined by UV/Vis-spectroscopy measuring the decrease of absorbance of unphosphorylated species at around 320 nm and the increase of absorbance of phosphorylated species at around 395 nm.<sup>[151,152,248]</sup> To a solution containing 2  $\mu\text{M}$  *pdxK* or SaPLK and 1 mM **PL**-probe, ATP was added to a final concentration of 1 mM in 100  $\mu\text{L}$  kinase-buffer (50 mM HEPES, 50 mM KCl, 10 mM  $\text{MgCl}_2$ , pH = 7.9). The assays were conducted in a 96-well plate (Nunclon<sup>™</sup>Delta Surface, *Thermo Scientific*) and absorbance spectra were recorded from 285 to 600 nm every 40 min on a *Tecan* Infinite<sup>®</sup> M Nano plate reader at 37 °C.

### 4.2.7 Loading State Studies

---

To 10  $\mu\text{M}$  protein in PBS (25  $\mu\text{L}$ ), 2  $\mu\text{L}$  of 250 mM  $\text{NaBH}_4$  (fresh in 0.1 M NaOH) or PBS (enzyme only) were added and the mixture was incubated for 30 min at room temperature. The reaction was stopped by adding 8  $\mu\text{L}$  0.5% formic acid (pH  $\approx$  5-6) and neutralized with 5  $\mu\text{L}$  0.1 M NaOH (pH  $\approx$  7-8). All samples were then diluted to 50  $\mu\text{L}$  with PBS in order to obtain 5  $\mu\text{M}$  protein solutions.<sup>[151,248]</sup> Measurements were conducted as described in the next paragraph.



### 4.2.8 Intact Protein Mass Spectrometry

IP-MS measurements were carried out on an Ultimate 3000 RSLC system (*Thermo Scientific*) coupled to an LTQ Orbitrap XL mass spectrometer (*Thermo Scientific*).<sup>[151,248]</sup> Protein desalting was performed using a MassPREP desalting column (*Waters*) at 25 °C. Gradient elution was carried out with 0.1% formic acid (LC-MS grade, *Fisher Analytic*) in water (LC-MS grade, *Fisher Analytic*) (A) and 0.1% formic acid in acetonitrile (MeCN, LC-MS grade, *Fisher Analytic*) (B). After 2 min pre-equilibration with 6% B, protein samples were injected and eluted with a linear gradient from 6% to 95% B over 1.5 min and 2 min at 95% B at 300  $\mu\text{L}/\text{min}$  flow rate. The column was re-equilibrated with 6% B for 1 min. Mass spectrometric measurements were conducted in HESI positive mode (H-ESI-II source, *Thermo Scientific*) with the following parameters: 4.0 kV capillary voltage, 350 °C capillary temperature, 31 V capillary voltage, 110 V tube lens, 30 L/h sheath gas, 15 L/h aux gas. Full scan measurements were accomplished in a range from 300-2000 m/z in profile mode in the orbitrap at a resolution of 100,000. Raw spectra were processed with UniDec 2.6.7 for deconvolution.

### 4.2.9 Assay for *PA2683* Activity

Kinetics of *PA2683* were measured by a coupled assay: the product pyruvate gets reduced by lactate dehydrogenase (LDH) while consuming one equivalent of nicotinamide adenine dinucleotide (NADH) causing a decrease of NADH absorbance at 340 nm. Reaction solutions of 2  $\mu\text{M}$  *PA2683*, 25  $\mu\text{g}$  LDH (5 mg/mL stock solution, *Roche*), 100  $\mu\text{M}$  **PLP** (1  $\mu\text{L}$  of a 10 mM stock in ddH<sub>2</sub>O), 6 mM adenosine monophosphate (AMP, 3  $\mu\text{L}$  of a 300 mM stock in ddH<sub>2</sub>O), 2.5 mM NADH (5  $\mu\text{L}$  of a 50 mM stock in ddH<sub>2</sub>O) and varying concentrations of L-Ser (1, 2, 5, 10, 20, 50, 100, 200, 400, 600, 800, 1000, 1500, 2000, 2500 mM, stocks in ddH<sub>2</sub>O) in a total volume of 100  $\mu\text{L}$  in buffer (10 mM TRIS, 1 mM MgCl<sub>2</sub>, pH = 7.5), were transferred into a 96-well plate (Nunclo<sup>TM</sup>Delta Surface, *Thermo Scientific*) and absorbance at 340 nm was recorded every 30 s on a Tecan Infinite<sup>®</sup> M Nano plate reader at 37 °C with shaking intervals 5 s prior to measurement. All conditions were performed in triplicates with a series of control experiments (at 600 mM L-Ser): w/o NADH, w/o *PA2638*, w/o L-Ser, w/o LDH, w/o AMP, w/o **PLP**. Reaction rates and MICHAELIS-MENTEN kinetics were calculated in *Graphpad Prism* 5.03 considering the following parameters

$$E = \varepsilon \cdot c \cdot d \leftrightarrow c = \frac{E}{d \cdot \varepsilon}$$

- for NADH:  $\frac{1}{d \cdot \varepsilon} = 535.91 \mu\text{mol}/\text{L}$  at 340 nm with  $\varepsilon = 6.22 \frac{1}{\text{M} \cdot \text{cm}}$ <sup>[345]</sup>

- with  $d = 0.3$  cm for  $100 \mu\text{L}$  in 96-well plate

#### 4.2.10 EMSA – Electrophoretic Mobility Shift Assay

The protocol was adapted from *Kunzmann et al.* with modifications.<sup>[346]</sup> The TAMRA dye labelled *ydcR* promoter fragment  $\text{PR}_{\text{ydcR}}$  and the intergenic region fragment  $\text{PR}_{\text{ydcR-ydcS}}$  (see table 4.5) of *E. coli* K12 were generated as described in chapter 4.2.2.1. Proteins were diluted in  $11 \mu\text{L}$  EMSA binding buffer (100 mM TRIS, 150 mM NaCl, 1 mM EDTA, 5% v/v glycerol, pH = 8.0) to the following concentrations: 2, 5, 10, 25, 50, 75, 100, 200, 400 nM. Control samples were performed at 200 nM protein concentration. **PLP** control samples were diluted in  $10.8 \mu\text{L}$  instead of  $11 \mu\text{L}$ . Then,  $0.5 \mu\text{L}$  salmon sperm DNA (4 mg/mL stock in ddH<sub>2</sub>O, *Carl Roth*) and  $0.5 \mu\text{L}$   $\text{PR}_{\text{ydcR}}$  or  $\text{PR}_{\text{ydcR-ydcS}}$  (20 ng/ $\mu\text{L}$  stock in ddH<sub>2</sub>O, 10 ng total) were added. To **PLP** control samples,  $0.2 \mu\text{L}$  **PLP** (120  $\mu\text{M}$  stock in ddH<sub>2</sub>O, 2  $\mu\text{M}$  total) were further added. After incubation for 20 min at room temperature,  $2 \mu\text{L}$  of loading buffer (EMSA binding buffer, 0.1% bromphenol blue) were added to the samples and they were loaded onto a NativePAGE™ 3-12% bis-tris polyacrylamide gel (*Invitrogen*, 150 V, 90 min). Fluorescence imaging was conducted on a *GE Healthcare* ImageQuant™ LAS-4000 equipped with a 575DF20 Cy3 filter.

#### 4.2.11 Growth Studies

**Table 4.7:** Bacterial strains.

Strain	Source	Antibiotic Pressure
<i>S. aureus</i> USA300 TnpdxS	Nebraska Transposon Mutant Library within the Network on Antimicrobial Resistance in <i>S. aureus</i> (NARSA) <sup>[254]</sup>	Erythromycin 5 $\mu\text{g}/\text{mL}$
<i>S. aureus</i> USA300	<sup>[254]</sup>	–
<i>E. coli</i> K12 $\Delta\text{pdxJ}$	Kindly provided by Prof. Kirsten Jung from the LMU Originated from the Keio Collection <sup>[243]</sup>	Kanamycin 25 $\mu\text{g}/\text{mL}$
<i>E. coli</i> K12 MG1655	Keio Collection <sup>[243]</sup>	–
<i>P. aeruginosa</i> PAO1	Institute Pasteur in France	–

First, minimal concentration of **PL** or probe supplementation in chemically defined media (CDM) in order to reach normal growth was determined. Therefore, an overnight culture of *E. coli* K12  $\Delta$ pdxJ was grown in LB-medium containing 25  $\mu$ g/mL kanamycin (25 mg/mL stock in ethanol) and washed with CDM<sub>EC</sub> containing kanamycin (2 $\times$ 5 mL) the next day. Bacteria were resuspended in CDM<sub>EC</sub> containing kanamycin to an OD<sub>600</sub> = 0.08. To each well containing 198  $\mu$ L bacterial suspension in a 96-well plate (Nunclon™ Delta Surface, *Thermo Scientific*), different concentrations of **PL** (2  $\mu$ L; 1, 10, 250, 500 nM final) or probe (2  $\mu$ L; 1, 10, 100, 250  $\mu$ M final) were added and growth was recorded by measuring the absorbance at 600 nm on a *Tecan Infinite*® M Nano plate reader at 37 °C over 24 h with shaking intervals prior to the measurements. All conditions were performed in quadruplicates. Sterile controls (duplicates) were added for each condition as blanks. Growth curves for larger cultures (100 mL in 500 mL flasks or 500 mL in 2 L baffled flasks containing 250 nM **PL** and the corresponding antibiotic as given in table 4.7) were recorded manually by measuring the OD<sub>600</sub> every hour. Flasks were incubated at 37 °C with shaking (200 rpm). Early stationary phases were reached in CDM after 8 h for *E. coli* K12  $\Delta$ pdxJ, after 6 h for *P. aeruginosa* PAO1 and after 10 h for *S. aureus* USA300 TnpdxS. For comparison reasons, growth curves for *S. aureus* USA300 TnpdxS in B-medium were also performed. Here, early stationary phase was reached after 6 h.

## 4.3 Proteomics

Analytical labelling and proteomics were conducted as described previously with modifications.<sup>[151,248]</sup>

### 4.3.1 Analytical Labelling

*E. coli* K12  $\Delta$ pdxJ were inoculated from an overnight culture 1:100 in 100 mL CDM<sub>EC</sub> containing kanamycin (25  $\mu$ g/mL) and 0.25  $\mu$ M **PL** (25  $\mu$ L of a 1 mM stock in DMSO). Bacteria were grown for 10 h at 37 °C, harvested (6000 $\times$ g, 4 °C, 10 min) and washed with CDM<sub>EC</sub> containing kanamycin (2 $\times$ 5 mL). Pelletised bacteria were resuspended in CDM<sub>EC</sub>, adjusted to an OD<sub>600</sub> = 40 and 200  $\mu$ L of the suspension were either incubated with 2  $\mu$ L probe (10 mM stock in DMSO) or DMSO for 2 h at 37 °C with shaking. Labelled cells were harvested (6000 $\times$ g, 4 °C, 10 min) and washed with cold PBS (2 $\times$ 500  $\mu$ L). For the lysis, cells were resuspended in 200  $\mu$ L PBS and sonicated (30 s at 80%, 3 cycles; *Bandelin* Sonolus HD 2070). Lysate was clarified by centrifugation (21,000 $\times$ g, 30 min, 4 °C) and the supernatant (150  $\mu$ L) was transferred into a fresh tube for reduction with sodium borohydride (6  $\mu$ L of 500 mM stock, freshly made

in 0.1 M NaOH). After incubation for 30 min at room temperature, proteins were precipitated by adding 600  $\mu\text{L}$  cold acetone ( $-80^\circ\text{C}$ ). Proteins were then pelletized by centrifugation ( $21,000\times g$ ,  $4^\circ\text{C}$ , 20 min) and washed with cold methanol ( $2\times 500 \mu\text{L}$ ) with resuspending steps by sonication (10 s at 10%, 1 cycle). Protein pellets were re-suspended in 100  $\mu\text{L}$  0.4% SDS in PBS and incubated with a click chemistry mix (5  $\mu\text{L}$  10 mM BTAA in ddH<sub>2</sub>O, 2  $\mu\text{L}$  50 mM CuSO<sub>4</sub> in ddH<sub>2</sub>O, 2  $\mu\text{L}$  5 mM rhodamine-azide in DMSO and 2  $\mu\text{L}$  100 mM sodium ascorbate freshly prepared in ddH<sub>2</sub>O) for 30 min at room temperature. Click reactions were quenched with addition of 100  $\mu\text{L}$  loading buffer and a SDS-polyacrylamide gel (12.5%, 150 V, 3.5 h) is performed.

### 4.3.2 Preparative Labelling

#### 4.3.2.1 *S. aureus* USA300 TnpdxS Growth, Labelling and Lysis

*S. aureus* USA300 TnpdxS overnight cultures were grown in 300 mL flasks containing 50 mL B-medium and 5  $\mu\text{g}/\text{mL}$  erythromycin (25  $\mu\text{L}$  of a 10 mg/mL stock in ethanol). After harvesting ( $6000\times g$ ,  $4^\circ\text{C}$ , 10 min), pellets were washed with CDM<sub>SA</sub> containing 5  $\mu\text{g}/\text{mL}$  erythromycin ( $2\times 10 \text{ mL}$ ) and adjusted to an OD<sub>600</sub> = 6. Large cultures of 500 mL CDM<sub>SA</sub> containing 5  $\mu\text{g}/\text{mL}$  erythromycin and 0.25  $\mu\text{M}$  PL (50  $\mu\text{L}$  of a 2.5 mM stock in DMSO) were then inoculated with 1:100 overnight culture and incubated for 10 h at  $37^\circ\text{C}$  with shaking. Bacteria were harvested ( $6000\times g$ ,  $4^\circ\text{C}$ , 10 min), washed with CDM<sub>SA</sub> containing 5  $\mu\text{g}/\text{mL}$  erythromycin ( $2\times 20 \text{ mL}$ ) and diluted with CDM<sub>SA</sub> to an OD<sub>600</sub> = 40. To 1 mL bacterial suspension, 100  $\mu\text{M}$  probe (10  $\mu\text{L}$  of a 10 mM stock in DMSO) or 10  $\mu\text{L}$  DMSO were added and incubated for 2 h at  $37^\circ\text{C}$  with shaking. Bacteria were harvested ( $6000\times g$ ,  $4^\circ\text{C}$ , 10 min) and washed with cold PBS ( $2\times 1 \text{ mL}$ ). Lysis was performed by addition of lysostaphin (5  $\mu\text{L}$  of a 10 mg/mL stock in 20 mM NaOAc, pH = 4.5, *Sigma Aldrich*, Lysostaphin from *Staphylococcus simulans*) and incubation for 1 h at  $37^\circ\text{C}$  and 1400 rpm shaking (*Eppendorf Thermomixer*<sup>®</sup> R). The resulting lysate was clarified by centrifugation ( $20,000\times g$ , 30 min,  $4^\circ\text{C}$ ) and the supernatant (900  $\mu\text{L}$ ) was transferred into a fresh 15 mL falcon prior to reduction. For competitive labelling experiments, bacteria were treated with phenelzine (75, 100, 1000  $\mu\text{M}$ , from 20 $\times$  stocks in ddH<sub>2</sub>O), benserazide (0.1, 1, 10 mM, from 20 $\times$  stocks in ddH<sub>2</sub>O) or CCG-50014 (100, 500, 2500  $\mu\text{M}$ , from 100 $\times$  stocks in DMSO) for 30 min at  $37^\circ\text{C}$  with shaking, prior to probe labelling.

**4.3.2.2** *E. coli* K12  $\Delta$ pdxJ Growth, Labelling and Lysis

*E. coli* K12  $\Delta$ pdxJ overnight cultures were grown in 300 mL flasks containing 50 mL LB-medium and 25  $\mu$ g/mL kanamycin (50  $\mu$ L of a 25 mg/mL stock in ddH<sub>2</sub>O). After harvesting (6000 $\times$ g, 4 °C, 10 min), pellets were washed with CDM<sub>EC</sub> containing 25  $\mu$ g/mL kanamycin (2 $\times$ 10 mL) and adjusted to an OD<sub>600</sub> = 20. Large cultures of 500 mL CDM<sub>EC</sub> containing 25  $\mu$ g/mL kanamycin and 0.25  $\mu$ M **PL** (50  $\mu$ L of a 2.5 mM stock in DMSO) were then inoculated with 1:100 overnight culture and incubated for 8 h at 37 °C with shaking. Bacteria were harvested (6000 $\times$ g, 4 °C, 10 min), washed with CDM<sub>EC</sub> containing 25  $\mu$ g/mL kanamycin (2 $\times$ 20 mL) and diluted with CDM<sub>EC</sub> to an OD<sub>600</sub> = 60. To 1 mL bacterial suspension, 100  $\mu$ M probe (10  $\mu$ L of a 10 mM stock in DMSO) or 10  $\mu$ L DMSO were added and incubated for 2 h at 37 °C with shaking. After labelling, bacteria were harvested (6000 $\times$ g, 4 °C, 10 min) and washed with cold PBS (2 $\times$ 1 mL). Lysis was performed by sonication (30 s at 80%, 4 cycles; *Bandelin* Sonolus HD 2070) and the resulting lysate was clarified by centrifugation (20,000 $\times$ g, 30 min, 4 °C). The supernatant (900  $\mu$ L) was transferred into a new 15 mL falcon prior to reduction. For competitive labelling experiments, bacteria were treated with MAC173979 (100, 500, 2500  $\mu$ M, from 100 $\times$  stocks in DMSO) for 30 min at 37 °C with shaking, prior to probe labelling.

**4.3.2.3** *P. aeruginosa* PAO1 Growth, Labelling and Lysis

*P. aeruginosa* PAO1 wt overnight cultures were grown in 300 mL flasks containing 50 mL LB-medium. After harvesting (6000 $\times$ g, 4 °C, 10 min), pellets were washed with CDM<sub>PA</sub> and adjusted to an OD<sub>600</sub> = 20. Large cultures of 500 mL CDM<sub>PA</sub> containing 0.25  $\mu$ M **PL** (50  $\mu$ L of a 2.5 mM stock in DMSO) were then inoculated with 1:100 overnight culture and incubated for 6 h at 37 °C with shaking. Bacteria were harvested (6000 $\times$ g, 4 °C, 10 min), washed with CDM<sub>PA</sub> (2 $\times$ 20 mL) and diluted with CDM<sub>PA</sub> to an OD<sub>600</sub> = 40. To 1 mL bacterial suspension, 100  $\mu$ M probe (10  $\mu$ L of a 10 mM stock in DMSO) or 10  $\mu$ L DMSO were added and incubated for 2 h at 37 °C with shaking. After labelling, bacteria were harvested (6000 $\times$ g, 4 °C, 10 min) and washed with cold PBS (2 $\times$ 1 mL). Lysis was performed by sonication (30 s at 80%, 4 cycles; *Bandelin* Sonolus HD 2070) and the resulting lysate was clarified by centrifugation (20,000 $\times$ g, 30 min, 4 °C). The supernatant (900  $\mu$ L) was transferred into a fresh 15 mL falcon prior to reduction.

#### 4.3.2.4 Reduction and BCA Assay

---

Lysates were reduced by adding 10 mM sodium borohydride (2  $\mu$ L of 500 mM stock per 100  $\mu$ L lysate freshly prepared in 0.1 M NaOH) and incubation for 30 min at room temperature. Subsequently, proteins were precipitated by adding 4 $\times$  volume cold acetone ( $-80^{\circ}\text{C}$ ) and stored at  $-20^{\circ}\text{C}$  for at least 2 h. After pelleting of precipitated proteins by centrifugation (10,000 rpm,  $4^{\circ}\text{C}$ , 15 min, rotor SLA-3000; Sorvall RC 6+, *Thermo Scientific*), proteins were washed with cold methanol ( $-80^{\circ}\text{C}$ ,  $2\times 1$  mL). Then, protein pellets were solubilised by adding 1 mL 0.4% SDS in PBS (w/v) and they were adjusted to the same concentration by a BCA assay (ROTI<sup>®</sup>Quant, *Roth*) in a total volume of 1 mL 0.4% SDS in PBS (w/v).

#### 4.3.2.5 Click Chemistry

---

Samples were treated with 10  $\mu$ L biotin-azide (10 mM stock in DMSO, *Sigma Aldrich*), 50  $\mu$ L BTAA (10 mM stock in ddH<sub>2</sub>O, *Jena Bioscience*), 20  $\mu$ L CuSO<sub>4</sub> (50 mM in ddH<sub>2</sub>O) and 20  $\mu$ L sodium ascorbate (100 mM stock freshly prepared in ddH<sub>2</sub>O) and incubated for 1 h at room temperature. Proteins were precipitated by adding 4 $\times$  volume cold acetone ( $-80^{\circ}\text{C}$ ) and stored at  $-20^{\circ}\text{C}$  for at least 2 h. After pelleting of precipitated proteins by centrifugation (20,000 $\times g$ ,  $4^{\circ}\text{C}$ , 15 min), proteins were washed with cold methanol ( $-80^{\circ}\text{C}$ ,  $2\times 1$  mL).

#### 4.3.2.6 Staudinger Ligation

---

Samples labelled with **PL3** were treated with 20  $\mu$ L EZ-Link<sup>™</sup> Phosphine-PEG3-Biotin (10 mM stock in DMSO, *Sigma Aldrich*) and samples were incubated for 4 h at  $37^{\circ}\text{C}$  with shaking, followed by 20 h at room temperature. Proteins were precipitated by adding 4 $\times$  volume cold acetone ( $-80^{\circ}\text{C}$ ) and stored at  $-20^{\circ}\text{C}$  for at least 2 h. After pelleting of precipitated proteins by centrifugation (20,000 $\times g$ ,  $4^{\circ}\text{C}$ , 15 min), proteins were washed with cold methanol ( $-80^{\circ}\text{C}$ ,  $2\times 1$  mL).

#### 4.3.2.7 MS Workflow

---

Protein pellets were resuspended in 1 mL 0.4% SDS in PBS (w/v) and centrifuged (20,000 $\times g$ , room temperature, 15 min) prior to avidin bead enrichment.

50  $\mu\text{L}$  of avidin-agarose bead slurry (*Sigma Aldrich*) were pre-washed with 0.4% SDS in PBS (w/v) ( $3\times 1\text{ mL}$ ,  $400\times g$ , room temperature, 5 min) prior to protein loading and incubation for 1.5 h at room temperature with rotation. Avidin beads with bound proteins were washed with 0.4% SDS in PBS (w/v) ( $3\times 1\text{ mL}$ ), 6 M urea in MS- $\text{H}_2\text{O}$  ( $2\times 1\text{ mL}$ ) and PBS ( $3\times 1\text{ mL}$ ). After removal of supernatants, beads were resuspended in 200  $\mu\text{L}$  X-buffer (7 M urea, 2 M thiourea in 20 mM 2-[4-(2-hydroxyethyl)piperazin-1-yl]ethane-1-sulfonic acid (HEPES) buffer, pH = 7.5) and proteins were reduced with 5 mM tris(2-carboxyethyl)phosphine (TCEP, 2  $\mu\text{L}$  of a 500 mM stock in MS- $\text{H}_2\text{O}$ ) for 1 h at  $37^\circ\text{C}$  with shaking. Then, alkylation with 10 mM iodoacetamide [IAA, 4  $\mu\text{L}$  of a 500 mM stock in 50 mM triethylammonium bicarbonate (TEAB) buffer] was conducted for 30 min at  $25^\circ\text{C}$  before quenching samples with 10 mM dithiothreitol (DTT, 4  $\mu\text{L}$  of a 500 mM stock in MS- $\text{H}_2\text{O}$ ) for 30 min at  $25^\circ\text{C}$ . Proteins were then enzymatically digested using 1  $\mu\text{L}$  LysC (0.5  $\mu\text{g}/\mu\text{L}$ , MS-grade, *Fujifilm*) for 2 h at  $25^\circ\text{C}$ , followed by dilution with 600  $\mu\text{L}$  TEAB (50 mM) and digestion using 1.5  $\mu\text{L}$  trypsin (0.5  $\mu\text{g}/\text{mL}$  in 50 mM acetic acid buffer, sequencing grade, *Promega*) for additional 16 h at  $37^\circ\text{C}$ . Reactions were stopped by adding 10  $\mu\text{L}$  formic acid (Pierce<sup>TM</sup>, *Thermo Scientific*) and beads were removed by centrifugation ( $17,000\times g$ , room temperature, 5 min). Prior to desalting using Sep-Pak<sup>®</sup> C18 cartridges (50 mg, *Waters*), cartridges were first pre-equilibrated with MeCN ( $1\times 1\text{ mL}$ ), 80% MeCN containing 0.5% formic acid ( $2\times 1\text{ mL}$ ) and 0.1% trifluoroacetic acid ( $3\times 1\text{ mL}$ ). After sample loading, cartridges were washed with 0.1% trifluoroacetic acid ( $3\times 1\text{ mL}$ ), 0.5% formic acid ( $1\times 500\ \mu\text{L}$ ) and peptides were eluted with 80% MeCN containing 0.5% formic acid (750  $\mu\text{L}$ ). Solvents were removed *in vacuo* (centrifugal vacuum concentrator, *Eppendorf*) and lyophilized peptides were dissolved in 25  $\mu\text{L}$  1% formic acid (v/v) and filtered through Ultrafree-MC centrifugal filters (*Merck*) prior to the transfer into LC-MS vials. All proteomics experiments were simultaneously conducted in three biological replicates.

#### 4.3.2.8 MS Measurement and Analysis

Proteomics samples were analysed on an Orbitrap Fusion mass spectrometer (*Thermo Scientific*) coupled to an Ultimate3000 nano-HPLC (*Thermo Scientific, Dionex*) equipped with an Acclaim<sup>TM</sup>PepMap<sup>TM</sup>100 C18  $75\ \mu\text{m}\times 2\text{ cm}$  trap (*Thermo Scientific*) and an Acclaim<sup>TM</sup>PepMap<sup>TM</sup>RSLC C18 separation column ( $75\ \mu\text{m}\times 50\text{ cm}$ ; *Thermo Scientific*), both heated to  $50^\circ\text{C}$ , coupled to an EASY-spray<sup>TM</sup> source. Samples were loaded onto the trap at a flow rate of 5  $\mu\text{L}/\text{min}$  with 0.1% trifluoroacetic acid before being transferred to the separation column at 0.4  $\mu\text{L}/\text{min}$ . Separation of samples was performed as following: Starting from 5% buffer B (0.1% formic acid in MeCN) and 95% buffer A (0.1% formic acid in  $\text{H}_2\text{O}$ ) for 10 min, a linear gradient was applied from 5% to 22% buffer B in 105 min, followed by an increase of buffer B from 22% to 32%

in 10 min and a subsequent increase to 90% buffer B in 10 min, which was kept at 90% buffer B for 10 min. After this isocratic flow, concentration of buffer B was decreased back to 5% within 0.1 min and held at this concentration for another 10 min (total time 152 min). MS full scans were recorded at 120000 resolution in the orbitrap with the following parameters: Ion transfer tube temperature 275 °C, RF lens amplitude 60%, 350-1500 m/z scan range,  $2.0 \cdot e^5$  AGC target, 3 s cycle time and 50 ms maximal injection time. Peptides with an higher intensity than  $5 \cdot e^3$  and charge states from 2-7 were selected and fragmented in the higher-energy collisional dissociation (HCD) cell at 30% collision energy and analysed in the ion trap using the rapid scan rate. In the ion trap, following parameters were adjusted: isolation window 1.6 m/z, AGC target  $1.0 \cdot e^4$  and a maximal injection time of 100 ms.

#### 4.3.2.9 Statistical Analysis of MS/MS Data

Proteomics raw data were analysed using MaxQuant (ver. 1.6.2.10)<sup>[176]</sup> which uses the Andromeda search engine.<sup>[347]</sup> Settings were default except for LFQ-quantification and match between runs, which were activated during search. The following UniProtKB databases were used for the searches: *E. coli* K12 (taxon identifier: 83333, downloaded 09.04.2019), *P. aeruginosa* PAO1 (taxon identifier: 208964, downloaded 14.04.2020) and *S. aureus* USA300 (taxon identifier: 367830, downloaded 04.11.2020). Statistical analysis was conducted in Perseus (ver. 1.6.5.0). Protein-groups textfiles from the MaxQuant analysis were loaded into Perseus and first, LFQ intensities were transformed ( $\log_2$ ). Further, protein contaminants, ones only identified by site modification and reverse hits were removed from the matrix. Sample replicates were then equally annotated and the matrix was filtered for 2 out of 3 valid values in at least one group. Missing values were imputed for the whole matrix using the following settings: width 0.3, down shift 1.8. Finally, *p* values were calculated by a two-sided two sample *t*-test using a BENJAMINI-HOCHBERG false discovery rate correction (FDR, 0.05). Visualisation of data was realised using a scatter plot [x-axis: student's *t* test difference (probe/control or competitor plus probe/probe); y-axis:  $-\log$  student's *t*-test *p*-value (probe/control or competitor plus probe/probe)]. Heatmaps were created in OriginPro<sup>®</sup> (ver. 9.7.0.185) by plotting LFQ-intensities against PLP-dependent enzymes.



## 4.4 Targeted Metabolomics Assays

---

### 4.4.1 Substrate Screen for *PA2683*

---

A 5  $\mu\text{M}$  *PA2683* solution in buffer (10 mM TRIS, 1 mM  $\text{MgCl}_2$ , pH = 7.5) was incubated at 37 °C for 30 min with 10 mM L-Ser, D-Ser, L-Thr or D-Thr (100 mM stocks in ddH<sub>2</sub>O), 6 mM AMP (60 mM stock in ddH<sub>2</sub>O) and 100  $\mu\text{M}$  **PLP** (10 mM stock in ddH<sub>2</sub>O) in a total volume of 100  $\mu\text{L}$ . All conditions were conducted in triplicates and heat controls (protein pre-incubation at 95 °C for 5 min) were performed as negative controls. Samples were further treated as described in 4.4.5.

### 4.4.2 Substrate Screen for *PA3659* and *PA3798*

---

Substrate conversion was determined by quantifying transaminated aminoacids ( $\alpha$ -keto-aminoacids) by LC-MS/MS. A 5  $\mu\text{M}$  protein solution in buffer (10 mM TRIS, 1 mM  $\text{MgCl}_2$ , pH = 7.5) was incubated at 37 °C for 30 min with 10 mM L-Trp, L-Tyr or L-Phe for *PA3659* and L-Met or L-Gln for *PA3798* (100 mM stocks in ddH<sub>2</sub>O), 5 mM 2-ketoglutarate (100 mM stock in ddH<sub>2</sub>O) and 100  $\mu\text{M}$  **PLP** (10 mM stock in ddH<sub>2</sub>O) in a total volume of 100  $\mu\text{L}$ . All conditions were conducted in triplicates and heat controls (protein pre-incubation at 95 °C for 5 min) were performed as negative controls. Samples were further treated as described in subsection 4.4.5.

### 4.4.3 Inhibition Assay for *A0A0H2XII6* with Phenelzine

---

Inhibition was determined by quantifying the enzymes product cadaverine by LC-MS/MS. For this, protein *A0A0H2XII6* (5  $\mu\text{M}$ ) was preincubated for 40 min at 37 °C with different concentrations of phenelzine (1 mM, 100  $\mu\text{M}$ , 50  $\mu\text{M}$ , 25  $\mu\text{M}$ , 12.5  $\mu\text{M}$ ; from 100 $\times$  stocks in ddH<sub>2</sub>O) in buffer (10 mM TRIS, 1 mM  $\text{MgCl}_2$ , pH = 7.5). To the solutions, 10 mM L-Lys (100 mM stock in ddH<sub>2</sub>O) and 100  $\mu\text{M}$  **PLP** (10 mM stock in ddH<sub>2</sub>O) were added (final volume 100  $\mu\text{L}$ ) and the reactions were incubated at 37 °C for 30 min. All conditions were conducted in triplicates and a heat control (protein pre-incubation at 95 °C for 5 min) was performed as negative control. Samples were further treated as described in subsection 4.4.5.

#### 4.4.4 Inhibition Assay for *A0A0H2XHJ5* with Phenelzine

Inhibition was determined by quantifying the enzymes product alanine by LC-MS. For this, protein *A0A0H2XHJ5* (5  $\mu$ M) was preincubated for 40 min at 37 °C with different concentrations of phenelzine (10 mM, 1 mM, 100  $\mu$ M, 50  $\mu$ M, 10  $\mu$ M, 1  $\mu$ M; from 100 $\times$  stocks in ddH<sub>2</sub>O) in buffer [50 mM 3-(morpholin-4-yl)propane-1-sulfonic acid (MOPS), pH = 7.4]. To the solutions, 2  $\mu$ M protein *A0A0H2XJC0*, 10 mM L-Cys (500 mM stock in ddH<sub>2</sub>O), 5 mM DTT (500 mM stock in ddH<sub>2</sub>O) and 100  $\mu$ M PLP (10 mM stock in ddH<sub>2</sub>O) were added (final volume 100  $\mu$ L) and the reactions were incubated at 37 °C for 30 min. All conditions were conducted in triplicates. A heat control (protein pre-incubation at 95 °C for 5 min) and samples with only one of each of the two proteins were performed as control experiments. Samples were further treated as described in subsection 4.4.5.

#### 4.4.5 Further Sample Preparation

After incubation, reactions were stopped by adding 400  $\mu$ L cold acetone (−80 °C) and the samples were stored for 2 h at −20 °C to complete protein precipitation. Proteins were then removed by centrifugation (21,000 $\times$ *g*, 4 °C, 20 min) and the supernatants were transferred into fresh 1.5 mL tubes for subsequent evaporation of solvents (centrifugal vacuum concentrator, *Eppendorf*). Dried samples were reconstituted in 50  $\mu$ L H<sub>2</sub>O/MeCN = 2/1 + 0.1% formic acid, sonicated for 5 min and clarified by centrifugation (17,000 $\times$ *g*, room temperature, 10 min). Prior to MS, samples were transferred into LC-MS-vials.

#### 4.4.6 MS Measurement and Analysis

LC-MS/MS measurements were carried out on an Ultimate<sup>TM</sup>3000 RSLC system (*Thermo Scientific*) coupled to an LTQ Orbitrap XL mass spectrometer (*Thermo Scientific*).<sup>[151,248]</sup> Chromatographic separation was performed using an Accucore<sup>TM</sup> HILIC column (No. 17526-152130, 150 $\times$ 2.1 mm, 2.6  $\mu$ m, *Thermo Scientific*) at 25 °C. Gradient elution was carried out with 0.1% formic acid (LC-MS grade, *Fisher Analytic*) and 5 mM ammonium acetate (Optima<sup>TM</sup> LC-MS grade, *Fisher Scientific*) in H<sub>2</sub>O/MeCN = 50/50 (LC-MS grade, *Fisher Scientific*) (buffer A) and 0.1% formic acid and 5 mM ammonium acetate in H<sub>2</sub>O/MeCN = 5/95 (buffer B). After 2 min pre-equilibration with 5% buffer A, samples were injected and eluted with

---

a linear gradient from 5% to 50% buffer A over 12 min and from 50% to 100% buffer A over 3 min followed by backflushing the column to 5% buffer A over 3 min and re-equilibration at 5% buffer A for 2 min at 400  $\mu\text{L}/\text{min}$  flow rate. Mass spectrometric measurements were conducted in HESI positive or negative mode (H-ESI-II source, *Thermo Scientific*) with the following parameters:

**Table 4.8:** Mass spectrometry settings.

<b>Educt</b>	<b>Polarity</b>	<b>Capillary Voltage [kV]</b>	<b>Capillary Temp. [°C]</b>	<b>Capillary Voltage2 [V]</b>	<b>Tube Lens [V]</b>	<b>Sheat Gas [L/h]</b>	<b>Aux Gas [L/h]</b>	<b>Quant. Method</b>	<b>Scan Range full [m/z]</b>
Serine	–	3.80	350	–2.00	–40.00	50	10	PRM	50-600
Threonine	–	3.70	350	–16.00	–30.00	60	15	PRM	50-650
Tryptophane	–	3.80	350	–6.00	–75.00	65	0	PRM	50-1000
Tyrosine	–	3.50	350	–1.00	–65.00	34	0	PRM	50-1000
Phenylalanine	–	3.50	350	–8.00	–40.00	34	0	PRM	50-1000
Methionine	–	3.80	350	–2.00	–30.00	35	30	PRM	50-1000
Glutamine	–	3.80	350	–26.00	–50.00	45	0	PRM	50-1000
Lysine	+	3.00	350	5.00	30.00	22	5	PRM	50-1000
Cysteine	+	3.50	350	6.00	25.00	40	0	SIM	50-500

Full scan measurements were accomplished in profile mode in the orbitrap at a resolution of 60.000, PRM or SIM methods at 30.000 in the orbitrap. Fragmentation was accomplished by collision-induced dissociation (CID) with parameters given in table 4.9. Raw spectra were processed with *Thermo Scientific* XCalibur™ 1.2.

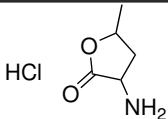
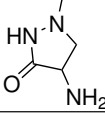
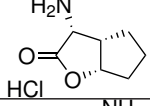
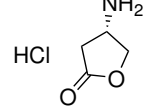
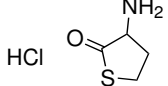
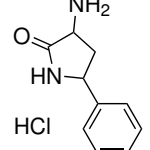
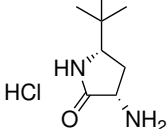
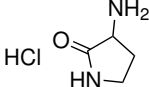
**Table 4.9:** Settings for MS/MS-methods.

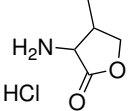
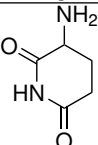
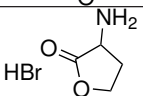
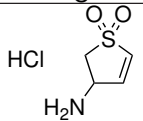
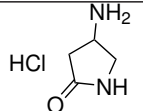
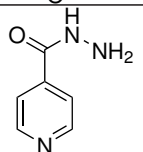
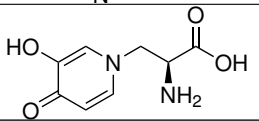
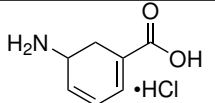
Educt Compound	Scan Range PRM [m/z]	Parent Mass [m/z]	Collision Energy	Activation Time [ms]
Serine	50-500	87.01	35.00	30.00
Threonine	50-500	101.02	35.00	30.00
Tryptophane	55-300	202.05	35.00	30.00
Tyrosine	50-300	179.03	35.00	30.00
Phenylalanine	50-300	163.04	35.00	30.00
Methionine	50-200	147.01	35.00	30.00
Glutamine	50-200	144.03	35.00	30.00
Lysine	50-250	103.12	35.00	30.00

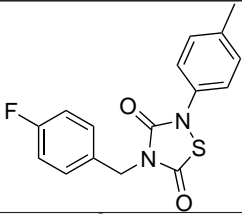
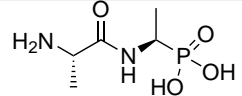
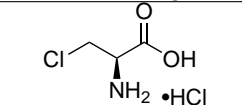
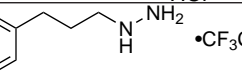
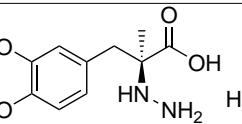
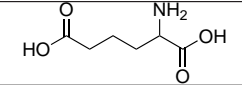
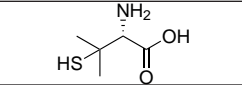
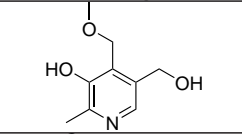
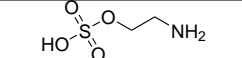
## 4.5 Compound Screen

5 mL overnight cultures of wild type strains *S. aureus* USA300 (B-medium), *E. coli* K12 (LB-medium) and *P. aeruginosa* PAO1 (LB-medium) were diluted 1:10000 in their corresponding media, distributed in a 96-well plate (Nunclo™ Delta Surface, *Thermo Scientific*) and compounds (table 4.10) were first applied at 500  $\mu$ M (from 50 mM stock, solvent see table 4.10) to a final volume of 100  $\mu$ L. Hit compounds were then fine-screened at 250, 100, 50 and 25  $\mu$ M. All experiments were carried out in triplicates and solvent-only and sterile samples were added as controls.

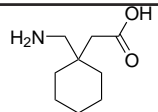
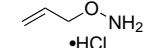
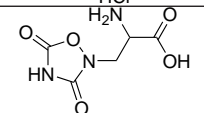
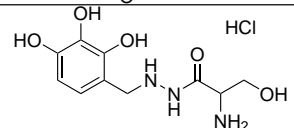
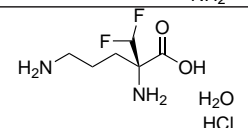
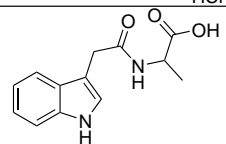
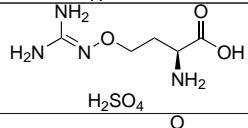
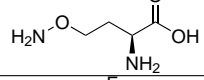
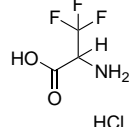
Table 4.10: List of screen compounds.

#	Compound	Structure	Mass [g/mol]	Source	Literature	Solvent
1	EN300-213294		151.59	Enamine		H <sub>2</sub> O
2	EN300-99743		115.14	Enamine		H <sub>2</sub> O
3	EN300-6489485		177.63	Enamine		H <sub>2</sub> O
4	EN300-219172		137.56	Enamine		H <sub>2</sub> O
5	EN300-17366		153.62	Enamine		H <sub>2</sub> O
6	EN300-7427659		212.68	Enamine		H <sub>2</sub> O
7	EN300-6735762		192.68	Enamine		H <sub>2</sub> O
8	EN300-298184		136.58	Enamine		H <sub>2</sub> O

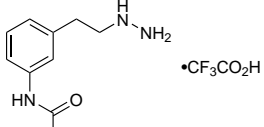
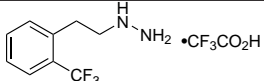
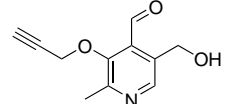
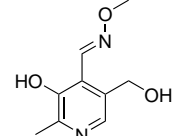
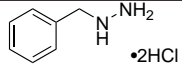
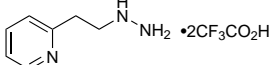
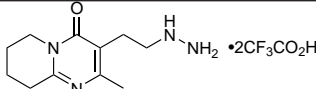
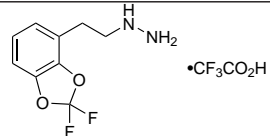
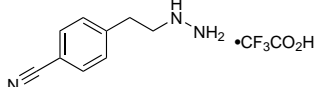
#	Compound	Structure	Mass [g/mol]	Source	Literature	Solvent
9	EN300-7445633		151.59	Enamine		H <sub>2</sub> O
10	BBV-38269949		128.13	Enamine		H <sub>2</sub> O
11	EN300-17331		182.02	Enamine		H <sub>2</sub> O
12	EN300-10694		168.62	Enamine		H <sub>2</sub> O
13	EN300-127487		136.58	Enamine		H <sub>2</sub> O
14	Isoniazid		137.14	Sigma	[35]	H <sub>2</sub> O
15	Mimosine		198.18	Sigma	[141]	30 mM NaOH
16	Gabaculine		175.61	Cayman	[9,348]	DMSO

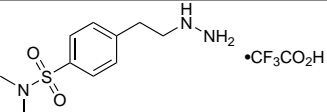
#	Compound	Structure	Mass [g/mol]	Source	Literature	Solvent
17	CCG-50014		316.35	Sigma	[103,104]	DMSO
18	Alafosfalin		194.14	Carbosynth	[101]	H <sub>2</sub> O
19	$\beta$ -Chloro-L-alanine		160.00	Carbosynth	[9,101]	H <sub>2</sub> O
20	TM-2-10		264.25	Synthesis		DMSO
21	Carbidopa		244.24	Arcos	[9]	DMSO
22	Amino adipic acid		161.16	Sigma	[9,145]	DMSO
23	Penicillamine		149.21	Sigma	[9]	H <sub>2</sub> O
24	Ginkgotoxin		183.21	Sigma	[349]	DMSO
25	Ethanolamin- <i>O</i> -sulfat		141.14	TCI	[9]	H <sub>2</sub> O



#	Compound	Structure	Mass [g/mol]	Source	Literature	Solvent
26	Gabapentin		171.24	TCI	[9]	H <sub>2</sub> O
27	<i>O</i> -Allyl hydroxyl amine		109.55	TCI	[9]	H <sub>2</sub> O
28	Quisqualic acid		189.13	Sigma	[9,145]	50 mM NaOH
29	Benserazide		293.70	TCI	[9]	H <sub>2</sub> O
30	Effornithine		236.64	TCI	[9]	H <sub>2</sub> O
31	Indole-3-acetyl alanine		246.27	Sigma	[9,350]	DMSO
32	Canavanine		274.25	Sigma	[9,144]	H <sub>2</sub> O
33	Canaline		134.14	Biomol	[9,144]	H <sub>2</sub> O
34	Trifluoralanine		179.53	Sigma	[9]	H <sub>2</sub> O

#	Compound	Structure	Mass [g/mol]	Source	Literature	Solvent
35	2-Aminobenzene sulfonate		173.19	TCI	[9]	DMSO
36	Gyromitrin		100.12	Toronto	[351]	H <sub>2</sub> O
37	Indole-3-acetyl glutamate		304.30	Toronto	[9,350]	DMSO
38	TM-2-11		310.27	Synthesis		DMSO
39	Phenelzine		234.27	Carbosynth	[9]	H <sub>2</sub> O
40	Aminoethylvinyl glycine		196.63	Carbosynth	[9]	H <sub>2</sub> O
41	Propargylglycine		113.12	Carbosynth	[9]	H <sub>2</sub> O
42	MAC173979		246.04	Synthesis	[294]	DMSO
43	TM-2-12		307.27	Synthesis		DMSO

#	Compound	Structure	Mass [g/mol]	Source	Literature	Solvent
44	TM-2-13		322.33	Synthesis		DMSO
45	TM-2-14		318.22	Synthesis		DMSO
46	PL15		205.21	Synthesis		DMSO
47	PL-methoxim		196.21	Synthesis		DMSO
48	EN300-295489		195.09	Enamine		DMSO
49	TM-2-15		365.23	Synthesis		DMSO
50	TM-2-16		450.34	Synthesis		DMSO
51	TM-2-17		330.21	Synthesis		DMSO
52	TM-2-18		275.23	Synthesis		DMSO

#	Compound	Structure	Mass [g/mol]	Source	Literature	Solvent
53	TM-2-19	 <chem>CN(C)S(=O)(=O)c1ccc(cc1)CCN=NH.[O-]C(=O)C(F)(F)F</chem>	375.35	Synthesis		DMSO

# REFERENCES

---

- [1] M. Richter, *Nat. Prod. Rep.* **2013**, *30*, 1324–1345.
- [2] J. D. Fischer, G. L. Holliday, S. A. Rahman, J. M. Thornton, *J. Mol. Biol.* **2010**, *403*, 803–824.
- [3] A. Kirschning, *Angew. Chem. Int. Ed.* **2020**, *60*, 6242–6269.
- [4] Casimir Funk, *J. State Med.* **1912**, *20*, 341–368.
- [5] T. B. Fitzpatrick, G. J. C. Basset, P. Borel, F. Carrari, D. DellaPenna, P. D. Fraser, H. Hellmann, S. Osorio, C. Rothan, V. Valpuesta, C. Caris-Veyrat, A. R. Fernie, *Plant Cell* **2012**, *24*, 395–414.
- [6] M. Eggersdorfer, D. Laudert, U. Létinois, T. McClymont, J. Medlock, T. Netscher, W. Bonrath, *Angew. Chem. Int. Ed.* **2012**, *51*, 12960–12990.
- [7] G. F. Combs, *The vitamins*, Elsevier Acad. Press, Amsterdam u.a., 4th ed., **2012**.
- [8] F. J. Leeper, A. G. Smith, *Nat. Prod. Rep.* **2007**, *24*, 923–926.
- [9] A. Amadasi, M. Bertoldi, R. Contestabile, S. Bettati, B. Cellini, M. L. Di Salvo, C. Borri-Voltattorni, F. Bossa, A. Mozzarelli, *Curr. Med. Chem.* **2007**, *14*, 1291–1324.
- [10] M. L. Di Salvo, R. Contestabile, M. K. Safo, *Biochim. Biophys. Acta* **2011**, *1814*, 1597–1608.
- [11] A. Tramonti, C. Nardella, M. L. Di Salvo, A. Barile, F. D’Alessio, V. de Crécy-Lagard, R. Contestabile, *EcoSal Plus* **2021**, *9*, eESP-0004–2021.
- [12] T. Mukherjee, J. Hanes, I. Tews, S. E. Ealick, T. P. Begley, *Biochim. Biophys. Acta* **2011**, *1814*, 1585–1596.
- [13] R. Contestabile, *Front. Biosci.* **2012**, *E4*, 897–913.
- [14] T. Ito, D. M. Downs, *J. Bacteriol.* **2020**, *202*, e00056–20.
- [15] Gerhard Mittenhuber, *J. Mol. Microbiol. Biotechnol.* **2001**, *3*, 1–20.
- [16] D. B. McCormick, H. Chen, *J. Nutr.* **1999**, *129*, 325–327.
- [17] D. E. Metzler, M. Ikawa, E. E. Snell, *J. Am. Chem. Soc.* **1954**, *76*, 648–652.
- [18] Martino L. Di Salvo, Nediljko Budisa, *Beilstein Bozen Symposium* **2012**, 27–66.
- [19] E. F. Oliveira, Cerqueira, Nuno M F S A, P. A. Fernandes, M. J. Ramos, *J. Am. Chem. Soc.* **2011**, *133*, 15496–15505.
- [20] S. Raboni, F. Spyrakis, B. Campanini, A. Amadasi, S. Bettati, A. Peracchi, A. Mozzarelli, R. Contestabile in *Comprehensive natural products II* (Eds.: L. N. Mander, H.-w. Liu), Elsevier, Amsterdam, **2010**, pp. 273–350.
- [21] M. D. Toney, *Biochim. Biophys. Acta* **2011**, *1814*, 1407–1418.
- [22] R. Percudani, A. Peracchi, *BMC Bioinf.* **2009**, *10*, 273.
- [23] H. C. Dunathan, *PNAS* **1966**, *55*, 712–716.
- [24] R. Graber, P. Kasper, V. N. Malashkevich, P. Strop, H. Gehring, J. N. Jansonius, P. Christen, *J. Biol. Chem.* **1999**, *274*, 31203–31208.
- [25] F. P. Seebeck, D. Hilvert, *J. Am. Chem. Soc.* **2003**, *125*, 10158–10159.
- [26] D. E. Metzler, E. E. Snell, *J. Biol. Chem.* **1952**, 353–361.
- [27] J. Olivard, D. E. Metzler, E. E. Snell, *J. Biol. Chem.* **1952**, 669–674.

- [28] P. Bilski, M. Y. Li, M. Ehrenshaft, M. E. Daub, C. F. Chignell, *Photochem. Photobiol.* **2000**, *71*, 129–134.
- [29] D. B. Tully, V. E. Allgood, J. A. Cidlowski, *FASEB J.* **1994**, *8*, 343–349.
- [30] J. M. Salhany, L. M. Schopfer, *J. Biol. Chem.* **1993**, *268*, 7643–7645.
- [31] K. A. Klotz, J. R. Lemke, R. Korinthenberg, J. Jacobs, *Neuropediatrics* **2017**, *48*, 199–204.
- [32] S. Ohtahara, Y. Yamatogi, Y. Ohtsuka, *Brain Dev.* **2011**, *33*, 783–789.
- [33] A. I. Denesyuk, K. A. Denessiouk, T. Korpela, M. S. Johnson, *J. Mol. Biol.* **2002**, *316*, 155–172.
- [34] I. D. Spenser, R. E. Hill, *Nat. Prod. Rep.* **1995**, *12*, 555.
- [35] M. P. Wilson, B. Plecko, P. B. Mills, P. T. Clayton, *J. Inherited Metab. Dis.* **2019**, *42*, 629–646.
- [36] R. Kajita, T. Goto, S. H. Lee, T. Oe, *Chem. Res. Toxicol.* **2013**, *26*, 1926–1936.
- [37] S. Christmann-Franck, S. Femandjian, G. Mirambeau, P. A. Der Garabedian, *Biochimie* **2007**, *89*, 468–473.
- [38] J. I. Garaycochea, G. P. Crossan, F. Langevin, L. Mulderrig, S. Louzada, F. Yang, G. Guilbaud, N. Park, S. Roerink, S. Nik-Zainal, M. R. Stratton, K. J. Patel, *Nature* **2018**, *553*, 171–177.
- [39] M. S. Ghatge, S. S. Karve, T. M. S. David, M. H. Ahmed, F. N. Musayev, K. Cunningham, V. Schirch, M. K. Safo, *FEBS Open Bio* **2016**, *6*, 398–408.
- [40] M. S. Ghatge, R. Contestabile, M. L. Di Salvo, J. V. Desai, A. K. Gandhi, C. M. Camara, R. Florio, I. N. González, A. Parroni, V. Schirch, M. K. Safo, *PloS one* **2012**, *7*, e41680.
- [41] P.-Y. Cheung, C.-C. Fong, K.-T. Ng, W.-C. Lam, Y.-C. Leung, C.-W. Tsang, M. Yang, M.-S. Wong, *J. Biochem.* **2003**, *134*, 731–738.
- [42] T. F. Fu, M. Di Salvo, V. Schirch, *Anal. Biochem.* **2001**, *298*, 314–321.
- [43] P. B. Mills, R. A. H. Surtees, M. P. Champion, C. E. Beesley, N. Dalton, P. J. Scambler, S. J. R. Heales, A. Briddon, I. Scheimberg, G. F. Hoffmann, J. Zschocke, P. T. Clayton, *Hum. Mol. Genet.* **2005**, *14*, 1077–1086.
- [44] H. Song, S.-i. Ueno, S. Numata, J.-i. Iga, S. Shibuya-Tayoshi, M. Nakataki, S. Tayoshi, K. Yamauchi, S. Sumitani, T. Tomotake, T. Tada, T. Tanahashi, M. Itakura, T. Ohmori, *Schizophr. Res.* **2007**, *97*, 264–270.
- [45] P. Lainé-Cessac, A. Cailleux, P. Allain, *Biochem. Pharmacol.* **1997**, *54*, 863–870.
- [46] U. Kästner, C. Hallmen, M. Wiese, E. Leistner, C. Drewke, *FEBS J.* **2007**, *274*, 1036–1045.
- [47] M. R. Weir, R. C. Keniston, J. I. Enriquez, G. A. McNamee, *Vet. Hum. Toxicol.* **1991**, *33*, 118–121.
- [48] P. T. Clayton, *J. Inherit. Metab. Dis.* **2006**, *29*, 317–326.
- [49] K. Stach, W. Stach, K. Augoff, *Nutrients* **2021**, *13*, 3229.
- [50] L. Galluzzi, E. Vacchelli, J. Michels, P. Garcia, O. Kepp, L. Senovilla, I. Vitale, G. Kroemer, *Oncogene* **2013**, *32*, 4995–5004.
- [51] P. Christen, P. K. Mehta, *Chem. Rec.* **2001**, *1*, 436–447.
- [52] N. V. Grishin, M. A. Phillips, E. J. Goldsmith, *Protein Sci.* **1995**, *4*, 1291–1304.
- [53] Nomenclature Committee of the International Union, *Enzyme nomenclature 1992. Recommendations of the Nomenclature Committee of the International Union of Biochemistry and*

- Molecular Biology on the ...*, Nomenclature Committee of the International Union, **1992**.
- [54] A. C. Eliot, J. F. Kirsch, *Annu. Rev. Biochem.* **2004**, *73*, 383–415.
- [55] P. K. Mehta, P. Christen, *Adv. Enzymol.* **2000**, *74*, 129–184.
- [56] A. M. Knight, A. Nobili, T. van den Bergh, M. Genz, H.-J. Joosten, D. Albrecht, K. Riedel, I. V. Pavlidis, U. T. Bornscheuer, *Appl. Microbiol. Biotechnol.* **2017**, *101*, 1499–1507.
- [57] F. Steffen-Munsberg, C. Vickers, H. Kohls, H. Land, H. Mallin, A. Nobili, L. Skalden, T. van den Bergh, H.-J. Joosten, P. Berglund, M. Höhne, U. T. Bornscheuer, *Biotechnol. Adv.* **2015**, *33*, 566–604.
- [58] E. Y. Bezsudnova, V. O. Popov, K. M. Boyko, *Appl. Microbiol. Biotechnol.* **2020**, *104*, 2343–2357.
- [59] G. Schneider, H. Käck, Y. Lindqvist, *Structure* **2000**, *8*, R1–R6.
- [60] F. Berkovitch, E. Behshad, K.-H. Tang, E. A. Enns, P. A. Frey, C. L. Drennan, *PNAS* **2004**, *101*, 15870–15875.
- [61] B. W. Lepore, F. J. Ruzicka, P. A. Frey, D. Ringe, *PNAS* **2005**, *102*, 13819–13824.
- [62] R. Percudani, A. Peracchi, *EMBO Rep.* **2003**, *4*, 850–854.
- [63] A. MacDougall, V. Volynkin, R. Saidi, D. Poggioli, H. Zellner, E. Hatton-Ellis, V. Joshi, C. O'Donovan, S. Orchard, A. H. Auchincloss, D. Baratin, J. Bolleman, E. Coudert, E. de Castro, C. Hulo, P. Masson, I. Pedruzzi, C. Rivoire, C. Arighi, Q. Wang, C. Chen, H. Huang, J. Garavelli, C. R. Vinayaka, L.-S. Yeh, D. A. Natale, K. Laiho, M.-J. Martin, A. Renaux, K. Pichler, *Bioinformatics* **2021**, *36*, 5562.
- [64] A. Bateman, M.-J. Martin, S. Orchard, M. Magrane, R. Agivetova, S. Ahmad, E. Alpi, E. H. Bowler-Barnett, R. Britto, B. Bursteinas, H. Bye-A-Jee, R. Coetzee, A. Cukura, A. Da Silva, P. Denny, T. Dogan, T. Ebenezer, J. Fan, L. G. Castro, P. Garmiri, G. Georghiou, L. Gonzales, E. Hatton-Ellis, A. Hussein, A. Ignatchenko, G. Insana, R. Ishtiaq, P. Jokinen, V. Joshi, D. Jyothi, A. Lock, R. Lopez, A. Luciani, J. Luo, Y. Lussi, A. MacDougall, F. Madeira, M. Mahmoudy, M. Menchi, A. Mishra, K. Moulang, A. Nightingale, C. S. Oliveira, S. Pundir, G. Qi, S. Raj, D. Rice, M. R. Lopez, R. Saidi, J. Sampson, T. Sawford, E. Speretta, E. Turner, N. Tyagi, P. Vasudev, V. Volynkin, K. Warner, X. Watkins, R. Zaru, H. Zellner, A. Bridge, S. Poux, N. Redaschi, L. Aimo, G. Argoud-Puy, A. Auchincloss, K. Axelsen, P. Bansal, D. Baratin, M.-C. Blatter, J. Bolleman, E. Boutet, L. Breuza, C. Casals-Casas, E. de Castro, K. C. Echioukh, E. Coudert, B. Cucho, M. Doche, D. Dornevil, A. Estreicher, M. L. Famiglietti, M. Feuermann, E. Gasteiger, S. Gehant, V. Gerritsen, A. Gos, N. Gruaz-Gumowski, U. Hinz, C. Hulo, N. Hyka-Nouspikel, F. Jungo, G. Keller, A. Kerhornou, V. Lara, P. Le Mercier, D. Lieberherr, T. Lombardot, X. Martin, P. Masson, A. Morgat, T. B. Neto, S. Paesano, I. Pedruzzi, S. Pilbout, L. Pourcel, M. Pozzato, M. Pruess, C. Rivoire, C. Sigrist, K. Sonesson, A. Stutz, S. Sundaram, M. Tognolli, L. Verbregue, C. H. Wu, C. N. Arighi, L. Arminski, C. Chen, Y. Chen, J. S. Garavelli, H. Huang, K. Laiho, P. McGarvey, D. A. Natale, K. Ross, C. R. Vinayaka, Q. Wang, Y. Wang, L.-S. Yeh, J. Zhang, P. Ruch, D. Teodoro, *Nucleic Acids Res.* **2021**, *49*, D480–D489.
- [65] M. Blum, H.-Y. Chang, S. Chuguransky, T. Grego, S. Kandasamy, A. Mitchell, G. Nuka, T. Paysan-Lafosse, M. Qureshi, S. Raj, L. Richardson, G. A. Salazar, L. Williams, P. Bork, A. Bridge, J. Gough, D. H. Haft, I. Letunic, A. Marchler-Bauer, H. Mi, D. A. Natale, M. Necci, C. A. Orengo, A. P. Pandurangan, C. Rivoire, C. J. A. Sigrist, I. Sillitoe, N. Thanki, P. D. Thomas, S. C. E. Tosatto, C. H. Wu, A. Bateman, R. D. Finn, *Nucleic Acids Res.* **2021**, *49*, D344–D354.

- [66] P. Gaudet, M. S. Livstone, S. E. Lewis, P. D. Thomas, *Briefings Bioinf.* **2011**, *12*, 449–462.
- [67] B. an Diep, S. R. Gill, R. F. Chang, T. H. Phan, J. H. Chen, M. G. Davidson, F. Lin, J. Lin, H. A. Carleton, E. F. Mongodin, G. F. Sensabaugh, F. Perdreau-Remington, *Lancet* **2006**, *367*, 731–739.
- [68] F. R. Blattner, G. Plunkett, C. A. Bloch, N. T. Perna, V. Burland, M. Riley, J. Collado-Vides, J. D. Glasner, C. K. Rode, G. F. Mayhew, J. Gregor, N. W. Davis, H. A. Kirkpatrick, M. A. Goeden, D. J. Rose, B. Mau, Y. Shao, *Science* **1997**, *277*, 1453–1462.
- [69] C. K. Stover, X. Q. Pham, A. L. Erwin, S. D. Mizoguchi, P. Warrener, M. J. Hickey, F. S. Brinkman, W. O. Hufnagle, D. J. Kowalik, M. Lagrou, R. L. Garber, L. Goltry, E. Tolentino, S. Westbrook-Wadman, Y. Yuan, L. L. Brody, S. N. Coulter, K. R. Folger, A. Kas, K. Larbig, R. Lim, K. Smith, D. Spencer, G. K. Wong, Z. Wu, I. T. Paulsen, J. Reizer, M. H. Saier, R. E. Hancock, S. Lory, M. V. Olson, *Nature* **2000**, *406*, 959–964.
- [70] Y.-L. Du, R. Singh, L. M. Alkhalaf, E. Kuatsjah, H.-Y. He, L. D. Eltis, K. S. Ryan, *Nat. Chem. Biol.* **2016**, *12*, 194–199.
- [71] Y.-L. Du, K. S. Ryan, *Nat. Prod. Rep.* **2018**, *36*, 430–457.
- [72] A. Tramonti, C. Nardella, M. L. Di Salvo, S. Pascarella, R. Contestabile, *FEBS J.* **2018**, *285*, 3925–3944.
- [73] B. R. Belitsky, A. L. Sonenshein, *Mol. Microbiol.* **2002**, *45*, 569–583.
- [74] B. R. Belitsky, *J. Mol. Biol.* **2004**, *340*, 655–664.
- [75] R. Wu, R. Sanishvili, B. R. Belitsky, J. I. Juncosa, H. V. Le, H. J. S. Lehrer, M. Farley, R. B. Silverman, G. A. Petsko, D. Ringe, D. Liu, *PNAS* **2017**, *114*, 3891–3896.
- [76] B. Cellini, R. Montioli, E. Oppici, A. Astegno, C. B. Voltattorni, *Clin. Biochem.* **2014**, *47*, 158–165.
- [77] H. Hayashi, *J. Biochem.* **1995**, *118*, 463–473.
- [78] R. Contestabile, A. Paiardini, S. Pascarella, M. L. Di Salvo, S. D’Aguanno, F. Bossa, *Eur. J. Biochem.* **2001**, *268*, 6508–6525.
- [79] F. W. Alexander, E. Sandmeier, P. K. Mehta, P. Christen, *Eur. J. Biochem.* **1994**, *219*, 953–960.
- [80] C. K. Savile, J. M. Janey, E. C. Mundorff, J. C. Moore, S. Tam, W. R. Jarvis, J. C. Colbeck, A. Krebber, F. J. Fleitz, J. Brands, P. N. Devine, G. W. Huisman, G. J. Hughes, *Science* **2010**, *329*, 305–309.
- [81] S. A. Kelly, S. Pohle, S. Wharry, S. Mix, C. C. R. Allen, T. S. Moody, B. F. Gilmore, *Chem. Rev.* **2018**, *118*, 349–367.
- [82] M. Chen, C.-T. Liu, Y. Tang, *J. Am. Chem. Soc.* **2020**, *142*, 10506–10515.
- [83] K. Chen, F. H. Arnold, *Nat. Catal.* **2020**, *3*, 203–213.
- [84] M. L. Di Salvo, K. Fesko, R. S. Phillips, R. Contestabile, *Front. Bioeng. Biotechnol.* **2020**, *8*, 52.
- [85] Mary P. Lambert, Francis C. Neuhaus, *J. Bacteriol.* **1972**, *110*, 978–987.
- [86] P. LeMagueres, H. Im, J. Ebalunode, U. Strych, M. J. Benedik, J. M. Briggs, H. Kohn, K. L. Krause, *Biochemistry* **2005**, *44*, 1471–1481.
- [87] C. D. Mitnick, S. S. Shin, K. J. Seung, M. L. Rich, S. S. Atwood, J. J. Furin, G. M. Fitzmaurice, F. A. Alcantara Viru, S. C. Appleton, J. N. Bayona, C. A. Bonilla, K. Chalco, S. Choi,



- M. F. Franke, H. S. F. Fraser, D. Guerra, R. M. Hurtado, D. Jazayeri, K. Joseph, K. Llaro, L. Mestanza, J. S. Mukherjee, M. Muñoz, E. Palacios, E. Sanchez, A. Sloutsky, M. C. Becerra, *N. Engl. J. Med.* **2008**, *359*, 563–574.
- [88] J. A. Caminero, G. Sotgiu, A. Zumla, G. B. Migliori, *Lancet Infect. Dis.* **2010**, *10*, 621–629.
- [89] C. de Chiara, M. Homšak, G. A. Prosser, H. L. Douglas, A. Garza-Garcia, G. Kelly, A. G. Purkiss, E. W. Tate, L. P. S. de Carvalho, *Nat. Chem. Biol.* **2020**, *5*, 183.
- [90] J. L. Strominger, E. Ito, R. H. Threnn, *J. Am. Chem. Soc.* **1960**, *82*, 998–999.
- [91] F. C. Neuhaus, *Antimicrob. Agents Chemother.* **1967**, *7*, 304–313.
- [92] T. S. Soper, J. M. Manning, *J. Biol. Chem.* **1981**, *256*, 4263–4268.
- [93] M. Kotnik, P. S. Anderluh, A. Prezelj, *Curr. Pharm. Des.* **2007**, *13*, 2283–2309.
- [94] K. Hoffmann, E. Schneider-Scherzer, H. Kleinkauf, R. Zocher, *J. Biol. Chem.* **1994**, *269*, 12710–12714.
- [95] T. Nomura, I. Yamamoto, F. Morishita, Y. Furukawa, O. Matsushima, *J. Exp. Zool.* **2001**, *289*, 1–9.
- [96] Daniel L. Milligan, Sieu L. Tran, Ulrich Strych, Gregory M. Cook, Kurt L. Krause, *J. Bacteriol.* **2007**, *189*, 8381–8386.
- [97] C. T. Walsh, *J. Biol. Chem.* **1989**, *264*, 2393–2396.
- [98] M Lobočka, J Hennig, J Wild, T Kłopotowski, *J. Bacteriol.* **1994**, *176*, 1500–1510.
- [99] J. Wild, J. Hennig, M. Lobočka, W. Walczak, T. Kłopotowski, *Mol. Gen. Genet.* **1985**, *198*, 315–322.
- [100] U. Strych, H.-C. Huang, K. L. Krause, M. J. Benedik, *Curr. Microbiol.* **2000**, *41*, 290–294.
- [101] M. A. Azam, U. Jayaram, *J. Enzyme Inhib. Med. Chem.* **2016**, *31*, 517–526.
- [102] F. R. Atherton, M. J. Hall, C. H. Hassall, R. W. Lambert, W. J. Lloyd, P. S. Ringrose, *Antimicrob. Agents Chemother.* **1979**, *15*, 696–705.
- [103] M. Ciustea, S. Mootien, A. E. Rosato, O. Perez, P. Cirillo, K. R. Yeung, M. Ledizet, M. H. Cynamon, P. A. Aristoff, R. A. Koski, P. A. Kaplan, K. G. Anthony, *Biochem. Pharmacol.* **2012**, *83*, 368–377.
- [104] Y. Lee, S. Mootien, C. Shoen, M. Destefano, P. Cirillo, O. A. Asojo, K. R. Yeung, M. Ledizet, M. H. Cynamon, P. A. Aristoff, R. A. Koski, P. A. Kaplan, K. G. Anthony, *Biochem. Pharmacol.* **2013**, *86*, 222–230.
- [105] L. J. Ejim, J. E. Blanchard, K. P. Koteva, R. Sumerfield, N. H. Elowe, J. D. Chechetto, E. D. Brown, M. S. Junop, G. D. Wright, *J. Med. Chem.* **2007**, *50*, 755–764.
- [106] K. Shatalin, E. Shatalina, A. Mironov, E. Nudler, *Science* **2011**, *334*, 986–990.
- [107] A. Asimakopoulou, P. Panopoulos, C. T. Chasapis, C. Coletta, Z. Zhou, G. Cirino, A. Giannis, C. Szabo, G. A. Spyroulias, A. Papapetropoulos, *Br. J. Pharmacol.* **2013**, *169*, 922–932.
- [108] C. Chao, J. R. Zatarain, Y. Ding, C. Coletta, A. A. Mrazek, N. Druzhyina, P. Johnson, H. Chen, J. L. Hellmich, A. Asimakopoulou, K. Yanagi, G. Olah, P. Szoleczky, G. Törö, F. J. Bohanon, M. Cheema, R. Lewis, D. Eckelbarger, A. Ahmad, K. Módis, A. Untereiner, B. Szczesny, A. Papapetropoulos, J. Zhou, M. R. Hellmich, C. Szabo, *Mol. Med.* **2016**, *22*, 361–379.
- [109] K. Shatalin, A. Nuthanakanti, A. Kaushik, D. Shishov, A. Peselis, I. Shamovsky, B. Pani,

- M. Lechpammer, N. Vasilyev, E. Shatalina, D. Rebatchouk, A. Mironov, P. Fedichev, A. Serganov, E. Nudler, *Science* **2021**, *372*, 1169–1175.
- [110] A. Mironov, T. Seregina, M. Nagornykh, L. G. Luhachack, N. Korolkova, L. E. Lopes, V. Kotova, G. Zavilgelsky, R. Shakulov, K. Shatalin, E. Nudler, *PNAS* **2017**, *114*, 6022–6027.
- [111] M. J. Wallace, S. Dharuman, D. M. Fernando, S. M. Reeve, C. T. Gee, J. Yao, E. C. Griffith, G. A. Phelps, W. C. Wright, J. M. Elmore, R. B. Lee, T. Chen, R. E. Lee, *ACS Infect. Dis.* **2020**, *6*, 467–478.
- [112] C. F. Baxter, E. Roberts, *J. Biol. Chem.* **1958**, *233*, 1135–1139.
- [113] A. W. Bown, B. J. Shelp, *Plant Physiol.* **1997**, *115*, 1–5.
- [114] N. J. Tillakaratne, L. Medina-Kauwe, K. Gibson, *Comp. Biochem. Physiol. A: Physiol.* **1995**, *112*, 247–263.
- [115] E. Metzger, Y. S. Halpern, *J. Bacteriol.* **1990**, *172*, 3250–3256.
- [116] J. I. Juncosa, K. Takaya, H. V. Le, M. J. Moschitto, P. M. Weerawarna, R. Mascarenhas, D. Liu, S. L. Dewey, R. B. Silverman, *J. Am. Chem. Soc.* **2018**, *140*, 2151–2164.
- [117] J. Bormann, *Trends Neurosci.* **1988**, *11*, 112–116.
- [118] N. G. Bowery, B. Bettler, W. Froestl, J. P. Gallagher, F. Marshall, M. Raiteri, T. I. Bonner, S. J. Enna, *Pharmacol. Rev.* **2002**, *54*, 247–264.
- [119] K. Obata, *Proc. Jpn. Acad. Ser. B* **2013**, *89*, 139–156.
- [120] R. A. Bakay, A. B. Harris, *Brain Res.* **1981**, *206*, 387–404.
- [121] J. Butterworth, C. M. Yates, J. Simpson, *J. Neurochem.* **1983**, *41*, 440–447.
- [122] N. Nishino, H. Fujiwara, S. A. Noguchi-Kuno, C. Tanaka, *Jpn. J. Pharmacol.* **1988**, *48*, 331–339.
- [123] T. Aoyagi, T. Wada, F. Kojima, M. Nagai, S. Harada, T. Takeuchi, K. Hirokawa, *Chem. Pharm. Bull.* **1990**, *38*, 1750–1752.
- [124] L. M. Gunne, J. E. Häggström, B. Sjöquist, *Nature* **1984**, *309*, 347–349.
- [125] M. A. Rogawski, R. J. Porter, *Pharmacol. Rev.* **1990**, *42*, 223–286.
- [126] L. J. Fowler, R. A. John, *Biochem. J.* **1972**, *130*, 569–573.
- [127] M. J. Jung, B. Lippert, B. W. Metcalf, P. Böhlen, P. J. Schechter, *J. Neurochem.* **1977**, *29*, 797–802.
- [128] B. E. Gidal, M. D. Privitera, R. D. Sheth, J. T. Gilman, *Ann. Pharmacother.* **1999**, *33*, 1277–1286.
- [129] E. J. Waterhouse, K. N. Mims, S. N. Gowda, *Neuropsychiatr. Dis. Treat.* **2009**, *5*, 505–515.
- [130] L. Frisén, K. Malmgren, *Acta Ophthalmol. Scand.* **2003**, *81*, 466–473.
- [131] J. R. Buncic, C. A. Westall, C. M. Panton, J. R. Munn, L. D. MacKeen, W. J. Logan, *Ophthalmology* **2004**, *111*, 1935–1942.
- [132] R. A. John, E. D. Jones, L. J. Fowler, *Biochem. J.* **1979**, *177*, 721–728.
- [133] P. Yogeewari, D. Sriram, R. Thirumurugan, J. V. Raghavendran, K. Sudhan, R. K. Pavana, J. Stables, *J. Med. Chem.* **2005**, *48*, 6202–6211.
- [134] H. Lee, E. H. Doud, R. Wu, R. Sanishvili, J. I. Juncosa, D. Liu, N. L. Kelleher, R. B. Silverman, *J. Am. Chem. Soc.* **2015**, *137*, 2628–2640.

- [135] M. Feja, S. Meller, L. S. Deking, E. Kaczmarek, M. J. During, R. B. Silverman, M. Gernert, *Epilepsia* **2021**, *62*, 3091–3104.
- [136] V. L. Schramm, *J. Biol. Chem.* **2007**, *282*, 28297–28300.
- [137] M. Hajizadeh, Z. Moosavi-Movahedi, N. Sheibani, A. A. Moosavi-Movahedi, *J. Iran. Chem. Soc.* **2021**.
- [138] V. M. D’Costa, C. E. King, L. Kalan, M. Morar, W. W. L. Sung, C. Schwarz, D. Froese, G. Zazula, F. Calmels, R. Debruyne, G. B. Golding, H. N. Poinar, G. D. Wright, *Nature* **2011**, *477*, 457–461.
- [139] G. S. Ducker, J. M. Ghergurovich, N. Mainolfi, V. Suri, S. K. Jeong, S. Hsin-Jung Li, A. Friedman, M. G. Manfredi, Z. Gitai, H. Kim, J. D. Rabinowitz, *PNAS* **2017**, *114*, 11404–11409.
- [140] N. Appaji Rao, R. Talwar, H. S. Savithri, *Int. J. Biochem. Cell Biol.* **2000**, *32*, 405–416.
- [141] H. B. Lin, R. Falchetto, P. J. Mosca, J. Shabanowitz, D. F. Hunt, J. L. Hamlin, *J. Biol. Chem.* **1996**, *271*, 2548–2556.
- [142] E. Oppenheim, P. J. Stover in *Biochemistry and molecular biology of vitamin B6 and PQQ-dependent proteins*, Vol. 9 (Eds.: A. Iriarte, H. M. Kagan, M. Martinez-Carrion), Birkhauser Verlag, Basel and Boston, **2000**, pp. 35–40.
- [143] B. J. Berger, *Antimicrob. Agents Chemother.* **2000**, *44*, 2540–2542.
- [144] A. K. Bence, D. R. Worthen, V. R. Adams, P. A. Crooks, *Anti-cancer drugs* **2002**, *13*, 313–320.
- [145] R. Schwarcz, R. Pellicciari, *J. Pharmacol. Exp. Ther.* **2002**, *303*, 1–10.
- [146] K. A. Denessiouk, A. I. Denesyuk, J. V. Lehtonen, T. Korpela, M. S. Johnson, *Proteins: Struct. Funct. Genet.* **1999**, *35*, 250–261.
- [147] N. M. Fleischman, D. Das, A. Kumar, Q. Xu, H.-J. Chiu, L. Jaroszewski, M. W. Knuth, H. E. Klock, M. D. Miller, M.-A. Elsliger, A. Godzik, S. A. Lesley, A. M. Deacon, I. A. Wilson, M. D. Toney, *Protein Sci.* **2014**, *23*, 1060–1076.
- [148] J. Catazaro, A. Caprez, A. Guru, D. Swanson, R. Powers, *Proteins* **2014**, *82*, 2597–2608.
- [149] J. Liang, Q. Han, Y. Tan, H. Ding, J. Li, *Front. Mol. Biosci.* **2019**, *6*, 4.
- [150] M. M. Whittaker, A. Penmatsa, J. W. Whittaker, *Arch. Biochem. Biophys.* **2015**, *568*, 64–70.
- [151] A. Hoegl, M. B. Nodwell, V. C. Kirsch, N. C. Bach, M. Pfanzelt, M. Stahl, S. Schneider, S. A. Sieber, *Nat. Chem.* **2018**, *10*, 1234–1245.
- [152] A. Fux, M. Pfanzelt, V. C. Kirsch, A. Hoegl, S. A. Sieber, *Cell chem. biol.* **2019**, *26*, 1461–1468.e7.
- [153] Y. Liu, M. P. Patricelli, B. F. Cravatt, *PNAS* **1999**, *96*, 14694–14699.
- [154] A. E. Speers, G. C. Adam, B. F. Cravatt, *J. Am. Chem. Soc.* **2003**, *125*, 4686–4687.
- [155] A. E. Speers, B. F. Cravatt, *J. Am. Chem. Soc.* **2005**, *127*, 10018–10019.
- [156] M. J. Evans, B. F. Cravatt, *Chem. Rev.* **2006**, *106*, 3279–3301.
- [157] B. F. Cravatt, A. T. Wright, J. W. Kozarich, *Annu. Rev. Biochem.* **2008**, *77*, 383–414.
- [158] M. J. Niphakis, B. F. Cravatt, *Annu. Rev. Biochem.* **2014**, *83*, 341–377.
- [159] B. D. Horning, R. M. Suci, D. A. Ghadiri, O. A. Ulanovskaya, M. L. Matthews, K. M. Lum, K. M. Backus, S. J. Brown, H. Rosen, B. F. Cravatt, *J. Am. Chem. Soc.* **2016**, *138*,

- 13335–13343.
- [160] D. Greenbaum, K. F. Medzihradzky, A. Burlingame, M. Bogyo, *Chem. Biol.* **2000**, *7*, 569–581.
- [161] J. A. Joyce, A. Baruch, K. Chehade, N. Meyer-Morse, E. Giraudo, F.-Y. Tsai, D. C. Greenbaum, J. H. Hager, M. Bogyo, D. Hanahan, *Cancer Cell* **2004**, *5*, 443–453.
- [162] A. M. Sadaghiani, S. H. Verhelst, M. Bogyo, *Curr. Opin. Chem. Biol.* **2007**, *11*, 20–28.
- [163] M. Fonović, M. Bogyo, *Expert Rev. Proteomics* **2008**, *5*, 721–730.
- [164] S. A. Sieber, *Activity-Based Protein Profiling, Vol. 324*, Springer Berlin Heidelberg, Berlin Heidelberg, 2012th ed., **2012**.
- [165] P. P. Geurink, L. M. Prely, G. A. van der Marel, R. Bischoff, H. S. Overkleeft, *Top. Curr. Chem.* **2012**, *324*, 85–113.
- [166] H. Fang, B. Peng, S. Y. Ong, Q. Wu, L. Li, S. Q. Yao, *Chem. Sci.* **2021**, *12*, 8288–8310.
- [167] E. Saxon, *Science* **2000**, *287*, 2007–2010.
- [168] M. Verdoes, B. I. Florea, U. Hillaert, L. I. Willems, W. A. van der Linden, M. Sae-Heng, D. V. Filippov, A. F. Kisselev, G. A. van der Marel, H. S. Overkleeft, *ChemBioChem* **2008**, *9*, 1735–1738.
- [169] D. Greenbaum, A. Baruch, L. Hayrapetian, Z. Darula, A. Burlingame, K. F. Medzihradzky, M. Bogyo, *Mol. Cell. Proteom.* **2002**, *1*, 60–68.
- [170] M. Pfanzelt, T. E. Maher, R. M. Absmeier, M. Schwarz, S. A. Sieber, *Angew. Chem. Int. Ed.* **2022**, e202117724.
- [171] E. S. Simon, J. Allison, *Rapid Commun. Mass Spectrom.* **2009**, *23*, 3401–3408.
- [172] W. X. Schulze, B. Usadel, *Annu. Rev. Plant Biol.* **2010**, *61*, 491–516.
- [173] X. Chen, S. Wei, Y. Ji, X. Guo, F. Yang, *Proteomics* **2015**, *15*, 3175–3192.
- [174] J. Cox, M. Y. Hein, C. A. Lubner, I. Paron, N. Nagaraj, M. Mann, *Mol. Cell. Proteomics* **2014**, *13*, 2513–2526.
- [175] S. Wang, Y. Tian, M. Wang, G.-B. Sun, X.-B. Sun, *Front. Pharmacol.* **2018**, *9*, 353.
- [176] S. Tyanova, T. Temu, J. Cox, *Nat. Protoc.* **2016**, *11*, 2301–2319.
- [177] J. M. Asara, H. R. Christofk, L. M. Freemark, L. C. Cantley, *Proteomics* **2008**, *8*, 994–999.
- [178] J. W. H. Wong, G. Cagney, *Methods Mol. Biol.* **2010**, *604*, 273–283.
- [179] N. M. Griffin, J. Yu, F. Long, P. Oh, S. Shore, Y. Li, J. A. Koziol, J. E. Schnitzer, *Nat. Biotechnol.* **2010**, *28*, 83–89.
- [180] W. P. Heal, T. H. T. Dang, E. W. Tate, *Chem. Soc. Rev.* **2011**, *40*, 246–257.
- [181] D. Leung, C. Hardouin, D. L. Boger, B. F. Cravatt, *Nat. Biotechnol.* **2003**, *21*, 687–691.
- [182] V. N. Malashkevich, P. Strop, J. W. Keller, J. N. Jansonius, M. D. Toney, *J. Mol. Biol.* **1999**, *294*, 193–200.
- [183] W. W. Yew, C. F. Wong, P. C. Wong, J. Lee, C. H. Chau, *Clin. Infect. Dis.* **1993**, *17*, 288–289.
- [184] G. A. Prosser, L. P. S. de Carvalho, *ACS Med. Chem. Lett.* **2013**, *4*, 1233–1237.
- [185] S. Halouska, R. J. Fenton, D. K. Zinniel, D. D. Marshall, R. G. Barletta, R. Powers, *J. Proteome Res.* **2014**, *13*, 1065–1076.

- [186] M. Gersch, J. Kreuzer, S. A. Sieber, *Nat. Prod. Rep.* **2012**, *29*, 659–682.
- [187] P. R. A. Zanon, F. Yu, P. Musacchio, L. Lewald, M. Zollo, K. Krauskopf, D. Mrdović, P. Raunft, T. E. Maher, M. Cigler, C. Chang, K. Lang, F. D. Toste, A. I. Nesvizhskii, S. M. Hacker, *Profiling the Proteome-Wide Selectivity of Diverse Electrophiles*, ChemRxiv, **2021**.
- [188] R. Haselbeck, D. Wall, B. Jiang, T. Ketela, J. Zyskind, H. Bussey, J. G. Foulkes, T. Roemer, *Curr. Pharm. Des.* **2002**, *8*, 1155–1172.
- [189] W. Korytnyk, H. Ahrens, *J. Med. Chem.* **1971**, *14*, 947–952.
- [190] W. Korytnyk, S. C. Srivastava, N. Angelino, P. G. G. Potti, B. Paul, *J. Med. Chem.* **1973**, *16*, 1096–1101.
- [191] I. B. Müller, F. Wu, B. Bergmann, J. Knöckel, R. D. Walter, H. Gehring, C. Wrenger, *PLoS one* **2009**, *4*, e4406.
- [192] W. Korytnyk, P. G. G. Potti, *J. Med. Chem.* **1977**, *20*, 567–572.
- [193] W. Korytnyk, G. B. Grindey, B. Lachmann, *J. Med. Chem.* **1973**, *16*, 865–867.
- [194] W. Korytnyk, N. Angelino, *J. Med. Chem.* **1977**, *20*, 745–749.
- [195] W. Korytnyk, R. P. Singh, *J. Am. Chem. Soc.* **1963**, *85*, 2813–2817.
- [196] W. Korytnyk, B. Paul, *J. Med. Chem.* **1970**, *13*, 187–191.
- [197] W. Korytnyk, S. C. Srivastava, *J. Med. Chem.* **1973**, *16*, 638–642.
- [198] Y.-C. Kim, K. A. Jacobson, *Synthesis* **2000**, *2000*, 119–122.
- [199] Y.-C. Kim, S. G. Brown, T. K. Harden, J. L. Boyer, G. Dubyak, B. F. King, G. Burnstock, K. A. Jacobson, *J. Med. Chem.* **2001**, *44*, 340–349.
- [200] M. Adamczyk, S. R. Akireddy, R. E. Reddy, *Tetrahedron* **2000**, *56*, 2379–2390.
- [201] L. Brown, G. A. Johnston, C. J. Suckling, P. J. Halling, R. H. Valivety, *J. Chem. Soc. Perkin Trans. 1* **1993**, 2777.
- [202] D. Heyl, E. Luz, S. A. Harris, *J. Am. Chem. Soc.* **1951**, *73*, 3437–3439.
- [203] P. F. Muhlradt, Y. Morino, E. E. Snell, *J. Med. Chem.* **1967**, *10*, 341–344.
- [204] D. Y. Yang, Y. Shih, H. W. Liu, *J. Org. Chem.* **1991**, *56*, 2940–2946.
- [205] M. Zhang, X. Zhang, J. Li, Q. Guo, Q. Xiao, *Chin. J. Chem.* **2011**, *29*, 1715–1720.
- [206] G. Knobloch, N. Jabari, S. Stadlbauer, H. Schindelin, M. Köhn, A. Gohla, *Bioorg. Med. Chem.* **2015**, *23*, 2819–2827.
- [207] M. L. Fonda, *J. Biol. Chem.* **1971**, *246*, 2230–2240.
- [208] M. L. Mechanik, Y. Torchinsky, V. L. Florentiev, M. Karpeisky, *FEBS Lett.* **1971**, *13*, 177–180.
- [209] K. D. Schnackerz, P. F. Cook, *Arch. Biochem. Biophys.* **1995**, *324*, 71–77.
- [210] F. Wu, P. Christen, H. Gehring, *FASEB J.* **2011**, *25*, 2109–2122.
- [211] N. D. Doktorova, L. V. Ionova, M. Karpeisky, N. Padyukova, K. F. Turchin, V. L. Florentiev, *Tetrahedron* **1969**, *25*, 3527–3553.
- [212] Y.-C. Kim, E. Camaioni, A. U. Ziganshin, X.-d. Ji, B. F. King, S. S. Wildman, A. Rychkov, J. Yoburn, H. Kim, A. Mohanram, T. K. Harden, J. L. Boyer, G. Burnstock, K. A. Jacobson, *Drug Dev. Res.* **1998**, *45*, 52–66.

- [213] W. R. Griswold, M. D. Toney, *J. Am. Chem. Soc.* **2011**, *133*, 14823–14830.
- [214] S. L. Blethen, E. A. Boeker, E. E. Snell, *J. Biol. Chem.* **1968**, *243*, 1671–1677.
- [215] Y. Morino, E. E. Snell, *PNAS* **1967**, *57*, 1692–1699.
- [216] V. Boekelheide, W. J. Linn, *J. Am. Chem. Soc.* **1954**, *76*, 1286–1291.
- [217] S. Müller, B. Liepold, G. J. Roth, H. J. Bestmann, *Synlett* **1996**, *1996*, 521–522.
- [218] G. Roth, B. Liepold, S. Müller, H. Bestmann, *Synthesis* **2003**, *2004*, 59–62.
- [219] D. Heyl, E. Luz, S. A. Harris, K. Folkers, *J. Am. Chem. Soc.* **1951**, *73*, 3430–3433.
- [220] E. M. Kaiser, W. R. Thomas, T. E. Synos, J. R. McClure, T. S. Mansour, J. R. Garlich, J. E. Chastain, *J. Organomet. Chem.* **1981**, *213*, 405–417.
- [221] Martin Pfanzelt, *Master's Thesis*, Technical University of Munich, Garching, **02.10.2017**.
- [222] W. Korytnyk, *J. Org. Chem.* **1962**, *27*, 3724–3726.
- [223] M. Saha, M. S. Hossain, S. Bandyopadhyay, *Angew. Chem. Int. Ed.* **2021**, *60*, 5220–5224.
- [224] D. Cahard, C. McGuigan, J. Balzarini, *Mini-Rev. Med. Chem.* **2004**, *4*, 371–381.
- [225] J. Rautio, N. A. Meanwell, L. Di, M. J. Hageman, *Nat. Rev. Drug Discovery* **2018**, *17*, 559–587.
- [226] P. J. Thornton, H. Kadri, A. Miccoli, Y. Mehellou, *J. Med. Chem.* **2016**, *59*, 10400–10410.
- [227] Y. Mehellou, J. Balzarini, C. McGuigan, *ChemMedChem* **2009**, *4*, 1779–1791.
- [228] A. Miccoli, B. A. Dhiani, Y. Mehellou, *MedChemComm* **2019**, *10*, 200–208.
- [229] M. Munier, D. Tritsch, D. Lièvreumont, M. Rohmer, C. Grosdemange-Billiard, *Bioorg. Chem.* **2019**, *89*, 103012.
- [230] C. McGuigan, R. N. Pathirana, N. Mahmood, K. G. Devine, A. J. Hay, *Antivir. Res.* **1992**, *17*, 311–321.
- [231] Y. Mehellou, H. S. Rattan, J. Balzarini, *J. Med. Chem.* **2018**, *61*, 2211–2226.
- [232] P. Kielkowski, I. Y. Buchsbaum, V. C. Kirsch, N. C. Bach, M. Drukker, S. Cappello, S. A. Sieber, *Nat. Commun.* **2020**, *11*, 517.
- [233] P. Kielkowski, I. Y. Buchsbaum, T. Becker, K. Bach, S. Cappello, S. A. Sieber, *ChemBioChem* **2020**, *21*, 1285–1287.
- [234] T. Rauh, S. Brameyer, P. Kielkowski, K. Jung, S. A. Sieber, *ACS Infect. Dis.* **2020**, *6*, 3277–3289.
- [235] A. Khazaei, A. Rostami, *Org. Prep. Proced. Int.* **2006**, *38*, 484–490.
- [236] M. M. Heravi, F. Derikvand, M. Ghassemzadeh, *Synth. Commun.* **2006**, *36*, 581–585.
- [237] G. Bauduin, D. Bondon, Y. Pietrasanta, B. Pucci, *Tetrahedron* **1978**, *34*, 3269–3274.
- [238] J. Sun, Y. Dong, L. Cao, X. Wang, S. Wang, Y. Hu, *J. Org. Chem.* **2004**, *69*, 8932–8934.
- [239] T. W. Greene, P. G. M. Wuts, *Greene's protective groups in organic synthesis*, Wiley-Interscience, Hoboken, NJ, 4th ed., **2007**.
- [240] A. Miccoli, B. Dhiani, P. Thornton, O. Lambourne, E. James, H. Kadri, Y. Mehellou, *ChemMedChem* **2020**, *15*, 671–674.
- [241] P. Prusevich, J. H. Kalin, S. A. Ming, M. Basso, J. Givens, X. Li, J. Hu, M. S. Taylor, A. M.

- Cieniewicz, P.-Y. Hsiao, R. Huang, H. Roberson, N. Adejola, L. B. Avery, R. A. Casero, S. D. Taverna, J. Qian, A. J. Tackett, R. R. Ratan, O. G. McDonald, A. P. Feinberg, P. A. Cole, *ACS Chem. Biol.* **2014**, *9*, 1284–1293.
- [242] M. B. Nodwell, M. F. Koch, F. Alte, S. Schneider, S. A. Sieber, *J. Org. Chem.* **2014**, *136*, 4992–4999.
- [243] T. Baba, T. Ara, M. Hasegawa, Y. Takai, Y. Okumura, M. Baba, K. A. Datsenko, M. Tomita, B. L. Wanner, H. Mori, *Mol. Syst. Biol.* **2006**, *2*, 2006.0008.
- [244] T. G. Slama, *Crit. Care* **2008**, *12 Suppl 4*, S4.
- [245] E. Tacconelli, E. Carrara, A. Savoldi, S. Harbarth, M. Mendelson, D. L. Monnet, C. Pulcini, G. Kahlmeter, J. Kluytmans, Y. Carmeli, M. Ouellette, K. Outterson, J. Patel, M. Cavaleri, E. M. Cox, C. R. Houchens, M. L. Grayson, P. Hansen, N. Singh, U. Theuretzbacher, N. Magrini, A. O. Aboderin, S. S. Al-Abri, N. Awang Jalil, N. Benzonana, S. Bhattacharya, A. J. Brink, F. R. Burkert, O. Cars, G. Cornaglia, O. J. Dyar, A. W. Friedrich, A. C. Gales, S. Gandra, C. G. Giske, D. A. Goff, H. Goossens, T. Gottlieb, M. Guzman Blanco, W. Hryniewicz, D. Kattula, T. Jinks, S. S. Kanj, L. Kerr, M.-P. Kieny, Y. S. Kim, R. S. Kozlov, J. Labarca, R. Laxminarayan, K. Leder, L. Leibovici, G. Levy-Hara, J. Littman, S. Malhotra-Kumar, V. Manchanda, L. Moja, B. Ndoye, A. Pan, D. L. Paterson, M. Paul, H. Qiu, P. Ramon-Pardo, J. Rodríguez-Baño, M. Sanguinetti, S. Sengupta, M. Sharland, M. Si-Mehand, L. L. Silver, W. Song, M. Steinbakk, J. Thomsen, G. E. Thwaites, J. W. M. van der Meer, N. van Kinh, S. Vega, M. V. Villegas, A. Wechsler-Fördös, H. F. L. Wertheim, E. Wesangula, N. Woodford, F. O. Yilmaz, A. Zorzet, *Lancet Infect. Dis.* **2018**, *18*, 318–327.
- [246] S. Zhao, J. W. Adamiak, V. Bonifay, J. Mehla, H. I. Zgurskaya, D. S. Tan, *Nat. Chem. Biol.* **2020**, *16*, 1293–1302.
- [247] Arie Geerlof, *M9 mineral medium*, **2010**, [https://www.helmholtz-muenchen.de/fileadmin/PEPF/Protocols/M9-medium\\_150510.pdf](https://www.helmholtz-muenchen.de/fileadmin/PEPF/Protocols/M9-medium_150510.pdf), visited on 2022-03-07.
- [248] A. Hoegl, *Dissertation*, Technische Universität München, München, **2018**.
- [249] D. Tomé, *ACS Food Sci. Technol.* **2021**, *1*, 487–494.
- [250] A. E. Speers, B. F. Cravatt, *Chem. Biol.* **2004**, *11*, 535–546.
- [251] V. V. Rostovtsev, L. G. Green, V. V. Fokin, K. B. Sharpless, *Angew. Chem.* **2002**, *114*, 2708–2711.
- [252] D. Jovanovic, P. Tremmel, P. S. Pallan, M. Egli, C. Richert, *Angew. Chem. Int. Ed.* **2020**, *59*, 20154–20160.
- [253] J. K. Lithgow, E. J. Hayhurst, G. Cohen, Y. Aharonowitz, S. J. Foster, *J. Bacteriol.* **2004**, *186*, 1579–1590.
- [254] P. D. Fey, J. L. Endres, V. K. Yajjala, T. J. Widhelm, R. J. Boissy, J. L. Bose, K. W. Bayles, *mBio* **2013**, *4*, e00537–12.
- [255] S. H. Kim, B. L. Schneider, L. Reitzer, *J. Bacteriol.* **2010**, *192*, 5304–5311.
- [256] Y. Takahashi, M. Nakamura, *J. Biochem.* **1999**, *126*, 917–926.
- [257] E. L. Holbrook, R. C. Greene, J. H. Krueger, *Biochemistry* **1990**, *29*, 435–442.
- [258] M. S. Mulani, E. E. Kamble, S. N. Kumkar, M. S. Tawre, K. R. Pardesi, *Front. Microbiol.* **2019**, *10*, 539.
- [259] Z. Pang, R. Raudonis, B. R. Glick, T.-J. Lin, Z. Cheng, *Biotechnol. Adv.* **2019**, *37*, 177–192.

- [260] Y. Kang, T. Durfee, J. D. Glasner, Y. Qiu, D. Frisch, K. M. Winterberg, F. R. Blattner, *J. Bacteriol.* **2004**, *186*, 4921–4930.
- [261] M. Hashimoto, T. Ichimura, H. Mizoguchi, K. Tanaka, K. Fujimitsu, K. Keyamura, T. Ote, T. Yamakawa, Y. Yamazaki, H. Mori, T. Katayama, J.-i. Kato, *Mol. Microbiol.* **2005**, *55*, 137–149.
- [262] S. Y. Gerdes, M. D. Scholle, J. W. Campbell, G. Balázsi, E. Ravasz, M. D. Daugherty, A. L. Somera, N. C. Kyrpides, I. Anderson, M. S. Gelfand, A. Bhattacharya, V. Kapatral, M. D'Souza, M. V. Baev, Y. Grechkin, F. Mseeh, M. Y. Fonstein, R. Overbeek, A.-L. Barabási, Z. N. Oltvai, A. L. Osterman, *J. Bacteriol.* **2003**, *185*, 5673–5684.
- [263] Z. Yang, C.-D. Lu, *J. Bacteriol.* **2007**, *189*, 3954–3959.
- [264] M. Y. Galperin, E. V. Koonin, *Nucleic Acids Res.* **2004**, *32*, 5452–5463.
- [265] T. Takenaka, T. Ito, I. Miyahara, H. Hemmi, T. Yoshimura, *FEBS J.* **2015**, *282*, 4201–4217.
- [266] L. P. S. de Carvalho, H. Zhao, C. E. Dickinson, N. M. Arango, C. D. Lima, S. M. Fischer, O. Ouerfelli, C. Nathan, K. Y. Rhee, *Chem. Biol.* **2010**, *17*, 323–332.
- [267] D. C. Sévin, T. Fuhrer, N. Zamboni, U. Sauer, *Nat. Methods* **2017**, *14*, 187–194.
- [268] F. Guo, P. Berglund, *Green Chem.* **2017**, *19*, 333–360.
- [269] M. Fuchs, J. E. Farnberger, W. Kroutil, *Eur. J. Org. Chem.* **2015**, *2015*, 6965–6982.
- [270] A. Mozzarelli, S. Bettati, *Chem. Rec.* **2006**, *6*, 275–287.
- [271] W. R. Griswold, M. D. Toney, *Bioorg. Med. Chem. Lett.* **2010**, *20*, 1352–1354.
- [272] K. D. Schnackerz, J. H. Ehrlich, W. Giesemann, T. A. Reed, *Biochemistry* **1979**, *18*, 3557–3563.
- [273] J. Jin, U. Hanefeld, *Chem. Commun.* **2011**, *47*, 2502–2510.
- [274] M. Goto, T. Yamauchi, N. Kamiya, I. Miyahara, T. Yoshimura, H. Mihara, T. Kurihara, K. Hirotsu, N. Esaki, *J. Biol. Chem.* **2009**, *284*, 25944–25952.
- [275] D. Amidani, A. Tramonti, A. V. Canosa, B. Campanini, S. Maggi, T. Milano, M. L. Di Salvo, S. Pascarella, R. Contestabile, S. Bettati, C. Rivetti, *Biochim. Biophys. Acta Gen. Subj.* **2017**, *1861*, 3474–3489.
- [276] I. A. Suvorova, D. A. Rodionov, *Microb. Genomics* **2016**, *2*, e000047.
- [277] E. Bramucci, T. Milano, S. Pascarella, *Biochem. Biophys. Res. Commun.* **2011**, *415*, 88–93.
- [278] S. El Qaidi, J. Yang, J.-R. Zhang, D. W. Metzger, G. Bai, *J. Bacteriol.* **2013**, *195*, 2187–2196.
- [279] N. Jochmann, S. Götker, A. Tauch, *Microbiology* **2011**, *157*, 77–88.
- [280] B. R. Belitsky, *Mol. Microbiol.* **2014**, *92*, 1113–1128.
- [281] A. Tramonti, A. Fiascarelli, T. Milano, M. L. Di Salvo, I. Nogués, S. Pascarella, R. Contestabile, *FEBS J.* **2015**, *282*, 2966–2984.
- [282] S. Kurihara, Y. Tsuboi, S. Oda, H. G. Kim, H. Kumagai, H. Suzuki, *J. Bacteriol.* **2009**, *191*, 2776–2782.
- [283] M. I. Prieto-Santos, J. Martín-Checa, R. Balaña-Fouce, A. Garrido-Pertierra, *Biochim. Biophys. Acta Gen. Subj.* **1986**, *880*, 242–244.
- [284] A. G. Albrecht, F. Peuckert, H. Landmann, M. Miethke, A. Seubert, M. A. Marahiel, *FEBS Lett.* **2011**, *585*, 465–470.



- [285] A. G. Albrecht, D. J. A. Netz, M. Miethke, A. J. Pierik, O. Burghaus, F. Peuckert, R. Lill, M. A. Marahiel, *J. Bacteriol.* **2010**, *192*, 1643–1651.
- [286] C. A. Roberts, H. M. Al-Tameemi, A. A. Mashruwala, Z. Rosario-Cruz, U. Chauhan, W. E. Sause, V. J. Torres, W. J. Belden, J. M. Boyd, *Infect. Immun.* **2017**, *85*, e00100–17.
- [287] B. Selbach, E. Earles, P. C. Dos Santos, *Biochemistry* **2010**, *49*, 8794–8802.
- [288] M. Blahut, C. E. Wise, M. R. Bruno, G. Dong, T. M. Makris, P. A. Frantom, J. A. Dunkle, F. W. Outten, *J. Biol. Chem.* **2019**, *294*, 12444–12458.
- [289] H. Mihara, N. Esaki, *Appl. Microbiol. Biotechnol.* **2002**, *60*, 12–23.
- [290] D. A. Bender, W. R. Smith, *Biochem. Soc. Trans.* **1978**, *6*, 120–122.
- [291] R. W. Vilter, *Vitam. Horm.* **1964**, *22*, 797–805.
- [292] D. E. Schwartz, R. Brandt, *Arzneim.-Forsch.* **1978**, *28*, 302–307.
- [293] D E Malcolm, P H Yu, R C Bowen, C O'Donovan, J Hawkes, and M Hussein, *J. Psychiatry Neurosci.* **1994**, *19*, 332–334.
- [294] S. Zlitni, L. F. Ferruccio, E. D. Brown, *Nat. Chem. Biol.* **2013**, *9*, 796–804.
- [295] J. M. Thiede, S. L. Kordus, B. J. Turman, J. A. Buonomo, C. C. Aldrich, Y. Minato, A. D. Baughn, *Sci. Rep.* **2016**, *6*, 38083.
- [296] J. Buigues, J. Vallejo, *J. Clin. Psychiatry* **1987**, *48*, 55–59.
- [297] J. G. Fiedorowicz, K. L. Swartz, *J. Psychiatr. Pract.* **2004**, *10*, 239–248.
- [298] V. A. Tanay, M. B. Parent, J. T. Wong, T. Paslawski, I. L. Martin, G. B. Baker, *Cell. Mol. Neurobiol.* **2001**, *21*, 325–339.
- [299] K. F. McKenna, D. J. McManus, G. B. Baker, R. T. Coutts, *J. Neural Transm.* **1994**, *41*, 115–122.
- [300] David L. Roman, Shodai Ota, Richard R. Neubig, *J. Biomol. Screening* **2009**, *14*, 610–619.
- [301] L. L. Blazer, H. Zhang, E. M. Casey, S. M. Husbands, R. R. Neubig, *Biochemistry* **2011**, *50*, 3181–3192.
- [302] J. Marcinkeviciene, M. Rogers, L. Kopcho, W. Jiang, K. Wang, D. J. Murphy, J. Lippy, S. Link, T. D. Chung, F. Hobbs, T. Haque, G. L. Trainor, A. Slee, A. M. Stern, R. A. Copeland, *Biochem. Pharmacol.* **2000**, *60*, 339–342.
- [303] H. Vashisth, A. J. Storaska, R. R. Neubig, C. L. Brooks, *ACS Chem. Biol.* **2013**, *8*, 2778–2784.
- [304] M. P. Hayes, C. R. Bodle, D. L. Roman, *Mol. Pharmacol.* **2018**, *93*, 25–35.
- [305] B. Roux, C. T. Walsh, *Biochemistry* **1992**, *31*, 6904–6910.
- [306] S. K. Wright, M. S. DeClue, A. Mandal, L. Lee, O. Wiest, W. W. Cleland, D. Hilvert, *J. Am. Chem. Soc.* **2005**, *127*, 12957–12964.
- [307] M. D. Plamann, G. V. Stauffer, *Gene* **1983**, *22*, 9–18.
- [308] D. H. Flint, *J. Biol. Chem.* **1996**, *271*, 16068–16074.
- [309] B. Laber, K. P. Gerbling, C. Harde, K. H. Neff, E. Nordhoff, H. D. Pohlenz, *Biochemistry* **1994**, *33*, 3413–3423.
- [310] R. S. Boddu, O. Perumal, D. K., *Biotechnol. Appl. Biochem.* **2020**, *68*, 1518–1530.

- [311] X. Dou, H. Huang, L. Jiang, G. Zhu, H. Jin, N. Jiao, L. Zhang, Z. Liu, L. Zhang, *Eur. J. Med. Chem.* **2020**, *201*, 112445.
- [312] Q. Z. Ye, J. Liu, C. T. Walsh, *PNAS* **1990**, *87*, 9391–9395.
- [313] E. A. Rayl, J. M. Green, B. P. Nichols, *Biochim. Biophys. Acta Protein Struct. Mol. Enzymol.* **1996**, *1295*, 81–88.
- [314] E. Procházková, J. Filo, M. Cigáň, O. Baszczyński, *Eur. J. Org. Chem.* **2020**, *2020*, 897–906.
- [315] S. B. Renwick, K. Snell, U. Baumann, *Structure* **1998**, *6*, 1105–1116.
- [316] E. Zigmund, A. Ben Ya'acov, H. Lee, Y. Lichtenstein, Z. Shalev, Y. Smith, L. Zolotarov, E. Ziv, R. Kalman, H. V. Le, H. Lu, R. B. Silverman, Y. Ilan, *ACS Med. Chem. Lett.* **2015**, *6*, 840–844.
- [317] T. M. Privalsky, A. M. Soohoo, J. Wang, C. T. Walsh, G. D. Wright, E. M. Gordon, N. S. Gray, C. Khosla, *J. Am. Chem. Soc.* **2021**, *143*, 21127–21142.
- [318] P. Le, E. Kunold, R. Macsics, K. Rox, M. C. Jennings, I. Ugur, M. Reinecke, D. Chaves-Moreno, M. W. Hackl, C. Fetzer, F. A. M. Mandl, J. Lehmann, V. S. Korotkov, S. M. Hacker, B. Kuster, I. Antes, D. H. Pieper, M. Rohde, W. M. Wuest, E. Medina, S. A. Sieber, *Nat. Chem.* **2020**, *12*, 145–158.
- [319] H. Lu, R. B. Silverman, *J. Med. Chem.* **2006**, *49*, 7404–7412.
- [320] J. Qiu, R. B. Silverman, *J. Med. Chem.* **2000**, *43*, 706–720.
- [321] H. Yuan, R. B. Silverman, *Bioorg. Med. Chem.* **2006**, *14*, 1331–1338.
- [322] A. Butrin, B. A. Beaupre, N. Kadamandla, P. Zhao, S. Shen, R. B. Silverman, G. R. Moran, D. Liu, *ACS Chem. Biol.* **2020**.
- [323] D. Liu, E. Pozharski, M. Fu, R. B. Silverman, D. Ringe, *Biochemistry* **2010**, *49*, 10507–10515.
- [324] R. Mascarenhas, H. V. Le, K. D. Clevenger, H. J. Lehrer, D. Ringe, N. L. Kelleher, R. B. Silverman, D. Liu, *Biochemistry* **2017**, *56*, 4951–4961.
- [325] M. J. Moschitto, P. F. Doubleday, D. S. Catlin, N. L. Kelleher, D. Liu, R. B. Silverman, *J. Am. Chem. Soc.* **2019**, *141*, 10711–10721.
- [326] W. Zhu, P. F. Doubleday, D. S. Catlin, P. M. Weerawarna, A. Butrin, S. Shen, Z. Wawrzak, N. L. Kelleher, D. Liu, R. B. Silverman, *J. Am. Chem. Soc.* **2020**.
- [327] G. R. Fulmer, A. J. M. Miller, N. H. Sherden, H. E. Gottlieb, A. Nudelman, B. M. Stoltz, J. E. Bercaw, K. I. Goldberg, *Organometallics* **2010**, *29*, 2176–2179.
- [328] E. C. Davison, I. T. Forbes, A. B. Holmes, J. A. Warner, *Tetrahedron* **1996**, *52*, 11601–11624.
- [329] S. Caddick, V. Delisser, V. Doyle, S. Khan, A. Avent, S. Vile, *Tetrahedron* **1999**, *55*, 2737–2754.
- [330] B. M. Trost, H. C. Shen, D. B. Horne, F. D. Toste, B. G. Steinmetz, C. Koradin, *Chemistry* **2005**, *11*, 2577–2590.
- [331] U. Groth, N. Richter, A. Kalogerakis, *Eur. J. Org. Chem.* **2003**, *2003*, 4634–4639.
- [332] J. Egger, C. Weckerle, B. Cutting, O. Schwardt, S. Rabbani, K. Lemme, B. Ernst, *J. Am. Chem. Soc.* **2013**, *135*, 9820–9828.
- [333] Y. Saito, K. Matsumoto, S. S. Bag, S. Ogasawara, K. Fujimoto, K. Hanawa, I. Saito, *Tetrahedron* **2008**, *64*, 3578–3588.
- [334] F. Himo, T. Lovell, R. Hilgraf, V. V. Rostovtsev, L. Noodleman, K. B. Sharpless, V. V. Fokin, *J. Am. Chem. Soc.* **2005**, *127*, 210–216.

- [335] T. Katoh, O. Ohmori, K. Iwasaki, M. Inoue, *Tetrahedron* **2002**, *58*, 1289–1299.
- [336] B. Witulski, U. Bergsträßer, M. Gößmann, *Tetrahedron* **2000**, *56*, 4747–4752.
- [337] E. Alicea-Matías, J. A. Soderquist, *Org. Lett.* **2017**, *19*, 336–339.
- [338] C. Sibbersen, J. Palmfeldt, J. Hansen, N. Gregersen, K. A. Jørgensen, M. Johannsen, *Chem. Commun.* **2013**, *49*, 4012–4014.
- [339] T. J. Dale, A. C. Sather, J. Rebek, *Tetrahedron Lett.* **2009**, *50*, 6173–6175.
- [340] E. J. Corey, A. Venkateswarlu, *J. Am. Chem. Soc.* **1972**, *94*, 6190–6191.
- [341] M. Quintiliani, L. Persoons, N. Solaroli, A. Karlsson, G. Andrei, R. Snoeck, J. Balzarini, C. McGuigan, *Bioorg. Med. Chem.* **2011**, *19*, 4338–4345.
- [342] M. Liebeke, K. Dörries, D. Zühlke, J. Bernhardt, S. Fuchs, J. Pané-Farré, S. Engelmann, U. Völker, R. Bode, T. Dandekar, U. Lindequist, M. Hecker, M. Lalk, *Mol. Biosyst.* **2011**, *7*, 1241–1253.
- [343] A. E. LaBauve, M. J. Wargo, *Curr. Protoc. Microbiol.* **2012**, *Chapter 6*, Unit 6E.1.
- [344] Thermo Fisher Scientific, *Gateway Cloning Protocols*, <https://www.thermofisher.com/de/de/home/life-science/cloning/gateway-cloning/protocols.html>, visited on 2022-03-07.
- [345] G. T. Höfler, E. Fernández-Fueyo, M. Pesic, S. H. Younes, E.-G. Choi, Y. H. Kim, V. B. Urlacher, I. W. C. E. Arends, F. Hollmann, *ChemBioChem* **2018**, *19*, 2344–2347.
- [346] M. H. Kunzmann, N. C. Bach, B. Bauer, S. A. Sieber, *Chem. Sci.* **2014**, *5*, 1158–1167.
- [347] J. Cox, N. Neuhauser, A. Michalski, R. A. Scheltema, J. V. Olsen, M. Mann, *J. Proteome Res.* **2011**, *10*, 1794–1805.
- [348] S. A. Shah, B. W. Shen, A. T. Brünger, *Structure* **1997**, *5*, 1067–1075.
- [349] A. K. Gandhi, J. V. Desai, M. S. Ghatge, M. L. Di Salvo, S. Di Biase, R. Danso-Danquah, F. N. Musayev, R. Contestabile, V. Schirch, M. K. Safo, *PloS one* **2012**, *7*, e40954.
- [350] A. Marabotti, P. Cozzini, A. Mozzarelli, *Biochim. Biophys. Acta Protein Struct. Mol. Enzymol.* **2000**, *1476*, 287–299.
- [351] D. Nagel, L. Wallcave, B. Toth, R. Kupper, *Cancer Res.* **1977**, *37*, 3458–3460.



# LIST OF FIGURES

---

1.1	Vitamins . . . . .	2
1.2	Vitamin B <sub>6</sub> . . . . .	3
1.3	Aldimines . . . . .	4
1.4	<b>PLP</b> Catalysis . . . . .	5
1.5	Reactions on the Substrates C <sub>α</sub> . . . . .	8
1.6	Inhibitors of <b>PLP</b> -DEs 1 . . . . .	11
1.7	Inhibitors of <b>PLP</b> -DEs 2 . . . . .	13
1.8	Activity- and Affinity-Based Probes . . . . .	17
1.9	Labelling Workflow . . . . .	18
1.10	Competitive ABPP . . . . .	20
2.1	<b>PLP</b> Derivatives . . . . .	25
2.2	Previously Synthesised Type A Derivatives . . . . .	27
2.3	Type A and Type B Derivatives . . . . .	29
2.4	Phosphoramidate Pro-Tides and Mechanism . . . . .	31
2.5	Acetal Equilibrium . . . . .	34
2.6	Phenelzine Derivatives . . . . .	40
2.7	Probe Phosphorylation . . . . .	42
2.8	Growth Studies in <i>E. coli</i> . . . . .	44
2.9	Analytical Labelling in <i>E. coli</i> . . . . .	46
2.10	Probe Phosphorylation . . . . .	47
2.11	Growth Studies with Pro-Tides in <i>E. coli</i> . . . . .	47
2.12	Analytical Labelling in HeLa Cells . . . . .	48
2.13	<b>PLP</b> ome Profiling in <i>S. aureus</i> . . . . .	52
2.14	<b>PLP</b> ome Profiling in <i>E. coli</i> . . . . .	54
2.15	<b>PLP</b> ome Profiling in <i>P. aeruginosa</i> . . . . .	56
2.16	<b>PLP</b> Loading State of Expressed Proteins . . . . .	58
2.17	UV/Vis Spectroscopy for Aminotransferase Substrate Screening . . . . .	60
2.18	MS Quantification of Aminotransferase Substrates . . . . .	61
2.19	Kinetics and MS Quantification of <i>PA2683</i> . . . . .	63
2.20	Investigation of the Transcriptional Regulator <i>ydcR</i> . . . . .	65
2.21	Activity of <i>A0A0H2XHJ5</i> . . . . .	67
2.22	Antibiotic Screen with Compound Library . . . . .	70
2.23	Competitive Labelling with Phenelzine in <i>S. aureus</i> . . . . .	73
2.24	Target Validation of Phenelzine Inhibition . . . . .	74
2.25	Competitive Labelling with Benserazide in <i>S. aureus</i> . . . . .	77
2.26	Competitive Labelling with CCG-50014 in <i>S. aureus</i> . . . . .	80
2.27	Competitive Labelling with MAC173979 in <i>E. coli</i> . . . . .	84
2.28	Spectroscopic Assay for <i>pabC</i> Target Validation . . . . .	86

---

3.1	Graphical Abstract . . . . .	90
A.1	Probe Phosphorylation of <i>S. aureus</i> PLK . . . . .	214
A.2	Probe Phosphorylation of <i>E. coli</i> PLK . . . . .	215
A.3	Additional Growth Curves of <i>E. coli</i> . . . . .	216
A.4	Growth Curves of <i>E. coli</i> , <i>P. aeruginosa</i> and <i>S. aureus</i> in CDM . . . . .	217
A.5	Additional Volcano Plots for <i>S. aureus</i> . . . . .	218
A.6	Additional Volcano Plots for <i>E. coli</i> . . . . .	219
A.7	Additional Volcano Plots for <i>P. aeruginosa</i> . . . . .	220
A.8	Additional EMSA gels . . . . .	221

# LIST OF SCHEMES

---

1.1	CPP-115 Inhibition Mechanism . . . . .	14
2.1	Synthesis Overview . . . . .	26
2.2	<b>PL2</b> Phosphoramidate Retrosynthesis . . . . .	32
2.3	The <b>PL</b> Phosphoramidate <b>PLPA</b> . . . . .	37
2.4	The <b>PL3</b> Phosphoramidate <b>PL3PA</b> . . . . .	38
2.5	Possible Side Reactions in <b>PL3PA</b> Labelling . . . . .	49
2.6	Mechanism of a Ser/Thr Dehydratase . . . . .	62
2.7	Mechanism of Cystein Desulfurases . . . . .	67
2.8	The PABA Biosynthesis . . . . .	81
2.9	Synthesis of MAC173979 and its Amine Derivative . . . . .	85





# LIST OF TABLES

---

2.1	Protective Groups for C3' in <b>PL2PA</b> Synthesis . . . . .	33
2.2	Methoxim Deprotection . . . . .	35
2.3	Acetal Deprotection . . . . .	36
2.4	List of Competed <b>PLP</b> -DE by Phenelzine . . . . .	72
2.5	List of Competed <b>PLP</b> -DE by Benserazide . . . . .	76
2.6	List of Competed <b>PLP</b> -DE by CCG-50014 . . . . .	78
2.7	List of Competed <b>PLP</b> -DE by MAC173979 . . . . .	83
4.1	List of used HPLC-gradients . . . . .	95
4.2	Buffer and Media . . . . .	162
4.3	PCR Conditions . . . . .	163
4.4	Thermocyclic Conditions . . . . .	163
4.5	Primer List . . . . .	164
4.6	Proteinexpression Conditions. . . . .	168
4.7	Bacterial Strains . . . . .	172
4.8	MS Settings . . . . .	182
4.9	MS/MS Settings . . . . .	183
4.10	List of Screen Compounds . . . . .	184
A.1	log <sub>2</sub> Enrichment Values for <i>S. aureus</i> . . . . .	222
A.2	log <sub>2</sub> Enrichment Values for <i>E. coli</i> . . . . .	224
A.3	log <sub>2</sub> Enrichment Values for <i>P. aeruginosa</i> . . . . .	227



# A

## APPENDIX

---

*Here, supplementary figures, tables and NMR-spectra of synthesised compounds are appended.*

### Contents

---

<b>A.1</b>	<b>Supplementary Figures . . . . .</b>	<b>214</b>
<b>A.2</b>	<b>Supplementary Tables . . . . .</b>	<b>221</b>
<b>A.3</b>	<b>NMR-Spectra . . . . .</b>	<b>230</b>
<b>A.4</b>	<b>Licences . . . . .</b>	<b>264</b>
<b>A.5</b>	<b>Curriculum Vitae . . . . .</b>	<b>265</b>

---

## A.1 Supplementary Figures

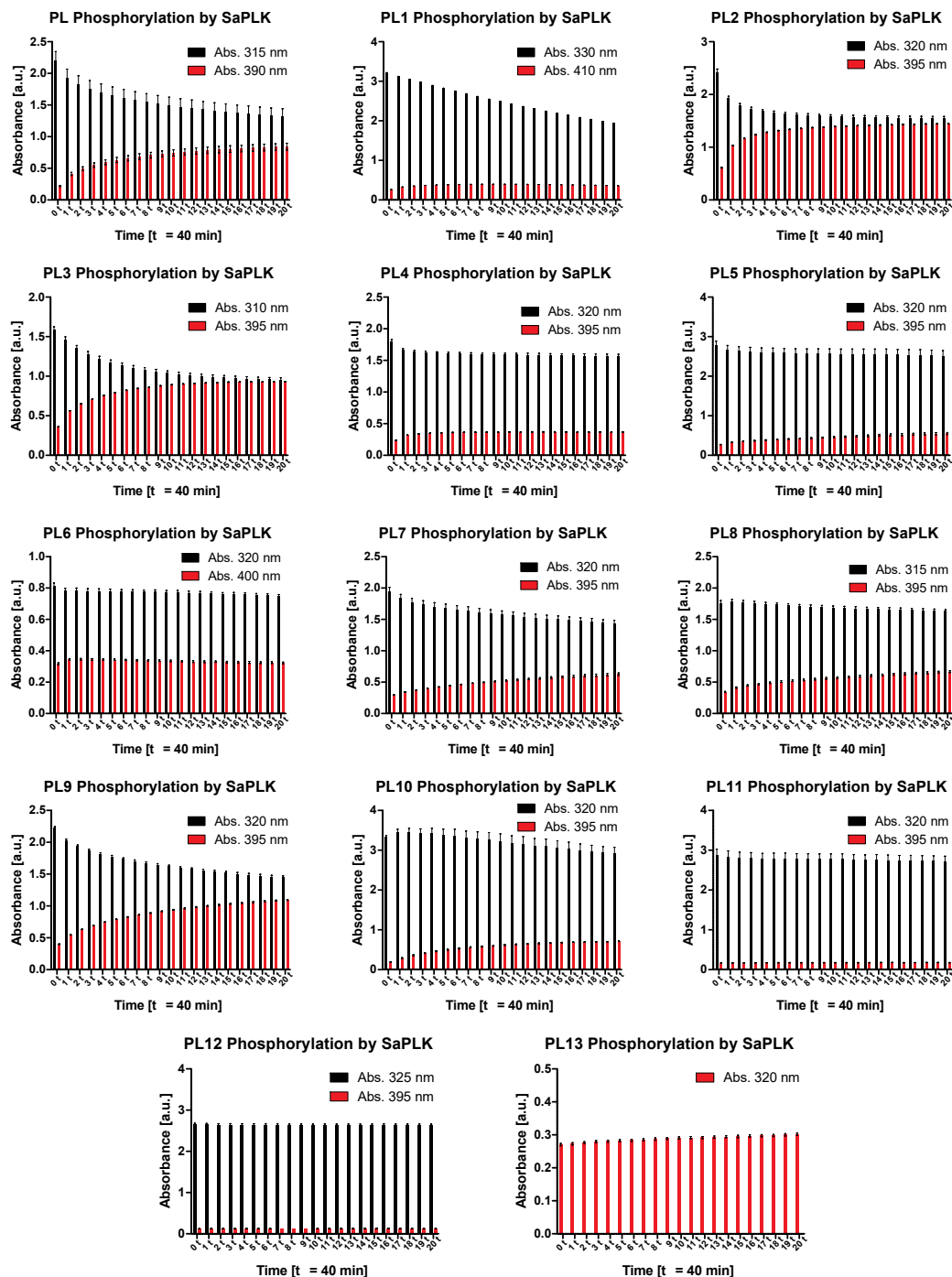


**Figure A.1:** Phosphorylation of PL probes *in vitro* by pyridoxal kinase (*S. aureus* SaPLK) were monitored by measuring UV/Vis absorbance over time (every 40 minutes, 20 cycles,  $n = 3$ , mean  $\pm$  SEM). Phosphorylated species absorb at around 395 nm. Phosphorylated **PL13** was measured at around 320 nm due to a different absorbance maximum of the phosphorylated species. Adapted from *Pfanzelt et al.*<sup>[170]</sup>

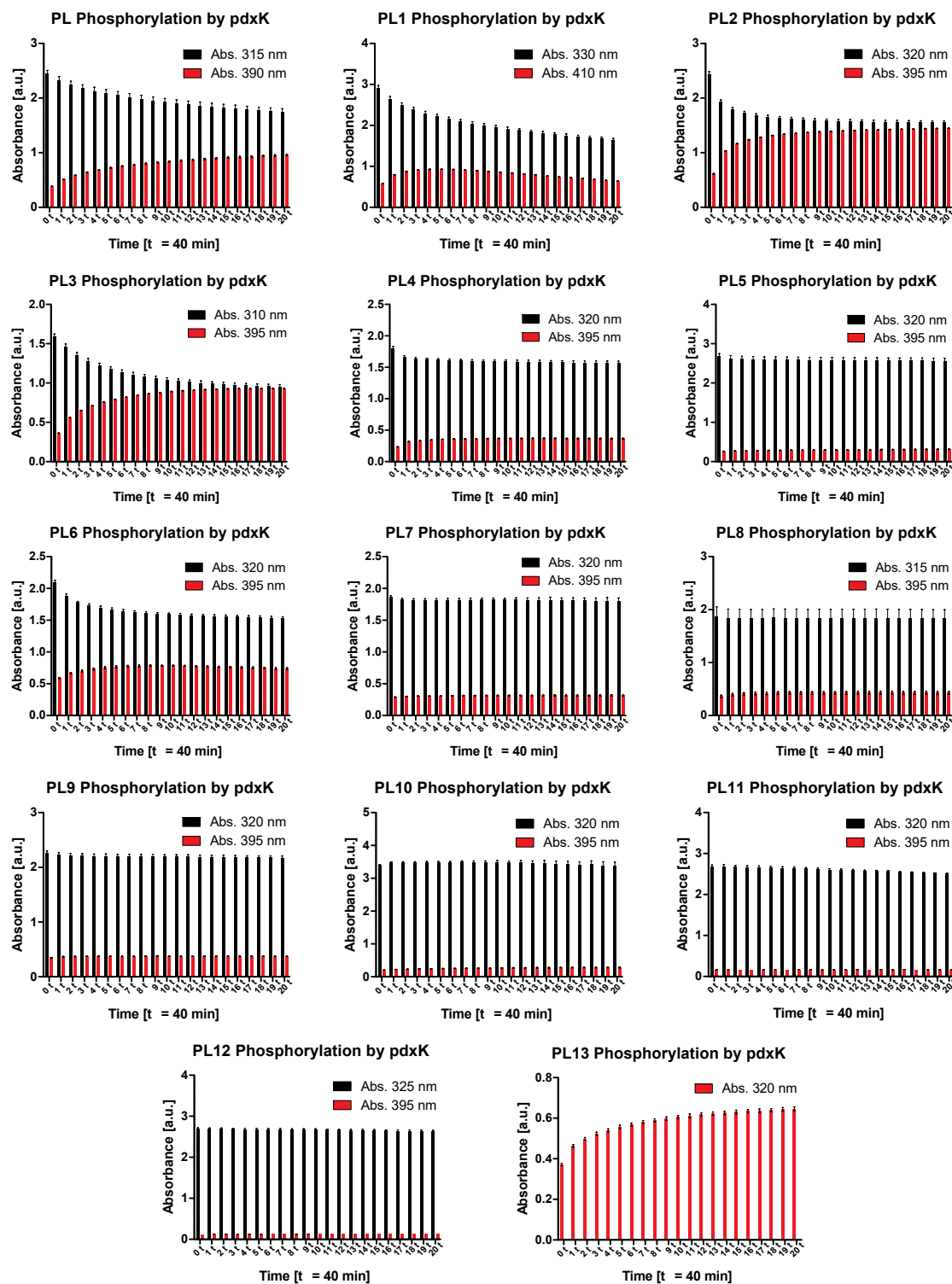


**Figure A.2:** Phosphorylation of PL probes *in vitro* by pyridoxal kinase (*E. coli pdxK*) were monitored by measuring UV/Vis absorbance over time (every 40 minutes, 20 cycles,  $n = 3$ , mean  $\pm$  SEM). Phosphorylated species absorb at around 395 nm. Phosphorylated **PL13** was measured at around 320 nm due to a different absorbance maximum of the phosphorylated species. Adapted from *Pfanzelt et al.*<sup>[170]</sup>

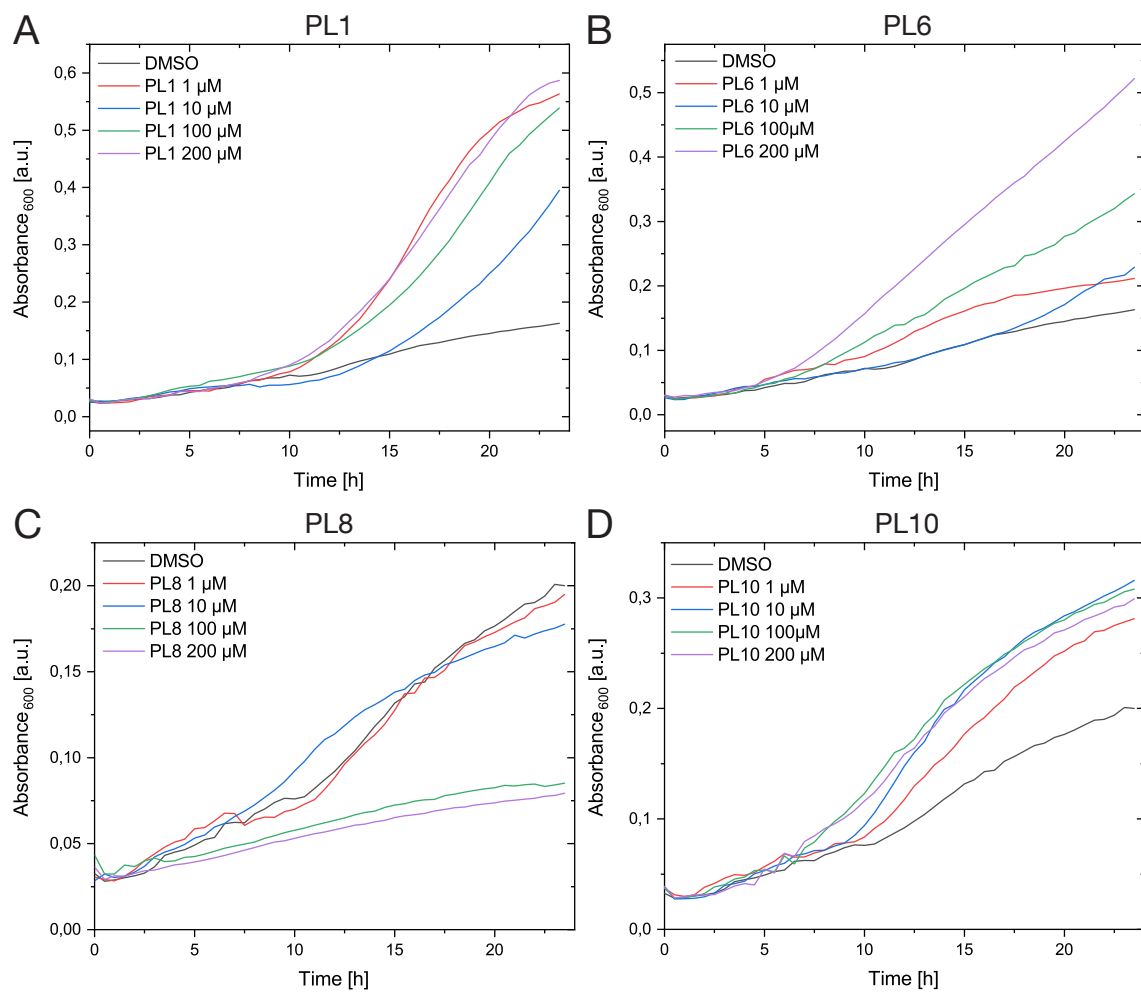


**Figure A.3:** Growth of *E. coli* K12  $\Delta$ pdxJ in CDM supplemented with different concentrations of PL1 (A), PL6 (B), PL8 (C) and PL10 (D). Adapted from Pfanzelt et al.<sup>[170]</sup>

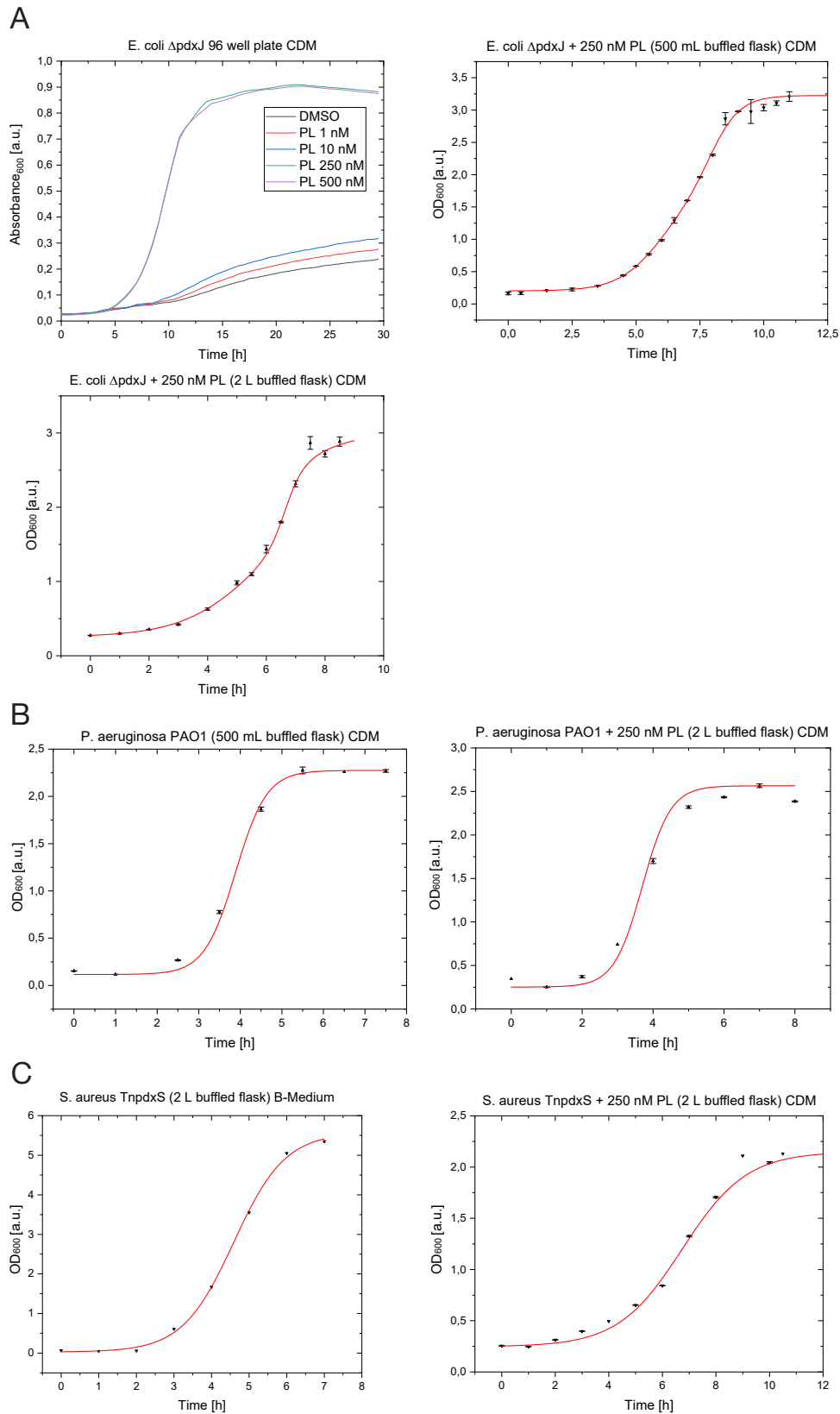


**Figure A.4:** (A) *E. coli* K12  $\Delta$ pdxJ growth curve studies. First, minimal **PL** concentration was determined for full growth in CDM. Then, growth curves in CDM (+250 nM **PL**) were monitored for 100 mL cultures in 500 mL buffered flasks and 500 mL cultures in 2 L buffered flasks. (B) For *P. aeruginosa* PAO1, growth studies in CDM (+250 nM **PL**) were performed for 100 mL cultures in 500 mL buffered flasks and 500 mL cultures in 2 L buffered flasks. (C) 500 mL *S. aureus* USA300 TnpdxS cultures in CDM (+250 nM **PL**) or B-medium were grown in 2 L buffered flasks. Adapted from Pfanzelt et al.<sup>[170]</sup>

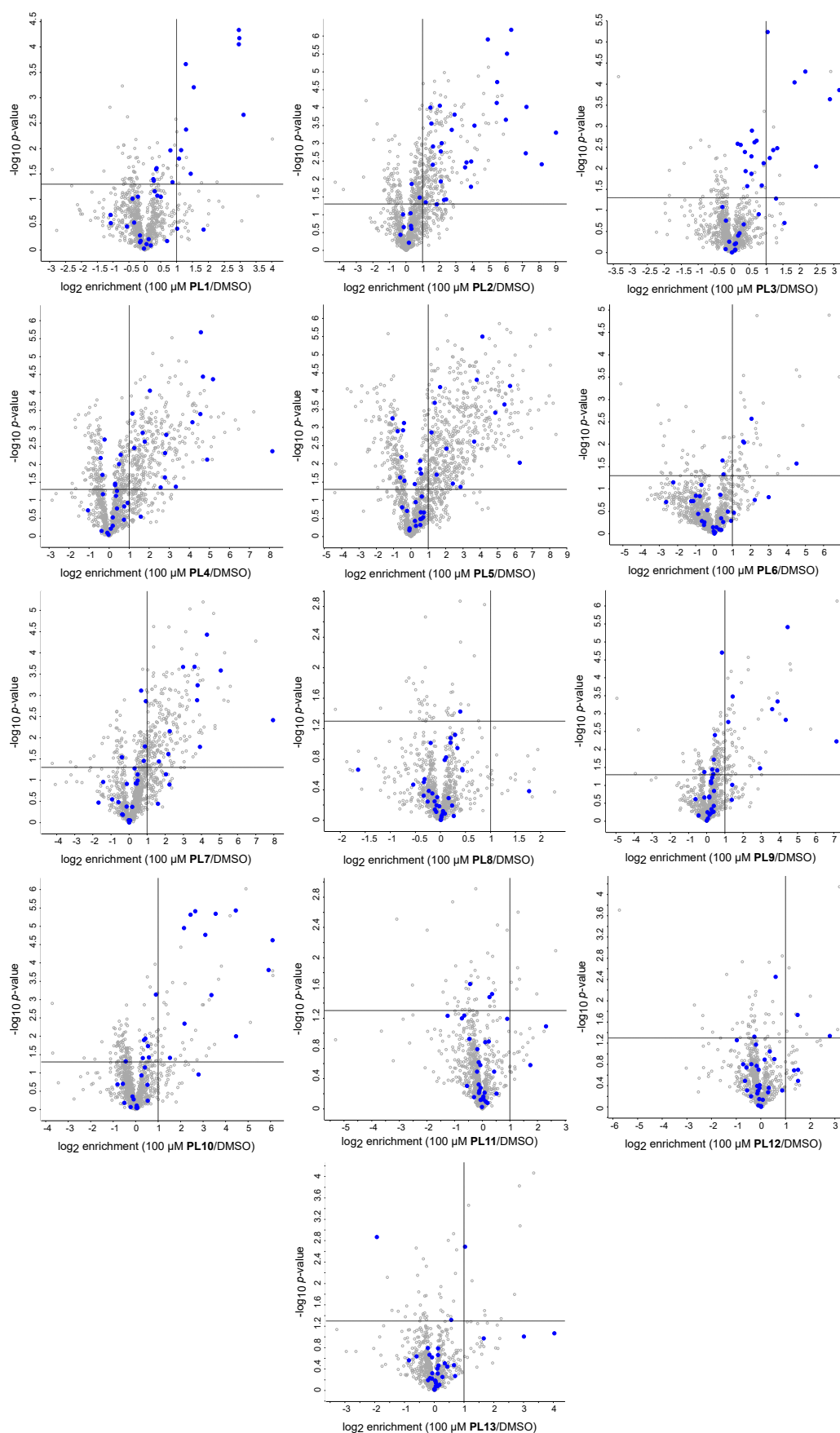


**Figure A.5:** Volcano plots for PL probe labelling in *S. aureus* USA300 TnpdxS. Proteins depicted in blue are assigned as PLP-dependent (table A.1). Adapted from Pfanzelt *et al.*<sup>[170]</sup>



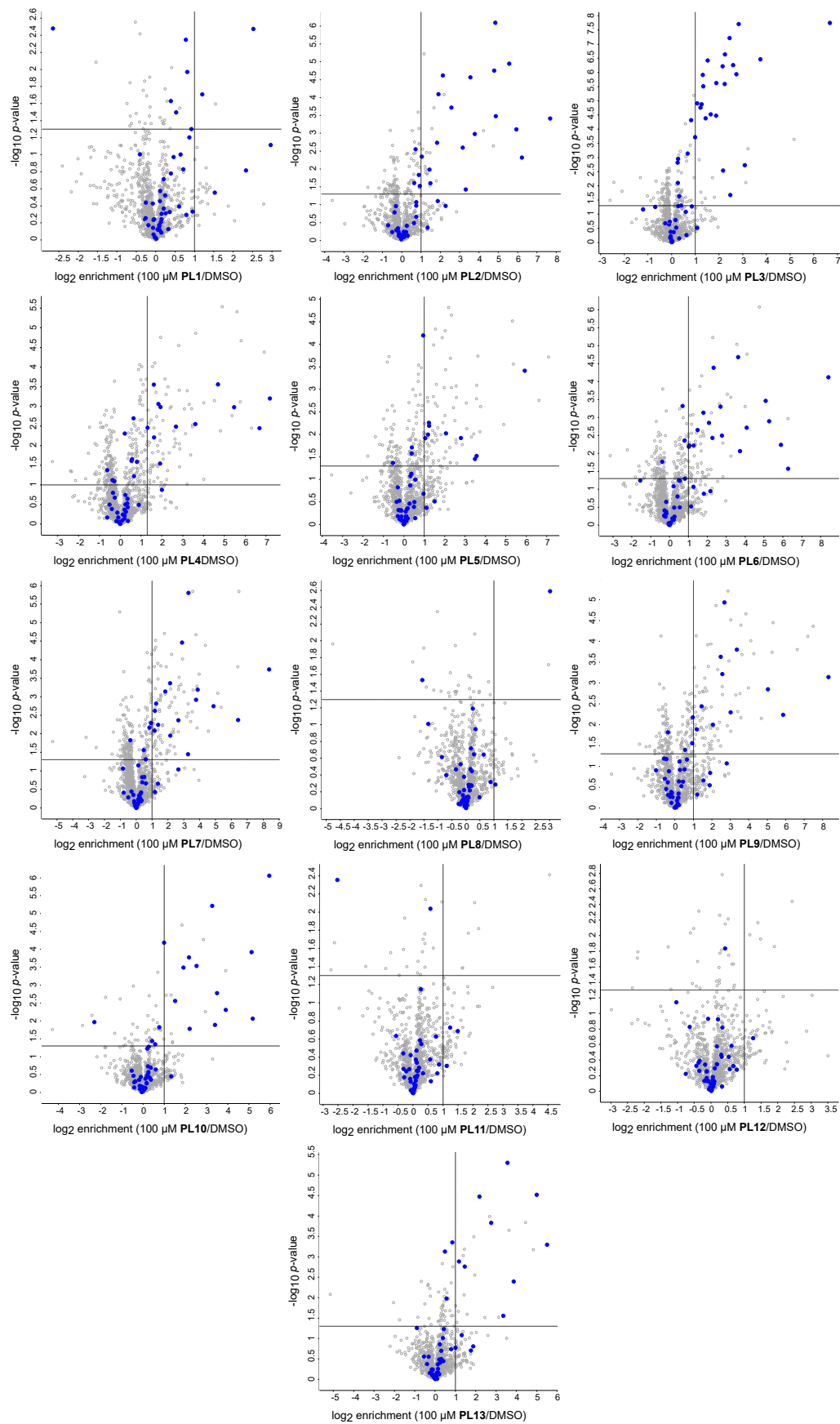


**Figure A.6:** Volcano plots for PL probe labelling in *E. coli* K12  $\Delta$ pdxJ. Proteins depicted in blue are assigned as PLP-dependent (table A.2). Adapted from Pfanzelt *et al.*<sup>[170]</sup>

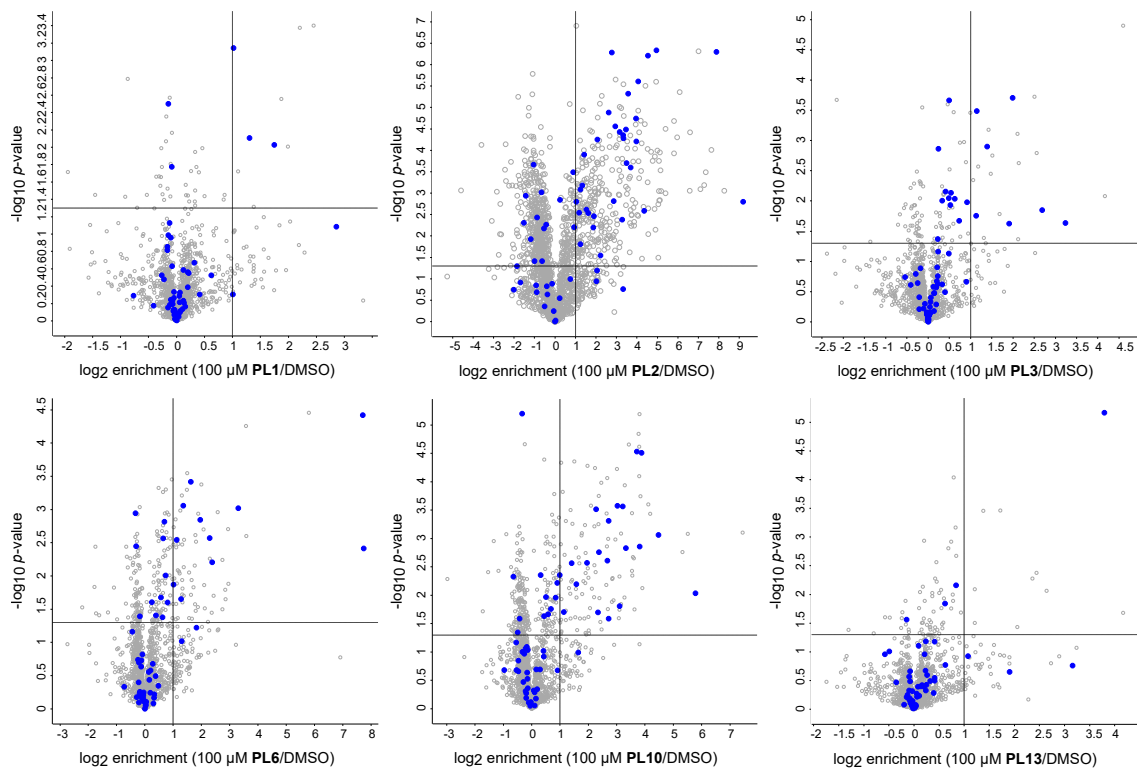


**Figure A.7:** Volcano plots for PL probe labelling in *P. aeruginosa* PAO1. Proteins depicted in blue are assigned as PLP-dependent (table A.3). Adapted from Pfanzelt *et al.*<sup>[170]</sup>

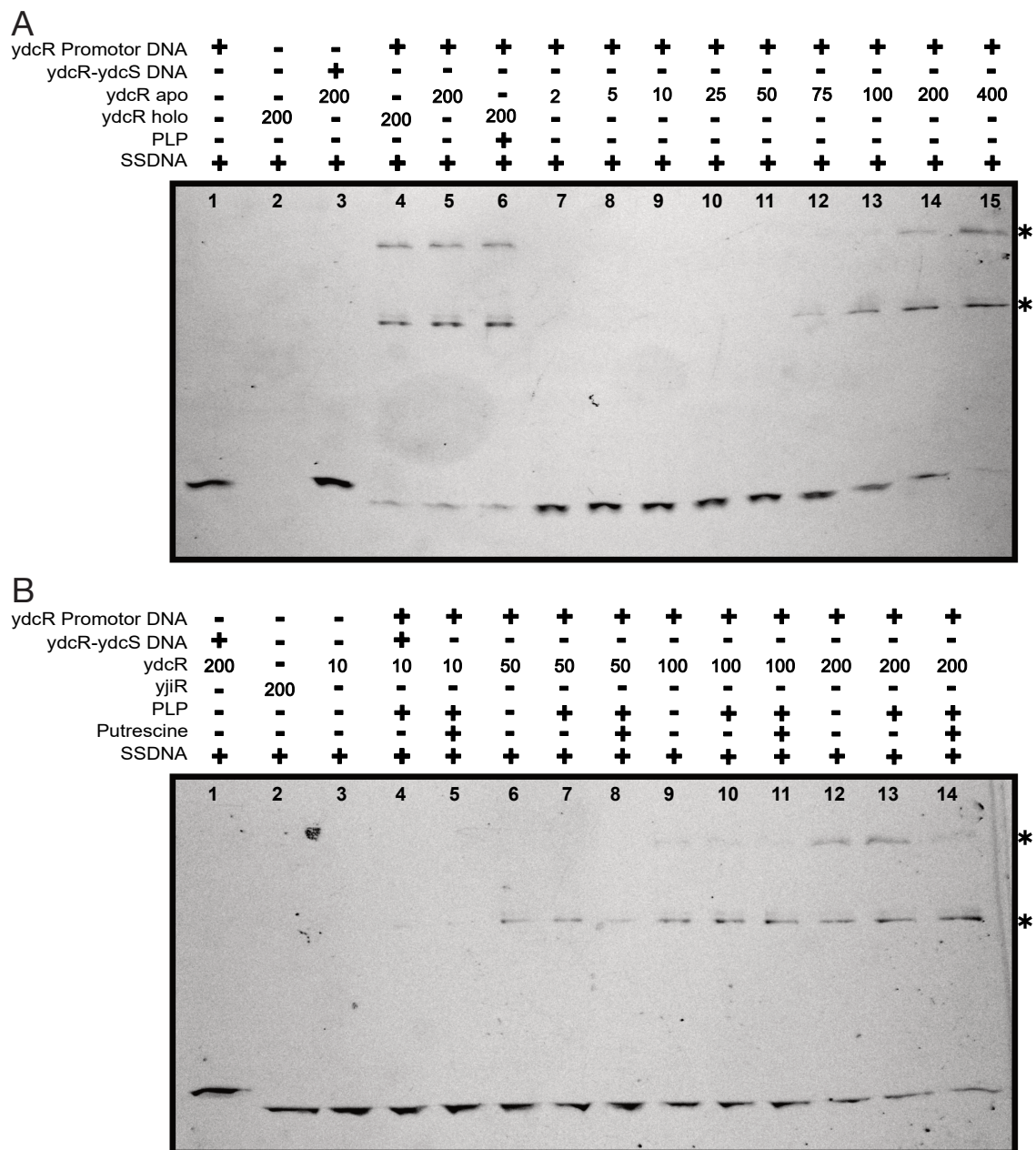


**Figure A.8:** (A) Investigation of the influence of **PLP** on the binding of *ycdR* to its promoter  $P_{ycdR}$ . Apo-*ycdR* was incubated with 100 eq hydroxylamine for 15 minutes prior to the EMSA to generate the apo-enzyme. Concentrations are given in [nM]. **PLP** was added at 10 eq. (B) Investigation of putrescine and **PLP** concentration on the binding of *ycdR* to its promoter  $P_{ycdR}$ . Concentrations are given in [nM]. **PLP** and putrescine were added at 500  $\mu$ M each. The two lines (\*) most likely correspond to different protein DNA complexes.<sup>[72]</sup> Adapted from Pfanzelt *et al.*<sup>[170]</sup>

**Table A.1:** log<sub>2</sub> enrichment (probe/DMSO) values for enrichment in *S. aureus* USA300 TnpdX. Putative, uncharacterised or poorly characterized PLP-DEs are highlighted with a \*. Adapted from Pfanzelt et al.<sup>[170]</sup>

Protein	PL1	PL2	PL3	PL4	PL5	PL6	PL7	PL8	PL9	PL10	PL11	PL12	PL13
A0A0H2XE82* (1)	–	–	–	–	–	–	–	–	–	–	–	–	–
A0A0H2XF80* (2)	-1,08414	–	0,09432	–	-0,38664	–	–	-0,11502	–	–	0,9022	1,48623	1,03155
A0A0H2XFA8* (3)	0,25965	4,91894	0,15771	4,57367	1,67137	1,63429	2,97393	0,20509	1,42732	0,04267	-0,19543	-0,00464	0,13914
A0A0H2XFB2* (4)	1,84397	0,16767	-0,18846	-0,03617	-0,52175	-2,63006	-1,70015	1,77034	0,2542	0,06352	-0,74329	-0,97785	-0,20897
A0A0H2XFD9 (5)	0,05026	5,4698	0,92426	1,67399	0,22793	1,58091	0,80045	0,00322	0,39225	0,03659	-0,12188	-0,14407	-0,14757
A0A0H2XFF8* (6)	0,6943	9,01239	0,77936	3,32377	0,69914	0,27489	-0,34338	0,26473	-0,46109	4,45942	–	-0,10962	-0,85312
A0A0H2XFH9 (7)	1,07418	4,10839	0,56717	2,03346	-0,56259	-0,87862	0,6581	0,01911	0,13771	2,64293	0,34626	0,54366	0,56523
A0A0H2XFQ3 (8)	1,44219	1,60868	1,10674	0,39134	-0,40473	-0,06312	-0,0205	0,011	0,83108	2,43423	-0,07541	-0,10177	-0,07485
A0A0H2XFR6* (9)	–	–	–	-0,09786	0,74575	–	–	–	–	–	–	–	–
A0A0H2XFY9* (10)	0,38814	7,20174	1,21086	4,89199	2,85207	0,39258	3,90895	0,2895	1,37536	-0,50516	0,51396	1,50015	0,6985
A0A0H2XG37* (11)	0,86332	6,06741	0,5819	1,1497	1,3705	0,04322	0,92263	0,0878	0,28895	2,14205	-0,13253	0,58922	0,09997
A0A0H2XG49 (12)	–	–	–	–	–	–	–	–	–	–	–	–	–
A0A0H2XG73* (13)	–	–	–	–	–	–	–	–	–	3,36617	–	–	–
A0A0H2XGP0* (14)	2,97034	7,23303	2,88196	4,67439	5,71146	0,92358	3,78551	0,16266	3,89286	6,0877	-0,65593	-0,59478	0,10394
A0A0H2XGU8* (15)	–	1,17082	–	0,73473	0,54279	–	–	–	–	0,52906	–	1,34282	–
A0A0H2XGZ5* (16)	–	2,74854	-0,18988	4,54615	5,39585	–	3,61679	–	–	–	–	–	–
A0A0H2XGZ7* (17)	-0,22195	1,83996	1,29404	2,77666	3,64382	-1,0067	2,15642	-0,19873	0,25795	-0,81604	-0,55704	-0,56564	-0,59669
A0A0H2XH24 (18)	1,2883	2,0164	1,84212	0,29437	0,20957	0,51291	0,4713	0,02074	0,43946	0,36291	-0,0226	-0,06331	0,12252
A0A0H2XHG0 (19)	–	–	–	-0,38093	–	–	–	–	–	–	–	–	–
A0A0H2XHH8 (20)	3,10404	8,15499	2,47296	8,13857	6,26825	4,51037	7,94715	0,4404	7,14618	2,79565	1,73538	1,50471	4,02898
A0A0H2XHJ5* (21)	1,53346	2,27641	2,15774	-1,06287	0,28394	-2,23184	-1,43996	0,19746	-0,62337	2,16575	0,42214	0,31981	0,42984
A0A0H2XHU6 (22)	0,30801	3,54928	0,66048	1,76843	1,1772	0,37864	1,64466	0,04942	0,58017	0,54394	0,08255	0,35441	0,11282
A0A0H2XHV8* (23)	-0,56558	2,91549	0,33737	0,49385	0,52662	-1,1468	0,30192	-0,33681	0,29632	0,43284	0,03926	-0,15556	0,00704
A0A0H2XI95 (24)	1,13634	3,90824	0,21697	2,84674	2,04555	2,22231	2,23194	0,22854	4,34528	–	–	2,79051	3,00801
A0A0H2XII6* (25)	-0,15332	6,00101	3,15812	4,15316	1,47259	2,98356	5,06614	-0,54265	3,59542	0,06757	-1,25623	-0,72271	0,16722

Protein	PL1	PL2	PL3	PL4	PL5	PL6	PL7	PL8	PL9	PL10	PL11	PL12	PL13
A0A0H2XIK4 (26)	0,3511	0,33819	0,25082	-0,23606	-0,46604	-0,78807	-0,0013	0,11117	0,0298	4,44618	0,1058	-0,05108	0,02828
A0A0H2XIR1* (27)	–	–	–	–	–	–	–	–	–	–	–	–	–
A0A0H2XIS2 (28)	2,96032	6,32416	1,3271	5,18209	4,11747	2,04804	4,29555	0,3358	4,44545	0,2528	-0,10654	0,00105	-0,16732
A0A0H2XIV3* (29)	–	3,63244	1,54046	0,7474	0,62582	1,08259	3,75021	–	0,37715	–	–	–	–
A0A0H2XJK0* (30)	-0,03317	0,32365	0,11078	0,34121	0,53002	0,01027	0,47104	-0,25801	0,14236	0,8949	-0,12884	-0,20586	-0,08189
A0A0H2XJW8* (31)	2,9582	0,26374	0,71998	-0,31942	-0,08523	-0,37004	-0,13267	0,39267	-0,13206	3,09163	-0,06648	-0,17502	0,03691
A0A0H2XJX6* (32)	1,29621	2,40061	-0,00221	0,92582	0,53751	0,49646	-0,93872	-0,31568	1,3975	-0,22389	0,18851	0,8587	0,65402
A0A0H2XK05* (33)	-1,07728	-0,33892	0,07632	0,38771	-0,09277	0,12209	-0,38331	-0,32978	0,0609	-0,57439	-0,47075	-0,40064	-1,92921
A0A0H2XKB4* (34)	0,18029	–	–	–	–	–	–	0,43603	–	–	–	–	–
A0A0H2XKI8 (35)	0,50165	3,89091	0,8738	2,56949	2,41327	–	2,03775	-0,11891	2,92699	1,52153	2,3031	–	1,65623
Q2FF15 (36)	0,36573	1,51848	1,04262	0,07867	0,26254	0,46078	0,41226	-0,06433	0,35079	0,40729	0,04821	-0,1234	0,04982
Q2FF55 (37)	0,80413	2,08203	0,37462	1,24948	-0,23586	0,74239	0,86226	-0,02319	1,17437	-0,14581	-0,06572	0,07417	0,04789
Q2FF63 (38)	1,01731	1,60416	0,56884	0,17038	0,6216	-0,53566	-0,59235	-1,64615	0,14622	0,5202	-0,3018	0,28774	0,34746
Q2FFN1 (39)	0,11804	2,08634	0,44034	2,7823	4,85744	-1,26585	2,24198	-0,23457	0,36894	5,9089	0,13014	-0,64678	0,27374
Q2FG69 (40)	-0,38989	-0,19348	0,0741	-0,43152	-0,77787	-0,7007	-0,14324	-0,08113	-0,13529	0,58117	-0,18495	-0,26679	-0,07347
Q2FGI6 (41)	-0,15851	-0,14892	0,1722	-0,34192	-0,63137	-0,67651	-0,39591	0,0441	-0,00758	0,31277	0,25354	0,14796	0,12486
Q2FGI7 (42)	0,27925	1,45725	0,39609	0,28693	-1,06872	-0,02084	0,36694	0,08008	0,22787	3,54894	0,23011	-0,00542	0,00597
Q2FH01 (43)	–	5,4445	–	1,57587	0,56103	–	1,59325	–	–	–	–	–	–
Q2FH64 (44)	–	2,12949	–	–	–	–	–	–	–	–	–	–	–
Q2FHT1 (45)	-0,136	0,28872	-0,29209	0,18082	0,57838	0,34243	0,16558	-0,0836	0,38449	-0,08831	-0,0121	-0,07426	0,01011
Q2FIR7 (46)	-0,33916	0,80627	-0,09147	0,57352	3,79416	-0,56243	0,05515	-0,16487	0,23725	-0,45107	-0,44557	-0,39551	-0,21629
Q2FKE3 (47)	–	–	–	–	–	–	–	–	–	–	–	–	–
Q2FKF1 (48)	–	–	–	–	–	–	–	–	–	–	–	–	–

**Table A.2:** log<sub>2</sub> enrichment (probe/DMSO) values for enrichment in *E. coli* K12 ΔpdxJ. Putative, uncharacterised or poorly characterized **PLP**-DEs are highlighted with a \*. Adapted from *Pfanzelt et al.*<sup>[170]</sup>

Protein	PL1	PL2	PL3	PL4	PL5	PL6	PL7	PL8	PL9	PL10	PL11	PL12	PL13
adiA (1)	–	3,77605	2,16488	3,5999	–	4,07095	3,7636	–	1,89969	–	–	–	–
alaA (2)	-0,05841	-0,28359	0,24267	-0,40858	-0,00548	-0,29424	-0,10791	-0,36247	-0,54974	-0,45286	-0,32564	-0,15729	-0,16233
alaC (3)	2,96456	1,20979	-0,27544	1,48379	1,09582	6,27226	1,16842	-0,26096	0,07501	-0,06246	0,59061	-0,7597	0,09895
alr (4)	-2,65317	3,14694	2,59375	2,67323	2,06293	2,76396	2,65239	-1,56388	2,0485	-2,29761	-2,52841	-1,03863	-0,54796
argD (5)	-0,0203	-0,45666	0,26912	1,93292	1,04638	-0,18254	0,37062	0,08641	2,56428	0,03024	0,09139	0,00745	0,13031
arnB (6)	–	–	–	–	–	–	–	–	–	–	–	–	–
aspC (7)	0,77569	3,54728	2,23612	0,53734	0,38024	3,62542	1,17758	0,24448	0,23921	3,26363	0,25732	0,20374	2,17955
astC (8)	0,25484	-0,15071	0,58774	-0,35119	0,09345	-0,05496	-0,3006	0,20058	-0,38936	0,30595	0,05794	0,30156	-0,04734
avtA (9)	0,45859	0,87522	0,67171	0,20578	-0,3538	0,48393	0,35876	-0,01748	0,64917	0,2168	-0,014	-0,13155	0,14395
bioA (10)	–	–	–	–	–	–	–	–	–	–	–	–	–
bioF (11)	–	–	–	–	–	–	–	–	–	–	–	–	–
cadA (12)	0,19853	1,47026	-1,20452	1,90305	0,11306	1,25257	2,1473	-0,04689	-0,18503	-0,41995	-0,30007	-0,19803	-0,06552
csdA (13)	–	–	1,07739	–	–	–	0,28864	–	–	–	0,32721	–	1,00418
cysK (14)	0,14693	1,82482	1,64858	0,34365	-0,19665	0,8085	0,50424	-0,11221	1,44711	0,36157	0,32721	0,0141	-0,07134
cysM (15)	2,51545	4,86738	3,74626	4,69114	0,51488	5,08407	3,86551	-0,12803	3,01287	-0,15118	0,56826	0,52792	0,78899
dadX (16)	0,10414	0,74322	0,3923	0,26596	-0,26896	0,52889	0,24467	0,62865	0,14905	0,37421	0,00773	0,06764	-0,40444
dcyD (17)	0,5261	0,24962	2,14512	-0,13773	-0,2257	1,03523	0,82	-0,19436	-0,16201	1,8998	0,0875	0,11217	4,9848
dsdA (18)	0,91984	0,30446	1,42757	0,88665	-0,29641	0,14592	-0,79822	-0,86328	0,21295	-0,16604	-0,05156	-0,06331	0,40213
epmB (19)	–	–	-0,697	–	–	–	–	–	–	–	–	–	2,75357
gabT (20)	0,09015	-0,17502	0,15882	-0,02069	0,03134	0,00803	0,135	0,08386	0,10654	0,16552	0,11	0,17059	0,05731
gadA (21)	0,13219	0,09329	-0,0712	0,12221	0,18505	-0,02751	0,17603	0,13495	0,34897	0,19193	-0,01579	0,07403	0,03967
gadB (22)	0,01455	-0,039	-0,0829	0,08795	0,11552	-0,04806	0,07497	0,05218	0,53805	0,09989	0,04275	-0,13242	-0,11466
gcvP (23)	0,07205	-0,19994	-0,04263	-0,03179	-0,1172	-0,21718	0,14982	0,18308	-0,22401	-0,0506	0,05765	0,07872	0,24034
glgP (24)	0,14908	0,92874	-0,1162	0,23985	0,0606	0,23601	0,01243	0,28473	-0,13325	0,25759	0,19642	0,17647	0,29828
glyA (25)	0,2051	2,12463	0,82052	1,60491	0,38351	1,78881	2,13055	0,17336	0,96142	0,25952	0,03251	0,04626	0,07132

Protein	PL1	PL2	PL3	PL4	PL5	PL6	PL7	PL8	PL9	PL10	PL11	PL12	PL13
hemL (26)	0,11152	-0,30588	-0,01222	-0,37113	-0,02883	-0,3982	-0,37543	-0,07381	-0,33051	0,19502	0,00922	0,05712	0,12743
hisC (27)	-0,04189	0,70694	0,2531	0,20994	0,00851	0,20851	0,13756	-0,0727	2,67599	0,99654	0,08803	-0,01695	0,47907
ilvA (28)	0,86356	2,56197	1,33491	0,56674	0,55725	1,27395	0,59603	0,1066	0,18587	0,76776	-0,07721	0,01865	0,23703
ilvE (29)	0,04728	0,8116	1,07396	0,86586	0,30926	0,52982	0,92924	0,04558	0,93287	0,56776	-0,00343	-0,037	1,17442
iscS (30)	0,81009	0,63837	1,26438	0,24885	0,3231	0,78506	0,47028	0,16016	0,20431	2,16938	0,06846	0,33864	0,4292
kbl (31)	0,70923	0,28807	1,30885	-0,06667	-0,11578	2,26237	0,1067	-0,23509	-0,26323	-0,05284	-0,23107	-0,34587	-0,14731
ldcC (32)	1,51926	6,22528	3,08163	6,67522	3,48656	5,88863	6,4106	1,05398	5,8537	1,33254	0,80595	0,33171	1,757
ltaE (33)	-0,25659	0,10068	-0,00275	-0,09985	-0,17301	-0,03406	-0,19332	-0,05834	-0,01091	-0,02623	0,1088	0,06909	-0,16069
lysA (34)	0,20636	4,78546	2,24716	1,62301	0,14356	2,08308	1,37017	0,08026	1,17941	-0,0785	-0,09748	-0,18021	0,00457
malP (35)	0,09185	0,74847	-0,04988	0,33364	0,27843	0,41273	0,1584	0,03927	0,16638	0,1006	0,27335	0,04885	0,05646
malY (36)	2,32845	3,30828	0,84771	–	1,50544	3,72664	0,38362	–	1,20154	0,60523	–	0,55577	3,34993
metB (37)	0,38925	4,84031	0,31856	0,63813	0,08622	2,32491	2,8757	0,09864	-0,20054	5,95928	0,57487	0,41756	0,55484
metC (38)	0,78562	2,26592	1,21685	1,99551	3,55889	2,14862	3,25607	0,87641	1,54293	5,17224	0,86423	0,76817	1,86785
pabC (39)	–	0,74603	1,86694	-0,51456	–	-0,04015	–	–	–	–	–	–	–
patA (40)	–	–	–	–	–	–	–	–	–	–	–	–	–
puuE (41)	-0,40892	-0,3845	0,19141	-0,6352	-0,54179	-0,27135	-0,83494	0,00313	-0,59221	-0,18773	-0,12992	-0,07783	-0,31806
selA (42)	0,94652	5,93252	1,87896	5,46203	2,79057	5,2626	4,86837	-0,19403	5,02598	3,90719	1,23625	1,25929	3,85745
serC (43)	0,63612	1,42404	0,9872	0,20112	0,02031	0,07001	0,26006	-0,01894	0,19872	1,51399	0,00566	0,08732	0,03444
speA (44)	-0,07461	0,54063	-0,04963	2,80382	0,9368	0,6822	3,28603	0,02142	-0,3741	-0,10645	-0,07822	-0,09224	0,8448
speC (45)	-0,06077	-0,04048	0,07583	-0,00479	-0,3052	-0,18735	-0,02844	0,2123	0,27154	0,10611	0,12449	0,00426	0,20385
speF (46)	–	–	–	–	–	–	–	–	–	–	–	–	–
sufS (47)	0,38689	1,0337	1,51751	-0,28198	0,09508	-0,22784	-0,13155	0,03237	-0,46951	0,03655	0,12717	0,01412	0,14103
tdcB (48)	0,32165	-0,72168	–	-0,19115	0,48518	-1,56231	-0,51108	-1,3492	-1,02081	-0,42225	-0,0754	-0,35293	-0,8989
tdcF (49)	-0,2919	0,2162	0,62266	0,19704	0,18292	0,24959	-0,09047	-0,1468	-0,48337	-0,54494	-0,56514	-0,63949	-0,26278
thrC (50)	0,3569	0,10776	6,67365	0,65027	1,18091	-0,00746	0,29842	-0,02331	0,43295	-0,0833	0,16448	-0,13199	0,07431
tnaA (51)	-0,02476	0,30762	0,27331	0,79921	1,23932	2,69557	1,15177	-0,03325	0,52247	0,16146	0,14665	0,09885	0,29532
trpB (52)	0,24009	5,56203	2,44409	1,83246	1,22585	1,01478	1,82819	-0,02474	2,47655	2,52427	0,02513	-0,11815	1,45314

Protein	PL1	PL2	PL3	PL4	PL5	PL6	PL7	PL8	PL9	PL10	PL11	PL12	PL13
tyrB (53)	0,10598	1,89819	2,82859	1,30526	0,37095	1,48013	1,24514	0,33821	3,34635	0,42197	0,111	0,17127	3,5521
wecE (54)	0,14297	1,86216	2,72861	-0,62638	0,55494	1,80855	2,65679	0,48061	2,80288	3,39486	1,49007	0,66464	1,30259
ybdL (55)	1,19739	0,61846	0,31913	–	0,95921	1,12839	0,33693	–	–	5,12839	0,75904	-0,44133	0,19442
ycbX* (56)	-0,07375	-0,07185	0,01966	-0,26851	-0,12191	-0,18387	6,19E-04	-0,09431	-0,38147	0,23133	0,2309	0,31761	0,38056
ydcR* (57)	–	–	–	–	–	–	–	–	1,87603	3,48933	–	–	–
ygeX (58)	–	–	–	–	–	–	–	–	–	–	–	–	–
yggS (59)	0,60256	7,68042	2,47062	7,17712	5,92414	8,40229	8,36773	3,0087	8,30433	2,19379	1,12036	0,60896	5,498
yhfS* (60)	–	–	–	–	–	–	–	–	–	–	–	–	–
yhfX* (61)	–	–	–	–	–	–	–	–	–	–	–	–	–
yiiM* (62)	-0,26223	-0,15132	0,01247	0,36017	-0,20599	0,21857	0,60709	-0,71043	0,0519	-0,36917	-0,32284	-0,37464	-0,13935
yjiR* (63)	–	–	–	–	–	–	–	–	–	–	–	–	–



**Table A.3:**  $\log_2$  enrichment (probe/DMSO) values for enrichment in *P. aeruginosa* PAO1. Putative, uncharacterised or poorly characterized **PLP**-DEs are highlighted with a \*. Adapted from Pfanzelt *et al.*<sup>[170]</sup>

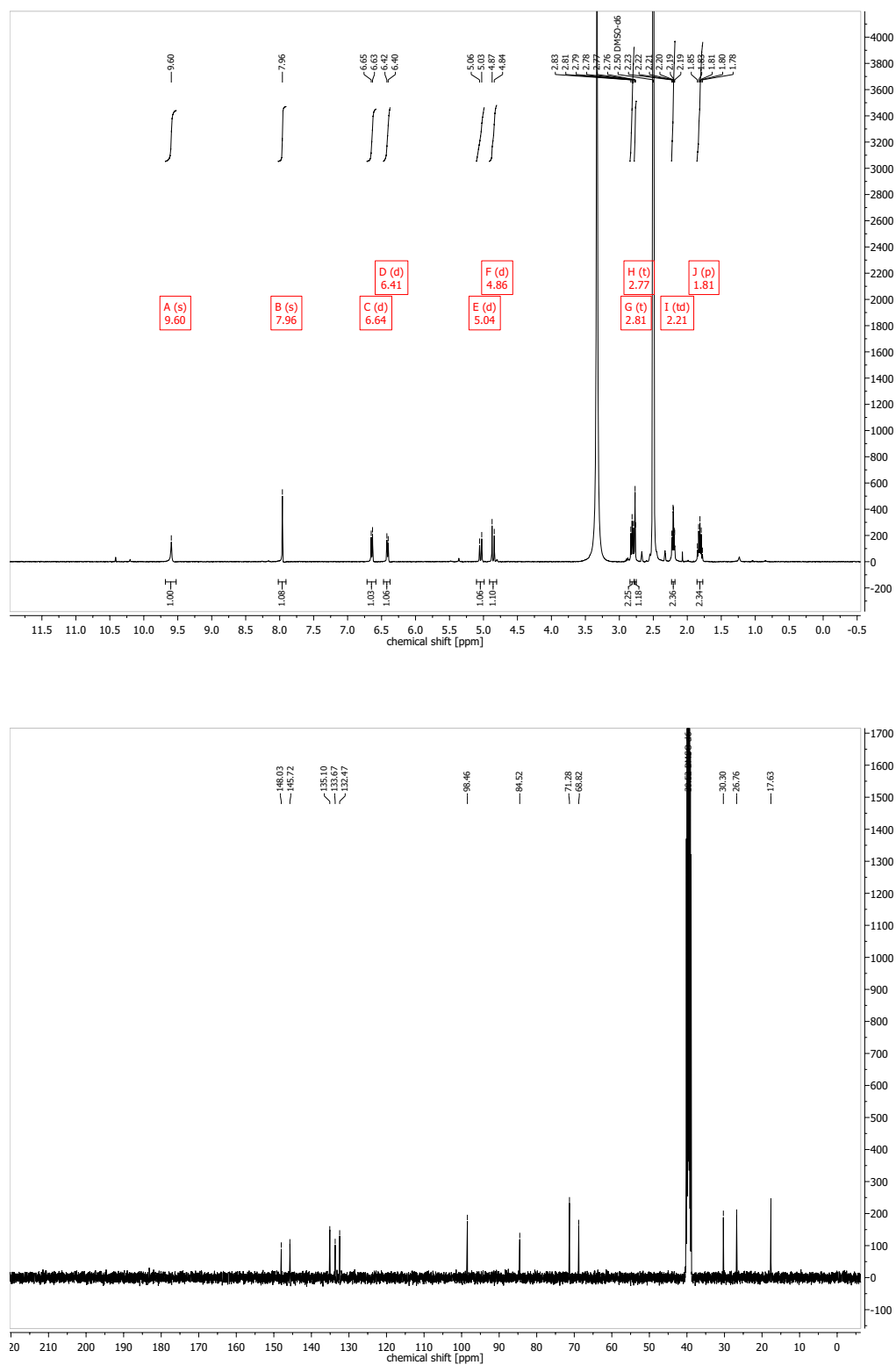
Protein	PL1	PL2	PL3	PL6	PL10	PL13
alr (1)	-0,16815	-0,66912	0,00101	0,03059	-0,64842	-0,58481
arnB (2)	–	3,27877	3,23667	1,81675	3,09822	–
aruC (3)	0,01932	-0,43569	-0,10567	-0,13914	-0,16901	-0,02996
aruH (4)	0,0596	0,92124	0,32619	0,27009	3,70337	0,83621
aspC (5)	-0,10748	1,22951	0,22697	-0,04356	0,98695	-0,10197
bauA (6)	-0,76929	-0,92811	-0,18488	-0,29373	-0,29602	-0,35666
bioA (7)	-0,01476	3,15613	0,51835	1,35033	3,87506	0,22646
cobC (8)	–	-0,8944	-0,2112	0,29277	–	–
csd (9)	-0,05418	-1,00397	0,39407	-0,24724	-0,26143	-0,02942
cysK (10)	0,0563	-0,1456	0,04647	-0,09225	0,16138	0,04843
cysM (11)	-0,07683	0,22401	0,20868	-0,06056	-0,42662	-0,052
dadX (12)	1,0176	4,53438	1,12851	1,95851	0,09589	0,32168
davT (13)	-0,15201	0,235	0,02809	-0,18007	-0,14998	-0,09815
dsdA (14)	0,03316	-0,4136	-0,03529	-0,0997	-0,218	-0,03632
gcvP1 (15)	-0,02184	-1,52035	0,0448	-0,11307	-0,47126	-0,01963
gcvP2 (16)	0,1956	-1,86268	-0,29068	0,1984	-0,10745	-0,49451
glgP (17)	–	-0,00889	–	0,33352	–	–
glyA1 (18)	-0,41106	4,34592	-0,00714	1,29759	1,64053	-0,20341
glyA2 (19)	0,04714	2,94149	0,22602	0,56561	0,9026	-0,03773
hemL (20)	-0,08616	-1,05592	0,05933	-0,33539	-0,34011	-0,08064
hisC1 (21)	0,19946	1,32696	-0,03684	0,04454	0,43291	0,13262
hisC2 (22)	–	–	–	–	–	–
ilvA1 (23)	-0,01289	1,03281	-0,01432	-0,04007	0,09776	0,01839
ilvA2 (24)	–	3,32546	–	–	–	3,15457
ilvE (25)	-0,02494	3,34234	0,91617	1,61583	0,06765	0,2092
iscS (26)	-0,1474	1,41719	0,40887	0,38238	0,50429	-0,15443
kynU (27)	-0,04626	-0,88817	-0,08224	-0,31845	-0,1472	-0,08308
ldcA (28)	-0,03118	2,85493	0,73031	2,37394	-0,19648	-0,01916
ltaE (29)	0,31529	0,01862	0,14549	0,01814	-0,33108	0,1929
lysA (30)	0,11806	4,05411	0,48495	0,63975	0,57108	0,07157
metY (31)	0,00415	1,88927	0,18785	-0,10065	1,12687	-0,04386
metZ (32)	-0,07313	3,48521	0,12321	0,7971	3,20468	0,40957
PA0221* (33)	–	–	–	–	–	–
PA0268* (34)	–	–	–	–	–	–
PA0394 (35)	1,74479	7,88023	1,90571	7,70313	2,2749	3,79348
PA0399* (36)	-0,16847	2,055	1,14543	0,13523	2,36552	0,0334
PA0400* (37)	-0,03986	3,68675	0,32593	0,24082	3,01691	0,23155
PA0529* (38)	–	–	–	–	–	–
PA0530* (39)	–	–	–	–	–	–

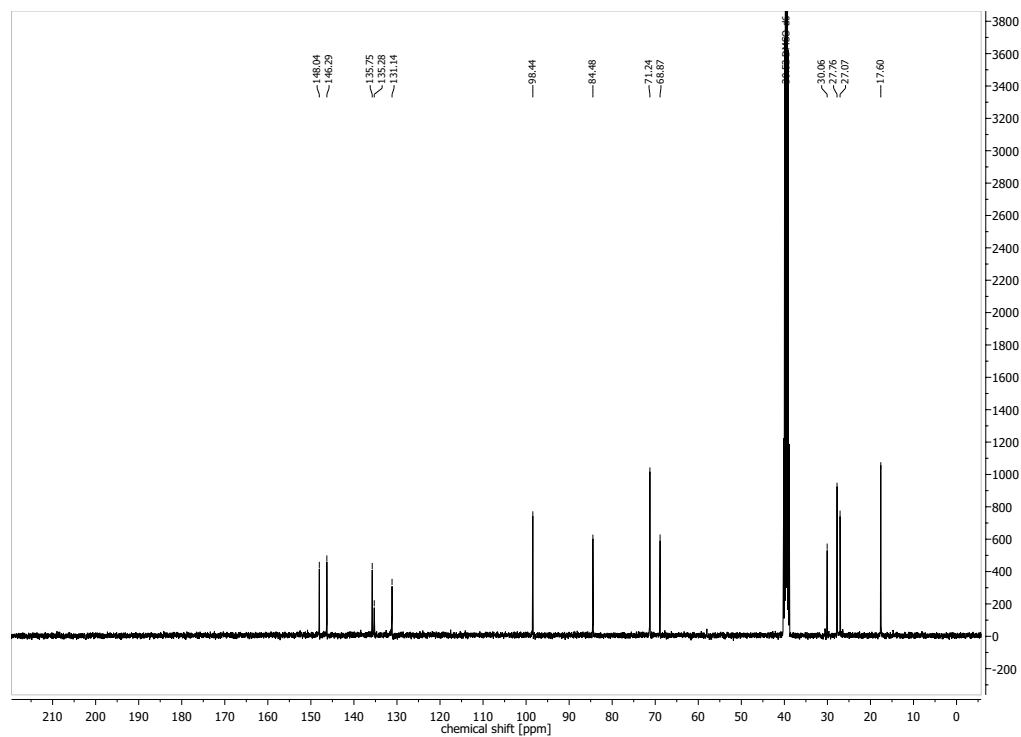
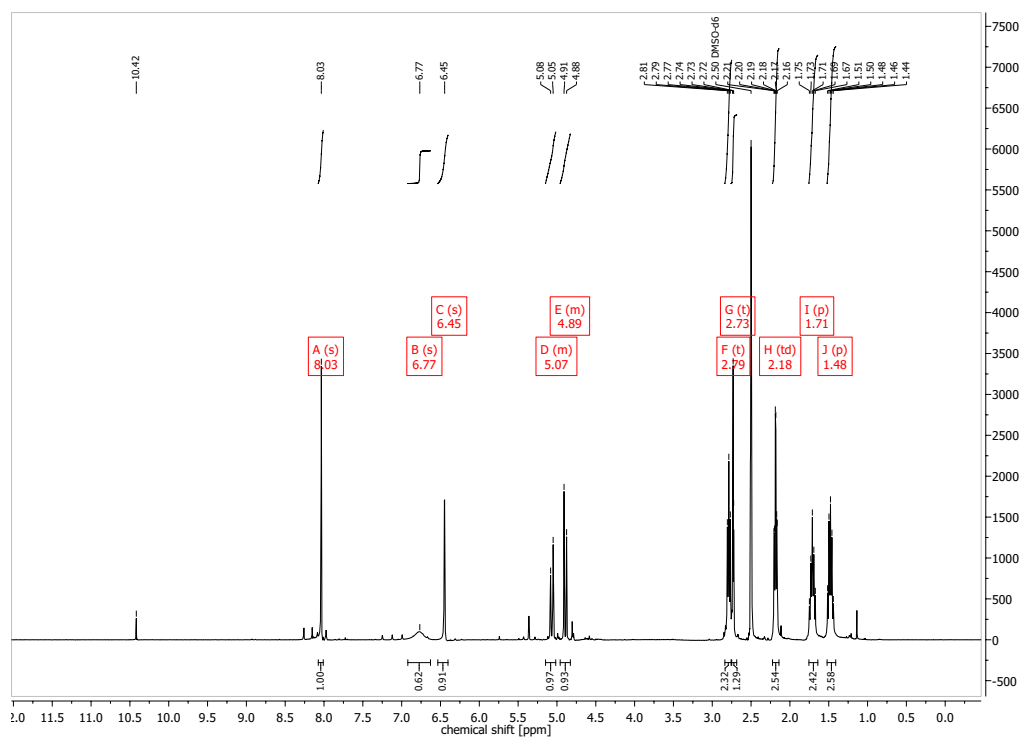
Protein	PL1	PL2	PL3	PL6	PL10	PL13
PA0813* (40)	–	–	–	–	-0,54108	–
PA0851* (41)	0,6207	2,0508	-0,5436	0,46907	0,90357	1,07339
PA0902 (42)	0,05155	-0,07439	-0,03397	-0,21151	-0,22254	0,00878
PA1061* (43)	-0,26964	-0,64178	0,48083	-0,22806	-0,55622	-0,14863
PA1346* (44)	–	–	–	–	–	–
PA1654* (45)	0,10465	-1,69945	-0,4161	-0,17814	-0,97283	0,22948
PA2032* (46)	0,4095	2,01835	0,90083	0,31811	2,33683	0,40828
PA2062 (47)	–	–	–	–	–	–
PA2100* (48)	–	2,21657	–	–	2,70976	–
PA2104* (49)	–	–	–	–	–	–
PA2229* (50)	–	–	–	–	–	–
PA2531* (51)	–	–	–	–	–	–
PA2683* (52)	1,00465	1,51816	0,05199	0,61376	0,29305	0,24182
PA2828* (53)	-0,08198	0,87961	-0,00274	-0,07697	-0,03392	0,09776
PA2897* (54)	–	–	–	–	3,32392	–
PA2958* (55)	1,30304	-0,51847	0,13924	-0,21715	4,47515	0,38595
PA3022* (56)	-0,15375	1,23315	0,20113	0,18334	-0,05398	0,40938
PA3659* (57)	0,13102	3,96187	0,13903	1,12221	0,83921	0,2585
PA3798* (58)	-0,02926	-0,54025	0,0402	-0,05767	1,40585	-0,02507
PA4088* (59)	–	–	–	–	–	–
PA4132 (60)	-0,04194	-0,38379	-0,24826	-0,13591	0,14489	0,02965
PA4165* (61)	–	–	–	–	–	–
PA4536* (62)	–	–	–	–	–	–
PA4715* (63)	-0,10224	3,45152	0,62657	2,28252	0,1871	-0,08757
PA4722 (64)	-0,22994	-1,44068	0,0092	-0,44762	-0,49604	-0,08079
PA4805* (65)	–	–	–	–	–	–
PA4875* (66)	–	–	–	–	–	–
PA5283* (67)	–	–	–	–	3,80607	–
PA5313* (68)	0,15271	0,74454	0,00118	0,37663	2,66955	0,62165
PA5431* (69)	–	–	–	–	–	–
PA5523* (70)	0,06097	-2,02042	0,18645	-0,73592	-0,19936	0,15453
pabC (71)	–	1,86076	–	–	–	–
phhC (72)	-0,0572	1,61292	-0,01181	0,15731	0,67934	0,02572
phnW (73)	–	–	–	–	1,94571	–
pvdH (74)	–	–	–	–	–	–
pvdN (75)	-0,01682	-1,18374	-0,21261	-0,19103	-0,47165	-0,07739
selA (76)	2,85092	9,17781	2,68217	7,73476	5,7718	1,90309
serC (77)	0,11834	1,16653	0,23289	-0,00196	0,41291	-0,09932
speA (78)	0,03074	0,32425	0,22166	1,27054	0,63761	0,03222
speC (79)	-0,08091	3,57223	0,48798	1,01293	0,22675	0,05431
spuC (80)	-0,04864	2,76178	0,24016	0,73384	0,31613	0,08904
thrC (81)	-0,0357	2,61586	1,98533	-0,13058	0,28814	-0,04355
trpB (82)	-0,12115	4,9452	1,39072	0,6838	1,57185	-0,13414

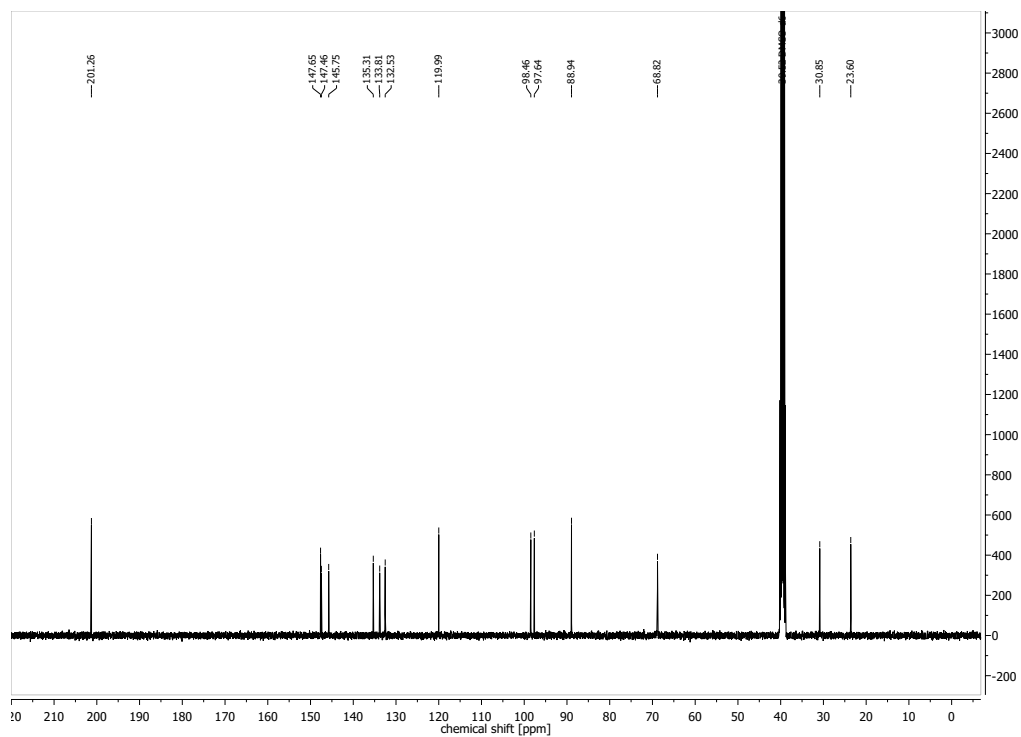
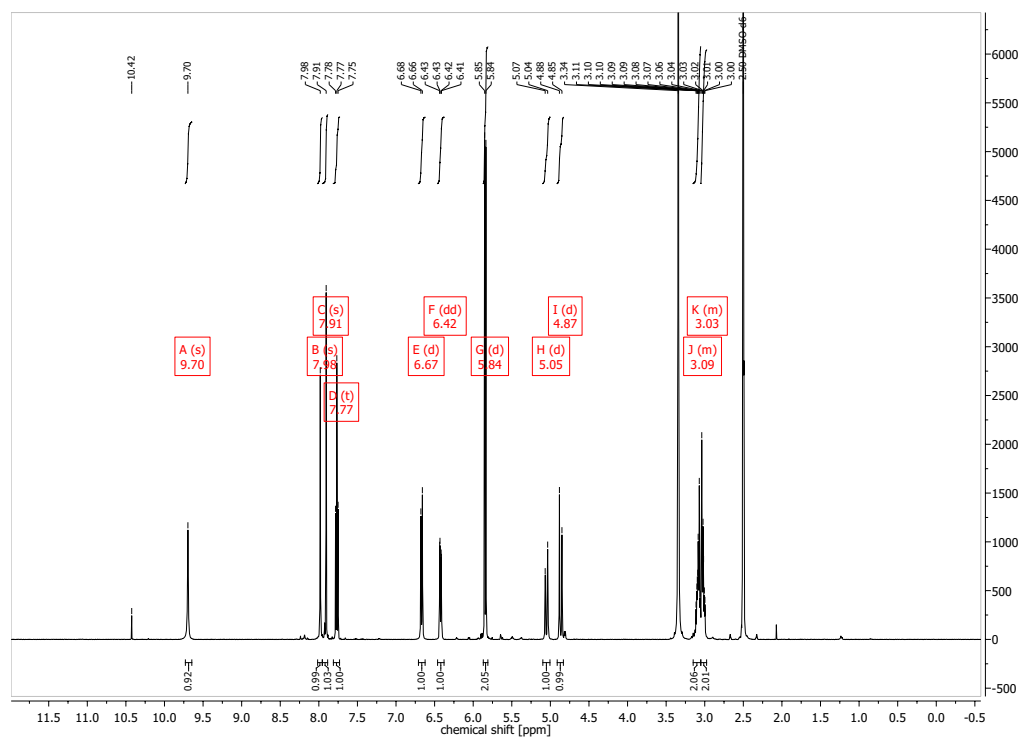
---

Protein	PL1	PL2	PL3	PL6	PL10	PL13
wbpE (83)	0,2145	3,95289	0,53482	3,30369	2,70911	0,61301

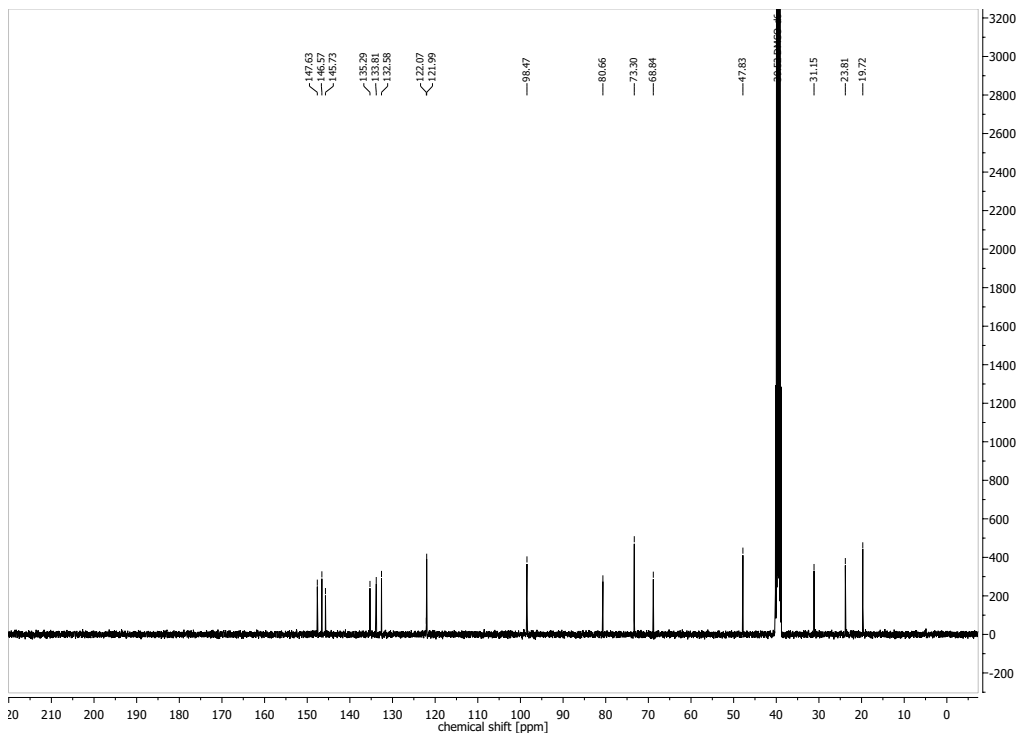
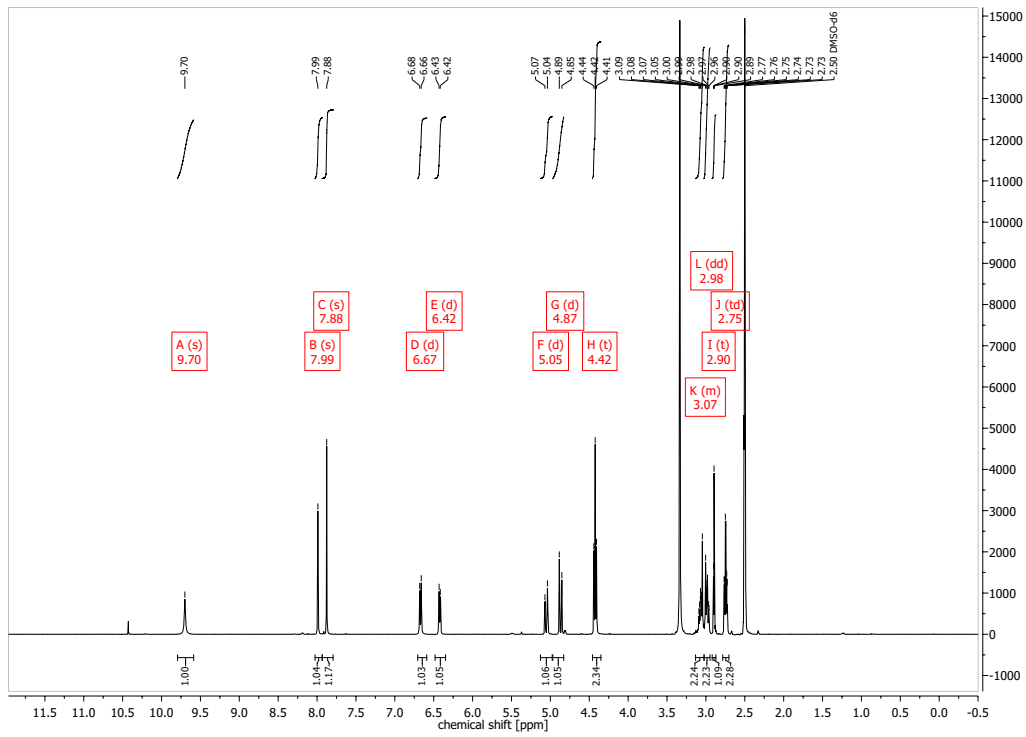
---

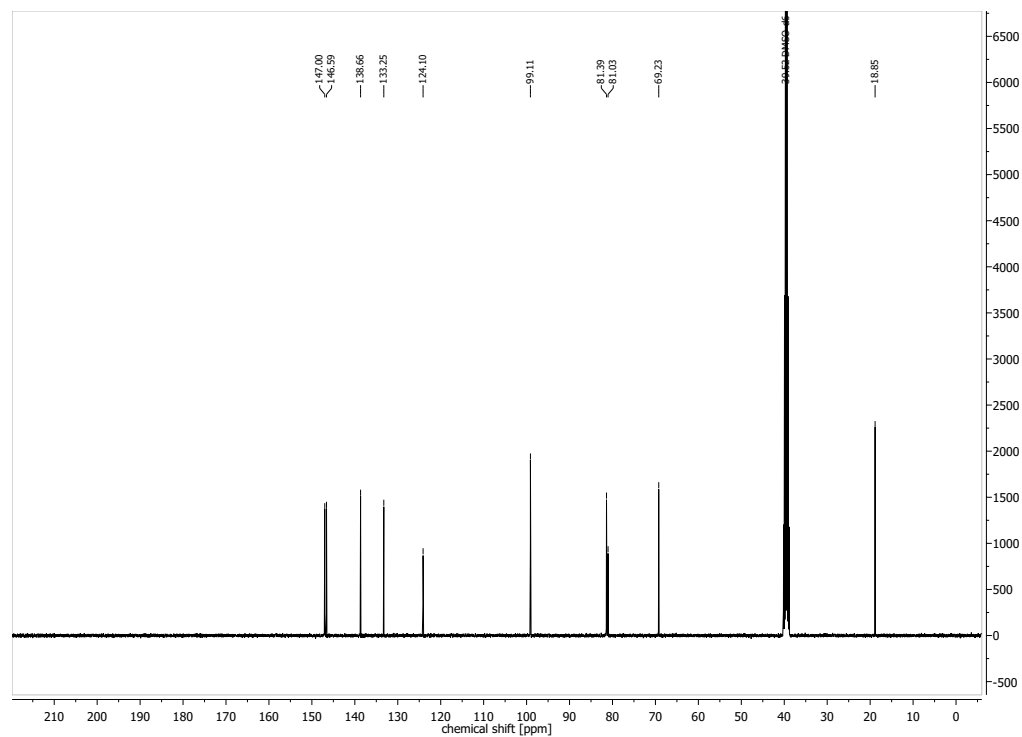
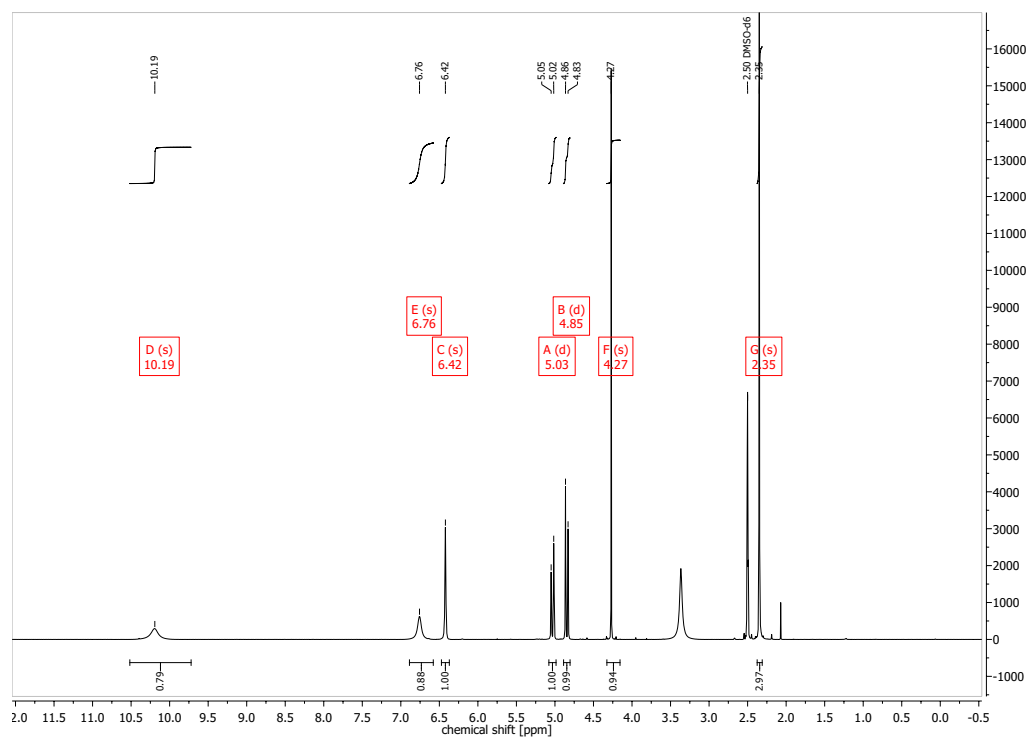
**A.3** NMR-Spectra $^1\text{H}$ - and  $^{13}\text{C}$ -spectra of PL6

$^1\text{H}$ - and  $^{13}\text{C}$ -spectra of PL7

$^1\text{H}$ - and  $^{13}\text{C}$ -spectra of PL8

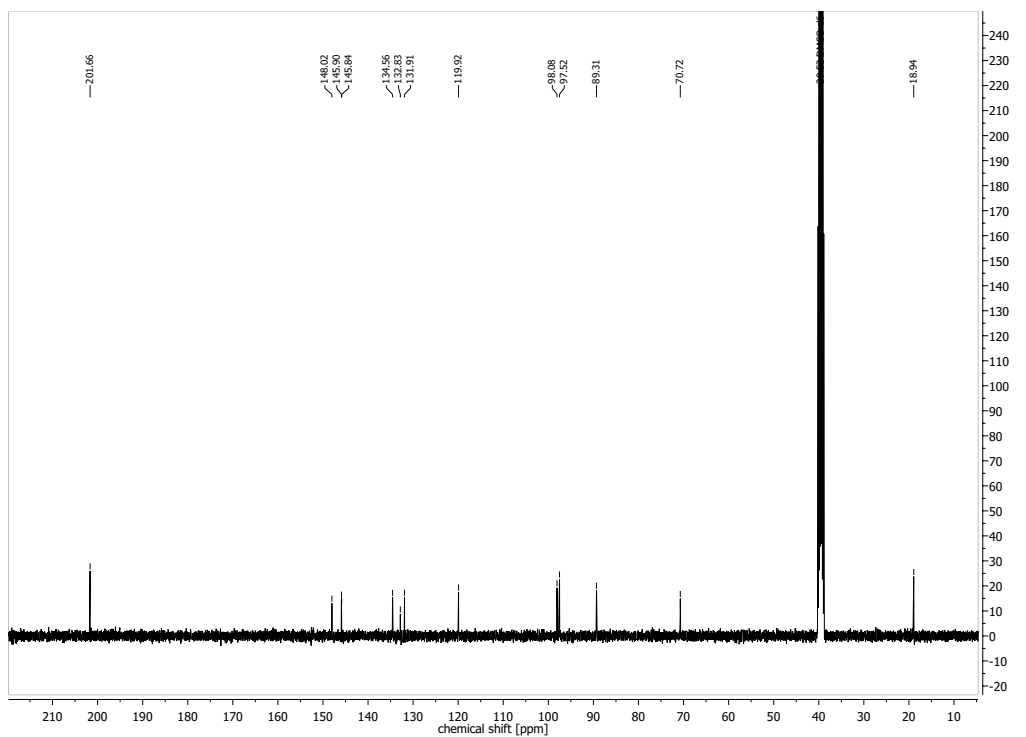
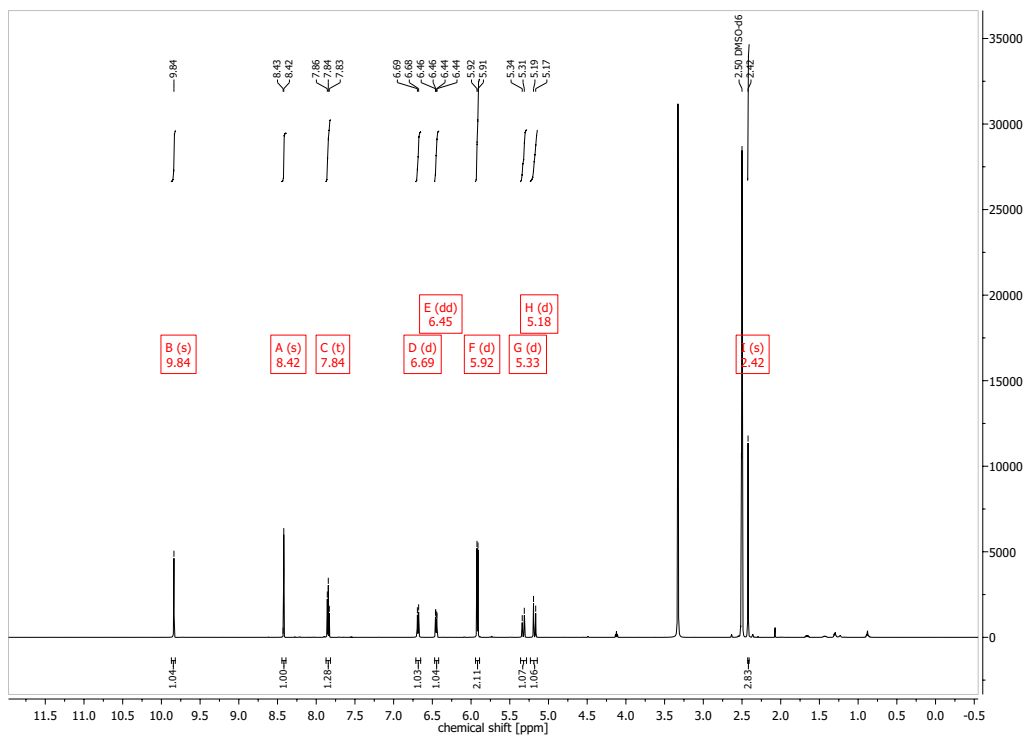
<sup>1</sup>H- and <sup>13</sup>C-spectra of PL9

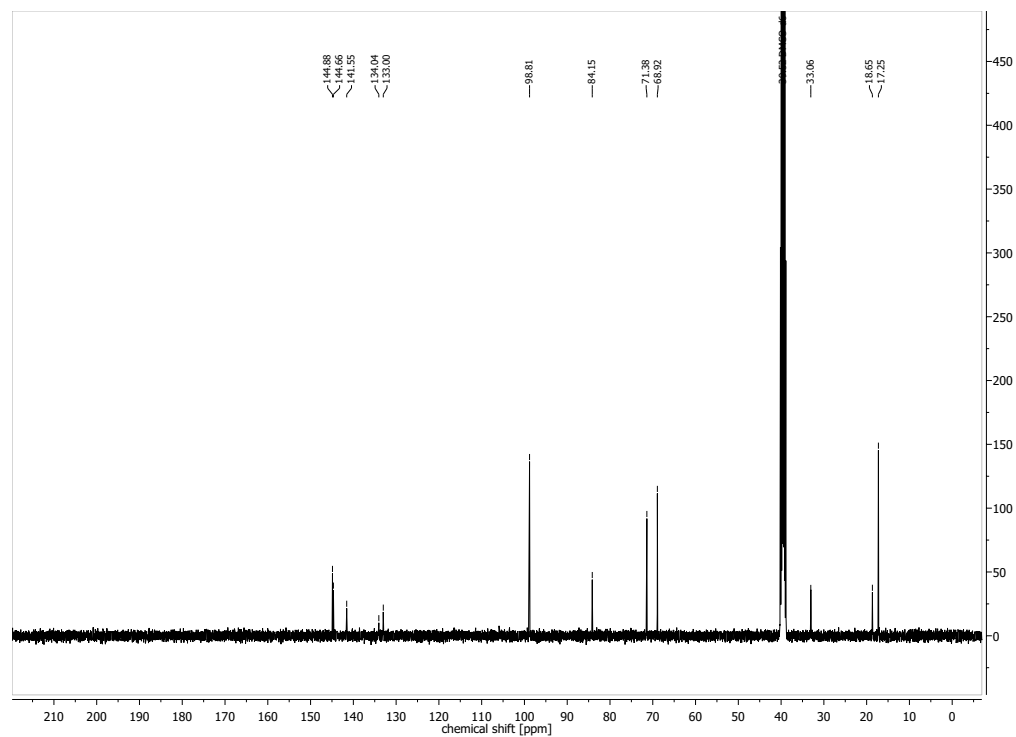
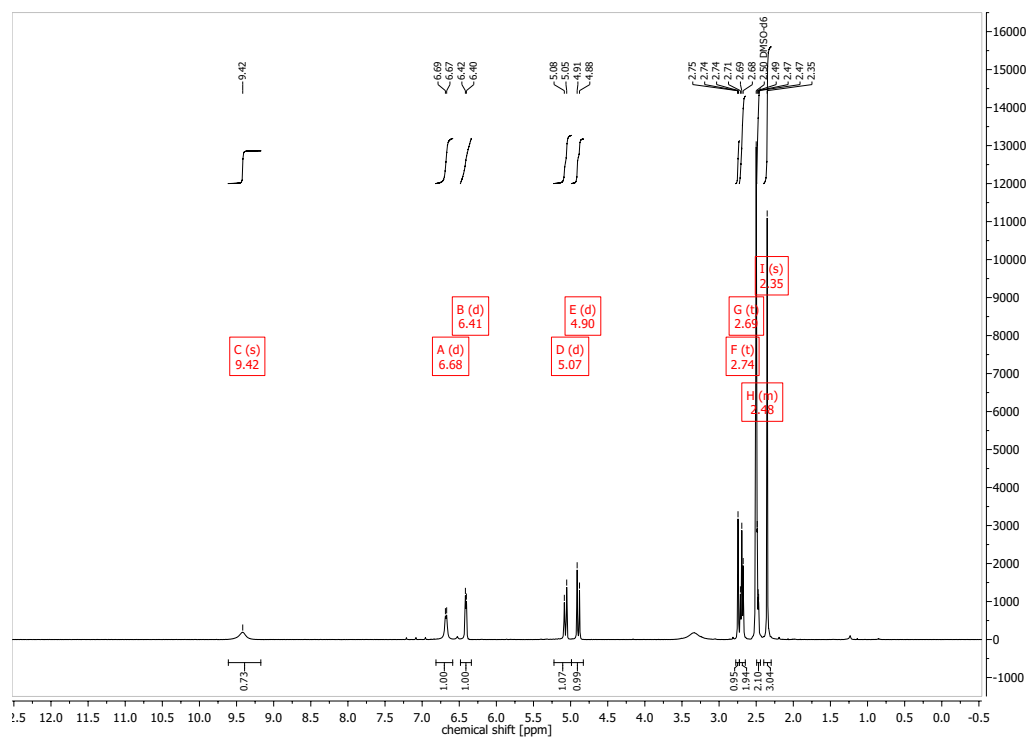


$^1\text{H}$ - and  $^{13}\text{C}$ -spectra of PL10

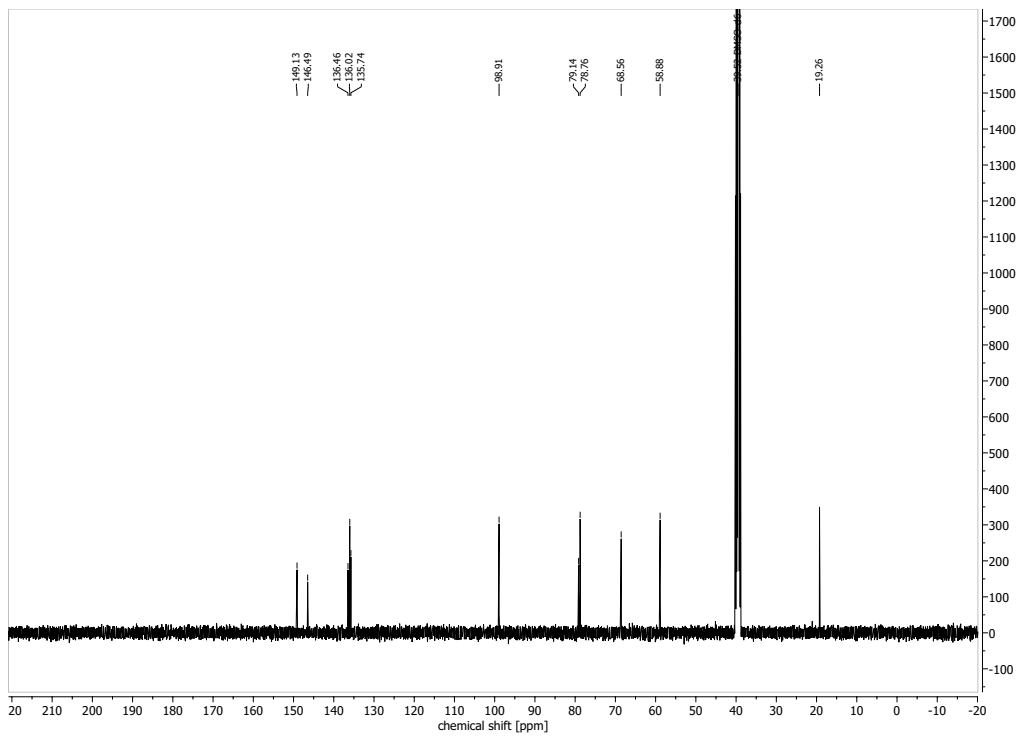
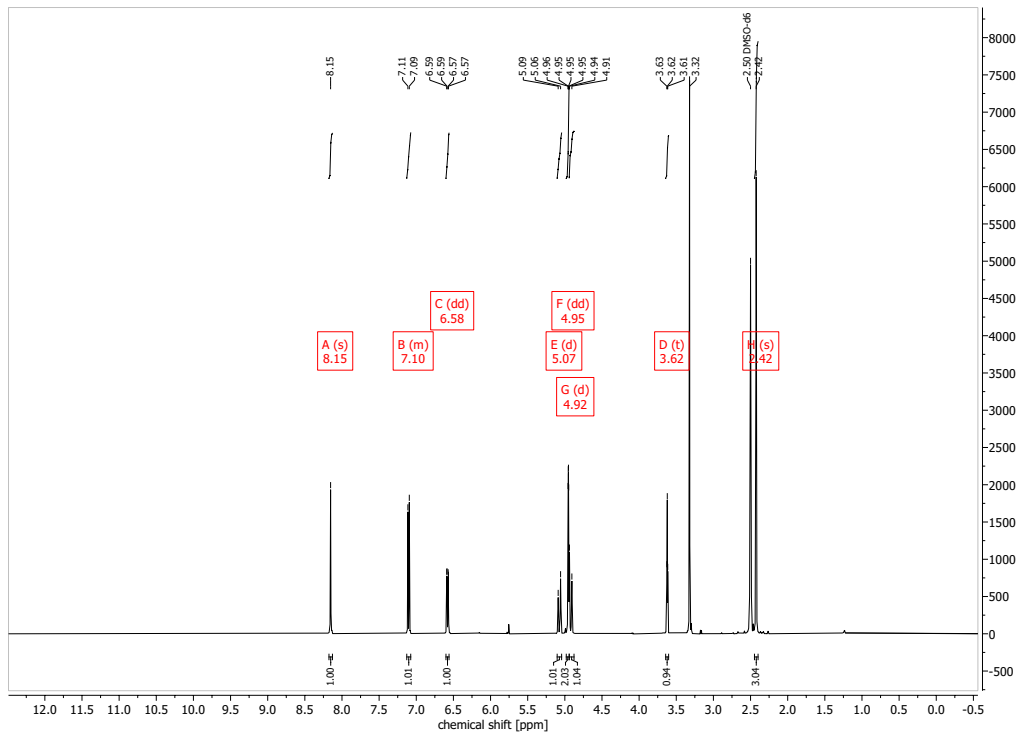


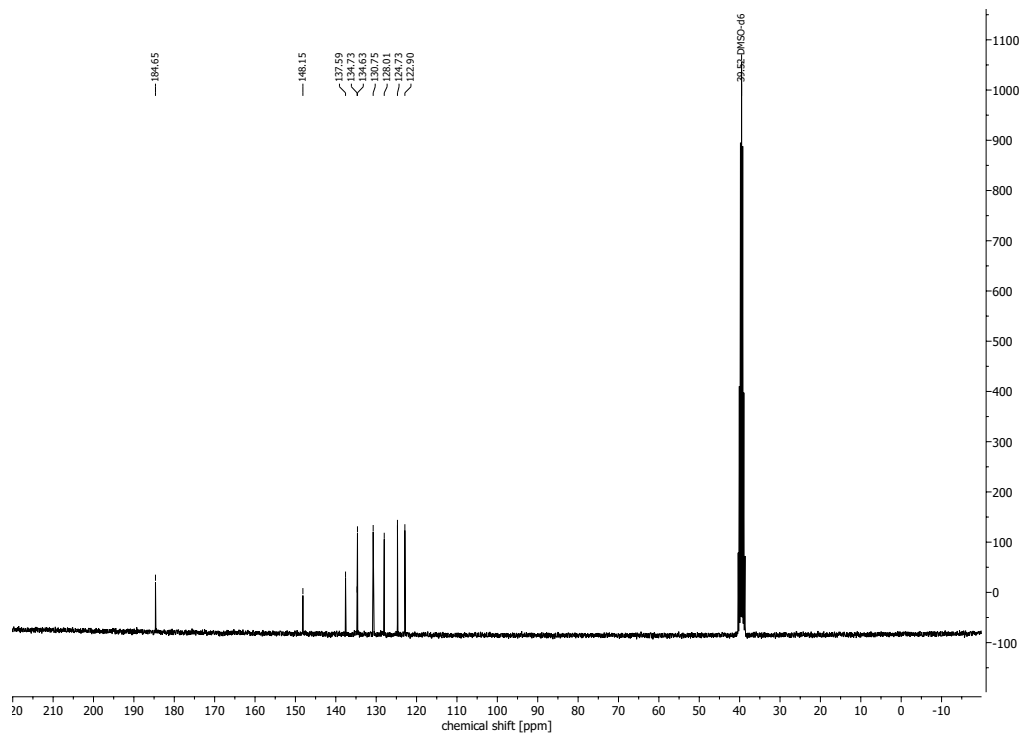
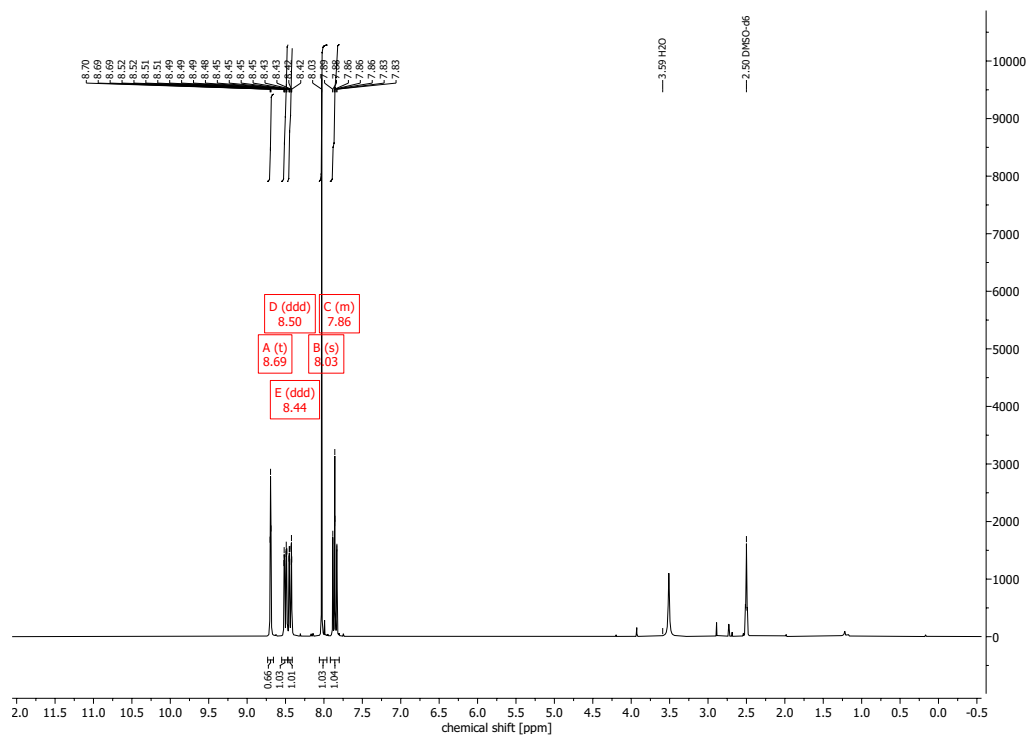
<sup>1</sup>H- and <sup>13</sup>C-spectra of PL11



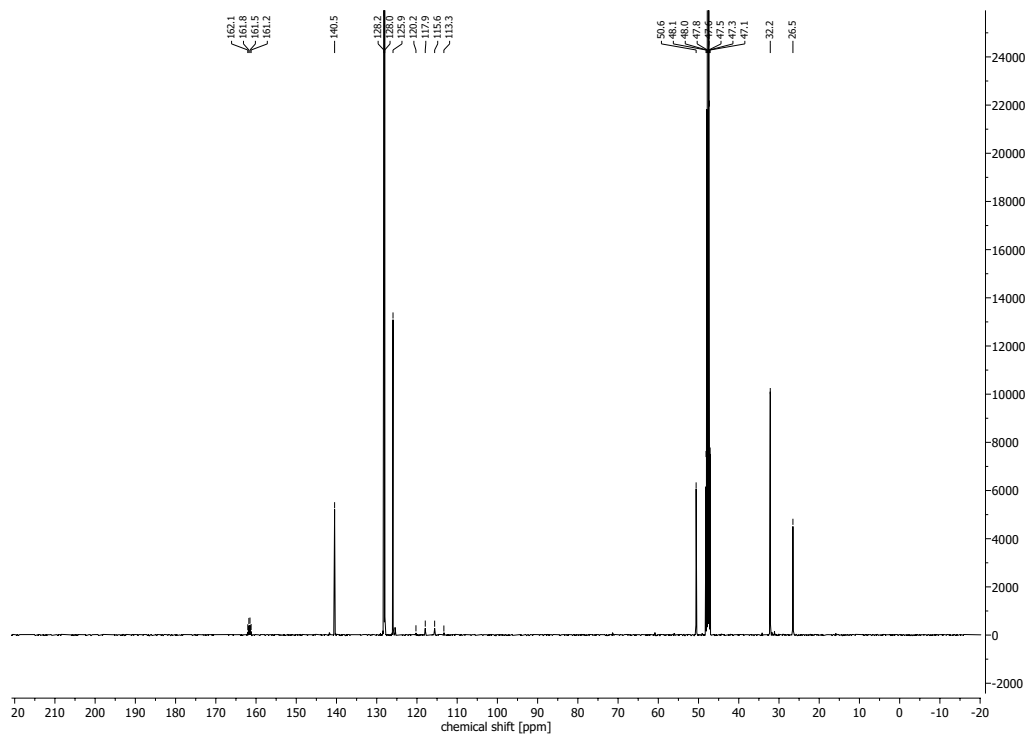
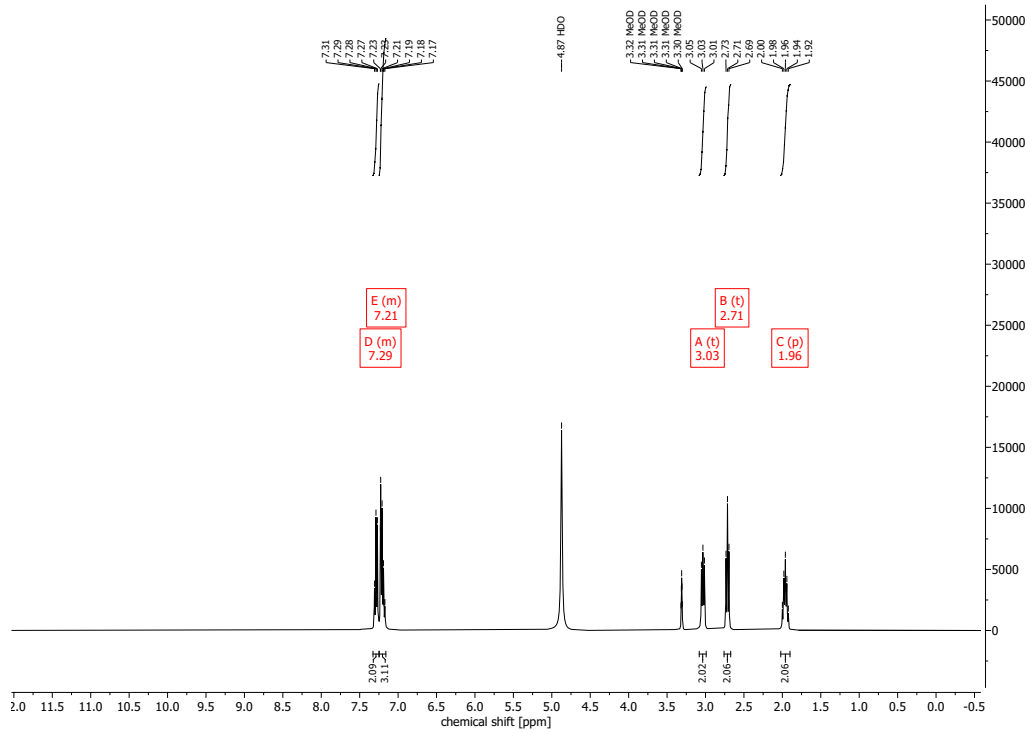
$^1\text{H}$ - and  $^{13}\text{C}$ -spectra of PL12

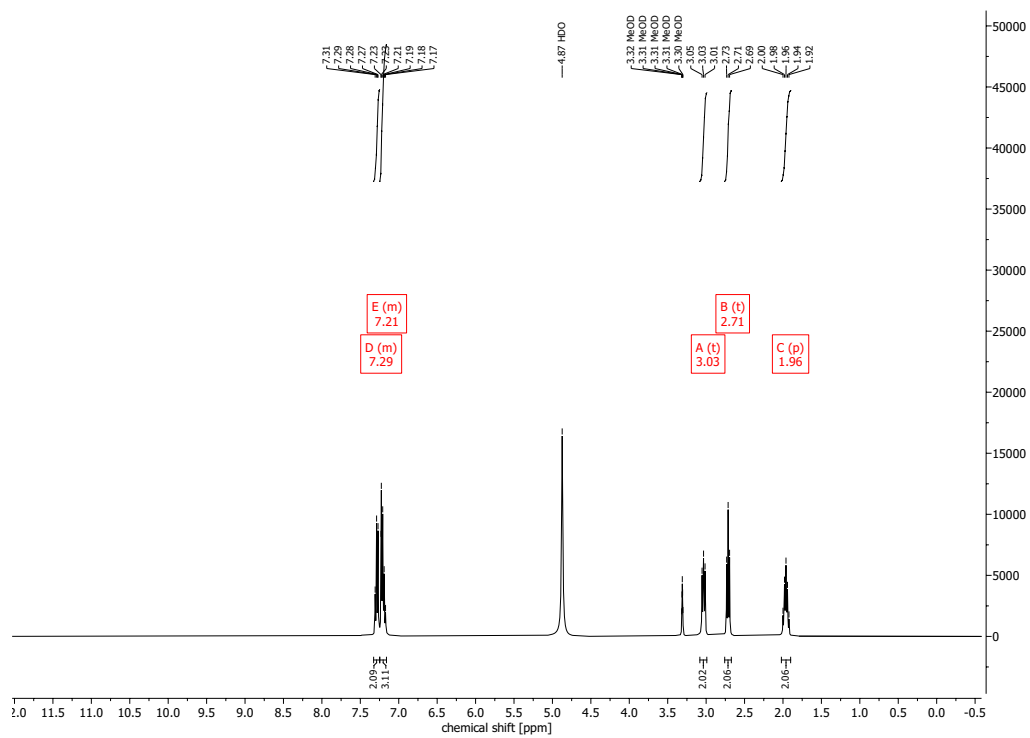
$^1\text{H}$ - and  $^{13}\text{C}$ -spectra of PL13



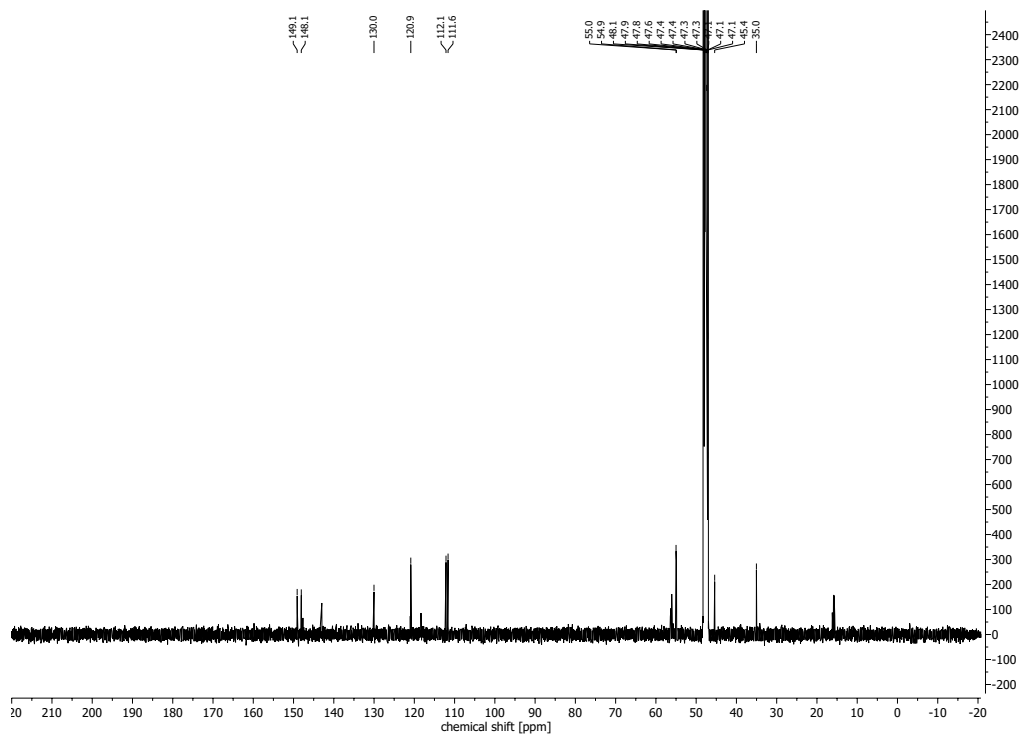
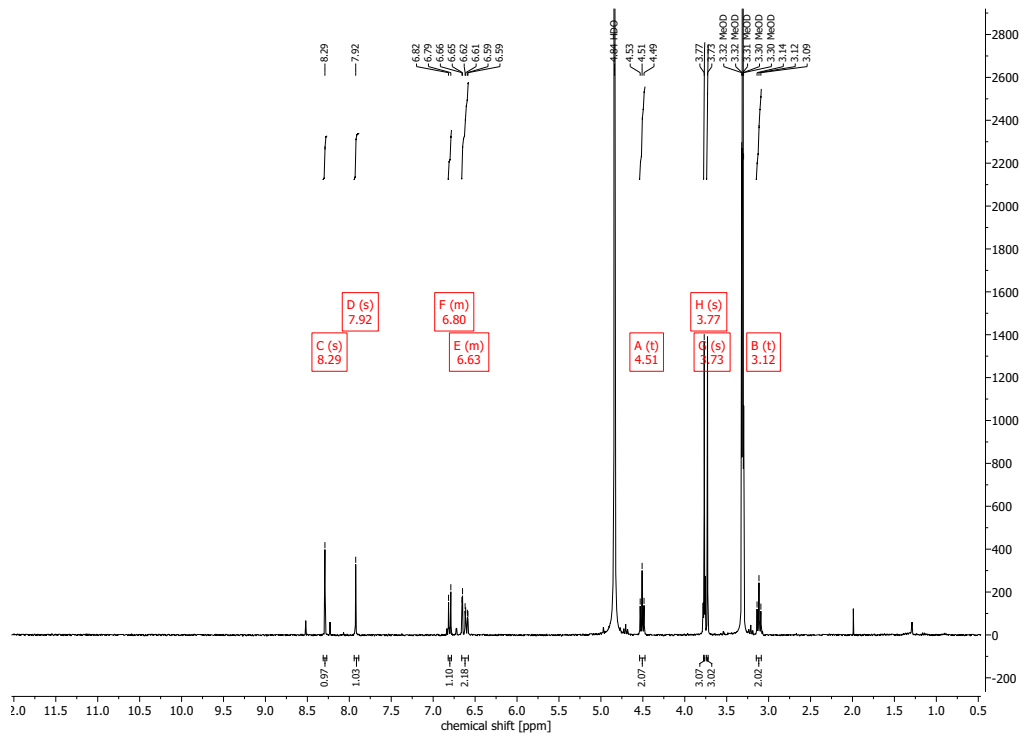
$^1\text{H}$ - and  $^{13}\text{C}$ -spectra of MAC173979

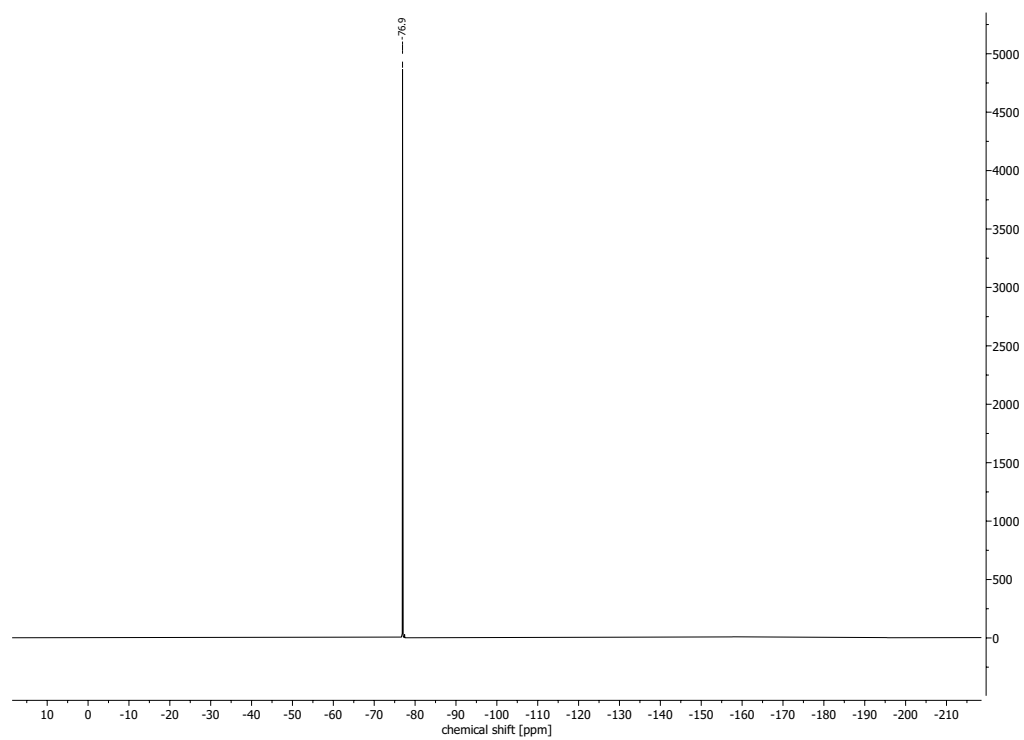
<sup>1</sup>H-, <sup>13</sup>C- and <sup>19</sup>F-spectra of TM-2-10



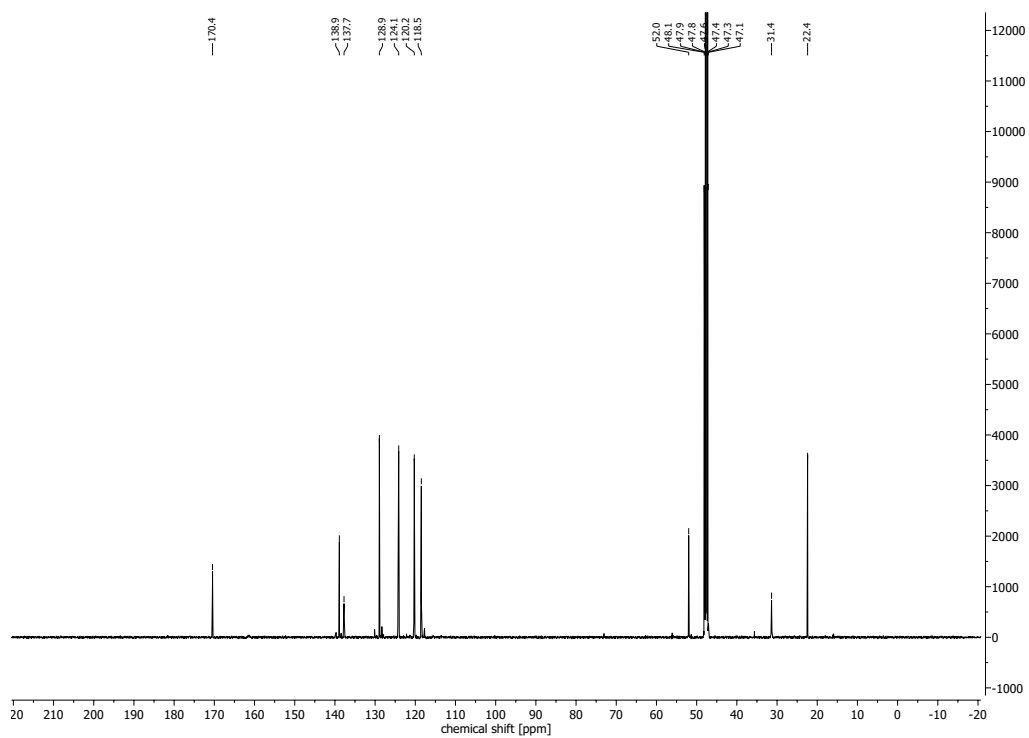
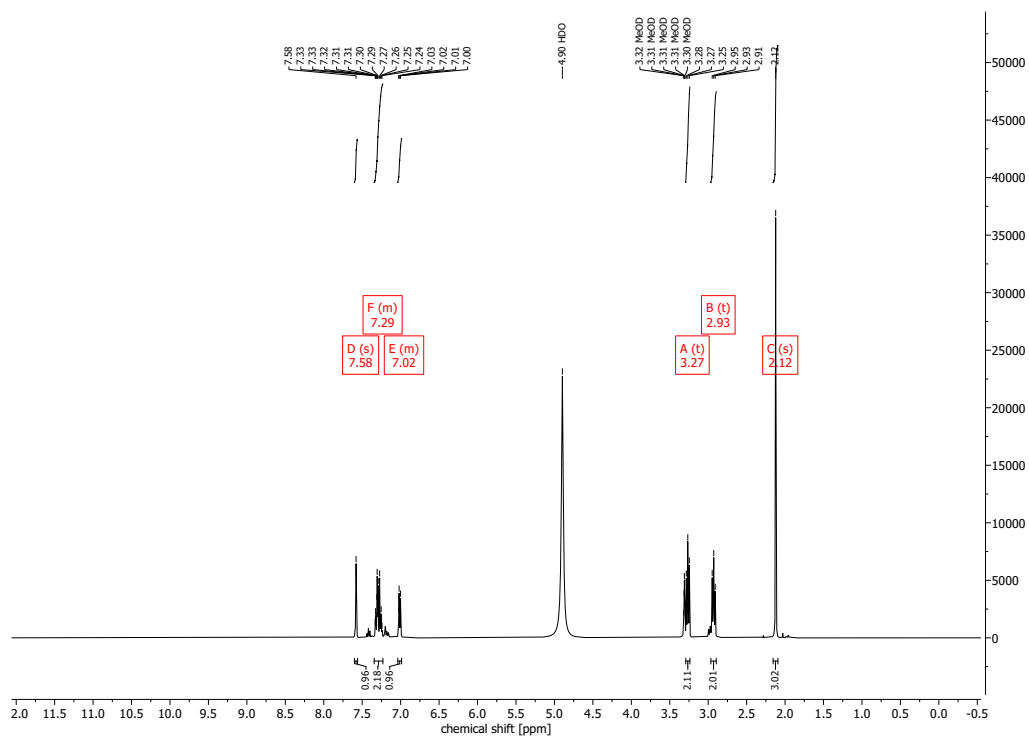


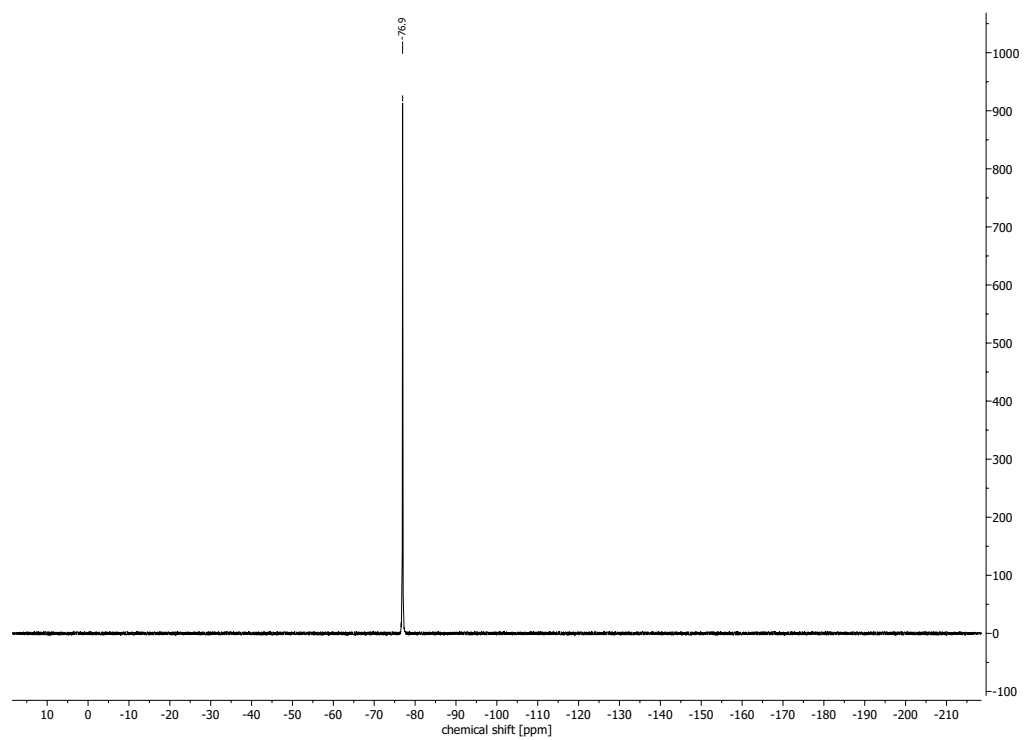
<sup>1</sup>H-, <sup>13</sup>C- and <sup>19</sup>F-spectra of TM-2-11



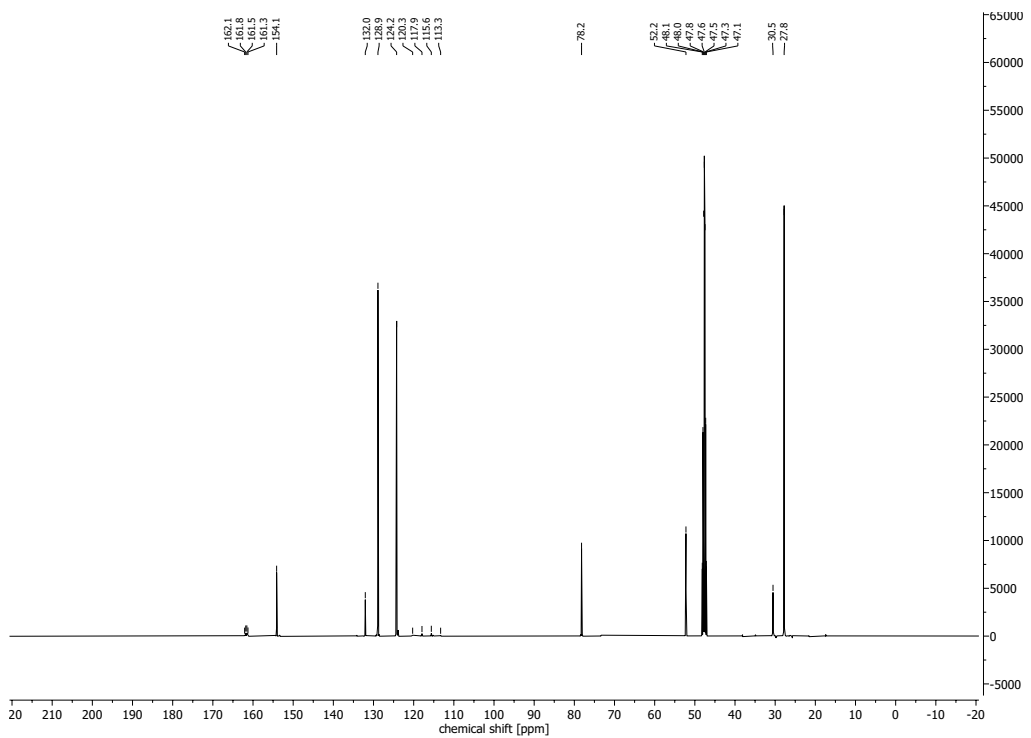
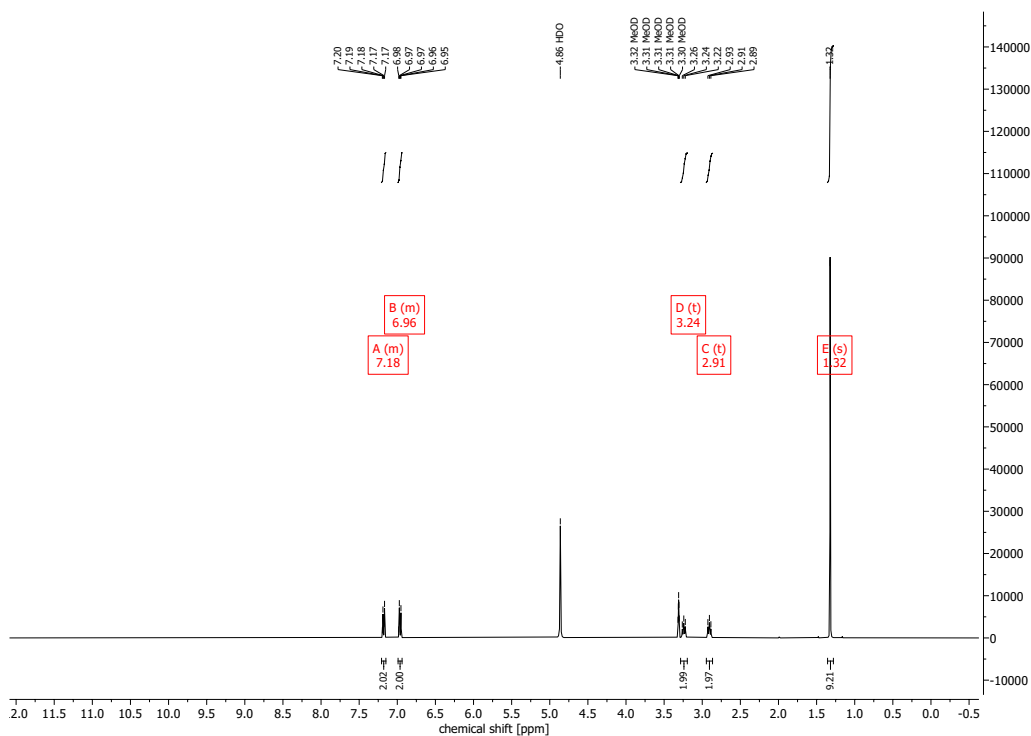


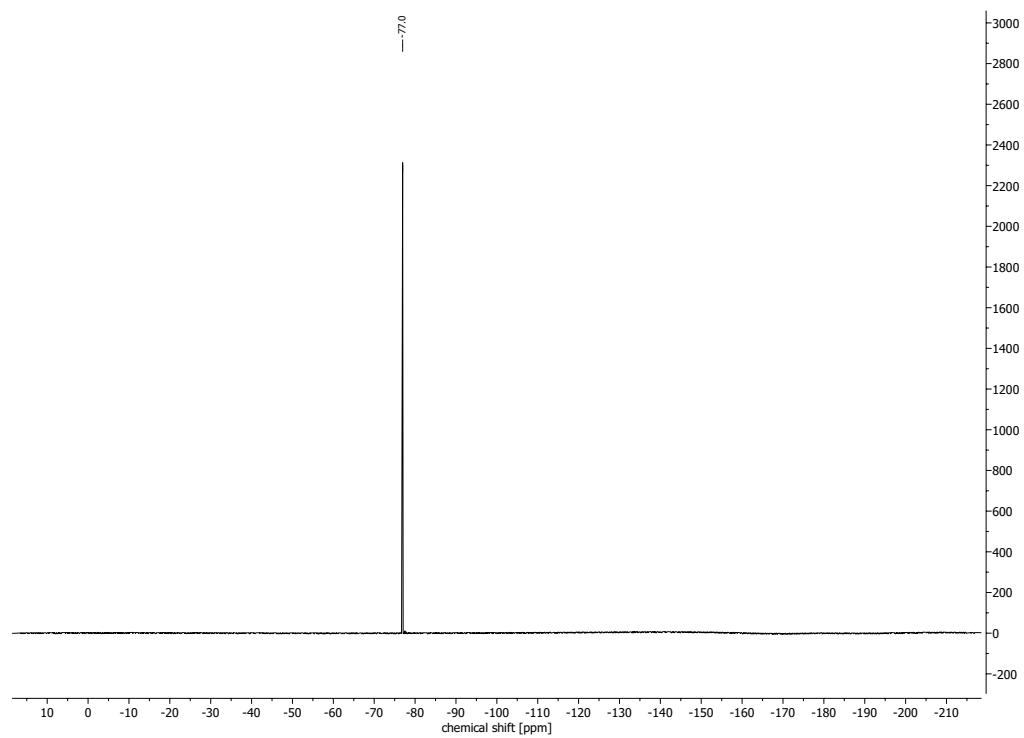


$^1\text{H}$ -,  $^{13}\text{C}$ - and  $^{19}\text{F}$ -spectra of TM-2-12

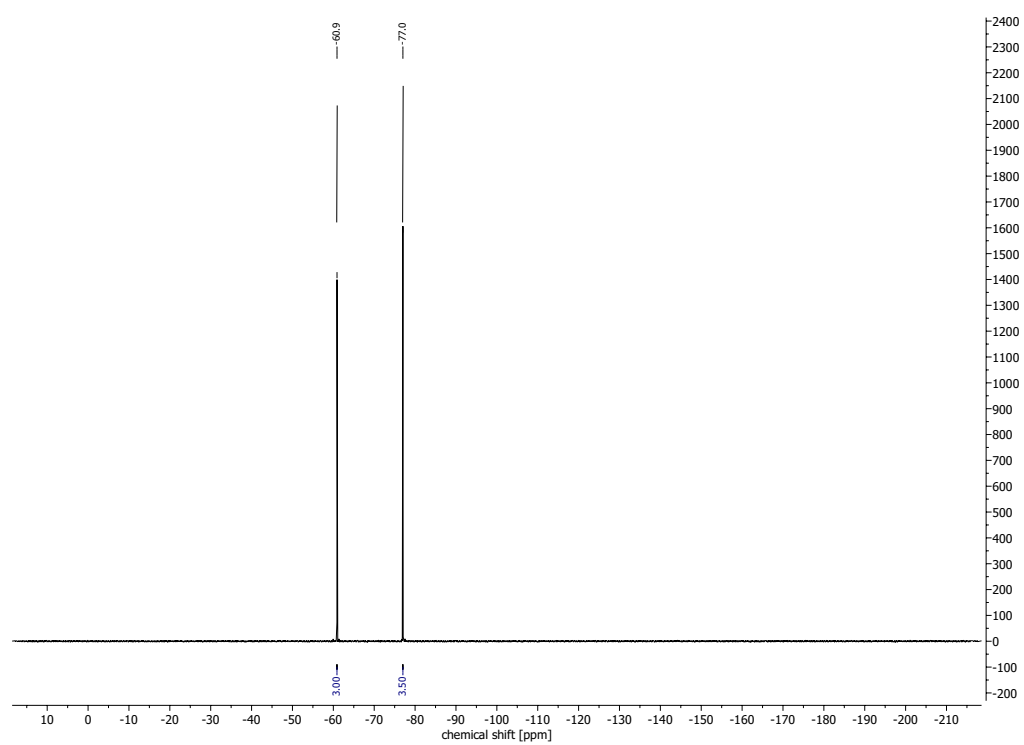


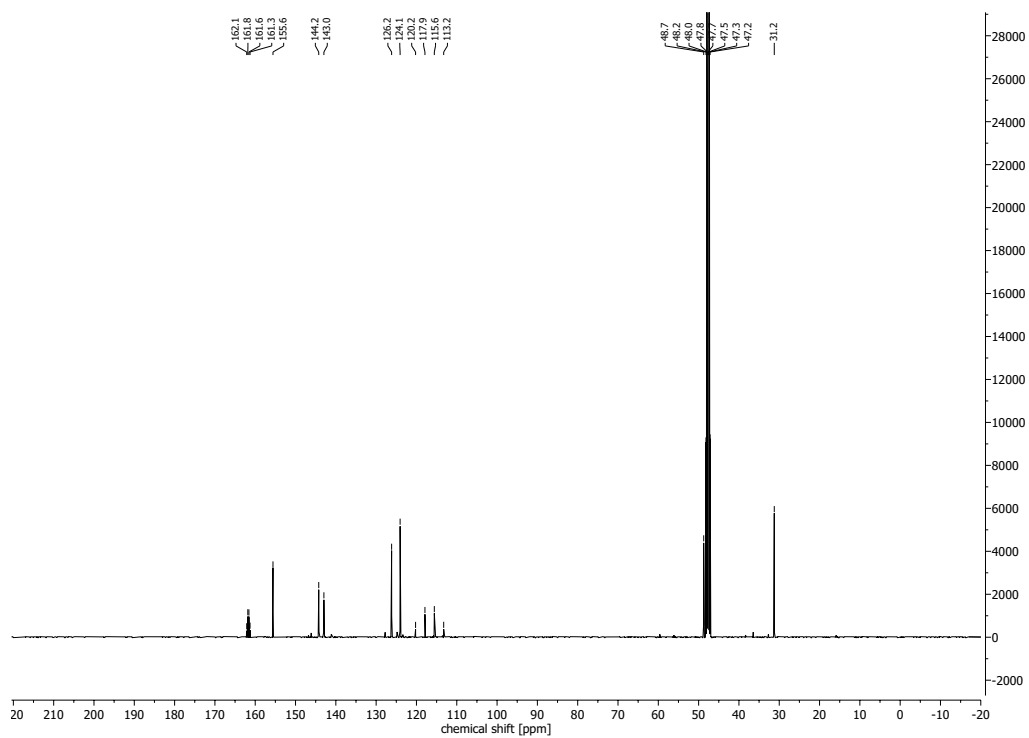
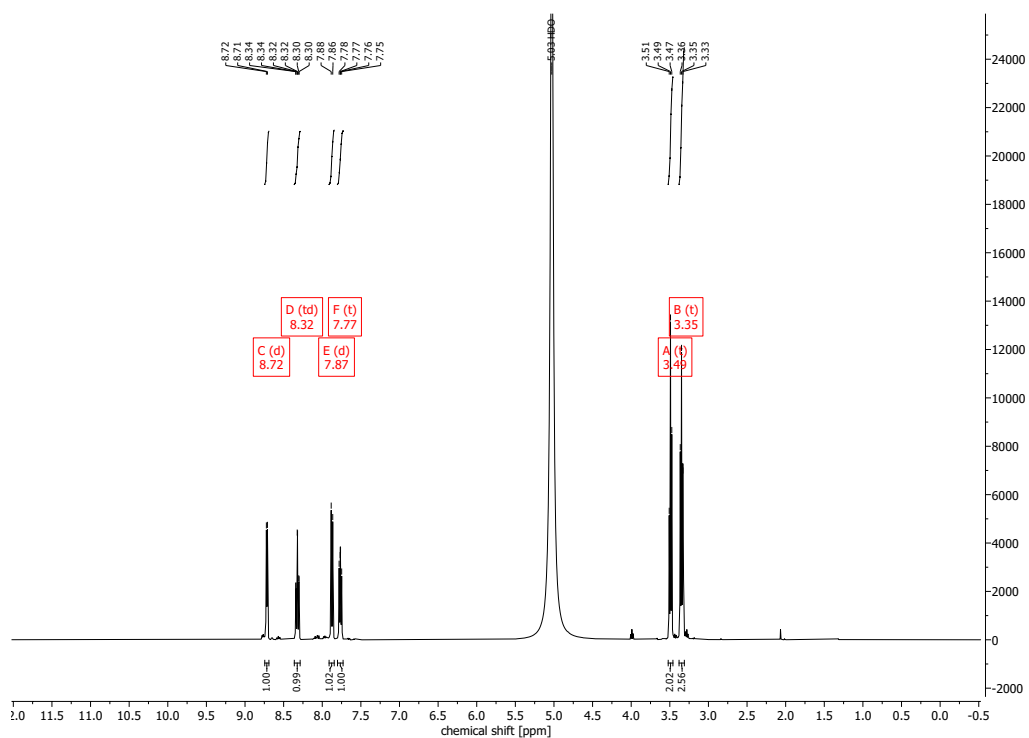
<sup>1</sup>H-, <sup>13</sup>C- and <sup>19</sup>F-spectra of TM-2-13

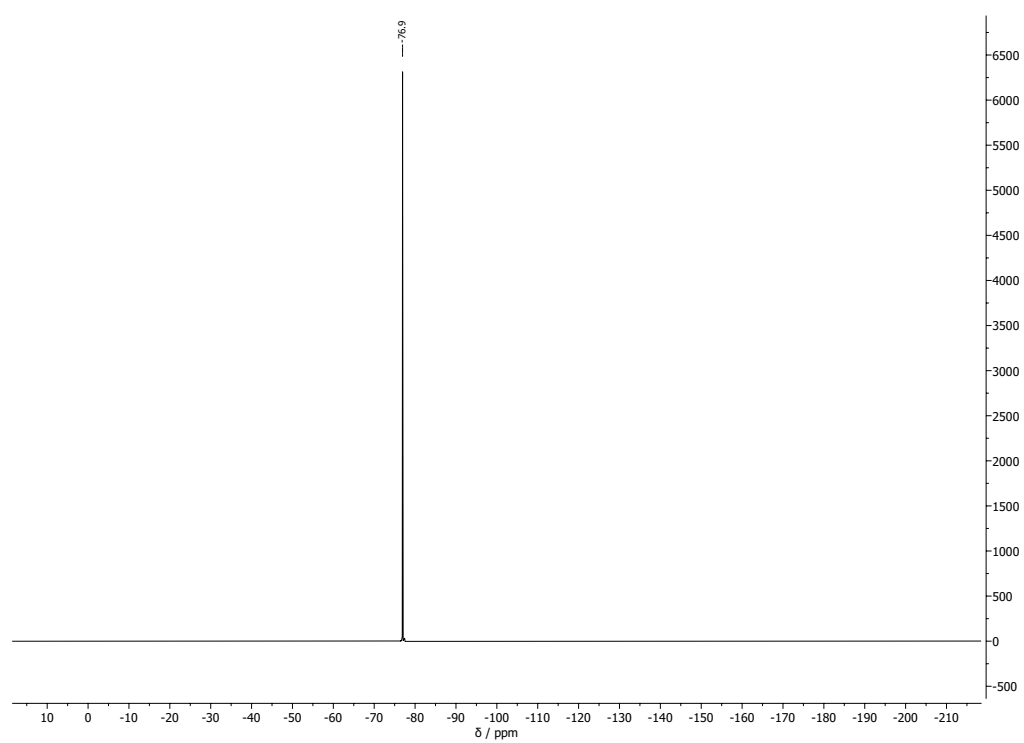






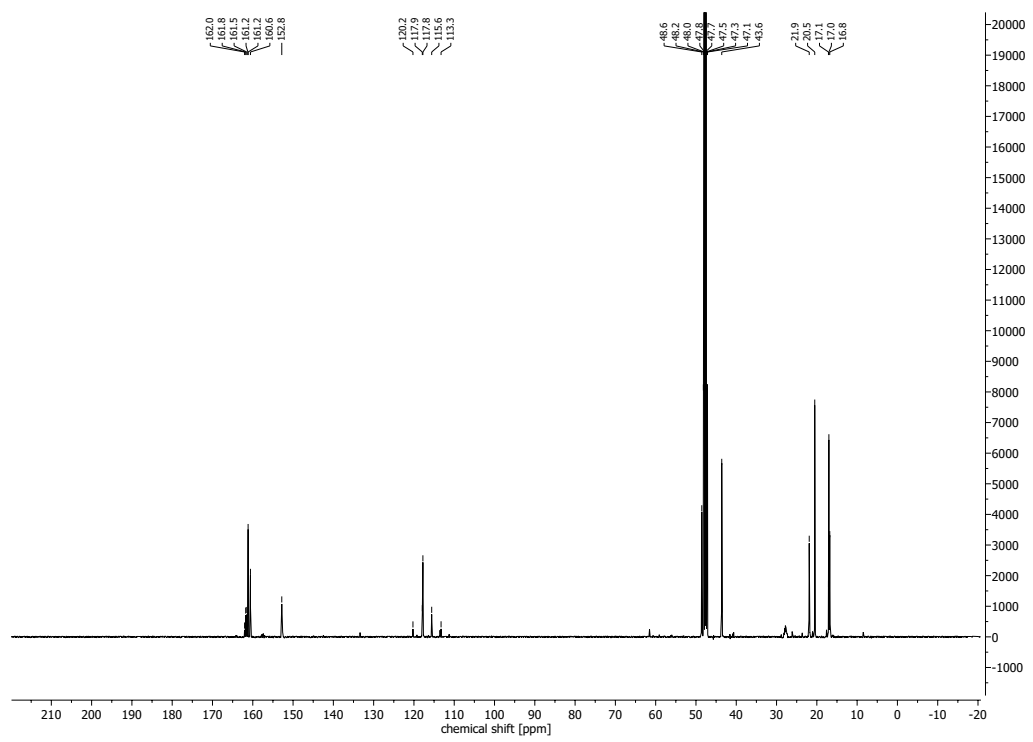
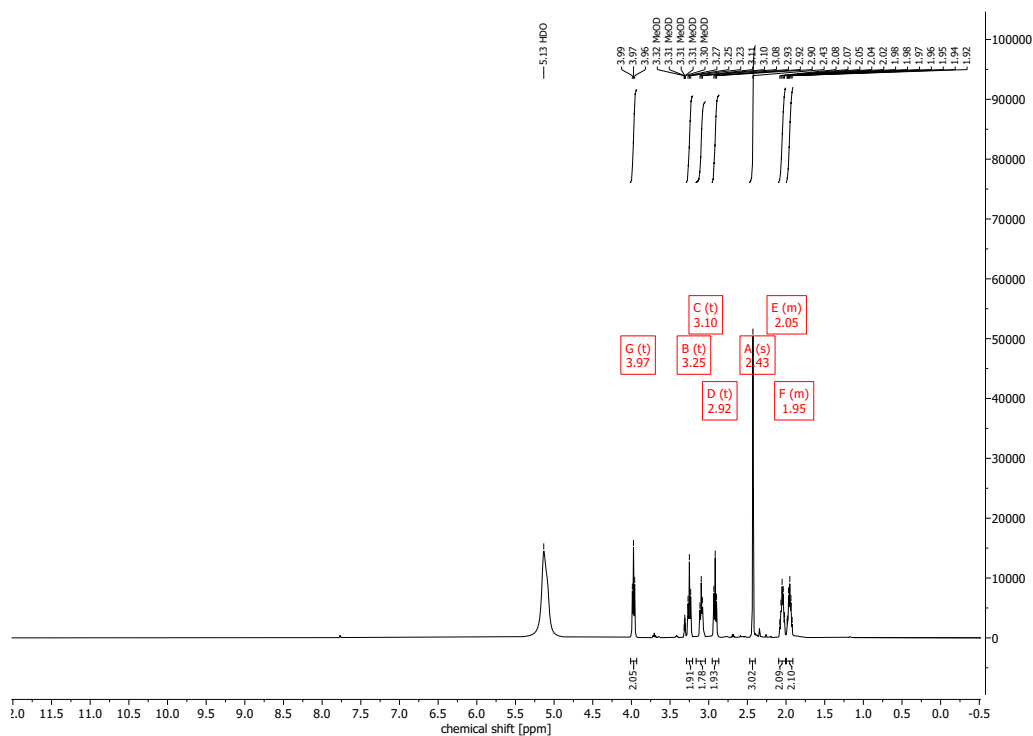


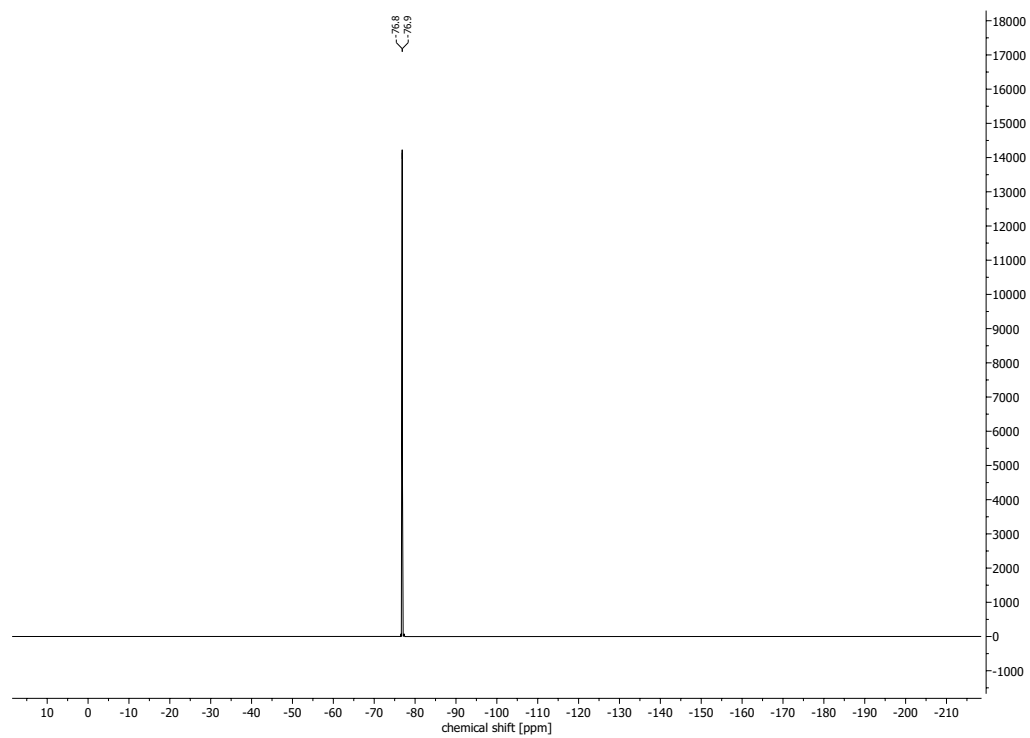
$^1\text{H}$ -,  $^{13}\text{C}$ - and  $^{19}\text{F}$ -spectra of TM-2-15

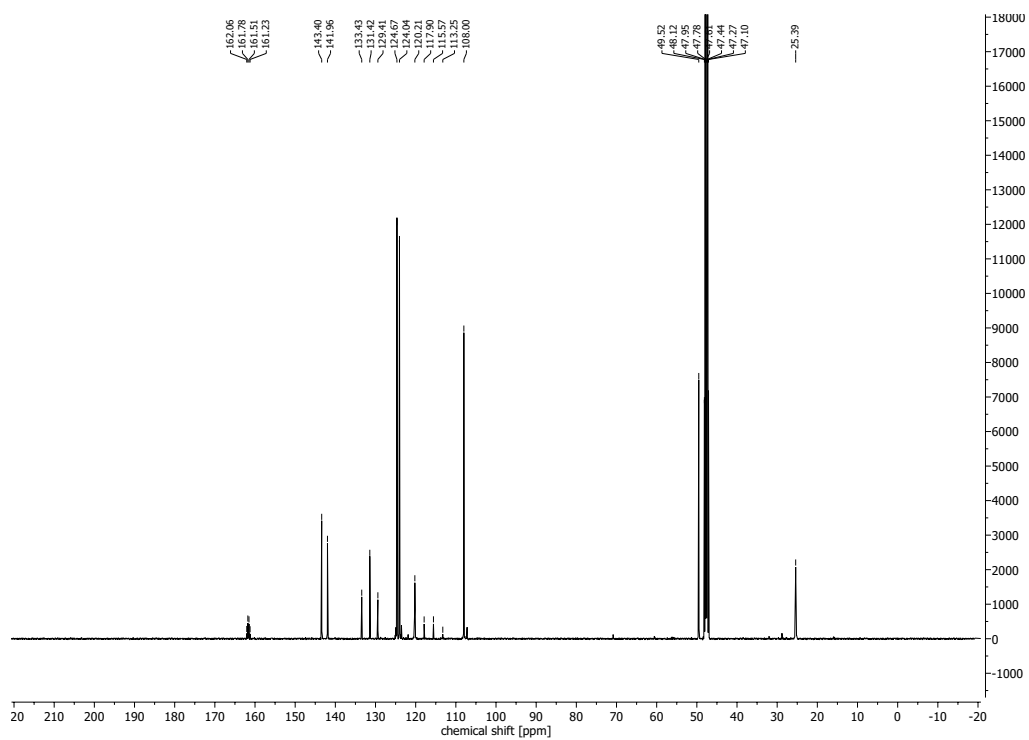
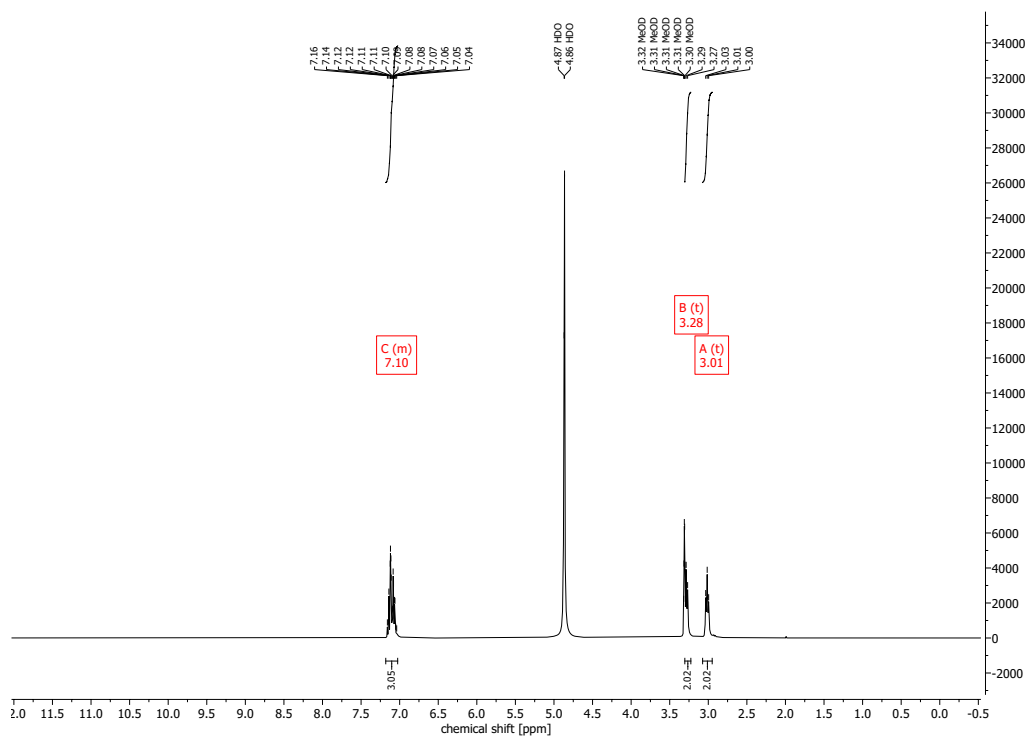


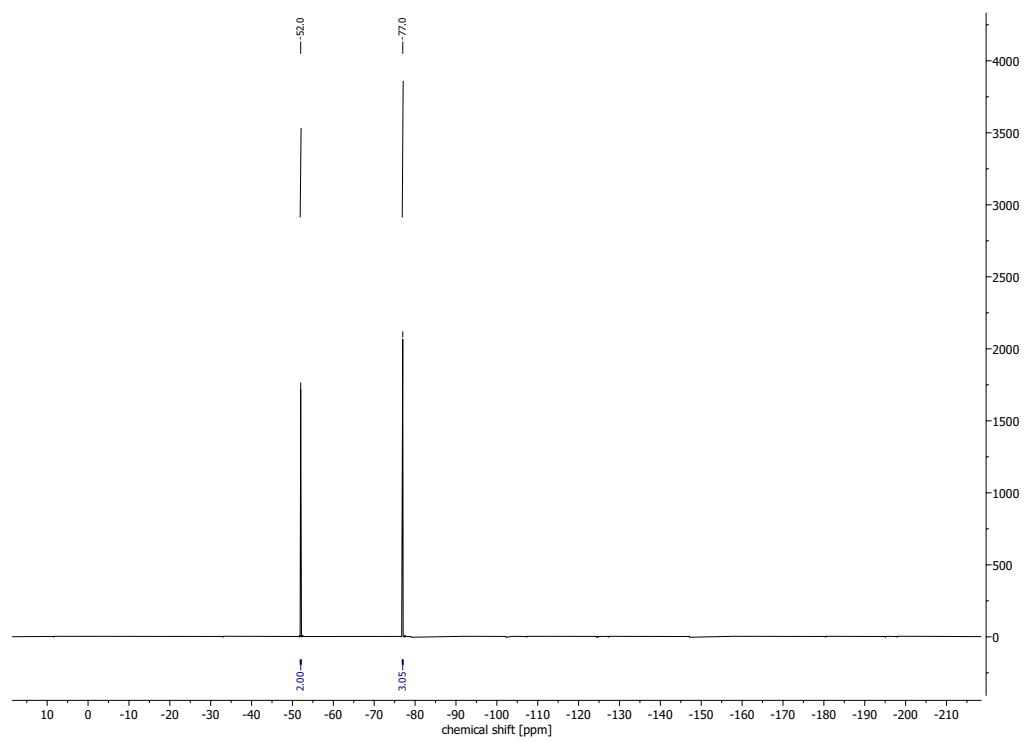


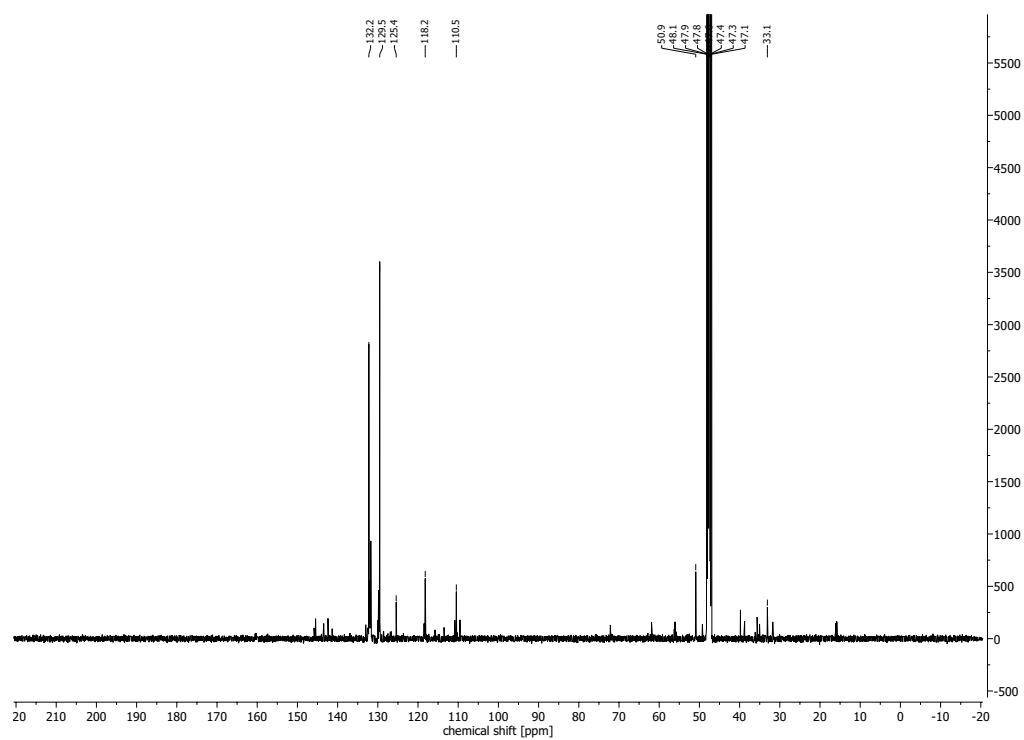
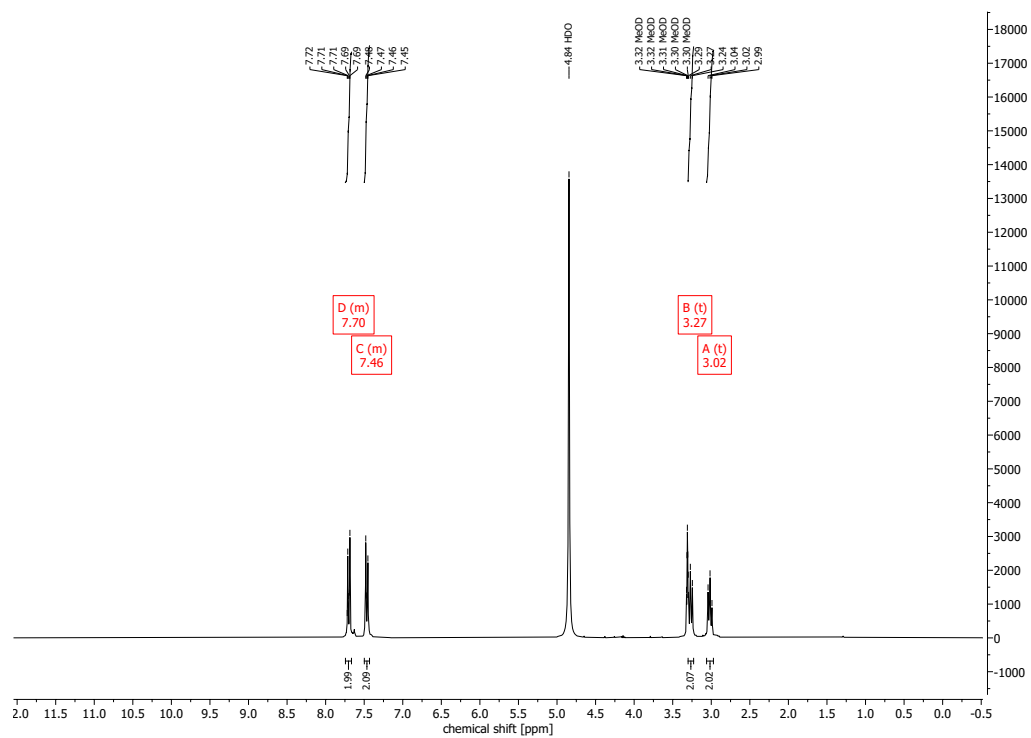
<sup>1</sup>H-, <sup>13</sup>C- and <sup>19</sup>F-spectra of TM-2-16

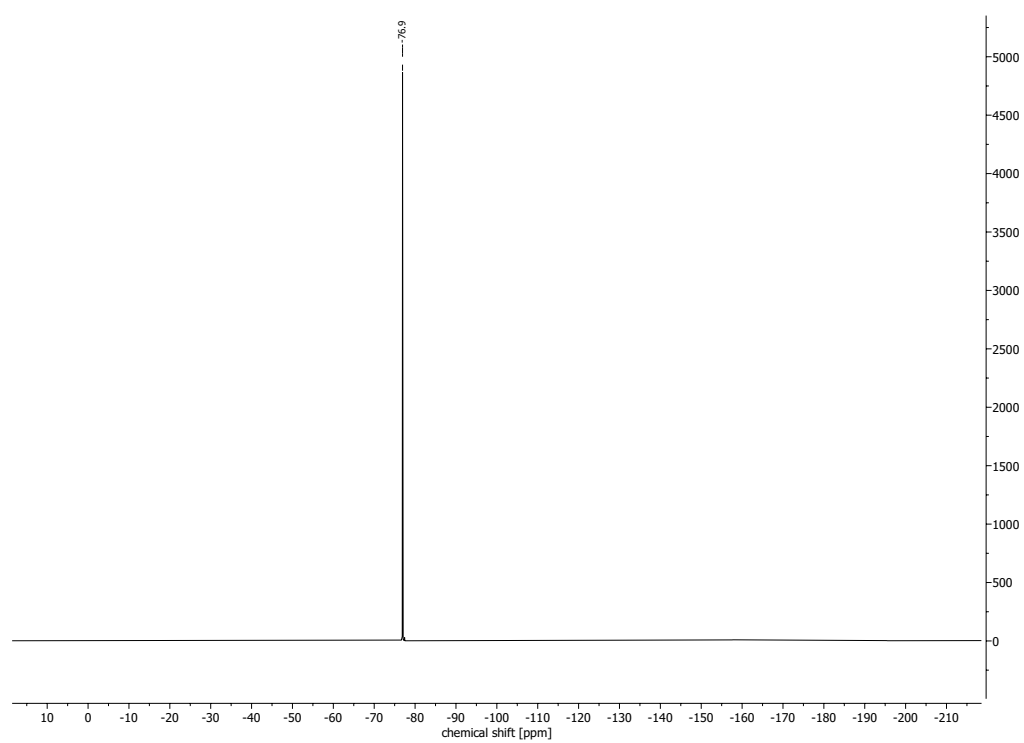




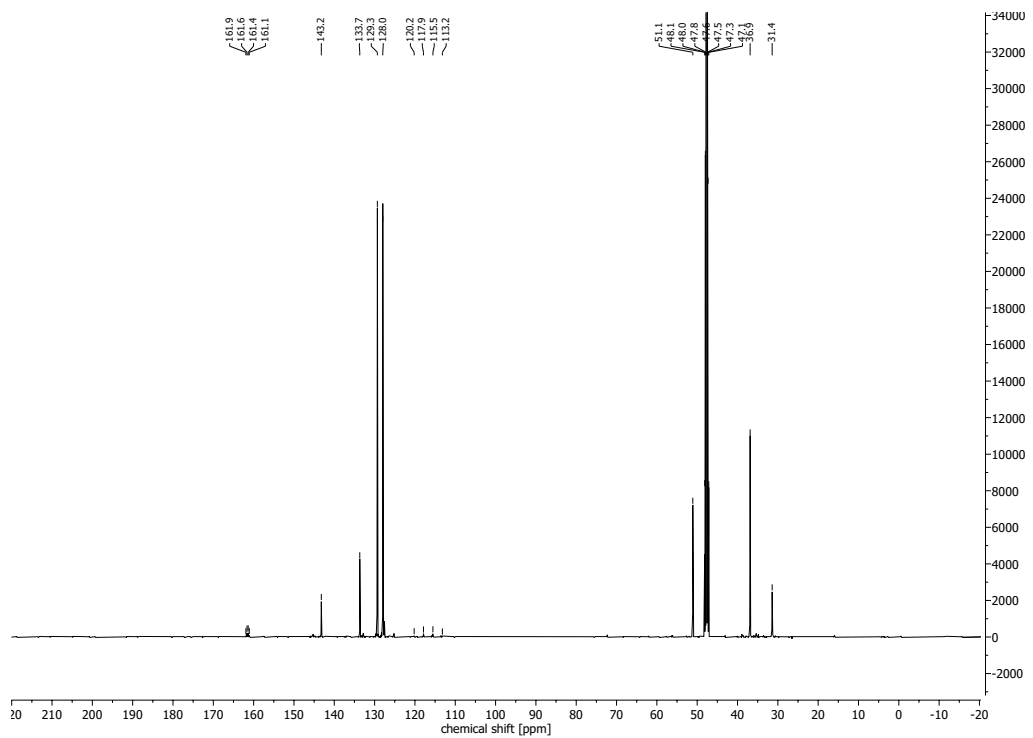
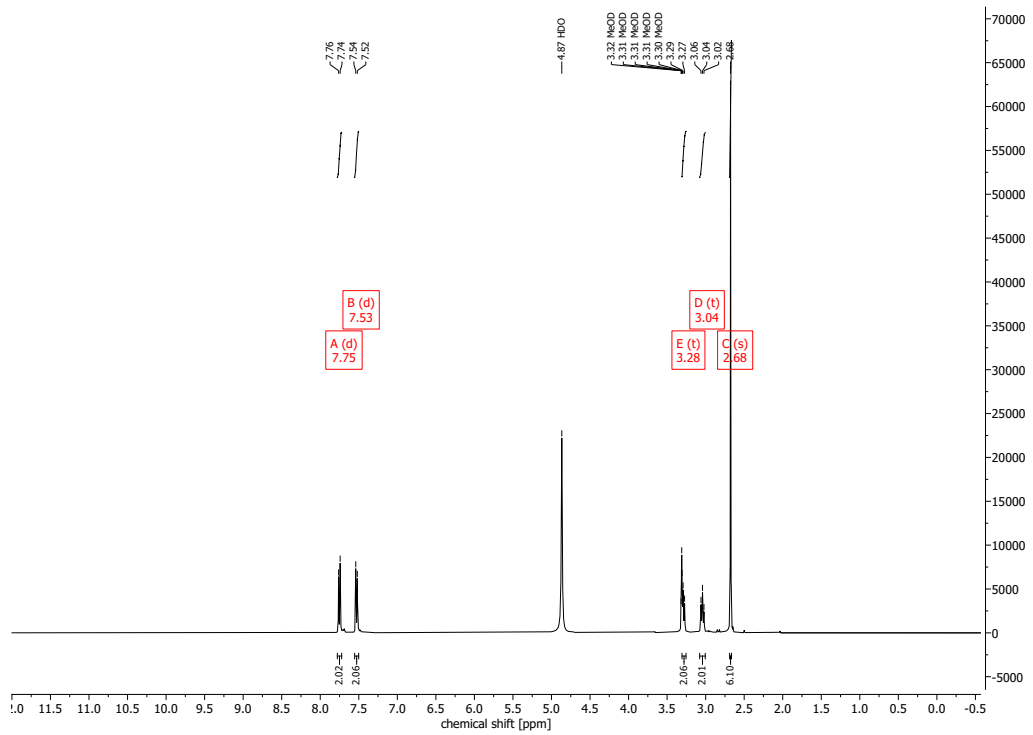
$^1\text{H}$ -,  $^{13}\text{C}$ - and  $^{19}\text{F}$ -spectra of TM-2-17

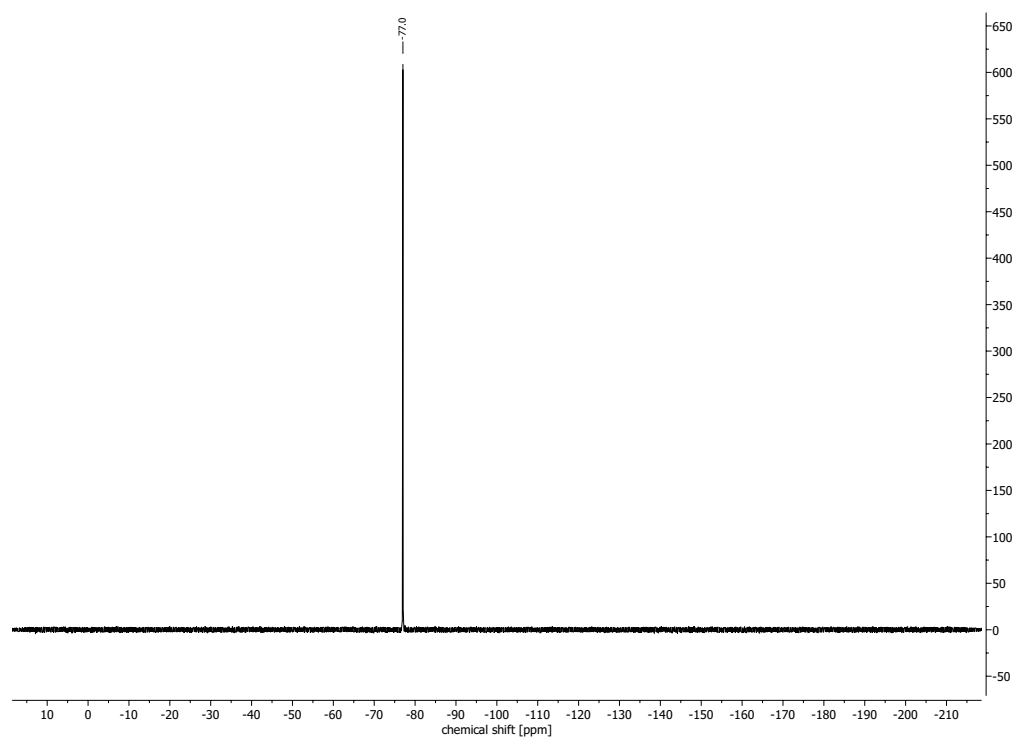


$^1\text{H}$ -,  $^{13}\text{C}$ - and  $^{19}\text{F}$ -spectra of TM-2-18

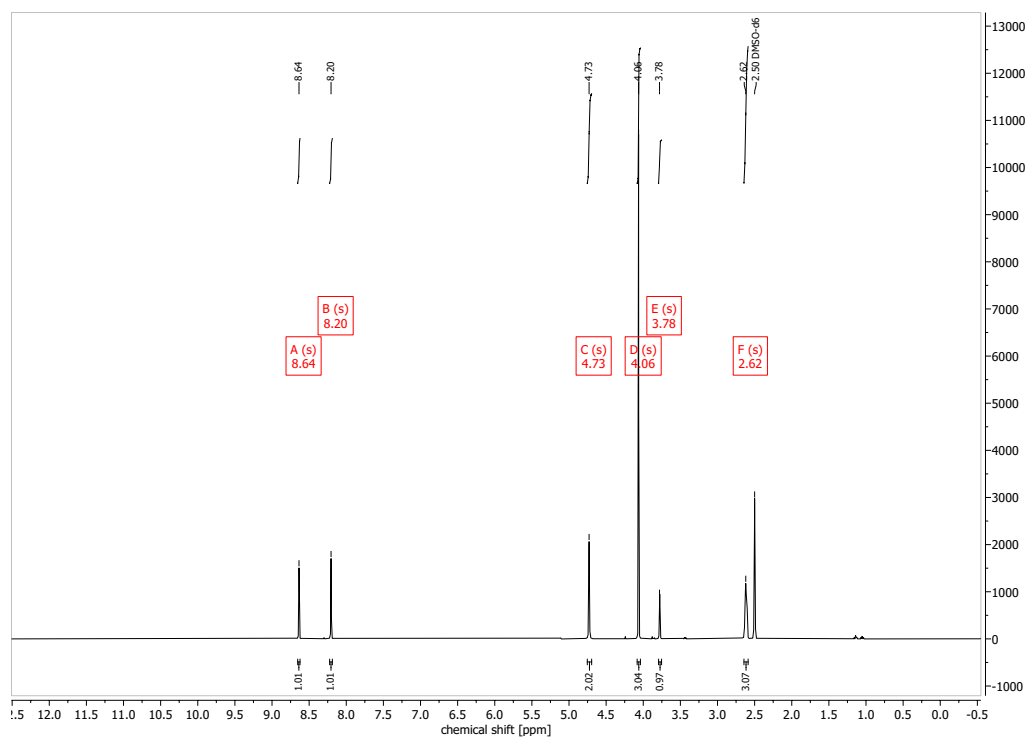


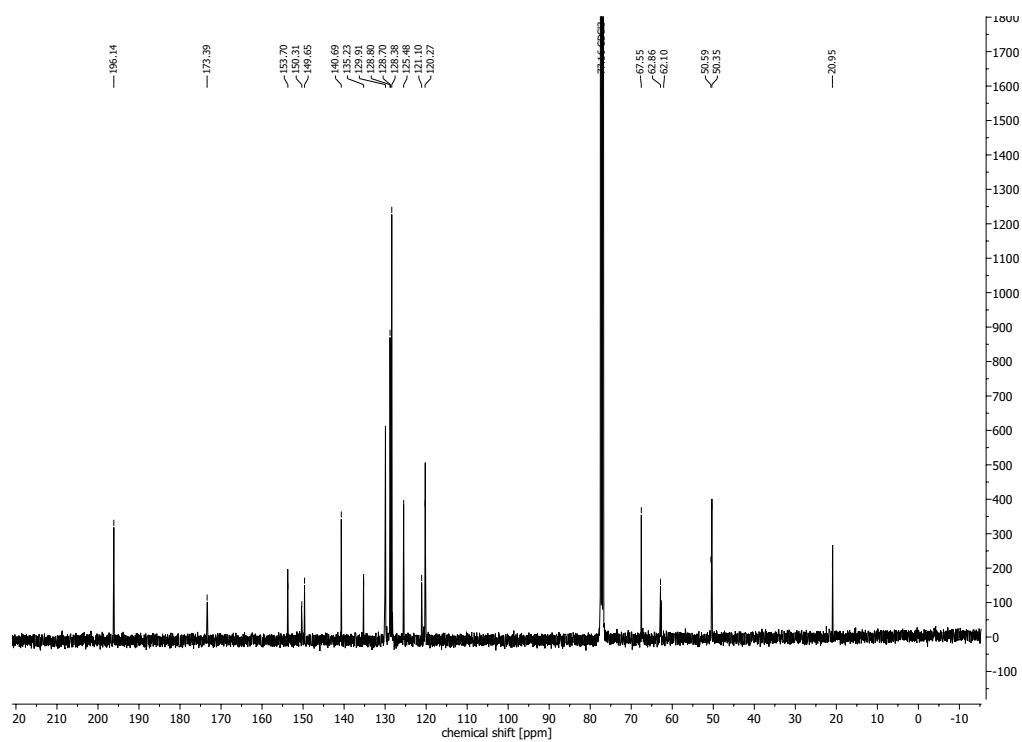
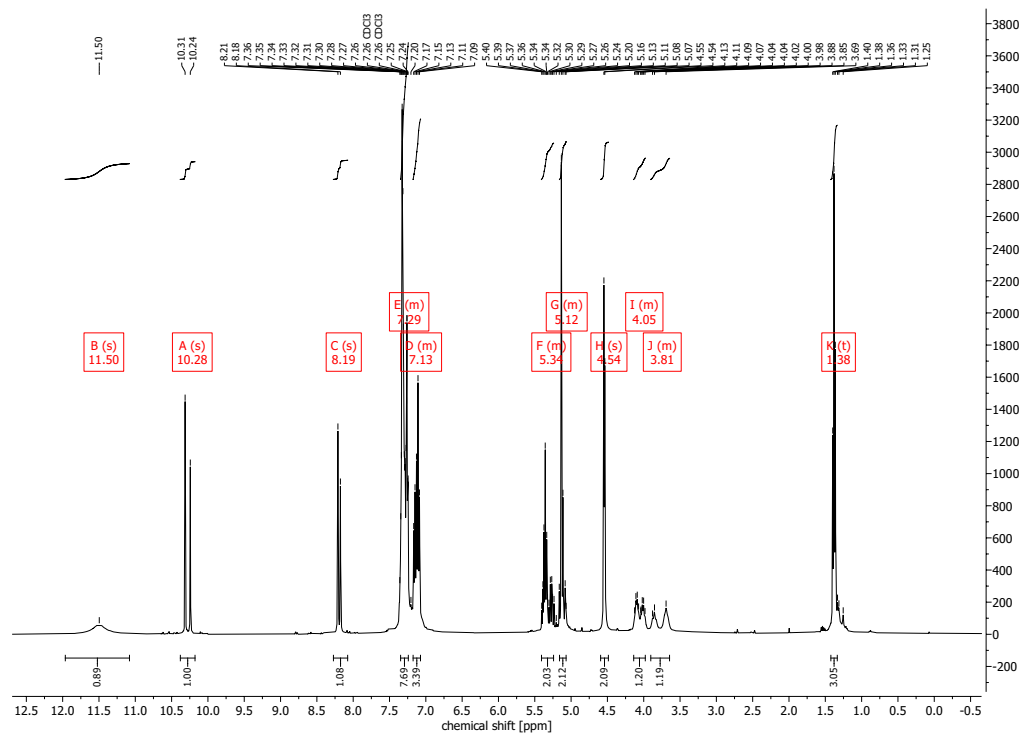
<sup>1</sup>H-, <sup>13</sup>C- and <sup>19</sup>F-spectra of TM-2-19

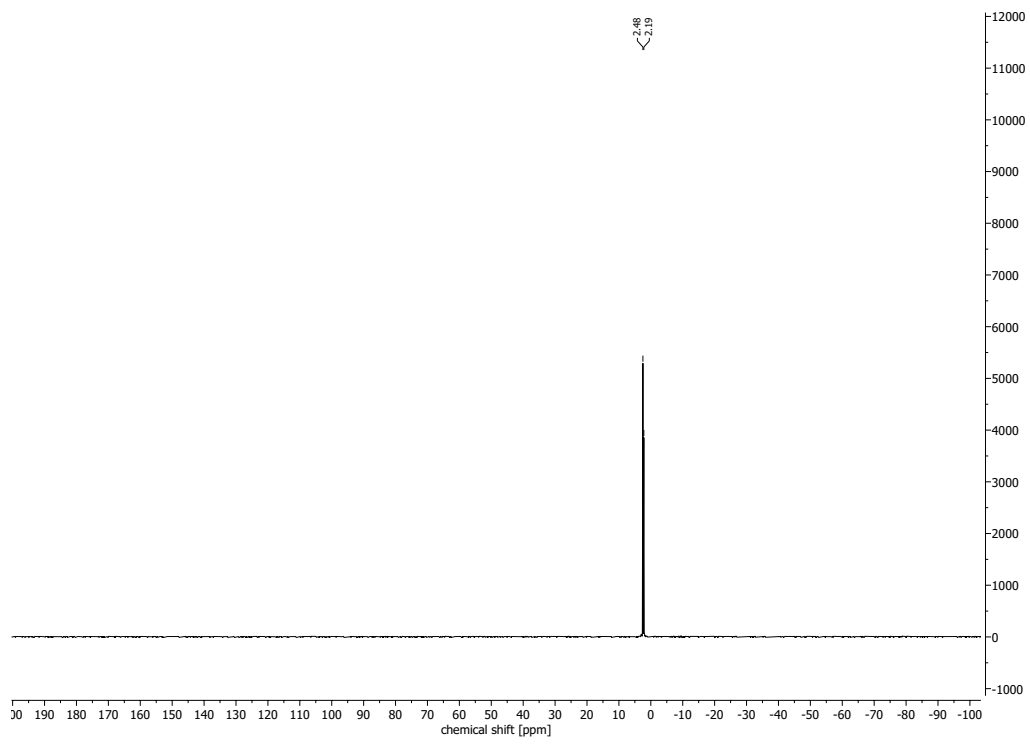




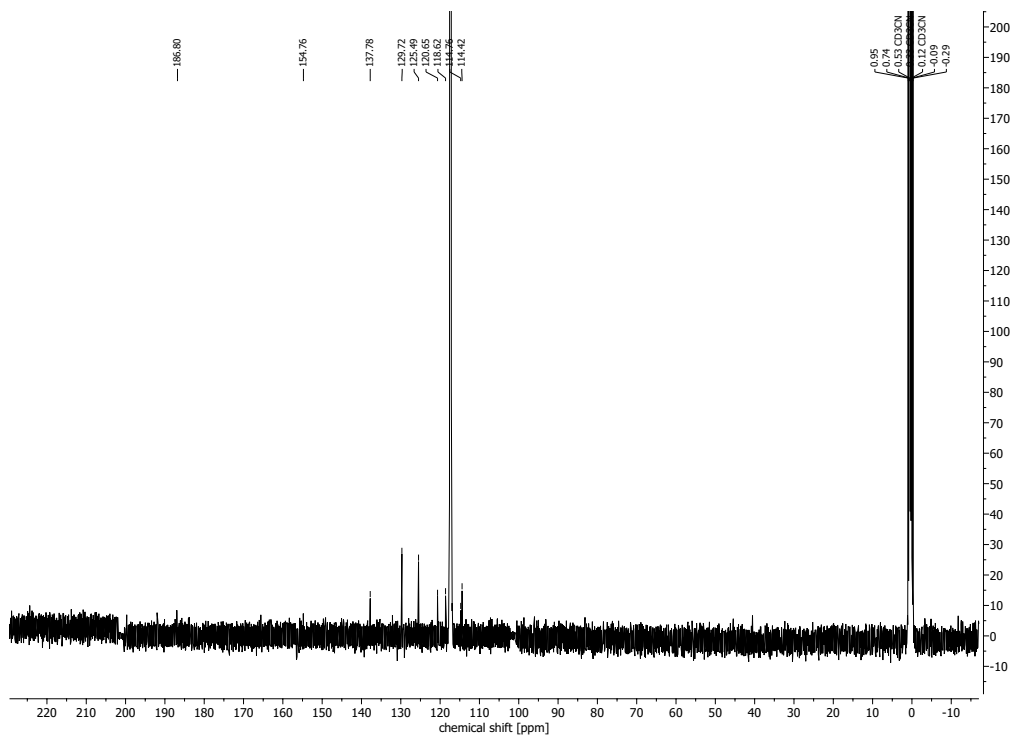
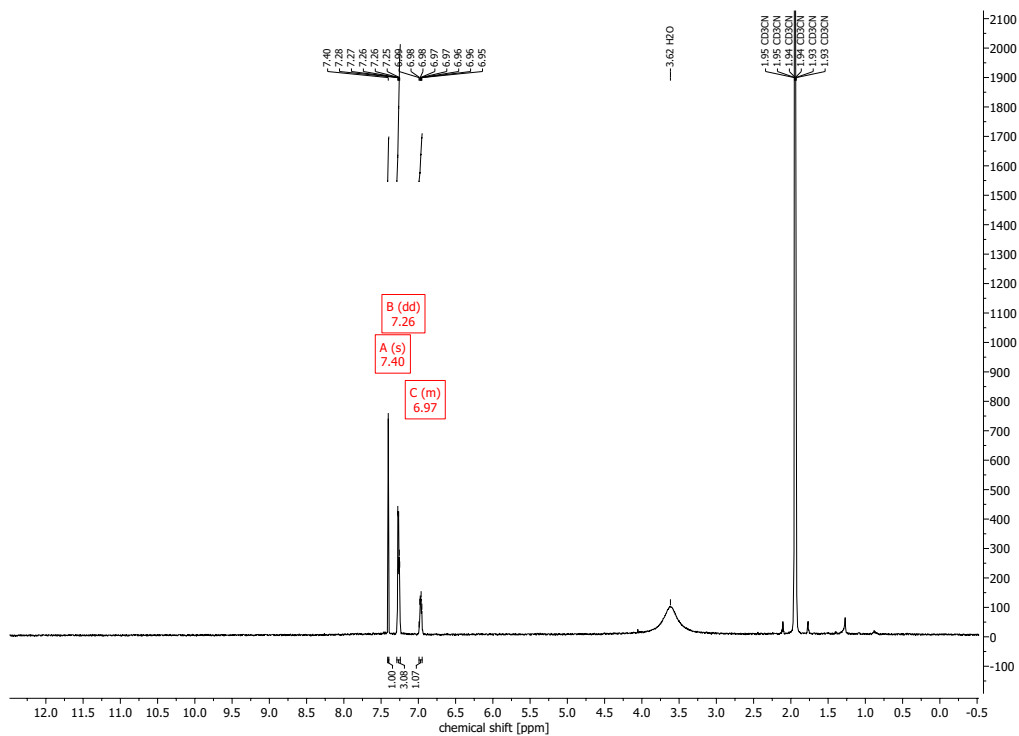


$^1\text{H}$ -spectrum of the PL methoxim

$^1\text{H}$ -,  $^{13}\text{C}$ - and  $^{31}\text{P}$ -spectra of PL3PA





$^1\text{H}$ - and  $^{13}\text{C}$ -spectra of MAC173979 amine

## A.4 Licences



This is a License Agreement between Martin Pfanzelt ("User") and Copyright Clearance Center, Inc. ("CCC") on behalf of the Rightsholder identified in the order details below. The license consists of the order details, the CCC Terms and Conditions below, and any Rightsholder Terms and Conditions which are included below. All payments must be made in full to CCC in accordance with the CCC Terms and Conditions below.

Order Date	28-Feb-2022	Type of Use	Republish in a thesis/dissertation
Order License ID	1193962-1	Publisher	JOHN WILEY & SONS, INC.
ISSN	1521-3373	Portion	Chart/graph/table/figure

### LICENSED CONTENT

Publication Title	Angewandte Chemie	Country	Germany
Article Title	Tailored Pyridoxal Probes Unravel Novel Cofactor-Dependent Targets and Antibiotic Hits in Critical Bacterial Pathogens	Rightsholder	John Wiley & Sons - Books
Author/Editor	Gesellschaft Deutscher Chemiker	Publication Type	eJournal
Date	01/01/1962	URL	http://www3.interscience.wiley.com/cgi-bin/jhome/1196572259
Language	English		

### REQUEST DETAILS

Portion Type	Chart/graph/table/figure	Distribution	Worldwide
Number of charts / graphs / figures requested	70	Translation	Original language of publication
Format (select all that apply)	Electronic	Copies for the disabled?	No
Who will republish the content?	Academic institution	Minor editing privileges?	Yes
Duration of Use	Life of current edition	Incidental promotional use?	Yes
Lifetime Unit Quantity	Up to 499	Currency	EUR
Rights Requested	Main product and any product related to main product		

### NEW WORK DETAILS

Title	Investigation of Pyridoxal Phosphate-Dependent Enzymes and Deciphering their Role as Novel Antibiotic Targets in Critical Bacterial Pathogens by a Chemical Proteomic Strategy	Institution name	Technical University of Munich
Instructor name	Stephan A. Sieber	Expected presentation date	2022-03-16

### ADDITIONAL DETAILS

The requesting person / organization to appear on the license	Martin Pfanzelt																
Reuse Content Details	<table border="1"> <tr> <td>Title, description or numeric reference of the portion(s)</td> <td>Figures, tables and supporting information</td> <td>Title of the article/chapter the portion is from</td> <td>Tailored Pyridoxal Probes Unravel Novel Cofactor-Dependent Targets and Antibiotic Hits in Critical Bacterial Pathogens</td> </tr> <tr> <td>Editor of portion(s)</td> <td>Pfanzelt, Martin; Maher, Thomas E.; Absmeier, Ramona M.; Schwarz, Markus; Sieber, Stephan Axel</td> <td>Author of portion(s)</td> <td>Pfanzelt, Martin; Maher, Thomas E.; Absmeier, Ramona M.; Schwarz, Markus; Sieber, Stephan Axel</td> </tr> <tr> <td>Volume of serial or monograph</td> <td>N/A</td> <td>Publication date of portion</td> <td>2022-02-24</td> </tr> <tr> <td>Page or page range of portion</td> <td>All</td> <td></td> <td></td> </tr> </table>	Title, description or numeric reference of the portion(s)	Figures, tables and supporting information	Title of the article/chapter the portion is from	Tailored Pyridoxal Probes Unravel Novel Cofactor-Dependent Targets and Antibiotic Hits in Critical Bacterial Pathogens	Editor of portion(s)	Pfanzelt, Martin; Maher, Thomas E.; Absmeier, Ramona M.; Schwarz, Markus; Sieber, Stephan Axel	Author of portion(s)	Pfanzelt, Martin; Maher, Thomas E.; Absmeier, Ramona M.; Schwarz, Markus; Sieber, Stephan Axel	Volume of serial or monograph	N/A	Publication date of portion	2022-02-24	Page or page range of portion	All		
Title, description or numeric reference of the portion(s)	Figures, tables and supporting information	Title of the article/chapter the portion is from	Tailored Pyridoxal Probes Unravel Novel Cofactor-Dependent Targets and Antibiotic Hits in Critical Bacterial Pathogens														
Editor of portion(s)	Pfanzelt, Martin; Maher, Thomas E.; Absmeier, Ramona M.; Schwarz, Markus; Sieber, Stephan Axel	Author of portion(s)	Pfanzelt, Martin; Maher, Thomas E.; Absmeier, Ramona M.; Schwarz, Markus; Sieber, Stephan Axel														
Volume of serial or monograph	N/A	Publication date of portion	2022-02-24														
Page or page range of portion	All																

The requesting person / organization to appear on the license

### REUSE CONTENT DETAILS

Title, description or numeric reference of the portion(s)	Figures, tables and supporting information	Title of the article/chapter the portion is from	Tailored Pyridoxal Probes Unravel Novel Cofactor-Dependent Targets and Antibiotic Hits in Critical Bacterial Pathogens
Editor of portion(s)	Pfanzelt, Martin; Maher, Thomas E.; Absmeier, Ramona M.; Schwarz, Markus; Sieber, Stephan Axel	Author of portion(s)	Pfanzelt, Martin; Maher, Thomas E.; Absmeier, Ramona M.; Schwarz, Markus; Sieber, Stephan Axel
Volume of serial or monograph	N/A	Publication date of portion	2022-02-24
Page or page range of portion	All		

### RIGHTSHOLDER TERMS AND CONDITIONS

No right, license or interest in any trademark, trade name, service mark or other branding ("Marks") of WILEY or its licensors is granted hereunder, and you agree that you shall not assert any such right, license or interest with respect thereto. You may not alter, remove or suppress in any manner any copyright, trademark or other notices displayed by the Wiley material. This Agreement will be void if the Type of Use, Format, Circulation, or Requestor Type was misrepresented during the licensing process. In no instance may the total amount of Wiley Materials used in any Main Product, Compilation or Collective work comprise more than 5% (if figures/tables) or 15% (if full articles/chapters) of the (entirety of the) Main Product, Compilation or Collective Work. Some titles may be available under an Open Access license. It is the Licensor's responsibility to identify the type of Open Access license on which the requested material was published, and comply fully with the terms of that license for the type of use specified. Further details can be found on Wiley Online Library <http://about.wiley.com/WileyCDO/section/114-410895.html>.

### CCC Terms and Conditions

- Description of Service: Defined Terms. This Reproduction License enables the User to obtain licenses for reproduction of one or more copyrighted works as described in detail on the relevant Order Confirmation (the "Works"). Copyright Clearance Center, Inc. ("CCC") grants licenses through the Service on behalf of the rightsholder identified in the Order Confirmation (the "Rightsholder"). "Republishing", as used herein, generally means the inclusion of a Work, in whole or in part, in a new work or works, also as described on the Order Confirmation. "User", as used herein, means the person or entity making such reproduction.
- The terms set forth in the relevant Order Confirmation, and any terms set by the Rightsholder with respect to a particular Work, govern the terms of use of Works in connection with the Service. By using the Service, the person transacting for a reproduction license on behalf of the User represents and warrants that he/she/it (a) has been duly authorized by the User to accept, and hereby does accept, all such terms and conditions on behalf of User, and (b) shall inform User of all such terms and conditions. In the event such person is a "freelancer" or other third party independent of User and CCC, such party shall be deemed jointly a "User" for purposes of these terms and conditions. In any event, User shall be deemed to have accepted and agreed to all such terms and conditions if User republishes the Work in any fashion.
- Scope of License: Limitations and Obligations.

3.1. All Works and all rights therein, including copyright rights, remain the sole and exclusive property of the Rightsholder. The license created by the exchange of an Order Confirmation (and/or any invoice) and payment by User of the full amount set forth on that document includes only those rights expressly set forth in the Order Confirmation and in these terms and conditions, and conveys no other rights in the Works) to User. All rights not expressly granted are hereby reserved.

3.2. General Payment Terms: You may pay by credit card or through an account with us payable at the end of the month. If you and we agree that you may establish a standing account with CCC, then the following terms apply: Remit Payment to: Copyright Clearance Center, 2918 Network Place, Chicago, IL 60673-1291. Payments Due: Invoices are payable upon their delivery to you (or upon our notice to you that they are

available to you for downloading). After 30 days, outstanding amounts will be subject to a service charge of 1-1/2% per month or, if less, the maximum rate allowed by applicable law. Unless otherwise specifically set forth in the Order Confirmation or in a separate written agreement signed by CCC, invoices are due and payable on "net 30" terms. While User may exercise the rights licensed immediately upon issuance of the Order Confirmation, the license is automatically revoked and is null and void, as if it had never been issued, if complete payment for the license is not received on a timely basis either from User directly or through a payment agent, such as a credit card company.

- Unless otherwise provided in the Order Confirmation, any grant of rights to User (i) is "one-time" (including the editions and product family specified in the license), (ii) is non-exclusive and non-transferable and (iii) is subject to any and all limitations and restrictions (such as, but not limited to, limitations on duration of use or circulation) included in the Order Confirmation or invoice and/or in these terms and conditions. Upon completion of the licensed use, User shall either secure a new permission for further use of the Work(s) or immediately cease any new use of the Work(s) and shall render inaccessible (such as by deleting or by removing or severing links or other locators) any further copies of the Work (except for copies printed on paper in accordance with this license and still in User's stock at the end of such period).
- In the event that the material for which a reproduction license is sought includes third party materials (such as photographs, illustrations, graphs, inserts and similar materials) which are identified in such material as having been used by permission, User is responsible for identifying, and seeking separate licenses (under this Service or otherwise) for, any of such third party materials, without a separate license, such third party materials may not be used.
- Use of proper copyright notice for a Work is required as a condition of any license granted under the Service. Unless otherwise provided in the Order Confirmation, a proper copyright notice will read substantially as follows: "Republished with permission of (Rightsholder's name), from (Work's title, author, volume, edition number and year of copyright); permission conveyed through Copyright Clearance Center, Inc." Such notice must be provided in a reasonably legible font size and must be placed either immediately adjacent to the Work as used (for example, as part of a by-line or footnote but not as a separate electronic link) or in the place where substantially all other credits or notices for the new work containing the republished Work are located. Failure to include the required notice results in loss to the Rightsholder and CCC, and the User shall be liable to pay liquidated damages for each such failure equal to twice the use fee specified in the Order Confirmation, in addition to the use fee itself and any other fees and charges specified.
- User may only make alterations to the Work if and as expressly set forth in the Order Confirmation. No Work may be used in any way that is defamatory, violates the rights of third parties (including such third parties' rights of copyright, privacy, publicity, or other tangible or intangible property), or is otherwise illegal, sexually explicit or obscene. In addition, User may not conjoin a Work with any other material that may result in damage to the reputation of the Rightsholder. User agrees to inform CCC if it becomes aware of any infringement of any rights in a Work and to cooperate with any reasonable request of CCC or the Rightsholder in connection therewith.
- Indemnity. User hereby indemnifies and agrees to defend the Rightsholder and CCC, and their respective employees and directors, against all claims, liability, damages, costs and expenses, including legal fees and expenses, arising out of any use of a Work beyond the scope of the rights granted herein, or any use of a Work which has been altered in any unauthorized way by User, including claims of defamation or infringement of rights of copyright, publicity, privacy or other tangible or intangible property.
- Limitation of Liability. UNDER NO CIRCUMSTANCES WILL CCC OR THE RIGHTSHOLDER BE LIABLE FOR ANY DIRECT, INDIRECT, CONSEQUENTIAL OR INCIDENTAL DAMAGES (INCLUDING WITHOUT LIMITATION DAMAGES FOR LOSS OF BUSINESS PROFITS OR INFORMATION, OR FOR BUSINESS INTERRUPTION) ARISING OUT OF THE USE OR INABILITY TO USE A WORK, EVEN IF ONE OF THEM HAS BEEN ADVISED OF THE POSSIBILITY OF SUCH DAMAGES. In any event, the total liability of the Rightsholder and CCC (including their respective employees and directors) shall not exceed the total amount actually paid by User for this license. User assumes full liability for the actions and omissions of its principals, employees, agents, affiliates, successors and assigns.
- Limited Warranties. THE WORK(S) AND RIGHT(S) ARE PROVIDED "AS IS". CCC HAS THE RIGHT TO GRANT TO USER THE RIGHTS GRANTED IN THE ORDER CONFIRMATION DOCUMENT, CCC AND THE RIGHTSHOLDER DISCLAIM ALL OTHER WARRANTIES RELATING TO THE WORK(S) AND RIGHT(S), EITHER EXPRESS OR IMPLIED, INCLUDING WITHOUT LIMITATION IMPLIED WARRANTIES OF MERCHANTABILITY OR FITNESS FOR A PARTICULAR PURPOSE. ADDITIONAL RIGHTS MAY BE REQUIRED TO USE ILLUSTRATIONS, GRAPHS, PHOTOGRAPHS, ABSTRACTS, INSERTS OR OTHER

PORTIONS OF THE WORK (AS OPPOSED TO THE ENTIRE WORK) IN A MANNER CONTEMPLATED BY USER. USER UNDERSTANDS AND AGREES THAT NEITHER CCC NOR THE RIGHTSHOLDER MAY HAVE SUCH ADDITIONAL RIGHTS TO GRANT.

- Effect of Breach. Any failure by User to pay any amount when due, or any use by User of a Work beyond the scope of the license set forth in the Order Confirmation and/or these terms and conditions, shall be a material breach of the license created by the Order Confirmation and these terms and conditions. Any breach not cured within 30 days of an written notice thereof shall result in immediate termination of such license without further notice. Any unauthorized (but licensable) use of a Work that is terminated immediately upon notice thereof may be liquidated by payment of the Rightsholder's ordinary license price therefor; any unauthorized (and unlicensable) use that is not terminated immediately for any reason (including, for example, because materials containing the Work cannot reasonably be recalled) will be subject to all remedies available at law or in equity, but in no event to a payment of less than three times the Rightsholder's ordinary license price for the most closely analogous licensable use plus Rightsholder's and/or CCC's costs and expenses incurred in collecting such payment.
- Miscellaneous.
  - User acknowledges that CCC may, from time to time, make changes or additions to the Service or to these terms and conditions, and CCC reserves the right to send notice to the User by electronic mail or otherwise for the purposes of notifying User of such changes or additions; provided that any such changes or additions shall not apply to permissions already secured and paid for.
  - Use of User-related information collected through the Service is governed by CCC's privacy policy, available online here: <https://marketplace.copyright.com/rsu-us-web/mp/privacy-policy>
  - The licensing transaction described in the Order Confirmation is personal to User. Therefore, User may not assign or transfer to any other person (whether a natural person or an organization of any kind) the license created by the Order Confirmation and these terms and conditions or any rights granted hereunder; provided, however, that User may assign such license in its entirety on written notice to CCC in the event of a transfer of all or substantially all of User's rights in the new material which includes the Work(s) licensed under this Service.
  - No amendment or waiver of any terms is binding unless set forth in writing and signed by the parties. The Rightsholder and CCC hereby object to any terms contained in any writing prepared by the User or its principals, employees, agents or affiliates and purporting to govern or otherwise relate to the licensing transaction described in the Order Confirmation, which terms are in any way inconsistent with any terms set forth in the Order Confirmation and/or in these terms and conditions or CCC's standard operating procedures, whether such writing is prepared prior to, simultaneously with or subsequent to the Order Confirmation, and whether such writing appears on a copy of the Order Confirmation or in a separate instrument.
  - The licensing transaction described in the Order Confirmation document shall be governed by and construed under the law of the State of New York, USA, without regard to the principles thereof of conflicts of law. Any case, controversy, suit, action, or proceeding arising out of, in connection with, or related to such licensing transaction shall be brought, at CCC's sole discretion, in any federal or state court located in the County of New York, State of New York, USA, or in any federal or state court whose geographical jurisdiction covers the location of the Rightsholder set forth in the Order Confirmation. The parties expressly submit to the personal jurisdiction and venue of each such federal or state court. If you have any comments or questions about the Service or Copyright Clearance Center, please contact us at 978-750-8400 or send an e-mail to [support@copyright.com](mailto:support@copyright.com).

v.1.1

## A.5 Curriculum Vitae

born 22<sup>nd</sup> July 1994 in  
Schongau, Germany

# Martin Pfanzelt

### Doctoral Studies

**Dec. 2017 – present: PhD in Chemical Biology**, *Technical University of Munich*, Garching, Germany  
Chair of Organic Chemistry II, Prof. Stephan. A. Sieber  
Topic: Investigation of Pyridoxal Phosphate-Dependent Enzymes and Deciphering Their Role as Novel Antibiotic Targets in Critical Bacterial Pathogens by a Chemical Proteomic Strategy

### Education

**Oct. 2015 – Nov. 2017: Master of Science, Chemistry**, *Technical University of Munich*, Garching, Germany, Grade 1.0  
Chair of Organic Chemistry II, Prof. Stephan. A. Sieber  
Topic: Synthesis of Pyridoxal Derivatives for the Investigation of Pyridoxal Phosphate Dependent Enzymes

**Oct. 2012 – Sep. 2015: Bachelor of Science, Chemistry**, *Technical University of Munich*, Garching, Germany, Grade 2.0  
Chair of Physical Chemistry, Prof. Ulrich Heiz  
Topic: Synthesis, Functionalisation and Characterisation of Small Gold Nanoparticles

**Jun. 2012: Abitur**, *Welfen-Gymnasium*, Schongau, Germany, Grade 1.4

### Workshops and Conferences

- Stress control workshop, Graduate School, 2021
- Leadership and personality workshop, Graduate School, 2021
- GMP workshop, GMP academy, 2021
- Scientific illustration workshop, Graduate School, 2020
- EMBO Chemical Biology conference, 2020
- Concepts of drug discovery workshop, Graduate School, 2020
- Communicating in teams and difficult situations workshop, Graduate School, 2019
- GMP workshop, Graduate School, 2019
- Biotech quality manager/regulatory affairs manager workshop, Graduate School, 2019
- ABPP conference in Leuven, Poster presentation, 2019
- PyMol course, Graduate School, 2018